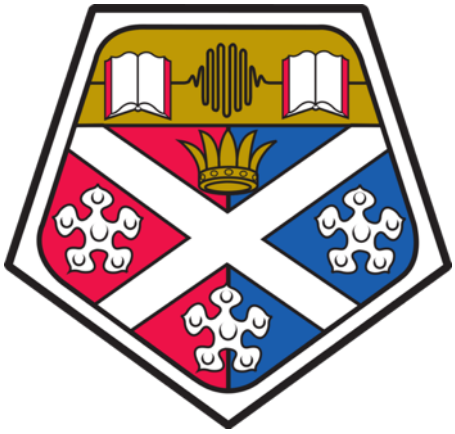

University of Strathclyde

Strathclyde Institute of Pharmacy and Biomedical Sciences

Understanding and exploiting the Mce proteins from *Streptomyces*

Emily Addington

Thesis presented in fulfilment of the requirements for the degree of

Doctor of Philosophy

2021

Declaration

This thesis is the result of the author's original research. It has been composed by the author and has not been previously submitted for examination which has led to the award of a degree.

Signed:

Date:

Acknowledgements

I would have been wholly incapable of completing this thesis without the help and support of so many people, to whom I will always be incredibly grateful. Thank you to all of Level 6 and all members of the MicroGroup for making my time at Strathclyde so enjoyable and providing ideas, encouragement, and friendship in equal measure. You are all so passionate, implausibly clever, and entirely unhinged. I miss you all already.

Thank you, in particular, to John Munnoch, who has been there since I was a summer student in Norwich and has remained ever a true and kind friend with an unwavering ability to help and care for others. Your advice and guidance, both within and outside of the lab, have been invaluable to me. There isn't enough room to write it all here, but I wouldn't have gotten to this point without you.

To my supervisor Paul, because there isn't another supervisor alive who could've gotten me through this PhD. I'll never be able to thank you enough for all your support and kindness. You've been the most inspiring, fun, and caring mentor, with infectious enthusiasm, unparalleled dedication, and unrelenting encouragement the many (many) times I've needed it. I will always feel incredibly fortunate to have been your student and a part of the Hoskie Lab.

To David, my heart, my support, my snack provider. Thanks, RB.

To my Mom and Dad.

Dad - Here it is. Thanks for all the war counsels.

Mom - You already know it all. I love you.

For Andy, forever missed. This can sit beside yours.

Abstract

Streptomyces are Gram-positive bacteria which are typically non-pathogenic saprophytes present in great abundance in soil. This genus is a member of the Actinobacteria phyla, which contains notable pathogens such as *Mycobacterium tuberculosis*, the causative agent of tuberculosis in humans.

Mammalian cell entry (*mce*) genes, originally discovered in *M. tuberculosis* as factors which enabled bacterial entry into human cells, have been identified wildly throughout Actinobacteria, in both pathogenic and non-pathogenic species. Bioinformatic analysis suggests all Actinobacterial operons descend from a singular ancestral operon which underwent proliferation and duplication with minimal gene reshuffling. In many Actinobacteria, *mce* operons have now been characterised as ABC transporters for lipids.

The genome of *Streptomyces coelicolor* encodes one copy of the *mce* operon which shares significant homology with the four *mce* operons of *M. tuberculosis*, known to be vital for the bacterium's virulence and persistence within hosts. Within *M. tuberculosis*, *mce1* and *mce4* encode ABC transporters for fatty acids and cholesterol respectively.

This thesis explores the function of the singular *mce* operon of *S. coelicolor* through knockout of the cluster and subsequent phenotypic analysis. Results from this work strongly suggest that the *mce* operon of *S. coelicolor* encodes an ABC transporter for sterol import which likely facilitates bacterial survival in the highly competitive rhizosphere. Further results demonstrate that deletion of the *mce* operon has profound effect on spore resistance, as well as on rate of sporulation and germination, and impacts interaction of the bacterium with soil protists.

“The data is the data.” – Dr Gordon Williamson

List of Tables

List of Figures

Table of contents

Chapter 1: Introduction

An overview of Actinobacteria

The phylum *Actinobacteria* is comprised of non-motile, Gram-positive bacteria characterized by the high guanine-plus-cytosine (G+C) content of their DNA. Many members of this phylum are found ubiquitously in terrestrial, fresh-water and marine environments where they perform vital ecological functions, including a broad range of metabolic processes and bio-transformations, and have key roles in carbon recycling. Actinobacteria are also of significant use in agriculture, biotechnology and medicine, with the phyla famously producing two-thirds of all naturally derived antibiotics and numerous anticancer, anthelmintic and antifungal compounds (Barka *et al.*, 2016). Conversely, the phyla Actinobacteria also contains eminent pathogens such as *Mycobacterium tuberculosis, Mycobacterium leprae,* and *Corynebacterium diphtheria,* which have significant impact on global morbidity and mortality.

Actinobacteria is one of the largest taxonomic units within the Bacteria domain and members of this phyla are accordingly diverse, including human pathogens (*Mycobacterium, Corynebacterium, Nocardia, Propionibacterium, Tropheryma)*, soil bacteria (*Streptomyces, Micromonospora)*, plant commensals (*Frankia spp*) and human gastrointestinal commensals (*Bifidobacterium spp.),* exhibiting a vast assortment of morphologies from coccoid to highly differentiated branched mycelial forms (Ventura *et al.*, 2007; Barka *et al.*, 2016). Some of these bacteria perform functions valuable to human health and nutrition, such as *Bifidobacterium*, which is particularly prolific in the human gut microbiome (O'Callaghan and van Sinderen, 2016). However, the Actinobacteria *Mycobacterium tuberculosis,* the causative agent of tuberculosis, remains the leading cause of death globally by any singular infectious bacterium too date (Moule and Cirillo, 2020). Whilst *Streptomyces* and *Mycobacterium* represent two of the most

highly studied and characterized genera, the phylum *Actinobacteria* contains over 300 other genera, including many which are greatly under researched in comparison (Zhi, Li and Stackebrandt, 2009; Gao and Gupta, 2012; Parte, 2014). This can be partially attributed to the considerable distribution of *Actinobacteria* members, particular with species colonizing extreme environments such as the Arctic tundra, radioactively or chemically contaminated sites, hyperarid deserts soils, or deep marine environments (Gao and Gupta, 2012).

Genomic characteristics of Actinobacteria are similarly diverse. Of known genomes, size varies from as small as 0.93 Mb in *Tropheryma whipplei* to 12 Mb in *Streptomyces bingchenggenis*. The Guanosine and Cytosine (GC) content of their DNA similarly differs from 41% in *Gardnerella vaginalis* ATCC 14019 to 74% in *Kineococcus radiotolerans* SR30216 (Bentley *et al.*, 2003; Bradshaw *et al.*, 2006; McLeod *et al.*, 2006; Bagwell *et al.*, 2008; Gao and Gupta, 2012). The genera *Streptomyces, Rhodococcus, Gordonibacter*, and *Kineococcus* have linear chromosomes with a central replication origin, *oriC*, and terminal inverted repeats (Chen *et al.*, 2002; McLeod *et al.*, 2006; Schrempf, 2006; Sekine *et al.*, 2006; Bagwell *et al.*, 2008; Kirby, 2011; Gao and Gupta, 2012). Other Actinobacteria, such as *Corynebacterium, Mycobacterium, Salinispora* and *Amycolatopsis,* have circular chromosomes (van Bergeijk *et al.*, 2020).

Mycelial forming Actinobacteria are often referred to as *Actinomycetes*, a designation utilized as early as 1877, meaning ‘ray fungus’. The term was coined by German botanist Carl Otto Harz due to the filamentous and hyphal structure of the bacteria and their morphological resemblance to fungi. Such mycelial Actinobacteria were indeed, at one point, believed to be transitional organisms between bacteria and fungi (Barka *et al.*, 2016). Certainly, their mycelial growth and reproduction through sporulation suggested a kinship with fungi, and names such as *‘Streptomyces’* (‘twisted fungus’) and

'Mycobacterium' ('fungus bacterium') reflected the possession of both fungal and bacterial properties and demonstrates the then uncertainty of how to classify these organisms (Hopwood, 2015). In the late 1970s 16S rRNA sequencing was developed by Carl Woese, a technique where 16S ribosomal RNA (rRNA), which contains both variable and highly conserved regions which can be amplified and compared in order to establish phylogenic relationships. Exemplifying this, *Streptomyces* has three variable regions, α, β and γ, which can be used for identification (Mehling, Wehmeier and Piepersberg, 1995). 16S sequencing confirmed that Actinobacteria are true bacteria, with only superficial similarities to fungi as a result of convergent evolution (Hopwood, 2015). However, classification of Actinobacteria remains a complex and ever-adjusting terrain as further sequencing and discovery of novel species and genera leads to regular updates in taxonomic structure and composition of the *Actinobacteria* phylogenic tree. Despite the use of 16S sequencing in architecting the actinobacterial taxa, this method has its limitations and issues remain in delineation, not only amongst species, but at family and genus levels (Nouioui *et al.*, 2018).

Current taxonomy for Actinobacteria divides the phyla into six classes, including the class Actinobacteria which itself contains 18 orders, including the *Actinomycetales*. In the most basic of terms, the Actinobacteria phylum contains the class *Actinobacteria*, which in turn contains the subclass *Actinobacteridae*. *Actinobacteridae* contains the order *Actinomycetales*, which further divides into thirteen suborders, including *Corynebacterineae* and *Streptomycineae*, of which the genera *Mycobacterium* and *Streptomyces* belong to respectively (Gao and Gupta, 2012; Barka *et al.*, 2016).

Pathogenic Actinobacteria

Although largely formed of saprophytic bacterium, Actinobacteria genera also contain some of the world's most well-known and deadliest pathogens, the most recognized of which originate from the genus *Mycobacterium,* which is composed of 188 species (Gupta, Lo and Son, 2018). Prominent human pathogens within this genus include *Mycobacterium tuberculosis, Mycobacterium leprae* and *Mycobacterium ulcerans,* the causative agents of tuberculosis, leprosy and Buruli ulcers respectively (Whittington *et al.*, 2012). Both *M. tuberculosis* and *M. leprae* are obligate intracellular microorganisms, having become highly adapted to infect their hosts and replicate inside mammalian cells. *M. leprae* in particular has a decayed 3.27 Mb genome resulting from severe loss of gene function, undergoing reductive evolution to become a host-dependent parasite (Vissa and Brennan, 2001). Together with two other Actinobacteria genera, *Corynebacterium* and *Nocardia*, *Mycobacteria* form the CNM group, notable for their acid- and alcohol-fast cell envelope composed of mycolic acids (Barka *et al.*, 2016). Both *Nocardia* and *Corynebacterium* species are causative agents of infections in humans. *Nocardia* infections are generally opportunistic in nature, arising largely in immunocompromised hosts and leading to disseminated nocardiosis and brain abscesses in humans (Simpson and Read, 2014; Barka *et al.*, 2016). The genera *Corynebacterium* and *Rhodoccocus* contain notable human pathogens, such as *C. diphtheria,* the causative agent of diphtheria, and *R. equi* (Barka *et al.*, 2016). Almost antithetically to these pathogens, *Streptomyces* are mycelial and commonly found in soil, being most well known for their production of antibiotics and other medicinal compounds. However, a number of species are prominent plant pathogens, notably *S. scabies,* and others, such as, *S somaliensis* cause opportunistic infections in humans such as actinomycetomas. Mycetomas are severe infections that may spread to deep tissues and bone and are the most commonly seen clinical infections associated with *Streptomyces* species (Kapadia, Rolston and

Han, 2007; Kirby *et al.*, 2012). Incidences of other *Streptomyces*-associated disease include invasive infections resulting in lung abscess, pneumonitis and bloodstream infections caused by diverse *Streptomyces* species acting in a highly opportunistic manner in individuals with pre-existing health conditions (Kapadia, Rolston and Han, 2007).

Mycobacterium tuberculosis

Arguably the most prominent of *Actinobacteria*, *Mycobacterium tuberculosis* (*Mtb*) is a highly host-adapted obligate-intracellular pathogen and the etiological agent of tuberculosis (TB) in humans. TB is responsible for significant morbidity and mortality world-wide, being the leading cause of death worldwide due to a singular infectious organism, other than Covid-19 (WHO, 2019). *Mtb* is a Gram-positive, non-sporulating and rod-shaped bacillus which is strictly aerobic in nature and grows at an optimum temperature of 37°C. It is relatively slow-growing, with division time of 18-24 hours in rich medium (Logsdon and Aldridge, 2018).

TB may manifest in various forms dependent on where the disease originates and develops in the host. The lungs are the most common site of primary infection, resulting in Pulmonary tuberculosis. Pulmonary tuberculosis is contracted by inhalation of aerosol droplets containing the tubercle bacilli, some of which are phagocytosed by alveolar macrophages or alveolar epithelial type II pneumocytes (Smith, 2003). *Mtb* is able to avoid destruction and parasitize macrophages by modulating phagosome progression and avoidance of a localized, productive immune response which would activate the host cell (Russell, 2001). In this manner, *Mtb* is able to reside within the phagocytic vacuole until death of the host cell. *Mtb*-parasitized macrophages show reduced ability to induce cellular immune responses. A localized immune response to *Mtb* invasion results in

recruitment of a plethora of inactivated monocytes, lymphocytes and neutrophils to the site of infection in the lungs (Smith, 2003; Pieters, 2008). The aggregation of these cells - which are largely ineffective at killing the mycobacteria - results in formation of the characteristic granulomas of TB. Granulomas, also known as Tuberculomas, consist of a center of infected macrophages interned by foamy giant cells, macrophages and T-lymphocytes (Pieters, 2008). In this manner, the bacterium is contained from spreading and may remain dormant for many decades. As a result, though it is believed that approximately one-third of the human population is infected with *Mtb*, most show no signs of illness, as the infection is in an asymptomatic and non-transmissible state. This is known as latent TB infection or LTBI (Smith, 2003; Pieters, 2008; Talbot and Raffa, 2014). Approximately 10% of LTBIs may become active again, causing an active pulmonary infection, with mycobacteria disseminating throughout the body and causing extrapulmonary TB (Talbot and Raffa, 2014). Active infection is more common in those with compromised immune systems, the elderly, or those with underlying conditions. Typical symptoms include cough, weight loss, fever and anorexia, with systemic infections having a high mortality rate (Delogu, Sali and Fadda, 2013).

Mtb possesses a highly complex cell wall which basic structure may be broken down into three segments: plasma membrane, cell wall core and outermost layer. The cell wall 'core', above the plasma membrane, is composed of peptidoglycan covalently linked to arabinogalactan which is respectively attached to mycolic acids. This insoluble core is referred to as the mycolyl arabinogalactan-peptidoglycan (mAGP) complex and is essential for cell viability (Brennan, 2003; Hett and Rubin, 2008; Grzegorzewicz *et al.*, 2016). The outer (upper) compartment is composed of lipids, interspersed with cell-wall proteins and lipid-linked polysaccharides (Brennan, 2003; Hett and Rubin, 2008).

The complete *M. tuberculosis* H37Rv genome sequence was published in 1988, the singular circular chromosome is approximately 4.41 Mb (4,411,532 bp) in size and contains approximately 4000 genes (Cole *et al.*, 1998). Of these, over 200 (approx. 6%) appear to encode enzymes for fatty acid metabolism. As such, it was proposed that enzymes which degrade fatty acids may be involved in some manner in the ability of *Mtb* to survive and replicate within the infected host, an aspect of pathogenesis which is addressed later in this study (Smith, 2003).

The genus *Streptomyces*

The family *Streptomycetaceae* contains the genus *Streptomyces*, which may be translated as "twisted chain fungus". *Streptomyces* is the largest genus of the *Actinobacteria* phylum and consists of Gram-positive, mycelial bacteria which colonize terrestrial soil, as well as fresh-water and marine sediment. Very few species are pathogenic towards plants or mammals, with the majority being saprophytic organisms which inhabit the soil rhizosphere or rhizoplane (Olanrewaju and Babalola, 2019). In fact, plant commensal *Streptomyces* species are of great agricultural importance; the initial reason these organisms were studied. Today, *Streptomyces* are most famously known for their production of a vast array of secondary metabolites of significant medicinal value. The genus produces a roughly estimated 70-80% of all commercial antibiotics, as well as many antifungals, antivirals, antiparasitics, chemotherapeutics, immunosuppressants and other therapeutically useful compounds (de Lima Procópio *et al.*, 2012; Kämpfer *et al.*, 2014).

Optimal environmental conditions for the majority of *Streptomyces* species are temperatures between 25 and 30°C, with low humidity and a neutral pH, although growth is also possible between pH6 and pH9 (Barka *et al.*, 2016). *Streptomyces* are aerobic,

non-motile and non-acid-alcohol fast, chemoorganotrophic organisms which are capable of nitrate to nitrate reduction and carbon cycling through the degradation of various organic matter (Hasani, Kariminik and Isaazadeh, 2014; Barka *et al.*, 2016). Approximately 600 species of *Streptomyces* have been identified, with two species, *S. griseus* and *S. coelicolor,* being of particular clinical importance (Bontemps *et al.*, 2013). *Streptomyces* is the most abundant of endosymbionts and may also be found living symbiotically on arthropods, such as leaf cutter ants, bees and wasps (Currie *et al.*, 1999; Chater, 2016; Kim *et al.*, 2019). Pathogenic species of the genus include *S. somaliensis* and *S. sudanensis* as well as a number of phytopathogens, of which *S. scabies* is likely the most notorious (Fyans *et al.*, 2013).

Streptomyces are believed to have originated around 400 million years ago, following colonization of the land by green plants and coinciding with the oxygenation of Earth's atmosphere (Chater and Chandra, 2006). *Streptomyces* possess a number of genes involved in the degradation and recycling of the polysaccharides composing organic fungal and plant matter, including chitin, cellulose xylan, agar, and other simple and complex carbohydrates (Barka *et al.*, 2016; Chater, 2016) *Streptomyces* spp. typically have a singular large linear chromosome, with the origin of chromosomal replication, *oriC*, centrally located. The 'core' region of the genome, including all genes essential for growth, comprises approximately half the chromosome and includes genes for DNA replication, transcription and translation, amino acid biosynthesis and cell division (Dyson, 2019). It has been noted that this core region of the *Streptomyces* genome bares significant synteny with that of circular genomes of other *actinomycetes* such as *M. tuberculosis,* suggesting common ancestry in primary cell functions (Dyson, 2019). Conversely, the chromosome arms are largely genes encoding non-essential functions, either acquired by *Streptomyces* following divergence from a common actinomycete ancestor or lost by other *actinomycetes* as they have become adapted to specialized

niches. Such genomic formatting suggests that chromosomal arms bare novel genetic attributes acquired by individual species as they adapt to their environment. These end regions, of approximately 1-2 Mb, are the primary reciprocal for horizontally transferred segments of DNA and are unstable in-terms of long-term gene retention. It is likely the case that genes which are of benefit to the organism may selectively find themselves migrated to more stable core regions of the genome (Chater and Chandra, 2006; Dyson, 2019).

Morphology and lifecycle of *Streptomyces*

Streptomyces are slow-growing organisms which superficially resemble fungi, producing mold-like sporogenic aerial hyphae. The complex lifecycle of *Streptomyces* involves significant morphological differentiation and transitions which are governed by strict and complex regulatory systems.

Streptomyces reproduce via spores which are disseminated through the environment, with growth commencing when the spore encounters a suitable milieu (Fig. 1.1). The spore germinates, beginning with swelling and break-down of the spore-coat, producing one or two germ tubes which grow apically by tip elongation, forming a branching, multichromosomal filamentous network known as the vegetative mycelium (Flärdh and Mark J Buttner, 2009; McCormick and Flärdh, 2012) Dormant spores have low metabolic activity and are tolerant to deleterious stressors such as desiccation and heat due to their thick cell wall. However, this cell wall is refractory towards outward growth, therefore spore germination involves ‘resuscitation-promoting factors’ or Rpfs, which are specialized peptidoglycan hydrolases which aid in initiating active growth of previously dormant spores by cell wall lysis (Sexton *et al.*, 2015). The polarisome component, DivIVA, which is localized to the hyphal tips, interacts with two other coiled-coil proteins,

Scy (*Streptomyces* cytoskeletal element) and FilP (Filament-forming protein) to co-ordinate and drive hyphal tip growth (Fröjd and Flärdh, 2019). To briefly discuss their roles, DivIVA is a vital component of the polarisome, acting to recruit cell wall biosynthetic machinery and determine where cell wall growth and branching occur. Scy colocalizes with DivIVA and appears to aid assembly of the polarisome, as well as recruiting the protein ParA, which is responsible for partitioning chromosomes, to the apical tip to initiate sporulation. FilP is located directly behind DivIVA and Scy at the apical tip and forms filaments along hyphae, organizing cell shape (Bush *et al.*, 2015; Dyson, 2019). Branching occurs as the apical polarisome splits to form a secondary tip focus on the lateral membrane. In this manner, the highly branching vegetative, or 'substrate', mycelium is formed (Bush *et al.*, 2015).

During this first phase of growth, the vegetative mycelium often expands deep into its environment seeking available nutrients and degrading polymeric substrates by secretion of hydrolytic enzymes (McCormick and Flärdh, 2012). This vegetative hyphae contains multinucleate compartments, separated by variably-placed cross-walls (Barka *et al.*, 2016; Yagüe *et al.*, 2016). The second phase of growth, which is initiated in response to various stressors such as nutrient depletion, environmental changes and extra-cellular signaling, involves formation of unbranched, sporogenic aerial hyphae (Bush *et al.*, 2015). These aerial hyphae, believed to be partially parasitic on the vegetative mycelium, are hydrophobic and grow upwards into the open air, providing *Streptomyces* with its distinctive 'fluffy' appearance (Chater and Chandra, 2006; Sigle *et al.*, 2015). Formation of aerial hyphae coincides with production of secondary metabolites in *Streptomyces*. Prevailing theories for this phenomenon suggest that the vegetative mycelium undergoes an autolytic degradation process similar to programmed-cell death, providing amino acids, aminosugars, nucleotides and lipids for the growth of aerial mycelium. In order to defend such precious nutrients from

scavenging by competing microbes, bioactive secondary metabolites are produced by *Streptomyces* in a coordinated process (Chater and Chandra, 2006; Barka *et al.*, 2016).

The formation of aerial hyphae requires a cascade of *bld* regulatory genes, so called for the 'bald' phenotype seen with deletions of these genes; with mutants being unable to erect aerial hyphae (Barka *et al.*, 2016). Such mutants also show disrupted antibiotic production, reinforcing the link between growth development and secondary metabolism. Similarly, DivIVA is regulated by the serine/threonine kinase, Afsk, which is also involved in the regulation of antibiotic production (Barka *et al.*, 2016; Dyson, 2019). Whilst vegetative hyphae are smooth and hydrophilic, aerial hyphae have an outwardly hydrophobic fibrous layer which allows hyphae to break through the surface tension of the aqueous-air interface for upwards growth (Dyson, 2019). Aerial hyphae are also sporogenic, forming septal cross walls which separate them into pre-spore compartments which will ultimately become spore chains (Sigle et al, 2015; Flardh & Buttner, 2009). Ultimately, this process gives rise to chains of 50-100 spores which are released as single spores into the environment (Ryding et al, 1999).

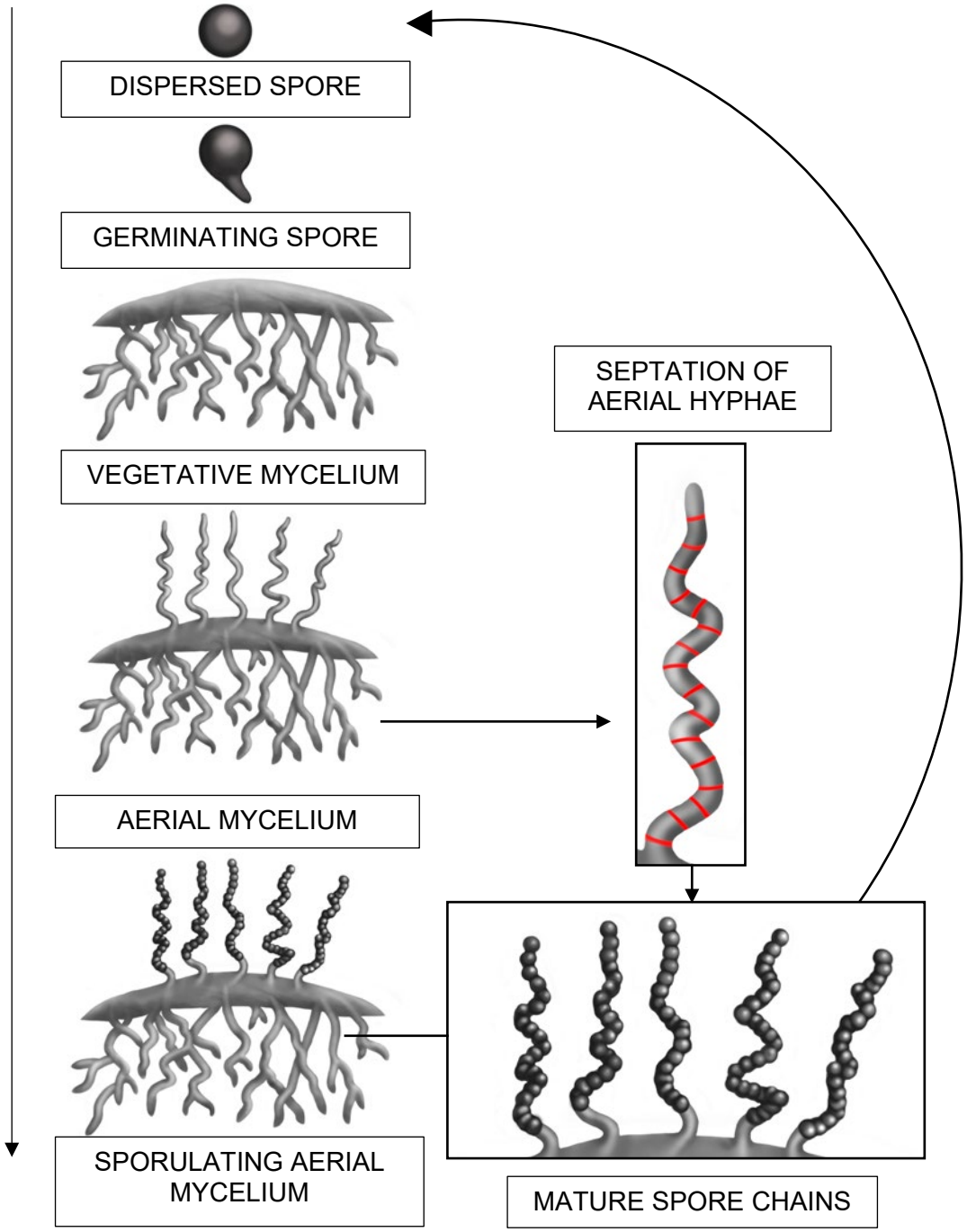

Figure 1.1: Lifecycle and morphology of *Streptomyces*. Upon encountering suitable conditions, a dispersed spore switches on germination machinery and produces one or two germ-tubes. Germ-tubes grow by tip-extension into a branching, vegetative mycelial network which may expand deeply into the environment. In response to nutrient depletion, amongst other signals, this vegetative mycelium is degraded for nutrients to erect aerial hyphae which are unbranched and sporogenic. Aerial hyphae undergo septation to produce individual unigenomic spore compartments. Spore chains are formed of mature spores which may be disseminated into the environment to begin the cycle once again.

Streptomyces spore structure, sporogenesis and germination

As non-motile microorganisms, *Streptomyces* reproduce through disseminated spores similar to those produced by eukaryotic fungi. Dispersal is aided by the upwards growth of the sporogenic aerial hyphae from the vegetative mycelium, meaning spores may be widely spread to encounter more favorable environmental conditions (Barka *et al.*, 2016; Dyson, 2019).

As priorly mentioned, the growth of aerial hyphae is regulated by the *bld* (bald) genes, with the master regulator being BldD, orchestrating the developmental transition from vegetative to aerial hyphal growth to sporulation (Bush *et al.*, 2015). BldD is responsible for the repression of approximately 170 sporulation genes during vegetative growth, including genes of the core transcriptional regulatory cascade and genes encoding cell division and chromosome segregation machineries necessary for sporulation septation (Bush *et al.*, 2015). This latter group includes FtsZ, SsgA and SsgB, and SspA, the roles of which are discussed later in this section. Other key regulatory genes, including the *whi* genes, are also repressed by BldD. Once BldD repression is abrogated, these genes may be expressed and morphological differentiation occurs (Bush *et al.*, 2015).

The membranes of aerial hyphae are stabilized by hopanoids, which act to decrease membrane permeability and therefore prevent against desiccation. Outwardly, amyloid-like fibrils coat the aerial hyphae in a amphipathic sheathe (Sigle *et al.*, 2015). In *S. coelicolor* this layer is composed of three classes of protein, including eight types of chaplin proteins (ChpA-H), which are either long or short chaplins and are anchored to the cell wall. Chaplins are organized by the rodlin proteins, RdlA and RdlB, together forming the major components of the hydrophobic sheathe in what is known as the rodlet layer. The third class of protein involved in construction of the aerial hyphal sheathe are

the spore-associated protein B (SapB) proteins. These lantibiotic-like peptides act as a surfactant, allowing emergence of the aerial hyphae into the atmosphere (Flärdh and Mark J. Buttner, 2009; Barka *et al.*, 2016).

Once aerial hyphae are erected, there is a tightly controlled switch from extension to septation, initiating a developmental program which ultimately leads to apical cell differentiation into a spore chain. Involved in this process are the developmental regulators, WhiA and WhiB. The *whiA* and *whiB* genes belong to the WhiB-like (Wbl) family of proteins and mutants of these genes fail to terminate aerial growth and initiate septation and chromosome partition (Bush *et al.*, 2015). It is now well-established that *whiA* and *whiB* are required for the switch from elongation to division, alongside the cell division activator SsgB, discussed further below (Barka *et al.*, 2016).

Creation of spores is known as ‘sporogenesis’ and requires the reorganization of several fundamental growth and cell-cycle processes (Flärdh and Mark J Buttner, 2009). Initially, a ‘sporogenic cell’ is formed. This is a long, non-septated apical compartment which will differentiate to become the spore chain. Each sporogenic cell is capable of producing up to 100 copies of the linear *Streptomyces* chromosome, which will be separated to allow the formation of unigenomic spores (Flärdh and Mark J Buttner, 2009; Bush *et al.*, 2015). Chromosome segregation occurs simultaneously with the separation of aerial hyphae at specific sites, resulting in the formation of unigenomic pre-spore compartments. This process is a type of cell division known as sporulation septation and is controlled by a family of SSgA-like proteins (SALP) which are found only in sporulating actinobacteria (Barka *et al.*, 2016). The SALP SsgA, alongside the small membrane protein SepG, facilitates the correct localization of SsgB to future-division sites, where the latter protein recruits FtsZ and, together with SsgA, stimulates its polymerization, therefore controlling the symmetrical spacing of septation (Willemse *et al.*, 2011; Chater, 2016). FtsZ is

homologous to the protein tubulin and initially polymerizes as helical filaments along the sporogenic cell, before being remodeled as cytokinetic rings, known as Z rings. Z rings form at regularly spaced 1.3 μm intervals along the sporogenic cell to form sporulation septa, which ultimately constrict to produce long chains of pre-spore compartments (Flärdh and Mark J Buttner, 2009). To perform this process, other cell-division proteins are recruited to the Z-ring to form a complex sometimes referred to as the divisome, and is comprised of proteins FtsW, FtsI, FtsL, FtsQ and DivIC (Flärdh and Mark J Buttner, 2009).

The septation of the sporogenic cell occurs simultaneously with the segregation of chromosomes into pre-spore compartments. This process will ultimately lead to the formation of unigenomic spores, with complete partitioning of individual nucleoids ensuing in the final stages of septation (Flärdh and Mark J Buttner, 2009). Chromosome segregation is orchestrated by two systems, ParAB and FtsK. ParA is a Walker A cytoskeletal ATPase, whilst ParB is a DNA-binding protein. ParA forms dynamic helical filaments which run downwards from the apical tip of the aerial hyphae along the sporogenic cell. It also aids ParB in binding and forming complexes on the DNA at the chromosomal *OriC*. Septation begins over the top of unsegregated nucleoids and FtsK, a DNA translocase, targets division sites and positions and transports the DNA to avoid closing septa (Flärdh and Buttner, 2009).

Once aerial hyphae are dissected by septation and pre-spore compartments have been formed containing nucleoids, transition to mature spores begins. During septation, the spore wall is 10-12nm, which will increase to 30-50 nm in mature spores. Another SALP member, SsgD, initiates formation of this thick, lysozyme-resistant spore wall, the development of which is accompanied by the rounding of pre-spores into a more ovoid shape associated with mature spores (Flärdh and Buttner, 2009; Bobek, Šmídová and

Čihák, 2017). The further thickening of this spore wall is controlled by the *Streptomyces* spore synthesizing complex (SSSC) comprised in part by two cytoskeletal actin-like proteins known as MreB and Mbl. During sporulation, Mre and Mbl proteins are localized to sites of peptidoglycan synthesis, directing incorporation of peptidoglycan at the lateral walls (Sigle *et al.*, 2015; Bobek, Šmídová and Čihák, 2017). DNA is condensed as the spores mature and, in *S. coelicolor*, a grey polyketide spore pigment is synthesized. The expression of this pigment is controlled by the regulatory *whi* (white) genes, which are further involved in early stages of sporulation. WhiA and WhiB appear to regulate the switch from aerial hyphal growth to initiation of sporulation septation, whilst WhiD, WhiH and WhiI are involved in spore formation and maturation (Bush *et al.*, 2015; Bush, 2018). Finally, a rodlet layer is formed around the spore wall in a thin, fibrous sheath. Two SALP members, SsgE and SsgF, control the action of cell wall hydrolases to separate the spores, allowing individual dispersal (Bobek, Šmídová and Čihák, 2017).

Although *Streptomyces* spores are less resilient to deleterious conditions than firmicutes endospores, they nevertheless serve to protect the genetic material, with-standing desiccation and relatively high temperatures to remain viable for decades. This makes *Streptomyces* spores well-suited to their role in dispersal and dissemination of the organism (Flärdh and Buttner, 2009). The resilience of *Streptomyces* spores is largely owed to their hydrophobic spore coat and the presence of protective small molecules such as trehalose and heat-shock proteins (Bobek, Šmídová and Čihák, 2017). Spores are often cited as being ‘dormant’ or at ‘metabolic zero’ whilst in this state, however this is not entirely accurate. Spores retain their viability by slowly degrading internal stores of carbon compounds such as trehalose and are able to respire by reducing either oxygen or nitrate via endogenous electron sources. Although respiration is very low in dormant spores, it is nevertheless detectable (Fischer, Falke and Sawers, 2014; Falke *et al.*, 2019). A spore-specific respiratory nitrate reductase which is not present in

mycelium has been identified and characterized (Fischer, Falke and Sawers, 2013). Furthermore, spores maintain permanently active enzymes including trehalase, trehalose phosphate synthase and enzymes required for initiation of phospholipid biosynthesis. Spores contain only small amounts of glycogen, but large amounts of trehalose and amino acids (Fischer, Falke and Sawers, 2013). Both dry and 'wetted' spores, show this respiration. Wetted spores have typically lost their hydrophobic sheathe but not begun the processes of germination. Such spores exhibit enhanced catalysis and increased glucose uptake and further have active pentose phosphate and TCA cycles (Fischer, Falke and Sawers, 2013). Older studies of *S. viridochromogenes* reports that wetting spores resulted in an increase in endogenous respiration that lasted for several days absent germination (Ensign, 1978). More recently, studies have demonstrated the metabolic activity of dormant spores, with spores oxidizing atmospheric H_2 to supply maintenance energy (Constant, Poissant and Villemur, 2008; Liot and Constant, 2016). A further, more ostentatious example of metabolic activity of actinomycete spores is that of the flagellated spores (zoo spores) of the soil-inhabiting *Actinoplanes,* which are able to swim chemotactically towards sugars, amino acids, aromatic compounds and mineral ions (Jang *et al.*, 2016). Therefore whilst 'dormant' may be used to describe spores pre-germination, this does not mean absence of respiration or all metabolic activity. Whilst much work has been devoted to secondary metabolism of *Streptomyces* and hyphal formation, more is needed to determine the true metabolic activity of spores.

Germination is induced when the spore encounters various stimuli, leading it to restart gene expression and metabolic processes (Fig. 1.2). These stimuli may include nutrient availability (the presence of peptidoglycan residues), heat shock or mechanical disruption of the spore envelope (Bobek, Šmídová and Čihák, 2017; Čihák *et al.*, 2017). Heat shocking spores at a temperature of approximately 50°C for ten minutes is a

method routinely used to initiate and synchronize spore germination in *Streptomyces* (Kieser, 2000). The proportion of spores in a population which germinate and the rate of germination varies across *Streptomyces* species, with *S. coelicolor* showing slower germination and lower spore viability than species such as *S. viridochromogenes* and *S. granaticolor* (Bobek, Šmídová and Čihák, 2017). Various sporulation inhibitors are doubtless in play in dormant *Streptomyces* spores; however, a great deal remains to be elucidated. It has been shown that the small, insoluble cell-wall protein NepA has a role in maintenance of spore dormancy, though the mechanism by which it prevents spore germination is unknown (De Jong *et al.*, 2009). Other germination inhibitors have been detected, including one with antibiotic activity which was secreted into medium surrounding spores of *S. viridochromogenes* (Hirsch and Ensign, 1976). The chemical structure of this compound, named Germicidin, was determined years later, and subsequently shown to be produced by *S. coelicolor* also (Petersen *et al.*, 1993; Song *et al.*, 2006).

The exact mechanisms by which spores are able to detect nutrient availability in their surroundings and induce germination remain to be elucidated. However, in the case of *B. subtitis* spores, this process appears to be stochastic. It has also been shown that, in optimal environments, germinating *Streptomyces* spores are able to stimulate the development of other dormant spores in close proximity (Bobek, Šmídová and Čihák, 2017).

The highly regulated process of germination may be classified into three stages; darkening, swelling, and germ-tube emergence. Darkening involves the exogenous divalent cations Ca^{2+}, Mg^{2+}, Mn^{2+} and Fe^{2+} and spore energy reserves, with stores of trehalose being consumed during the early stages of germination. This initial step involves uncoating and reconstruction of the cell-wall, in which spores lose their

hydrophobicity and therefore rapidly intake water to result in swelling and loss of heat resistance. Spore hydrolases, such as RpfA and SwlA, are reactivated, performing lysis and reconstruction of the cell wall peptidoglycan, allowing intake external nutrients (Bobek, Šmídová and Čihák, 2017). The spore then enters the swelling stage of germination, where enzymatic activities are recovered and the store of trehalose is rapidly depleted, in what appears to be an essential step in germination. Resultingly, the break-down of trehalose leads to an increase in glucose level, providing energy to revive enzymes and to utilize for initial development (Bobek, Šmídová and Čihák, 2017). The cytoplasm is re-hydrated, supporting re-activation of proteins and ribosomes, with ribosomes being fully functional within several minutes of germination instigation. Reactivation of proteosynthetic apparatus and nascent proteins is aided by GroEL, Trigger factor and DnaK (Strakova *et al.*, 2013). External carbon, nitrogen and energy is obtained and DNA replication re-starts slightly before or concurrently with germ-tube emergence (Bobek, Šmídová and Čihák, 2017). The final stage is germ-tube emergence, with one or two germ tips emerging and growing by apical tip extension. This process, as previously mentioned, is orchestrated by the polarisome, consisting of the proteins DivIVA, Scy and Filp. DivIVA is phosphorylated by the serine/threonine kinase, AfsK, and recruits the cell wall biosynthetic machinery, thus determining where cell wall growth and branching will occur. The protein Scy co-localizes with DivIVA and recruits chromosome-partitioning protein ParA to hyphal tips. The intermediate filament protein Filp, localizes directly behind DivIVA forms a cytoskeletal network that provides rigidity and elasticity to ultimately control cell-shape (Bush *et al.*, 2015)(Bobek, Šmídová and Čihák, 2017).

The rate of spore germination, germ-tube emergence and growth differs across *Streptomyces* species and is highly dependent on environmental conditions and nutrient supply. In *S. coelicolor* on mannitol-soya flour (MS) agar, swelling and germ-tube

emergence is typically seen between 3-5 hours (Haiser, Yousef and Elliot, 2009; Bobek, Šmídová and Čihák, 2017).

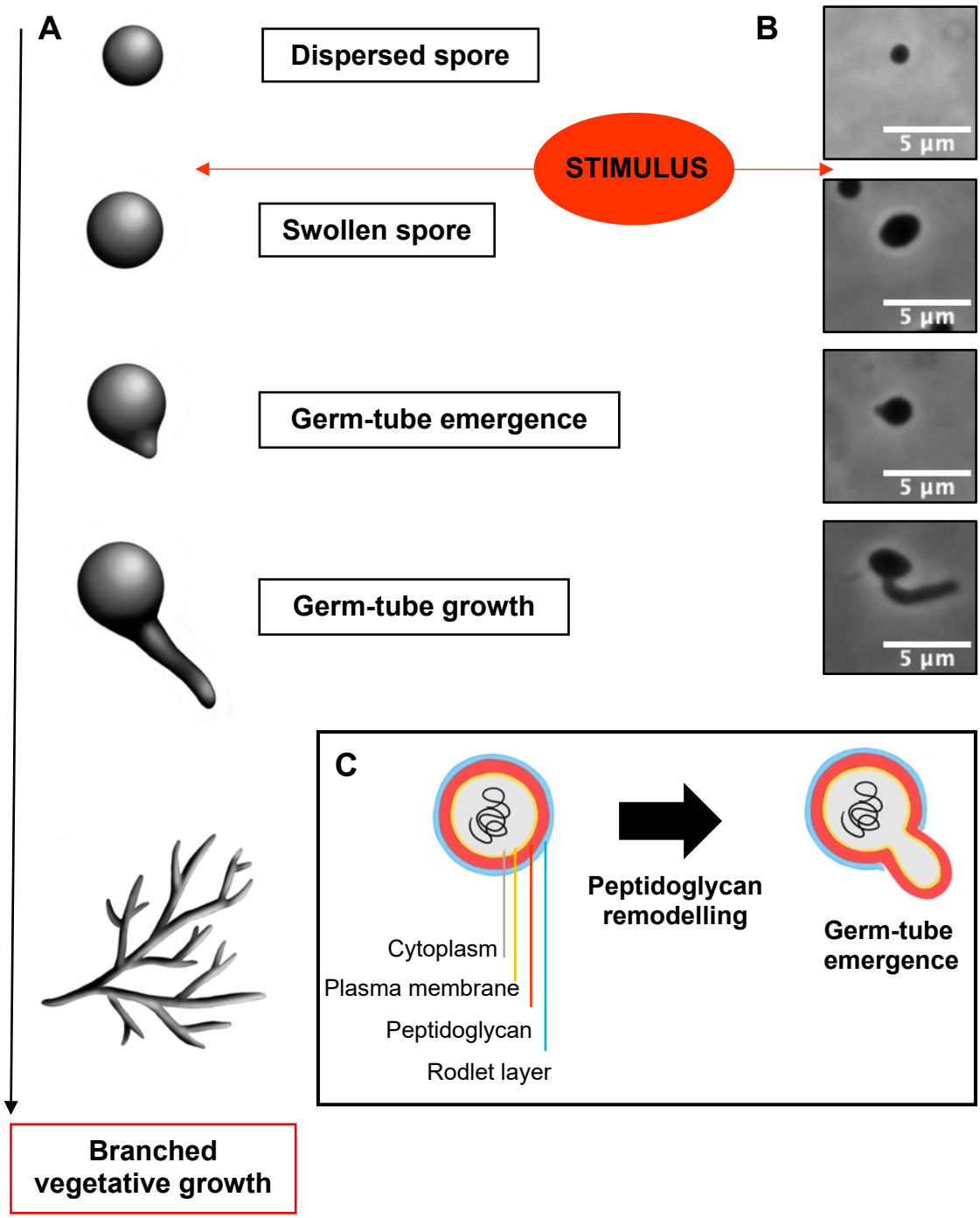

Figure 1.2: Spore germination and germ-tube emergence. (A) The stages of spore germination, beginning with a dispersed spore. A stimulus is encountered and the spore switches on germination machinery, starting to swell. A germ-tube emerges and grows by apical tip extension. The result is a vegetative mycelium. **(B)** Light microscopy of germination. **(C)** The spore envelope consisting of a rodlet layer, peptidoglycan layer, and plasma membrane surrounding the cytoplasm. Peptidoglycan modelling occurs to lead to break down of the cell wall and germ-tube emergence.

Architecture of the *Streptomyces* cell envelope and mechanisms of membrane protein transport

Streptomyces are Gram-positive bacteria, therefore possessing a cell envelope composed of a plasma membrane and a thick peptidoglycan layer, but lacking the outer membrane found in Gram-negative bacteria.

The plasma membrane is the innermost layer of the cell envelope of *Streptomyces*, with cryo-electron micrograph suggesting it is approximately 7 nm in width (Zuber *et al.*, 2008) This layer is a phospholipid bilayer composed of polar lipids and proteins which serves to delineate the intracellular space from the extracellular. The major constituent of plasma membranes are phospholipids, including phosphatidylglycerol (DPG), phosphatidylethanolamine (PE), phosphatidylinositol (PI), and phosphatidylinositol mannoside (PIMS) and other less abundant lipids such as cholesterol (or hopanoids) and sphingomyelin (Kämpfer *et al.*, 2014; Yeagle, 2016). *S. coelicolor* also possesses monolyso-cardiolipin (LCL) and dilyso-cardiolipin (DLCL) as part of their membrane, two unusual molecules that appear essential under some growth conditions (Sandoval-Calderón, Guan and Sohlenkamp, 2017). Phospholipids are amphipathic, with a polar headgroup at one end of the molecule and a nonpolar hydrocarbon chain on the other. Typically for phospholipids, this structure is a phosphate esterified to an alcohol at the 3' position, with the hydrocarbon chains generally being fatty acids of varying lengths which are esterified to the alcohol at 1' and 2' positions (Yeagle, 2016). As a result of their shape and amphipathic nature, these lipid molecules arrange themselves to spontaneously form bilayers such as the plasma membrane lipid bilayer of cells.

The *S. coelicolor* genome encodes 7825 proteins, 25% of which are targeted to the cytoplasmic membrane (1119) or the extracellular environment (819). Membrane proteins also form a large constituent of plasma membranes and may be categorized

into two types, integral (intrinsic) membrane proteins or peripheral (extrinsic) membrane proteins. Integral membrane proteins are embedded within the lipid bilayer and can only be removed by disruption of the membrane itself. Conversely, peripheral membrane proteins are those which are associated with the plasma membrane, and may be anchored by various means, but are not integrated within the lipid bilayer (Yeagle, 2016). Integral membrane proteins may be further subdivided into transmembrane proteins, which traverse the membrane, and anchored proteins, which have a hydrophobic portion embedded within the lipid bilayer which serves to anchor the protein. Typically, integral membrane proteins have a hydrophobic regions of 19-23 amino acids folded into an alpha-helix able to traverse the typical width of the hydrophobic portion of the lipid bilayer (Yeagle, 2016). Proteins may have one or many helices to form a helix bundle. Integral membrane proteins may also be formed from a beta-barrel, which are multiple strands of beta-sheet wound into a cylindrical shape so that hydrophobic residues face outwards. Beta-barrel transmembrane proteins are often, but not always, open in the middle to function as transporter proteins (Yeagle, 2016).

One type of peripheral membrane proteins are the lipoproteins, which are anchored to the plasma membrane by lipid-modification of a cysteine residue (Zückert, 2014a). Lipoproteins are important for envelope stability, sporulation, nutrient acquisition, transport and numerous other bacterial physiological processes. Lipoproteins often act as substrate binding proteins for the numerous ABC transporters in Gram-positive bacteria (Thompson *et al.*, 2010). Approximately 2.7% of the *S. coelicolor* proteome are lipoproteins anchored to the cell membrane (Widdick *et al.*, 2006). In Gram-positive bacteria lipoproteins function in the subcellular region between the extracellular side of the plasma membrane and the peptidoglycan and other layers of the cell wall (Hutchings *et al.*, 2009).

Bacteria possess two main pathways for protein secretion across the cytoplasmic membrane. These are the general Secretion route, known as the Sec pathway, and the Twin-arginine translocation pathway, or Tat-pathway. The Sec pathway is highly conserved in all organisms, whilst only 50% of bacteria, plants and archaea possess the Tat secretion pathway (Natale, Brüser and Driessen, 2008). The Sec pathway is largely responsible for transporting unfolded proteins across the membrane, whilst the TAT pathway serves to transport folded proteins. Proteins are targeted to the Sec pathway through either co-translational or post-translational targeting (Natale, Brüser and Driessen, 2008). In bacteria, secretory proteins are primarily trafficked along the post-translational Sec pathway, whilst co-translational targeting is utilized for integral membrane proteins (Natale, Brüser and Driessen, 2008). In post-translational targeting, a signal sequence in the secretory protein targets it to the Sec-translocase, a process that in Gram-negative bacteria involves the chaperone protein SecB, which is not found in Gram-positive bacteria (Van Wely *et al.*, 2001). In co-translational targeting, the signal sequence of the secretory protein is bound by the signal recognition particle (SRP), another chaperone protein, whilst the secretory protein is being translated and this complex of SRP-ribosome nascent chain (SRP-RNC) are targeted to the Sec-translocase. The SRP-RNC complex interacts with FtsY, the bacterial SRP receptor (SR). FtsY is partially membrane associated on the cytoplasmic side of the plasma membrane and can deposit the ribosome/secretory protein to the Sec-translocase (Angelini, Deitermann and Koch, 2005). The Sec-translocase consists of a protein conducting channel (PCC) formed of three integral membrane proteins, SecY, SecE and SecG, which associates with SecA, a peripheral associated ATPase, and the chaperon protein SecB, which guides secretory proteins to the complex (Natale, Brüser and Driessen, 2008).

The TAT system similarly consists of integrated membrane proteins, TatA and TatC or TatA, TatB and TatC which form the receptor and protein conducting machinery. Proton motor force supplies the energy for translocation of secretory proteins, which are typically already folded (Natale, Brüser and Driessen, 2008). The chaperone proteins SlyD and DnaK may interact with Tat substrates to prevent mis-targeting to the Sec pathway, whilst substrate specific chaperones prevent the protein from binding to the Tat system before correct assembly. During this time insertion of cofactors into the complex occurs, including TMAO Reductase and Hydrogenase. The Tat pathway is a major protein export route in *S. coelicolor* (Widdick *et al.*, 2006).

The YidC membrane insertase is also present in *S. coelicolor* and functions to correctly fold and insert integral membrane proteins into the plasma membrane, both dependently and independently of the Sec translocase complex. Integral membrane proteins which are translocated through SecYEG may be properly folded and assembled by YidC. YidC may also function independently of the Sec pathway to insert membrane spanning proteins into the membrane (Lewis and Brady, 2015).

Secretory proteins are marked for translocation by signal-sequences. For proteins targeted to the Sec pathway, these signal sequences are found at the amino-terminus (N-terminal) and have a conserved structure. Typically, signal sequences are approximately 20 amino acids in length and consist of a positively charged amino-terminal (n-region), a hydrophobic core (h-region) and a polar carboxyl-terminal (c-region). The c-region contains the Type I signal peptidase recognition site, (A-X-A), a membrane-bound enzyme which cleaves the signal sequence from the secretory protein domain during, or closely following, translocation. Lipoprotein precursor proteins contain a cleavage site in the c-region which is recognized and cleaved by Type II signal peptidase enzymes, These prolipoproteins also possess a lipoprotein box, a four-amino-

acid motif, L-X-X-C, in the c-region which overlaps with the cleavage site. The lipoprotein box motif contains a conserved cystine residue at the +1 position, after the cleavage site, which is lipid-modified, post-translocation and -signal sequence cleavage, to anchor this protein at the membrane surface (Natale, Brüser and Driessen, 2008; Zückert, 2014a). The Tat signal sequence also has a tripartite structure with an n-region of variable length. It contains a conserved sequence motif that includes twin arginines found at the interface of the n- and h-regions and a c-region with typical A-X-A Type I signal peptidase recognition site which is cleaved. The twin-arginine motif pattern is Z-R-R-x-Φ-Φ (Z = any polar residue and Φ = hydrophobic residues). The c-region also typically contains a positively charged amino acid, which functions to direct secretory proteins away from the Sec pathway (Natale, Brüser and Driessen, 2008).

The TAT secretion system appears to be the major pathway of lipoprotein export in *S. coelicolor* (Widdick *et al.*, 2006) The cysteine residue possesses a sulphydryl group, and following translocation, the enzyme lipoprotein diacylglycerol transferase (Lgt) catalyzes a thioether linkage of a lipid moiety to this sulphydryl group. Following this, the signal sequence is cleaved by a Type II signal peptidase enzyme on the N-terminal side of the lapidated cysteine (Thompson *et al.*, 2010).

The peptidoglycan layer of *Streptomyces* has an estimated thickness of approximately 35 nm, a considerable size in comparison with *Mycobacterium*, in which the peptidoglycan layer is 7 nm (Rahlwes, Sparks and Morita, 2019). Peptidoglycan, also known as murein, is composed of linear glycan strands cross-linked by short peptides (Vollmer, Blanot and De Pedro, 2008). It is an essential component of the bacterial cell wall which protects and provides integrity to the cell. In *Streptomyces*, with their complex lifecycle, the peptidoglycan layer frequently undergoes remodeling to allow the organism

to grow. The *Streptomyces* peptidoglycan layer also contains teichoic acids, lipoteichoic acids and other polysaccharides and proteins (Kleinschnitz, Latus, *et al.*, 2011).

Streptomyces coelicolor

Perhaps the most prominently known *Streptomyces* is the species *Streptomyces coelicolor*, which is often used as a model organism. *S. coelicolor* is a free-living saprophytic bacterium with key roles in many metabolic processes and biotransformations in soil, and which has a morphologically complex lifecycle.

S. coelicolor A3(2) is the model organism for the *Streptomyces* genus and it is the M145 strain of *S. coelicolor* A3(2) which is employed as the wild-type organism in this study (Hoskisson and van Wezel, 2019). *Streptomyces coelicolor* M145 is a derivative of the A3(2) strain, with deletions of the native linear 363 Kb plasmid SPC1 and circular 31.4 Kb SPC2 plasmids (Yamasaki, Redenbach and Kinashi, 2001; Haug *et al.*, 2003).
Originally discovered by R. Müller in 1908, *S. coelicolor* was named for production of a striking blue pigment; coelicolor being translated as ‘sky color’ from Latin. In 1916 Waksman and Curtis also identified an actinomycete which produced a red and blue pigment and designated it *Actinomyces violaceusruber* (violaceus being Latin for purple, ruber being Latin for red). Due to their physiological similarities, these separate organisms were once mistakenly classed as the same species. When Professor Sir David Hopwood began his study of *Streptomyces* genetics, he chose what he believed to be a strain of *S. coelicolor* as his model organism, later to become A3(2), as the red and blue pigments would make for ideal markers. In fact, as advances in genetic analysis techniques would show, this strain is more closely related to Waksman and Curtis’ *Streptomyces violaceoruber* ISP5049, than *S. coelicolor* Müller. However, to reduce confusion the A3(2) strain remains referred to as *S. coelicolor*.

S. coelicolor A3(2) has a singular chromosome of approximately 8.66 Mbp with a centrally located origin of replication and a G+C content of 72.12% (Bentley *et al.*, 2002). The chromosome may be considered to have a tripartite structure; a core, which contains essential genes, and two arms, containing genes of non-essential function for the survival of the organism. The core extends from approximately 1.5 Mb to 6.4 Mb, with the left arm being 1.5 Mb in length and shorter than the 2.3 Mb of the right arm (Bentley *et al.*, 2003). The genome encodes some 7825 proteins, with ends of the chromosome carrying terminal inverted repeats with covalently linked proteins to protect the free 5' ends. A loss of more than 1 Mbp of genome sequence at either chromosome end is tolerable to the organism (Hoskisson and van Wezel, 2019). The red and blue pigments produced by *S. coelicolor* are the prodiginine antibiotic, undecylprodigiosin, and the polyketide antibiotic, actinorhodin, respectively. Actinorhodin is the blue/red pigment noticed by Hopwood and is red at an acidic pH and blue at an alkaline pH. Although not key to this study, *S. coelicolor* also contains more than 20 clusters coding for secondary metabolites.

S. coelicolor possesses a restriction system which cleaves DNA methylated by *E. coli* modification systems and thus any plasmids conjugated into *S. coelicolor* must be done so through a non-methylating strain of *E. coli,* such as ET12567 [pUZ8002].

The role and survival of *Streptomyces coelicolor* in soil

Streptomyces are soil bacteria, being so pervasive in number that they are responsible for soil odor through their production of the volatile compound geosmin (Latin for "earth smell"). As saprotrophic organisms *Streptomyces* are important in the decomposition of organic material and carbon recycling and accordingly produce a multitude of secreted

proteases, chitinases, cellulases, amylases and other enzymes capable of breaking down various insoluble polymers (Bentley *et al.*, 2002; Chater, 2016).

Streptomyces are well-known for their colonization of the rhizosphere; the region of soil which is the plant-root interface, abundant in free oxygen, water, ionic secretions, enzymes, proteins, amino and organic acids, phenolics and sugars (Sousa and Olivares, 2016). Unsurprisingly, the rhizosphere is therefore host to a vast microbial community which benefit from these varied metabolites released by plant roots, whilst in turn plants benefit from various microbial activity which aid their growth. In fact, the number of microbial genes in the rhizosphere is greater than that of plant genes. Studies have shown that microorganisms associated with plants exert effects on seedling vigor, plant growth and development, nutrition and diseases. The rhizosphere is also inhabited by fungi, oomycetes, nematodes, protozoa, algae, viruses, archaea and arthropods, some of which are beneficial to plant health and others which are detrimental, but all of which benefit from the vast amount of nutrition released by the plant either directly or indirectly (Mendes, Garbeva and Raaijmakers, 2013).

The survival of *Streptomyces* in this environment relies on its ability to inhibit or kill a plethora of competing bacteria, fungi and archaea, a feat thought to be accomplished through production of anti-microbial secondary metabolites. *Streptomyces* are also under threat by bacteriophages, with *S. coelicolor* employing the phage growth limitation (Pgl) system to avoid re-infection (Kronheim *et al.*, 2018). Included in the numerous bioactive metabolites *Streptomyces* is capable of producing are antifungal and antiprotozoal amphotericin B, the broad-spectrum antibiotic oxytetracycline, the beta-lactamase inhibitor clavulanic acid, and the anti-Gram-negative compounds daptomyin, streptomycin and viomycin, constituting a considerable arsenal against competing or predatory adjacent microorganisms (Clark, 2011). Nematode predation is also likely

avoided by the production of various anthelmintics and nematicides, which serve to defend against organisms such as *C. elegans* (Tran *et al.*, 2017).

Streptomyces must also contend with bacterivorous protists present in the soil, and how *Streptomyces* avoids predation by such eukaryotic organisms is poorly understood. Unlike stationary microbes which may be targeted via localized high concentrations of secreted antimicrobial compounds, protists are highly motile. Furthermore, whilst *Streptomyces* does appear to produce some compounds with antiprotozoal activity, such as amphotericin B, phenazine-1-carboxylic acid (PCA) and amphomycin, the effectiveness of such compounds is limited (Pagmadulam *et al.*, 2020). It has been shown that *Streptomyces lysosuperificuss* secretes tunicamycin, which is able to prevent cell adhesion and interfere with aggregation of *Dictyostelium discoideum in vitro* (Takatsuki, Arima and Tamura, 1971; McDonald and Sampson, 1983; Nasser *et al.*, 2013).

A key question is why *Streptomyces* produces compounds with antitumor and immunomodifiers, such as doxorubicin and bleomycin, the first of which functions by blocking the eukaryotic topoisomerase II (Tan *et al.*, 2015). It seems likely that the production of such compounds evolved as an anti-eukaryotic defense mechanism against predatory soil protists that *Streptomyces* encountered in the environment. Other physical defense mechanisms may also have arisen in part due to selective pressure from interactions with protists. For example, it has been proposed that the rodlet layer of *Streptomyces* spores, and even the polyketide pigments produced by spores, may contribute resistance to lytic or digestive enzymes of protists (Chater *et al.*, 2010).

Of the entire *Streptomyces* genus, only a dozen or so species are pathogenic towards plants, with the most infamous being *S. scabies,* the causative agent of potato scab

(Bignell *et al.*, 2010). More typically, species of *Streptomyces* are plant commensals or endophytes which benefit the plant, increasing availability of micro and macro molecules for the plant via degradation of insoluble materials, producing phytohormones and providing protection from phytopathogenic microorganisms via antimicrobial compounds (Seipke, Kaltenpoth and Hutchings, 2012).

The symbiotic relationship of plants with the majority of *Streptomyces* species is a give and take, with *Streptomyces* providing a wealth of micro- and maco-nutrients for the plant via nitrogen fixation and the breakdown of insoluble organic material. In turn, the plant-root soil-interface is an ideal area for *Streptomyces* to colonize, as plants produce large amounts of nutrients, including carbon-containing compounds, known as rhizodeposits. Such rhizodeposits include water-soluble exudates (sugars, amino acids, organic acids), and water-insoluble material (sloughed cells and mucilage). Included in these secretions are fatty acids and sterols, making the plant roots a rich source of lipids. Fatty acids released by plant roots included linoleic, linolenic, oleic, palmitic and stearic fatty acids. Whilst sterols include campesterol, cholesterol, sitosterol and stigmasterol (Dennis, Miller and Hirsch, 2010).

Carbon sources for *Streptomyces*

Streptomyces possess an arsenal of secreted proteins including proteases, chitinases, cellulases, endoglucanases, amylases and pectate lysases to allow them to degrade various large polymers into compounds *Streptomyces* may use as carbon sources (Bentley *et al.*, 2002). Although able to breakdown complex insoluble substrates such as cellulose and agar for carbon sources, *Streptomyces* also utilizes simple sugars. For *S. coelicolor* A3(2), glucose is a preferred carbon source (Banchio and Gramajo, 1997). It has been long known that *Streptomyces* is also capable of utilizing cholesterol as a sole

carbon source, and that an ability to uptake sterols may be key to colonization of the rhizosphere (Brown and Peterson, 1966; Clark *et al.*, 2013).

Prokaryotic ABC transporters

All organisms rely on transport of materials across their plasma membranes for survival, whether this is the import of extracellular nutrients or the removal of intracellular waste products. Transport across a chemical gradient and across a membrane relies on the free energy change associated with the hydrolysis of ATP and is known as primary transport (Wilkens, 2015).

Primary transporters consist of the rotary motor ATPases (F-, A-, and V-ATPases), P-type ATPases, and the ATP-binding cassette transporters, also known as 'ABC' transporters (Wilkens, 2015). The ABC transporters share a highly conserved structure, composed of two nucleotide-binding domains (NBDs) and two trans-membrane domains (TMDs). ATP molecule binding causes dimerization of the NBDs, with hydrolysis of ATP via these domains driving a conformational change in the TMD which allows the substrate to cross the membrane lipid bilayer (Locher, 2016). In prokaryotes these domains are usually separate protein subunits, whilst in eukaryotes they are composed of a single polypeptide chain (Jones and George, 2002).

The ABC transporter superfamily is one of the largest, with ABC transporters being ubiquitous amongst all-manner of life-forms where they play fundamental roles in biological processes. ABC transporters may belong to one of three functional categories; importers, exporters and a third category not involved in transport but in mRNA translation and DNA repair (Davidson *et al.*, 2008; Locher, 2016; El-Awady *et al.*, 2017). Prokaryotes possess both importers, which are typically involved in the uptake of

nutrients, and exporters, which may function to remove unwanted toxins and drugs from the cell and include MDR-pumps (Locher, 2016). By contrast, of the 48 distinct human ABC transporters, most appear to be exporters and have considerable roles in human health and disease. In both eukaryotes and prokaryotes, the substrates for these transporters vary widely on a spectrum from small molecules such as amino acids to larger compounds such as lipids and polysaccharides. Bacteria typically require additional domains or proteins associated with ABC-transporters which serve to capture and deliver the desired solute to the TMD binding site, known as substrate binding proteins (SBP). SBPs are periplasmically-located soluble proteins in Gram-negative bacteria, whilst in Gram-positive bacteria these subunits are lipoproteins attached to the outer plasma membrane (Wilkens, 2015). SBPs vary in size, being approximately 25-70 kDa, and share a conserved three-dimensional structure, containing two domains connected by a hinge. The substrate, or ligand, to be transported is captured between these two domains (Berntsson *et al.*, 2010; Maqbool *et al.*, 2015). The two domains may be called the C- and N-lobes and together with the flexible hinge may form an 'open-unliganded' conformation with high substrate affinity or a 'closed-unliganded' state with low-affinity for substrates, with ligand binding causing the conformation change (Poolman and van der Heide, 2002; de Boer *et al.*, 2019).

Prokaryotic ABC importers may be classified into three types: Type I importers, Type II importers and energy coupling factors (ECF) transporters, also known as Type III importers. Type I ABC importers are involved in bacterial uptake of diverse nutrients, Type II importers are generally involved in high-affinity uptake of metal chelates, iron-containing complexes, and cobalamin. Finally, ECF or Type III importers facilitate high-affinity of various vitamins into bacteria (Locher, 2004).

ABC transporters are a large family with many members and vary in their specific mechanisms of action. Several models of ABC transporter mechanisms have been proposed, with some debate in which order certain steps occur. However, models all share the same basic elementary steps that may be roughly and simply described as follows. The binding of two ATP molecules to each of the NBDs causes the domains to dimerize with the ATPase active sites at the interface. The TMDs, which are tethered to the NBD via a coupling helix, are simultaneously manipulated by this dimerization. In ABC importers, prior to ATP-binding, the NBD are dissociated and the TMD are in an open-facing conformation on the intracellular side of the plasma membrane. The binding of ATP to the NBD causes dimerization, TMD conformational change and the opening of a substrate-binding cavity formed by the TMD on the extracellular side of the plasma membrane. Binding of the substrate or substrate-binding protein to the TMD may then trigger ATP hydrolysis and release of ADP and phosphate from the NBD. This leads to dissociation of the NBD and TMD conformational change to induce an intracellular-facing cavity through which the substrate may be released and transported into the cytoplasm (Procko *et al.*, 2009). For exporters, prior to ATP binding to the NBD, TMD are in an inward-facing conformation. The intracellular substrate binds to the inward-facing TMD. Binding of ATP to the NBD causes dimerization which in turn triggers a change in the TMD to an outwards-facing configuration, allowing the substrate to be exported. ATP hydrolysis and release results in separation of the NBDs and the TMD return to an inward-facing configuration (Procko *et al.*, 2009) (Fig. 1.3).

The two NBD of the ABC transporters are usually denoted NBD1 and NDB2, and may also be called ATPases or ABCs. Each NBD is composed of two subdomains, a larger RecA-like subdomain which is found in other P-loop ATPases and an alpha-helical domain which is unique to ABC transporters (Ter Beek, Guskov and Slotboom, 2014). The RecA-like domain is sometimes referred to as the catalytic domain of the NDB and

contains a number of highly conserved sequence motifs. These include the Walker A motif or P-loop, (G/A)XXXXGK(T/S), where “X” can be any amino acid, and the Walker B motif, φφφφDE, where φ is a hydrophobic residue, situated downstream of the Walker A motif. Also present are the A-loop, Q-loop, D-Loop and switch region or H-loop. It is the Walker A, Walker B, Q-loop, and switch region which form the nucleotide binding site of the NBD (Davidson *et al.*, 2008). The helical subdomain of the NBD contains the ABC signature motif or C-motif, LSGGQ, which is characteristic of the ABC superfamily (Ter Beek, Guskov and Slotboom, 2014). The functions of these motifs are described in detail below.

Adenosine triphosphate (ATP) consists of a nitrogenous base (adenine), a ribose sugar, and three phosphate groups bonded through phosphodiester bonds. These bonds contain a high energy content and when hydrolyzed release energy, resulting in a free phosphate group and Adenosine diphosphate (ADP). If another bond is hydrolyzed, another free inorganic phosphate is released and ADP is converted to Adenosine monophosphate (AMP) (Dunn and Grider, 2020). ATP must be bound to a magnesium ion to be biologically active, making it MgATP. It is MgATP which binds the NBD of ABC transporters. Hydrolysis of ATP on NBD of ATP transporters involve nucleophilic attack of a lytic water molecule at the γ-phosphate which cleaves the phosphate bond. The exact mechanism of this is still debated, but involves the highly conserved glutamate residue in the Walker B motif (discussed below) seemingly acting as a catalytic base and also involves changes of the Mg^{2+} ion coordination (Prieß *et al.*, 2018). It still remains to be elucidated whether it is the binding of the ATP or the cleavage of ATP which provides the ‘power stroke’ for conformational change of the transporter (Prieß *et al.*, 2018).

The Walker A motif is crucial for phosphate binding and the Walker B motif is essential for ATP hydrolysis. The serine/threonine hydroxyl in the Walker A motif interacts with the

Mg^{2+} of Mg^{2+}-ATP, whilst the ε-amino group of the lysine residue interacts with the β– and γ– phosphates of ATP to allow positioning and binding. In the Walker B motif, the aspartate residue coordinates the Mg^{2+} required for ATP hydrolysis, and the glutamate residue is believed to activate water for the hydrolysis of ATP (Hanson and Whiteheart, 2005; Wilkens, 2015). The D-loop is believed to contribute to the dimer interface of the NBD by making contact with the Walker A motif on the opposite NBD. The A-loop motif contains an aromatic residue thought to interact with the adenine of ATP and be essential for ATP binding. The switch region or H-loop contains a histidine which contacts the resides of the Walker A and B motifs across the dimer interface and form a tight coupling between the ATP molecule and the NBD dimer. Finally, a Q-loop glutamine mediates communication between the NBDs and TMDs (Procko *et al.*, 2009; Wang *et al.*, 2011).

Like the NBDs, the TMD are usually notated TMD1 and TMD2. Each TMD typically contains 6 to 10 hydrophobic transmembrane alpha-helixes, to total 12-20 transmembrane segments for a full transporter. Most common are 6 alpha-helices to give a total of 12 transmembrane segments per functional unit. The transmembrane helices form a pore which, depending on configuration, may be accessible from the cytoplasm or extracellular space to allow substrates to traverse the membrane. Unlike NBD which may be identified via significantly conserved sequences, TMD typically have no identifiable conserved motifs, likely reflecting chemical diversity of their varied substrates, but instead may be identified by shared structure and topology. In both importers and exporters, the substrate must interact with residues of the transmembrane alpha-helices that compose the transmembrane spore (Biemans-Oldehinkel, Doeven and Poolman, 2006). In importers with SBP, TM domains form the docking site for SBPs.

The substrate-binding proteins (SBP) were the first component of ABC transporters identified (Biemans-Oldehinkel, Doeven and Poolman, 2006). In Gram-negative

bacteria, SBP are typically water-soluble proteins which are found in the periplasmic space. Conversely, SBP in Gram-positive bacteria are usually lipoproteins which are anchored to the plasma membrane via a lipid-anchor or fused to the TMD of the ABC transporter (Biemans-Oldehinkel, Doeven and Poolman, 2006).

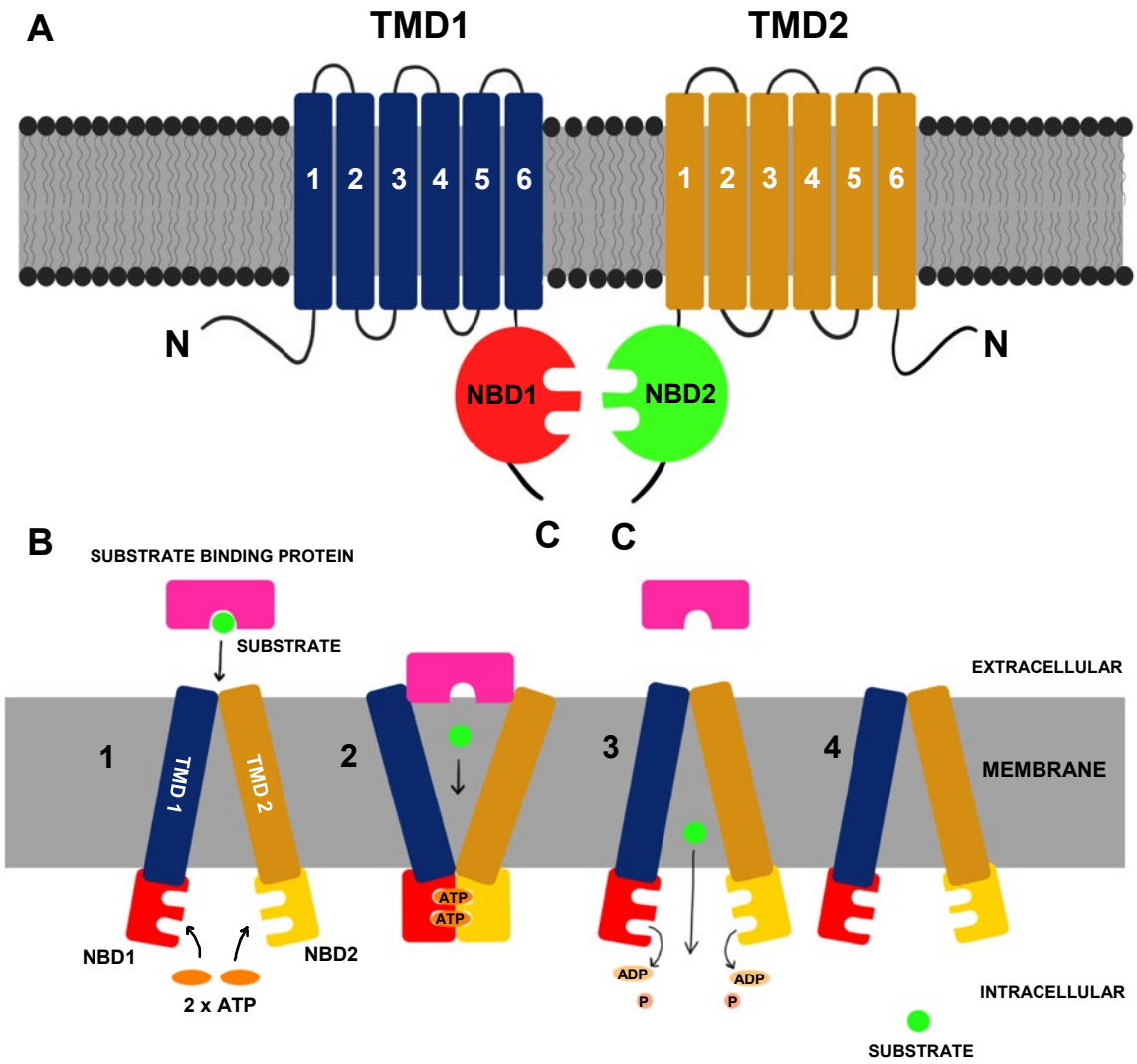

Figure 1.3: General structure and mechanism of ABC transporters. (A) Generalised topology of ABC transporters, consisting of two transmembrane domains (TMDs), and two cytoplasmic nucleotide-binding domains (NBDs). These four domains may be fused together as a singular polypeptide chain, or formed by four separate polypeptide chains, or by two polypeptides each forming a TMD and NBD which associate to form a homodimer or heterodimer. The arrangement shown in **A** is that of a single polypeptide with one TMD and one NBD fused together, with the active transporter functioning as a homodimer. **(B)** Shows the general proposed mechanism of function of an ABC importer. **(1)** The NBD are dissociated and the TMD are in an open intracellular-facing conformation. The binding of ATP to the NBD causes dimerization, TMD conformational change and the opening of a substrate-binding cavity formed by the TMD on the extracellular side of the plasma membrane. **(2)** Binding of the substrate or substrate-binding protein to the TMD triggers ATP hydrolysis and release of ADP and phosphate from the NBD. **(3)** This leads to dissociation of the NBD and TMD conformational change to induce an intracellular-facing cavity through which the substrate may be released and transported into the cytoplasm. **(4)** The transporter has returned to the original conformation and the substrate has been transported.

Nutrient uptake in *Streptomyces*

As a saprophytic organism, efficient nutrient uptake is vital to the survival of *S. coelicolor*, particularly in the highly competitive rhizosphere. *S. coelicolor* is capable of degrading complex organic polymers produced by plants and fungi, such as cellulose, ligocellulose, xylan and lignin, via production and extracellular secretion of lytic enzymes (Romano-Armada *et al.*, 2020). As the nutrients released by these processes are in high demand with rivalling microbes, *Streptomyces* must also possess highly efficient nutrient import systems to outcompete other micro-organisms. Correspondingly, transporters compose approximately 12.1% of the *S. coelicolor* proteome, with most of these being ABC transporters (Zhou *et al.*, 2016). ABC transporters are one of the major routes by which *Streptomyces* import carbon sources and nutrients (Thomas, 2010). As previously mentioned, *Streptomyces* is capable of utilizing exogenous lipids, such as fatty acids and sterols as a sole carbon source (Banchio and Gramajo, 1997; Clark *et al.*, 2013). Although, *S. coelicolor* possess genes which are putatively associated with sterol metabolism, it appears incapable, as are most bacteria, of synthesizing sterols and must instead import these from the environment (McLean *et al.*, 2006). Cholesterol is not able to diffuse to the bacterial cytoplasm and must instead by imported via a specific uptake system (García, Uhía and Galán, 2012).

Mammalian Cell Entry (*mce*) genes

The mammalian cell entry (*mce*) operon was originally discovered in the Actinobacteria and human pathogen *Mycobacerium tuberculosis* (*Mtb*) as part of efforts to characterise genes involved in cell invasion. In 1993, a non-pathogenic strain of *E. coli* transformed with a recombinant vector containing a 1535-bp DNA fragment from *Mtb* was shown to invade non-phagocytic HeLa cells and was preferentially phagocytosed by human macrophages. Furthermore, *E. coli* recombinant clones were shown to survive within

macrophages for at least 24 hours post-internalization, past that of wild-type controls (Arruda *et al.*, 1993). This putative virulence gene (Rv0169) was designated mammalian cell entry locus 1A (mce1A), with genome sequencing of *Mtb* identifying it as one gene of an eight-gene operon present four times within the genome (Casali and Riley, 2007). The operon was subsequently termed the *mammalian cell entry* operon, with copies designated *mce1-4* (Fig. 1.4). Each of the *Mtb mce* operons share an identical structure; two *yrbE* genes (*yrbE, yrbB*) (PF02405) directly upstream of six *mce* genes (*mceA-F*). These proteins are defined as '*mce* proteins' by their possession of a *'mce*-like' domain (PF02470), comprised of an estimated 81 amino acids with well-conserved hydrophobic residues (Isom *et al.*, 2017). In some Actinobacteria *mce* operons, including *Streptomyces* and *Mycobacterium*, *mce* genes are succeeded by one or more *mas* genes (*mce* associated genes), encoding Mam (Mce-associated membrane) proteins.

Due to their cell-invasive properties and their discovery in an intracellular human pathogen, investigations into the Mce proteins initially focused entirely on their role in virulence. Such analyses demonstrated a clear role for the *mce* operons in *Mtb* pathogenicity. Whilst not all *mce* genes promote cell entry, knockouts of some *mce* result in decreased virulence or complete attenuation of *Mtb* (Gioffré *et al.*, 2005; Mohn *et al.*, 2008; Pandey and Sassetti, 2008). An in-depth analysis of the Mce proteins of *Mtb* and their roles in bacterial virulence and intracellular survival is included later in this study. Key to note, however, is that as well as their role in pathogenicity, studies of the *mce* operons also strongly indicated involvement in lipid transport (Mohn *et al.*, 2008; Pandey and Sassetti, 2008; Cantrell *et al.*, 2013).

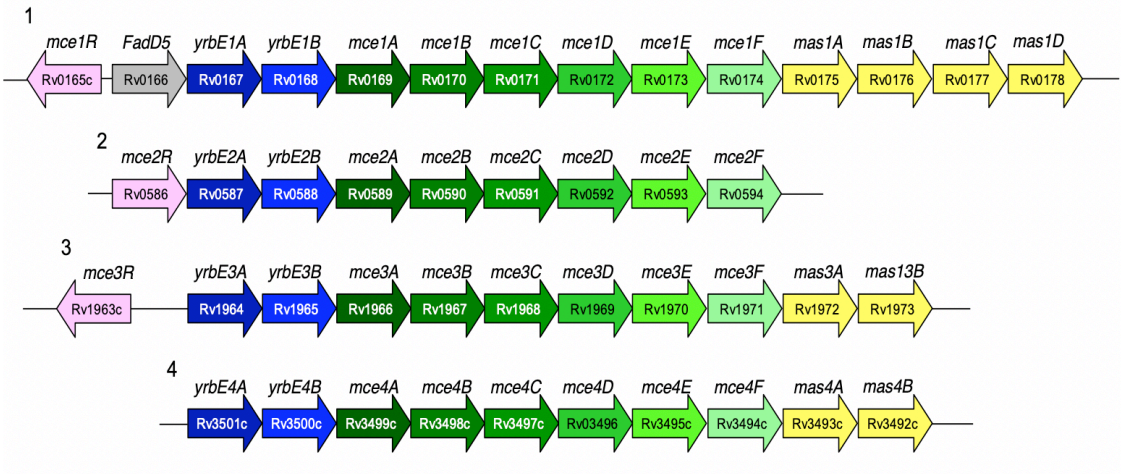

Figure 1.4: The four *mce* operons of *Mycobacterium tuberculosis*. The four *mce* operons present in the *Mtb* genome share a conserved structure, encoding two integral membrane proteins, yrbEA/B, upstream of six *mce* proteins. Figure by Paul Hoskisson.

Homologous *mce* operons with highly conserved structure have subsequently been identified in all *Mycobacterium*, as well as numerous other Actinobacteria members such as *Nocardia*, *Rhodococcus* and *Streptomyces*, and also in some diderm bacteria and eukaryotic chloroplasts (Casali and Riley, 2007; Mohn *et al.*, 2008; Forrellad *et al.*, 2014). A search of Pfam returns over 21,000 protein sequences containing the *mce*-motif*,* the vast majority of these belonging to Actinobacteria. *Streptomyces* species appear to typically contain a singular complete copy of the operon, with the notable exception of the plant pathogen *S. scabies* which lacks any *mce* sequences. Actinobacteria may have a full copy of the operon, or only select Mce proteins. In Mycobacteria, the decayed genome of *M. Leprae* contains only a singular copy of the *mce1* operon, whilst *M. bovis* possess the complete *mce1, mce2* and *mce4* operons but is missing the *mce3* operon. (Casali & Riley, 2007). It has been suggested by Casali & Riley (2007) that number of *mce* sequences in a genome may be influenced in part by the environment in which the organism reside. The greatest number of sequences appear to be found in fast-growing and soil-dwelling *Mycobacterium* species, such as *M. vanbaalenii*, which has 65 Mce proteins, whilst fewer copies are present in host-specialized, slow-growing pathogenic species, such as *M. leprae* which contains only 6 (Casali and Riley, 2007). Phylogenetic analysis indicates that all *Actinomycetales mce* operons likely arise from a singular ancestral 8-gene operon which has undergone proliferation and deletion within Actinobacteria members with minimal shuffling of genes (Casali and Riley, 2007). Notably, although *mce* proteins were originally examined as virulence factors, *mce* homologues are also present in non-pathogenic species; suggesting a role for the operon outside of virulence. It is now apparent that *mce* operons encode ABC transporter assemblies for lipids. It has been conclusively shown that the *mce4* loci of *Mycobacteria* and *Rhodoccocus* encodes an ATP-dependent steroid uptake transporter (Mohn et al, 2008). More recently, *mce1* in *Mtb* has been characterised as an ABC transporter for fatty acids (Nazarova *et al.*, 2019). It is further known that Mce proteins of Gram-negative

bacteria are crucial in lipid transport between the inner and outer bacterial membranes, discussed later in this study. Mce proteins therefore appear to be involved in lipid transport, with *Mce* operons in *Actinobacteria* encoding ABC transporters for lipids.

ABC-transporters utilise ATP to drive conformation changes in associated transporter proteins and thus assemblies include an ATPase. In *Nocardia*, *Streptomyces* and *Rhodoccocus*, the associated ATPase is encoded within the *mce* operon, however in *Mtb* the ATPase is MceG of the MLK family, which is encoded elsewhere in the genome and energises all four operons (Pandey and Sassetti, 2008; García-Fernández *et al.*, 2017b). The two integral membrane proteins, YrbEA and YrbEB, bare homology to the permease subunits of ABC transporters, whilst Mce proteins resemble the substrate binding proteins associated ABC transporters (Casali and Riley, 2007). Mas or Mam proteins, positioned directly downstream of the *mce* genes, encode proteins which are thought to have a role in stabilisation of the ABC transporter complex (Perkowski *et al.*, 2016).

There is significant sequence divergence in non-*mce* motifs of Mce proteins which may be due to varied substrate specificity, and this may be the purpose of multiple *mce* systems in a single organism, with operons having distinct substrates (as is seen in *Mycobacterium*) or even directionality in transport (Ekiert *et al.*, 2017). *Mce4* is now known to be a cholesterol importer in *Mycobacterium*, whilst *Mce1* of *Mtb* appears to function as a fatty acid transporter (Pandey and Sassetti, 2008). These operons are expressed at differential times in pathogenesis, again indicating that they possess non-redundant functions (Joshi *et al.*, 2006; Casali and Riley, 2007; Klepp *et al.*, 2012; Fenn, Wong and Darbari, 2020). Of further note, is that Mce ABC transporters contain 6 Mce proteins though to function as substrate binding proteins, instead of the typical one or two associated with canonical ABC transporters. It is possible that each of the Mce

proteins functions to bind a distinct substrate, or that they interact to form a hetero-octomeric complex for a singular substrate, with co-ordination of the Mce proteins required for function and stabilisation of the complex (Casali and Riley, 2007). The *E. coli* Mce proteins, *mlaD*, *letB* and *pqib* appear to function as individual complexes (Ekiert *et al.*, 2017; Isom *et al.*, 2020).

Bacterial virulence is thought to have arisen from interactions with predatory bacterivorous amoebae. Specifically, predation of protists applied a selection pressure which lead to the evolution of virulence mechanisms against eukaryotes. It has been proposed that the *mce* operon originated as a nutrient uptake system in non-pathogenic saprophytic bacteria and later evolved a virulent function in eukaryotic pathogens such as *Mtb*. From the singular ancestral *Actinobacteria mce* operon, niche specialisation of Actinobacteria to soil environments or eukaryotic hosts has resulted in divergence of *mce* operons in different genera (Clark *et al.*, 2013). Whilst the *mce* operons aid virulence in pathogenic bacteria, they likely serve as nutrient uptake systems allowing colonisation of the soil in bacteria such as *Rhodoccocus* and *Streptomyces.*

The *mce* operons of *Mycobacterium tuberculosis*

The *Mtb* genome encodes four dispersed homologous copies of the *mce* operon, (Mce(1-4) A-F), which appear to have arisen from duplication events from a singular ancestral operon (Singh *et al.*, 2016). The highest degree of sequence identity (60-69%) is found between *mce1* and *mce2* operons, therefore making these copies likely the most recent duplication (Haile *et al.*, 2002; Casali and Riley, 2007). All operon consists of two transmembrane proteins which appear to function as the permease subunits of the ABC transporter, *yrbEA* and *yrbEB* respectively, and six Mce proteins, believed to act as substrate-binding proteins. The ATPase, encoded by *mceG*, is located elsewhere in the

genome and energizes all four of the *Mtb* operons (Joshi *et al.*, 2006). This ATPase, Rv0655/MceG, is a MLK ATPase, a family of ATPases believed to constitute a conserved pathway of lipid import (Dassa, 2011). The *mce1*, *mce3* and *mce4* operons also include a number of *mce*-associated (mas) proteins downstream, also sometimes referred to as Mams (mce-associated membrane proteins). *Mce4* also appears to have a number of orphaned *mam* genes, which are distally located from the *mce* operon (Perkowski *et al.*, 2016).

The *mce1* operon encodes the GntR-like regulator protein homologous to the FadR subfamily, *mce1R*, as well as *fadD5* (a fatty-acryl CoA synthetase) upstream of the *yrbE* genes. *Mce1R* appears to be responsible for negatively regulating the *mce1* operon (Casali and Riley, 2007). Whilst *Mce2* and *Mce3* also encode upstream transcriptional regulators *mce2R* and *mce3R* respectively (Casali and Riley, 2007; Perkowski *et al.*, 2016). *Mce3R* is a TetR-type of transcriptional repressor which regulates the *Mce3* operon (de La Paz *et al.*, 2009).

All Mce proteins of *Mtb* contain the conserved Mce-like domain PF02470 in their N-terminal region (Sutcliffe and Harrington, 2004; Fenn, Wong and Darbari, 2020). Similarly, all *Mtb* Mce proteins, excepting Mce1E, Mce3E and Mce4E, have transmembrane domains, strongly indicating that these are integral membrane proteins. It is further proposed that the non-membrane-embedded portions of these proteins are extracellular (Mohn *et al.*, 2008). Mce1E, Mce3E and Mce4E lack transmembrane domains, instead all encoding a lipoprotein attachment site which suggests they are anchored to the plasma membrane and surface exposed (Fenn, Wong and Darbari, 2020). Many of the Mce proteins (Mce1A, Mce1D Mce2A, Mce2F, Mce3A, Mce4A and Mce4D) also encode a cholesterol uptake porter (CUP) domain in their unique C-terminal regions, making it likely these proteins interact with cholesterol. Furthermore, Mce1D,

Mce1E, Mce2D, Mce2F, Mce3A, Mce3C, Mce4D and Mce4E, contain RGD motifs, potentially for integrin binding. While DEF, or (docking) D-, motifs are present in Mce2D, Mce3E and Mce4E, which may bind to ERK proteins in the MAPK/ERK signalling pathway (Fenn, Wong and Darbari, 2020).

It has been conclusively demonstrated that *mce4* encodes a cholesterol importer in *Mtb*, whilst Mce1A and Mce3E appear to play a role in adherence and cell entry. However, much still remains to be elucidated about the function of the *Mtb* Mce proteins (Kohwiwattanagun *et al.*, 2007; Mohn *et al.*, 2008). It appears likely that the *mce* operons of *Mtb* may have non-redundant functions, particularly as there is evidence of temporal differences in expression amongst the four copies (Joshi *et al.*, 2006; Casali and Riley, 2007; Klepp *et al.*, 2012; Fenn, Wong and Darbari, 2020). In support of this, mice infection studies indicate that *mce1* is vital immediately after infection, whilst *mce4* becomes necessary later (Joshi *et al.*, 2006). This is in keeping with *mce1* being involved in cell invasion, while *mce4* allows for intracellular bacterial survival by providing a carbon source through cholesterol uptake. It may be that whereas some of the *mce* operons are involved in nutrient acquisition, others have roles in transport of cell wall compounds in mycobacteria and others in cell adhesion and invasion (Klepp *et al.*, 2012). A further aspect to consider is that the number of Mce proteins, A-F, is considerably more substrate-binding proteins than are typical for ABC transporters and may suggest multiple substrates and functions for the transporters, or that the proteins form a complex.

As shown through immunoelectron microscopy, all six Mce1 proteins are known to localise to the cell wall fraction of *Mtb,* with Mce1A exposed on the cell surface (Chitale *et al.*, 2001; Stavrum *et al.*, 2012). As such, Mce1A is believed to interact with the host-immune system and be involved in cell adhesion and uptake. Mce1A-expressing *E.coli*

and Mce1A-coated polysterene latex beads are readily internalized by non-pathogenic HeLa cells, and Mce1A has been shown to promote bacterial adherence and internalisation of *E.coli* into epithelial cells (Kohwiwattanagun *et al.*, 2007). Moreover, *Mce1* knockouts in *Mtb* and *BCG* result in aberrant granuloma formation in infected mice lungs, with mice succumbing to death earlier than those infected with WT *Mtb.* An alternate study showed that *Mtb mce1* mutants, disrupted in *yrbE1B* to eliminate *mce1* expression, were virulence attenuated in mice. The study also found similar attenuation for *mce2*A and *mce3*A mutations (Gioffré *et al.*, 2005; Kohwiwattanagun *et al.*, 2007). Similar experiments performed in *Norcardia farcinica*, an opportunistic human pathogen, showed that Mce1E was expressed in the process of infection in animals, and facilitated internalization of latex beads by HeLa cells (Ji *et al.*, 2017). Such results are clearly indicative of a role for *mce1* in host cell invasion, and correspondingly it has been shown that *mce1* is expressed early during *Mtb* infection. However, the function of the *mce1* operon is likely more complex than is currently known. Surprisingly, an *Mtb mce1* knockout was shown to be hypervirulent in murine macrophages and BALB/c mice models, though hypervirulence in macrophages is likely due to absence of complete immune system. (Shimono *et al.*, 2003; Sellers *et al.*, 2012). This result was later complemented by Gioffré *et al*, a study which determined that mode of infection seems to impact whether *mce* mutants display hypervirulence or attenuation. Shimono *et al* infected BALB/c mice intravenously via a tail vein, whilst Gioffré *et al* utilised both intratracheal inoculation and intraperitoneally, with the latter resulting in hyperviulence of *mce1* mutants and the former resulting in attenuation in BALB/c mice. The authors proposed that an intraperitoneal or intravenous route introduces the bacilli to advantageous niches such epithelial cells, in which they may easily persist, whilst intracheal inoculation resulted in *mce* mutant bacilli immediately encountering aveolar macrophages (Gioffré *et al.*, 2005).

Within the last decade, *mce1* and *mce2* systems have been shown to be involved in uptake and transport of different cell wall lipid components, including mycolic acid importation (García-Fernández *et al.*, 2017). *FadD5* is a putative fatty acyl-CoA synthetase gene, which is located in the *mce1* operon of *Mtb* and has a putative fatty acid binding site. Disruption of this site lead to reduced growth of *Mtb* on mycolic acid as a sole carbon source, and attenuated growth *in vivo*. This raises the possibility that it may play a role in recycling mycolic acids from *Mtb* bacilli which die *in vivo* (Dunphy *et al.*, 2010; García-Fernández *et al.*, 2017). A study which disrupted *mce*2 in *Mtb* found that this change resulted in an accumulation of sulfolipids, a major cell wall lipid component. Other studies in *mce2* mutants showed *Mtb* was attenuated in mice and showed diminished stimulation of pro-inflammatory cytokine production in macrophages, which may be a result of sulfolipid accumulation (Marjanovic *et al.*, 2010; Marjanovic, Iavarone and Riley, 2011). A 2014 study showed that *mce1 Mtb* mutants accumulated mycolic acids, leading to supposition by the study that *mce1* serves as a mycolic acid importer (Forrellad *et al.*, 2014).

As recently as 2017, it appears to have been demonstrated that *mce1* is a fatty acid transporter in *Mtb* (Nazarova *et al.*, 2017). Foamy macrophages, the niche of *Mtb* in humans, are rich sources of both fatty acids and cholesterols, and there is strong evidence indicating that fatty acids are utilized by *Mtb* during infection. It has been established that *Mtb* preferentially metabolizes fatty acids ex vivo, as well as upregulating genes for fatty acid utilization during macrophage infection, in murine model infections and in human lung tissues. Studies have shown that *Mtb* is capable of importing and metabolizing fatty acids or acyl-chains from triacylglycerol and studies have visualized lipid inclusions within intracellular *Mtb* (Nazarova *et al.*, 2019). The protein LucA (lipid uptake coordinator A) was identified as facilitating both fatty acid and cholesterol uptake in *Mtb* by stabilizing protein subunits of the Mce1 and Mce4

transporters (Nazarova *et al.*, 2017). The study demonstrated a *mce1* mutant was defective in fatty acid uptake and metabolism, but unaffected in its ability to uptake cholesterol. LucA/Rv3723 appears to be an integral membrane protein and orthologs of *lucA* are present only in *Mycobacterium* species. *LucA* was found to interact with Mce1 and Mce4-associated proteins, or mams. Mams, which are located downstream of *mce1*, *mce3* and *mce4* and predicted to be exported membrane proteins, appear to be required for *mce4*-dependent cholesterol uptake. Research has now indicated that these proteins may function to stabilise the transporter complex (Perkowski *et al.*, 2016). The study determined that LucA interacted with the TM segment of mam proteins, subunits of the transporter, and participates in the functioning of these complexes (Nazarova *et al.*, 2017).

The *mce3* operon is present in *Mtb,* but not found in *M. bovis*, *M. smegmatis*, *M. microit* or *M. leprae* (Hemati *et al.*, 2019). The function of *mce3* in *Mtb* is currently unknown, although Mce3A and 3E proteins have shown to be involved in uptake and survival of Mycobacteria and Mce3A also appears to facilitate internalization of latex beads by HeLa cells (Sherief El-Shazly *et al.*, 2007; Uchiya *et al.*, 2013). *Mce3* is regulated by the tetR transcriptional regulator mce3R, which is also the regulator of *Ino1* and *FadA4* which are involved in lipid metabolism (Marjanovic *et al.*, 2010; Forrellad *et al.*, 2014). It has been clearly demonstrated that *mce2* and *mce3* operons are involved in the pathogenesis and virulence of *Mtb*. When used as a subcutaneous vaccine against a hypervirulent strain of *Mtb* (Bejing code 9501000), deletions of *mce2* or *mce3* induced a higher level of protection than BCG as well as being ‘safer’ (Aguilar *et al.*, 2006).

Mce4 is known to be a cholesterol importer in *Mycobacteria*, and appears to be expressed in latter, nutrient-deficient, stages of infection (Casali and Riley, 2007; Rathor *et al.*, 2016). It has been well established that *mce4* is required for bacterial survival in

prolonged infection, once macrophages have been activated by IFNγ. The intracellular environment of the macrophage is hostile for the bacterium, and nutrient-scarce. *Mtb* is able to degrade sterol rings and cholesterol side chains for sources of energy and carbon and *Mtb* bacilli has been shown to localise to cholesterol-rich areas of the host cell. This utilisation of cholesterol as a carbon source is necessary for the persistence of *Mtb* inside host cells and as such the bacterium requires a cholesterol uptake system. *Mce4*, which appears to be the major cholesterol import system of *Mtb*, likely fulfils this role in the infection process (Pandey and Sassetti, 2008). In *M. smegmatis*, which encodes 6 *mce* operons, deletions of *mce4*, eradicates survival of the bacteria on media with cholesterol as a sole carbon source. Individual deletions of each of the *mce4* genes similarly resulted in mutants being unable to grow on cholesterol, indicating that all genes are necessary for cholesterol import and their deletion cannot be compensated for by homologues genes in any of the other 5 *mce* operons (García-Fernández *et al.*, 2017). In mice, an *Mtb mce4* deletion was attenuated after two-four weeks post-infection, with an *mce1-mce4* double mutant even further attenuated (Joshi *et al.*, 2006). This may possibly suggest that *mce1* and *mce4* have redundant or partially redundant functions but may also be a result of a “sicker” strain, reduced in ability to invade cells as well as persist intracellularly. This is supported by the *mce1* deletion showing low CFU at 1-week post-infection compared to WT, whilst the *mce4* mutant grew normally at one week and showed defects only later in infection (Joshi *et al.*, 2006).

In more recent years, a clearer role for Mce proteins in signalling has emerged. It is well known that *Mtb* interferes with host cytokine production as a means of avoiding detection, and mce proteins have been implicated in this process. It appears that Mce3E binds ERK1/2 via the DEF motif in its C-terminal region and prevents ERK1/2 phosphorylation and downstream signalling that would otherwise lead to cytokine expression (Li *et al.*, 2015; Fenn, Wong and Darbari, 2020). Mce2E has also been shown to supress

macrophage immune responses by inhibiting ERK and JNK pathways and thereby preventing the production of cytokine and ILF-6 (Qiang *et al.*, 2019; Fenn, Wong and Darbari, 2020). Mce2E has further been shown to promote epithelial cell proliferation. Mce2E was shown to prevent K48-linked polyubiquitination of eEF1A1, therefore enhancing its stability and leading to tumour cell proliferation. The ubiquitination system is vital for regulating the majority of eukaryotic cellular processes, therefore pathogens often seek to hijack this system to its own advantage (Qiang *et al.*, 2019a; Fenn, Wong and Darbari, 2020). Such findings lead to questions of what further unidentified roles the Mce proteins have in host cells and how this relates to their function as lipid/steroid transporters.

To summarize, there is conclusive evidence that *mce4* is a cholesterol importer in *Mtb* and *mce1* appears to be a fatty acid importer, including transport of mycolic acids, and also has a function in host cell adhesion and invasion.

How the *mce* operons of *Mtb* function still remains to be elucidated. It is proposed that, as mutations of *yrbE1A, mce1A,* or *mce1E* result in abrogation of expression of all Mce1 proteins, the operon proteins may function as a complex (Casali and Riley, 2007). This has recently been shown to be the case for the Mce systems of *E. coli*, as described below (Ekiert *et al.*, 2017). It appears likely that the Mce proteins function as a complex, with mas or mam proteins serving to stabilize this complex (Nazarova *et al.*, 2017). In fact, a recent study of the Mycobacterial *mce4* operon found that all Mce4 and Mam4 proteins were required for cholesterol uptake, suggesting that cholesterol import is facilitated by multiprotein Mce4 transporter complex. Conversely, not all Omam proteins (orphaned Mam) proteins encoded outside the operon were necessary for cholesterol import. OmamA and OmamB were required and when these proteins were removed the levels of Mce4A and Mce4E declined. This suggests that these additional proteins

assemble or stabilize the multiprotein Mce4 transporter complex. Furthermore, immunoprecipitation-mass spectrometry showed every Mce, YrbE, MceG, Mam and Oman protein with a role in cholesterol transport associated with Mce4A. (Rank, Herring and Braunstein, 2021).

The *mce* operon of *Streptomyces coelicolor*

Streptomyces coelicolor contains a single copy of the entire *mce* operon, situated in a core region of the genome at 2.6 Mb (Clark *et al.*, 2013). The 13.4 Kb *mce* operon of *S. coelicolor* consists of nine genes, including an ATPase, two integral membrane proteins and six *mce* proteins, as well as two downstream *mce*-associated (mas) genes and a gene of unknown function (Clark *et al.*, 2013) (Fig. 1.5).

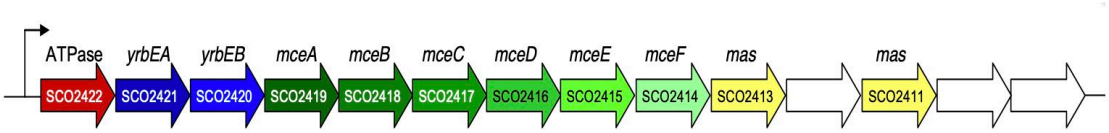

Figure 1.5: The *mce* operon of *S. coelicolor*. The operon encodes an ATPase, two putative transmembrane proteins, and six *mce* proteins containing a single mce domain each. Two *mas* genes of unknown function are also present downstream.

In *S. coelicolor* the apparent *mce* ATPase is SCO2422, which is 343 amino acids in size and contains the Walker A (P-loop), Walker B and LSGGQ motifs necessary for ATP binding and hydrolysis which are conserved in the nucleotide binding domains (NBD) of ABC transporters (Casali and Riley, 2007; Davidson *et al.*, 2008; Rees, Johnson and Lewinson, 2009). The integral membrane proteins thought to form the transmembrane domains (TMD) of the ABC-transporter are SCO2421 and SCO2420; sharing a respective 50.8 and 55.4% sequence identity to their *Mtb* homologous *yrbEA* and *yrbEB.* SCO2421 and SCO2420 have the highest homology to the *yrbEAB* proteins of the *mce4* operon of *Mtb.* SCO2421 is 254 amino acids and SCO2420, 268. Analysis using TMPred software suggests that these proteins are both transmembrane proteins with SCO2421 possessing a predicted 5 transmembrane domains and SCO2420, 6. In total, these proteins possess 11 transmembrane helices between them, predicted to be orientated with cytoplasmic N-terminals. 10-20 membrane-spanning helices are characteristic of ABC importer-associated TMDs (Rice, Park and Pinkett, 2014).

Directly downstream of SCO2421 and SCO2420 are the *mce* genes, SCO2419-SCO2414 which all contain a singular *mce*-like motif of 81-amino acids which characterizes them as Mce proteins. The *S. coelicolor mce* genes share a 33-37% homology with their *Mtb* homologues, with the greatest sequence similarity to the Mce proteins of the *Mtb mce3* operon. SCO2419 (418 aa), SCO2418 (354 aa), SCO2417 (351 aa), SCO2416 (337 aa), SCO2415 (413 aa) and SCO2414 (433 aa) are believed to function as the substrate binding proteins of the Mce ABC transporter. Interestingly, each Mce protein contains a putative substrate-binding domain required to deliver substrate to the membrane component of the ABC transporter (Casali and Riley, 2007). Typically, substrate binding proteins of ABC importers in Gram-positive bacteria contain a lipobox motif which is modified to anchor the protein to the cell membrane. MceE1, MceE3 and MceE4 proteins of *Mtb* have this lipobox, however it is absent in all *S.*

coelicolor mce proteins, possibly indicating that all *mce* proteins of *S. coelicolor* are secreted rather than membrane bound. A possibility supported by the fact that all Mce proteins of *S. coelicolor* contain probable N-terminal signal peptide sequences. As *Mtb* Mce proteins appear to be either integral membrane proteins or lipoproteins, this suggests that the transporter system may function differentially in *Streptomyces* than in *Mycobacterium*. It remains unknown whether the Mce proteins of *S. coelicolor* function as a complex to bind a single substrate, or individually to bind separate substrates.

Three genes of unknown function are directly downstream of the *mce* genes in *S. coelicolor*, including two *mas* genes. *Mas* genes are conserved in three *Streptomyces* species; *S. coelicolor, S. ghanaensis* and *S. lividans* and have been proposed to aid substrate binding, although this remains unconfirmed (Casali and Riley, 2007).

The *mce* operon of *S. coelicolor* appears to be constitutively expressed throughout the developmental lifecycle of the bacteria when grown on solid medium. However, the operon is not essential (Clark, 2011). Phenotype screening showed that deletion of the *mce* operon did not affect growth or viability of *S. coelicolor* on any carbon source tested (Clark, 2011). It was found, however, that expression of the *mce* operon was repressed on media containing high levels of cholesterol (Clark, 2011; Clark *et al.*, 2013). It was also determined that deletions of the *mce* operon appeared to result in a higher resistance to SDS (10% w/v) and lysozyme (0.5 mg/ml), possibly suggesting an effect on the cell envelope from the deletion of the Mce proteins (Clark *et al.*, 2013). An altered spore envelope phenotype in the *mce* mutant was observed via SEM, with spores being more wrinkled, prone to collapse, and with a smaller mean spore diameter. Spore chains in the *mce* mutant also displayed appendages which suggested that premature germination was occurring on the spore chain (Clark *et al.*, 2013). This precocious germination phenotype was proposed to be the mechanism via which *mce* mutants of *S.*

coelicolor also display enhanced virulence towards *Acanthamoeba polphaga* (Clark *et al.*, 2013). These phenotypes are explored further later in this study.

It also appears that the *mce* operon of *S. coelicolor* is regulated in part by the MtrAB two-component system. Mutating *mtrA* in *S. coelicolor* was shown to abolish *mce* expression; with deletions of *mrtA* producing identical phenotypes to a deletion of the *mce* operon (Clark *et al.*, 2013). MtrAB is a two-component system known to also regulate cell division and antibiotic production in *S. coelicolor* (Som *et al.*, 2017).

Whilst the function and substrates for the *mce* operon of *Streptomyces* remains to be fully elucidated, there is evidence suggesting that it also encodes a cholesterol importer such as in *Mycobacterium* (Clark *et al.*, 2013). *Streptomyces* colonises the rhizosphere, the region of soil at the plant-root interface and a highly competitive microbial niche. It is proposed that the *mce* operon may enhance *S. coelicolor* survival in the soil environment by scavenging sterols, which *S. coelicolor* is not capable of biosynthesising and must acquire from the environment (Lamb *et al.*, 2002). Plant roots are a source of phytosterols and fatty acids; thus a robust sterol uptake system may be vital for habitation and survival in this niche. It has been shown *S. coelicolor mce* mutants are impaired in their ability to colonise plant roots and that addition of high cholesterol represses expression of the *mce* operon; possibly suggesting that the *mce* operon of *S. coelicolor* encodes a high-affinity, low capacity sterol importer, transcribed when environmental sterol availability is low (Clark, 2011; Clark *et al.*, 2013). However, it is yet to be shown conclusively that the substrate for *mce* proteins in *S. coelicolor* are sterols, and with 6 *mce* proteins, it remains possible that the transporter binds multiple substrates.

The *mce* systems of Gram-negative bacteria and chloroplasts

Mce proteins (those possessing the conserved *mce* domain PF0470) are now known to be present in diderm bacteria and chloroplasts as well as Actinobacteria. In these organisms, the proteins have been linked to lipid homeostasis or cell adhesion (Fenn, Wong and Darbari, 2020). The homologue of the *mce* operon in Gram-negative bacteria is known as the Mla (Maintenance of OM Lipid Asymmetry) operon, and, in *E. coli*, forms the ABC transporter complex MlaFEDB. The Mla family has been shown to mediate lipid transport between the inner and outer membranes in *E. coli*, crucially maintain the integrity of the outer membrane (Ekiert *et al.*, 2017).

E. coli contains three Mce genes, *mlaD* (Maintenance of OM Lipid Asymmetry D), *pqiB* (paraquat inducible B) and *letB (*formally *yebT*), which are each part of three separate operons (Ekiert *et al.*, 2017). Each operon also encodes a TM protein, MlaE, PqiA and LetA (formally YebS), respectively. The *pqiB* and *MlaD* operons also encode an outer membrane lipoprotein, PqiC and MlaA, respectively.

The *mla* operon encodes an ABC-type ATPase, MlaF, the transmembrane protein MlaE, the Mce protein MlaD, a periplasmic protein MlaC, and the STAS domain protein, MlaB, all of which function together with MlaA, and an outer membrane lipoprotein encoded elsewhere in the genome. The currently proposed structure and mechanism of the transport system is that MlaF, E, D and B form an ABC transporter complex known as MlaFEDB in the cell cytoplasm, with MlaE spanning the inner membrane. The Mce protein, MlaD, contains a singular Mce domain and has been shown to bind phospholipids (Thong *et al.*, 2016). Six copies of MlaD form a homo-hexameric ring, with a central channel that allows passage of hydrophobic molecules such as phospholipids or sterols. This hexametric ring associates with the MlaFEDB ABC transporter complex

which provides the energy for transfer via ATP hydrolysis. MlaC, which is a periplasmic soluble lipid-binding protein, shuttles lipid substrates between the inner membrane MlaFEDB transporter an outer membrane complex. This outer membrane complex is composed of MlaA and the outer membrane porin protein OmpC. The direction of transport has not been concretely established and therefore the complex could function to either export lipids to the outer membrane or drive lipid import to the inner membrane. In the case of lipid import to the inner membrane, the mechanism is likely as follows; MlaC binds to MlaA-OmpC in the outer membrane, and the lipid to be transported is transferred to the hydrophobic pocked of MlaC, where it is protected from solvent as MlaC diffuses across the periplasm to the inner membrane MlaFEDB complex. ATP hydrolysis provides the energy to remove the lipid from MlaC and/or translocation of the lipid into the inner membrane. Conversely, MlaFEDB may utilise ATP hydrolysis to extract inner membrane lipids and MlaC may ferry these lipids to mlaA-OmpC which mediate their insertion into the outer membrane (Ekiert *et al.*, 2017). In either model, the Mce protein MlaD forms a hexameric ring complex to transport lipids, evidencing the commonality that Mce proteins are involved in lipid transport.

Conversely, PqiB, another of the Mce proteins, appears to form a complex of six polypeptides which assemble into a needle-and-syringe assembly across the periplasm, which is believed to provide a channel for the translocation of lipids. PiqB is believed to interact with the inner membrane protein PqiA and possibly PqiC, the outer membrane protein. As the operon lacks an ATPase it is not clear how transport is driven; it may be possible that the ATPase is encoded elsewhere in the genome, or that MlaF is shared by the PqiB system, or that proton motive force or passive equilibration is responsible for lipid translocation between the inner and outer membranes (Ekiert *et al.*, 2017).

LetB (Lipophilic Envelope-spanning Tunnel B) has recently been shown to form a stack of seven rings which create a hydrophobic tunnel between the inner and outer membrane. Lipids are capable of binding the inside of this tunnel, suggesting that its function is lipid transport between the inner and outer membranes. LetB encodes seven Mce domains in its primary sequence and has a N-terminal transmembrane helix. It has been shown that number of Mce domains corresponds to tunnel length, which directly affects protein function *in vivo* and matches the width of the *E.coli* periplasm (Isom *et al.*, 2020). The inner membrane protein LetA, which is encoded in the same operon, is proposed to function alongside LetB, by facilitating lipid insertion and extraction, although, like MlaD and PqiB, the directionality of transport remains to be confirmed. Furthermore, like the PqiB system, the driving force behind transport is unknown (Ekiert *et al.*, 2017; Isom *et al.*, 2020).

To summarise, Mce proteins in Gram-negative bacteria appear to have a role in lipid transport, and function by either ferrying systems or tunnels which span the periplasm. MlaE appears to function as an ABC transporter permease providing energy for lipid translocation, with MlaFEDB functioning as an ABC transporter for lipids similar to the *mce4* system in *Mycobacterium*. The PqiAB and LetAB systems appear to be evolutionarily unrelated to each other and MlaE, despite containing Mce proteins and correspondingly seem to function by different mechanisms. However, all three systems appear to be involved in lipid transport (Isom *et al.*, 2020).

Interactions of *Streptomyces coelicolor* and model protists

Streptomyces colonises a region of soil dense in a plethora of microorganisms, including free-living, bacterivorous amoebae. These phagotrophic microbial eukaryotes are abundant in soil, at a density of 10^3-10^7 per gram dry weight of soil, and thus it is

inevitable that *Streptomyces* will encounter them (Finlay and Esteban, 2019). Interestingly, it appears that rhizosphere bacteria, dependent on taxa, may be of varying quality as a food source for protozoa. Likely this is due to a variety of mechanisms that various bacteria have developed to avoid predation via protist (Rosenberg *et al.*, 2009). A species of the *Acanthamoeba* genus, *Acanthamoeba polyphaga* is an amoeba found in soil which has been shown to ingest *Streptomyces coelicolor* spores, though spores germinated in the phagocytic vacuoles and causes lysis of the protist (Clark *et al.*, 2013). Another soil protist, *Dictyostelium discoideum* also appears to be able to ingest *Streptomyces coelicolor* spores whilst in culture.

Dictyostelium discoideum

The eukaryotic unicellular protist *Dictyostelium discoideum*, stylized simply as *Dictyostelium*, is a member of the Amoebozoa kingdom which resides in deciduous forest soil and predates a wide range of bacteria and yeast (Ludwig, Francisco and Francisco, 2006). A single *Dictyostelium* amoeba is approximately 10-20 μm in diameter and is haploid, with six chromosomes, 4-7Mbp in size, a total of 13000 predicted genes, and a low G+C content (10-30%) (Filipski and Kumar, 2005; Annesley and Fisher, 2009; Steinert, 2011). The entire genome is approximately 34 Mb and has a high (77.6%) A+T content (Brock *et al.*, 2011; Leoni Swart *et al.*, 2018).

As a cellular slime mould, Dictyostelium has a varied and multifaceted lifecycle. Single-cell amoebae are ‘hatched’ from a spore into the environment where they employ phagocytosis of bacteria and fungi and micropinocytosis to obtain the nutrients needed for growth and division by binary fission (Dunn *et al.*, 2018). *Dictyostelium* amoebae secrete prestarvation factor (PSF) which is a glycoprotein autocrine factor which allows *Dictyostelium* to measure their own cell density in comparison with prey source available

(Clarke and Gomer, 1995; Colosimo and Katz, 2001). Upon nutrient depletion, starvation or other developmental triggers initiate a complex and fascinating series of morphological phases in which the amoebae act in a social and altruistic manner in order to ensure the survival of some of their number. *Dictyostelium* are chemotactic, sensing secreted folate to move towards their prey, and upon initiation of starvation, amoeba being to secrete waves of cAMP to chemotactically attract surrounding *Dictyostelium*. Aggregation of tens of thousands of cells occurs, which may be seen by the naked eye as 'streams' of cells flowing towards a central point. From here, cells may diverge onto one of two morphological pathways, including the eminent 'slug' form which has given *Dictyostelium* its 'slime mould' moniker. This involves the aggregated cells forming a psuedoplasmodium, or slug, composed of anywhere from a few hundred to 100,000 cells and varying from 0.1 to 2mm in size (Sunderland, 2009) . In fact, slugs of as little as 100 or as many as 2,000,000 cells have been reported (Gaudet *et al.*, 2008). Slugs may move at a speed of up to 2 mm per hour and migrate for a period up to two weeks, displaying thermotaxis and phototaxis in pursuit of locating a favourable environment (Gaudet *et al.*, 2008). Upon locating such an environment, the motile slug re-arranges and differentiates into a cellular stalk supporting a spore head or 'sorogen'; a morphology referred to as a fruiting body. The spore, from its height, may be scattered to germinate in a more supportive environment, whilst the cells which form the stalk are sacrificed. This ensures the survival of a portion of the amoebae, with the usual spore to stalk cell ratio being approximately 4:1 (Ludwig, Francisco and Francisco, 2006; Gaudet *et al.*, 2008). Alternatively, starving and aggregating *Dictyostelium* cells may by-pass the motile slug stage and form a 'standing' slug' which progresses directly to a fruiting body. The mature spore, or 'sorus' of the fruiting body is approximately 125-300 microns in diameter, whilst the stalk is some 5-15 microns in diameter and 1.5 to 3 cm in height. The spores display low metabolic activity, allowing them to survive without nutrients for up to several years if necessary (Gaudet *et al.*, 2008). Cells which form the stalk will die

within 24 hours, scarified to ensure the survival of the spore. In some 'farming' strains of *Dictyostelium*, cells will retain undigested food bacterium which they carry with them into the spore. *Dictyostelium* amoeba therefore incredibly show a primitive farming symbiosis with certain bacteria which includes dispersal and harvesting (Brock *et al.*, 2011).

When favourable environmental conditions are encountered, the dormant spore undergoes activation, where it prepares to germinate. Initially the spore begins to swell and then amoebae emerge from the spore coat. The process takes place over two to six hours and ultimately results in free individual amoebae which disperse to seek prey and proliferate via binary fission, therefore beginning the lifecycle anew. From initiation at starvation to formation of a viable spore, the entire differentiation cycle takes place within a 24-hour period (Steinert, 2011) (Fig. 1.6 & 1.7).

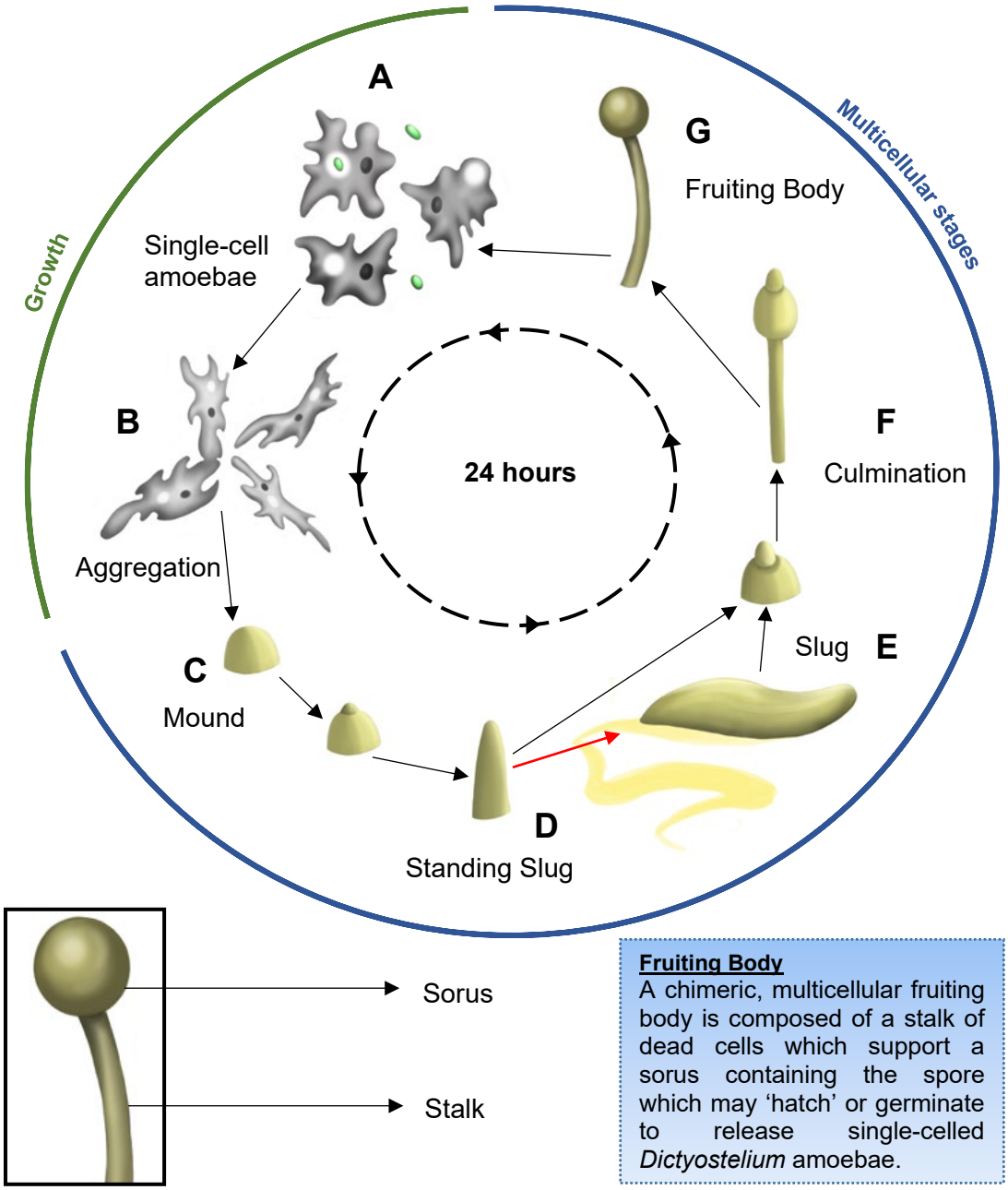

Figure 1.6: Lifecycle and development of *Dictyostelium discoideum*. (A) Single-cell amoebae prey on bacteria and replicate via binary fission. Upon depletion of food resources and initiation of starvation, cells secrete cAMP to recruit surrounding cells and cause mass aggregation **(B)**. Aggregation leads to a multicellular mound which is contained within an extracellular matrix of cellulose and mucopolysaccharide **(C)** which further develops into a standing slug **(D).** Depending on environmental conditions, the standing slug may fall over to become migratory **(E)** or begin culmination **(F)** to produce a fruiting body **(G)** which consists of a spore atop a stalk of dead cells. Under optimal conditions, where the migratory slug stage is bypassed, the lifecycle takes 24 hours. Migratory slugs survive and travel for a number of weeks before entering culmination (Figure adapted from Dunn et al., 2018).

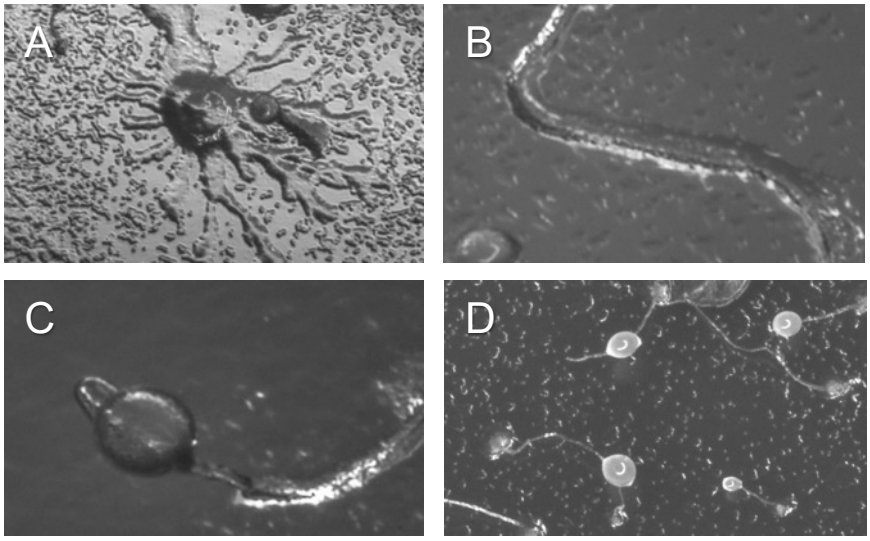

Figure 1.7: The diverse morphological lifecycle of *Dictyostelium*. (A) Starving single-celled amoebae begin to aggregate to form a slug via chemotaxis. **(B)** A motile slug is formed and travels around the plate. **(C)** The slug beings to culminate and organise cells for formation of a fruiting body. **(D)** Mature fruiting bodies with spores are formed. Stereo light micrographs taken at 11.25 x magnification on a SMZ1500 stereomicroscope using a DF 33UX264 CMOS camera system.

Dictyostelium as a model macrophage

Being easily cultured, unicellular, and phagocytic, *Dictyostelium* is a valuable model through which to study host-pathogen interactions, most prominently as a surrogate macrophage (Cosson and Lima, 2014). Unlike other amoebae*, Dictyostelium* is readily pliable in regard to genetic manipulation, whilst also being motile and displaying chemotaxis, cytokinesis, signal transduction and various other desirable qualities for a model organism. *Dictyostelium* are professional phagocytes which may be infected by various human and animal pathogens and therefore provide a simplistic model in which to study eukaryotic host-pathogen interactions in lieu of using more complex mammalian systems (Steinert, 2011). In fact, Froquet *et al* (2014) proposes that *Dictyostelium* are the simplest developed system by which to study bacterial virulence. Of great benefit is that the complete genome sequence of *Dictyostelium* is available, and it is a highly genetically tractable organism, making it easy to generate required mutations (Annesley and Fisher, 2009).

Studies of *Dictyostelium* laboratory strains have demonstrated that they are able to phagocytose 2-10 times faster than macrophages and neutrophils (Thilo, 1985; Gotthardt *et al.*, 2002). Vitally, as a soil amoebae and phagocyte, *Dictyostelium* is a natural predator of many opportunistic pathogenic bacteria and has accordingly developed mechanisms to circumvent their invasion, replication and colonization. It is therefore a practical organism to use when investigating the virulence traits of various intracellular bacterial pathogens, including those of *L. pneumophila*, *Mycobacteria* and *Salmonella* (Bozzaro and Eichinger, 2011). As *Dictyostelium* and macrophages employ highly similar mechanisms of phagocytosis*,* likewise bacteria also appear to utilize largely identical methods to escape *Dictyostelium* predation as they do for mammalian phagocytes (Cosson and Lima, 2014). The opportunistic intracellular pathogens

Legionella pneumophilia and *Mycobacterium marinum* use similar molecular mechanisms to survive and proliferate in *Dictyostelium* as in mammalian macrophages (Pears and Gross, 2021). Of particular benefit to this study, *Dictyostelium* inhabits the soil, the natural niche of the free-living *S. coelicolor*.

Foraging and predation strategies of *Dictyostelium*

Dictyostelium are able to predate and grow upon numerous bacteria, including *Proteobacteria*, *Bacterioidetes, Firmicutues* and *Actinobacteria*. Even bacteria which *Dictyostelium* may find itself unable to predate become edible when at lower densities, and likewise, when in higher densities itself, *Dictyostelium* is a more efficient predator (Shi *et al.*, 2020). This makes *Dictyostelium* a generalist predator, however, interestingly, *Dictyostelium* appears to adjust its feeding strategies depending on its prey, as shown by changes in its transcriptional profile depending on food-source bacteria. Interestingly, *Dictyostelium* appears to show differential gene expression when fed on Gram-positive bacteria compared to Gram-negative bacteria (Nasser *et al.*, 2013; Lamrabet *et al.*, 2020; Shi *et al.*, 2020).

Dictyostelium must first be able to sense food bacteria, recognize it (whilst avoiding pathogenic bacteria) and then move towards it. *Dictyostelium* are chemotactic, sensing and moving towards chemicals such as folate or cAMP which are produced by the food source bacteria. Interestingly, response to food source bacteria appears to be specific in *Dictyostelium*. Recent studies show that *Dictyostelium* discriminate between Gram-positive and Gram-negative bacteria, showing preferential migration towards Gram-negative bacteria. *Dictyostelium* also appear to display preferential sensing, where they may direct themselves towards particular bacteria regardless of chemical gradient. It is proposed that possibly *Dictyostelium* display a ‘muted response’ to Gram-positive

bacteria in comparison with Gram-negative bacteria due to the lack of cAMP production in Gram-positive bacteria (Rashidi and Ostrowski, 2019). How *Dictyostelium* recognize specific types of bacteria has yet to be elucidated, however the *Dictyostelium* genome includes numerous genes which may be involved in this process. *Dictyostelium* possess 61 putative G-protein coupled receptors, including Grl and GrlG which are implicated as receptors which facilitate the detection of folic acid. Whilst *Dictyostelium* do not possess Toll-like receptor orthologs, the genome does encode two cytosolic proteins with Toll/Interleukin1-Receptor domains, TirA and TirB, potentially involved in intracellular signaling. There are also more than 100 proteins containing leucin-rich repeats, and is possible that these may function as pattern recognition receptors (Rashidi and Ostrowski, 2019).

As mentioned, it also appears that *Dictyostelium* may use different molecular mechanisms to kill, depending on the ingulfed bacteria, responding to different bacteria by changing gene expression. For instance, intracellular killing of *Klebsiella pneumoniae* requires the proteins Kil1 and Kil2, which are not involved in killing of *Bacillus* (Lamrabet *et al.*, 2020). *Dictyostelium* may therefore be able to recognize microbe associated molecular patterns (MAMPs) and accordingly activate the appropriate intracellular signaling pathways for specific bacterial destruction (Rashidi and Ostrowski, 2019). This seems to be the case with pathogenic bacteria, such as *M. marinum*, as upon exposure to this bacterium *Dictyostelium* triggered transcriptional changes that upregulate host defense pathways which appeare to be specific to *M. marinum* infection (Rashidi and Ostrowski, 2019).

Phagocytic mechanisms of *Dictyostelium*

Dictyostelium perform both phagocytosis and macropinocytosis, both processes involving the internalization of extracellular material. Macropinocytosis is the mechanism utilized by cells to engulf large volumes of extracellular fluid and begins with actin cytoskeleton rearrangement and the extension of lamellipodia from the plasma membrane. Some of these lamellipodia will fold back on themselves, trapping fluid and soluble nutrients in a structure known as the macropinosome (Lim and Gleeson, 2011; Buckley *et al.*, 2016). Axenic strains of *Dictyostelium* are mutated in a manner which leads to increased performance of macropinocytosis and accordingly greater uptake of soluble nutrients, allowing *Dictyostelium* to survive in liquid culture without a bacterial food source (Bloomfield *et al.*, 2015).

The phagocytosis of solid material by *Dictyostelium* is a process which highly resembles that of professional phagocytic cells in multicellular organisms (Cosson and Lima, 2014). Indeed, it is believed that predatory phagocytosis and destruction of bacteria in mammalian organisms is a trait that initially originated from interaction of unicellular eukaryotic organisms, such as environmental amoebae, with bacteria (Cosson and Lima, 2014). Vegetative *Dictyostelium* amoebae forage for prey chemotaxically, detecting pterin-like compounds such as folate which are released by bacteria and fungi and migrating towards these and likely other chemical signals (Aufderheide and Janetopoulos, 2016; Kuburich, Adhikari and Hadwiger, 2016). *Dictyostelium* display considerable meandering while foraging and are constituently motile, meaning that even in the absence of chemoattractant such as folate they will continue to travel by random motion in search of food (Kuburich, Adhikari and Hadwiger, 2016).

Dictyostelium are prolific eaters, with a single amoeba being able to digest up to 300 bacteria in an hour period (Bozzaro, Bucci and Steinert, 2008). The endocytic process begins with the amoeba reversibly binding to the particle it seeks to phagocytose. This binding occurs between the particle and specialized phagocytic and signaling receptors on the amoeba cell surface. This binding leads to a cascade of downstream signaling inciting actin polymerization and membrane deformation to form what is known as the phagocytic cup. This phagocytic cup is formed by actin protrusion at the cell surface, with the cell membrane extending around the particle. Closure of this cup produces the early (or nascent) phagosome, which may then be internalized into the cell in the final step (Ishikawa *et al.*, 2003; Dunn *et al.*, 2018). Binding does not always lead to internalization and phagocytosis, even when actin is locally recruited. However, successful phagocytosis, when it occurs, is often an extremely rapid event. The process from initial actin recruitment to form the phagocytic cup to actin disassembly around the phagosome can take place in under 60 seconds (Bozzaro, Bucci and Steinert, 2008). The phagocytic receptors of *Dictyostelium* are largely unknown, with only a few being recently identified. One group includes the five integrin-like Sib receptors, SibA-E. It appears that SibA and SibC directly influence adhesion to the particle to be engulfed (Cornillon *et al.*, 2006; Dunn *et al.*, 2018). LmpA, B and C, three homologs of the scavenger receptor class B proteins which are found in mammals, are found in *Dictyostelium* and it has been proposed that these LmpB may function as a phagocytic receptor, as it is present at the plasma membrane and in early phagocytic compartments (Harris, Ravandi and Siu, 2001; Janssen *et al.*, 2001; Gotthardt *et al.*, 2002; Dunn *et al.*, 2018) *Dictyostelium* may also possess lectin-like receptors, as it is able to bind specifically to certain sugar derivatives (Vogel *et al.*, 1980; Bozzaro and Roseman, 1983; Dunn *et al.*, 2018). Most notable, *Dictyostelium* hunts via folate chemotaxis, and a G-protein coupled receptor for folic acid, fAR1, has been identified which appears to be involved in signaling and initiation of prey uptake, although not particle binding (Pan *et*

al., 2016; Dunn *et al.*, 2018). However, *Dictyostelium* requires further identification and characterization of its phagocytic receptors and how they are involved and interact in prey binding and phagocytosis.

Inside *Dictyostelium*, the nascent phagosome containing the ingested particle will mature into a microbicidal phagolysosome, ultimately culminating in the destruction of the ingested particle and exocytosis of undigested material. Early steps include the loss of the phagosome actin coat, and recruitment of proteins which regulate vesicle fusion and phagosome maturation (Rupper, Grove and Cardelli, 2001; Steinert, 2011; Dunn *et al.*, 2018). These proteins include Rab GTPases, notably Rab 5 and 7, which sequentially recruit effectors that facilitate docking and fusion of endocytic compartments with the nascent phagosome. As early as 1 minute after uptake, Rab7 is recruited to the phagosome, where it ensures fusion with lysosomal compartments to introduce lysosomal enzymes into the phagosome. This process appears to occur between 3 - 15 minutes post-uptake (Steinert, 2011; Dunn *et al.*, 2018). Concurrently, the WASH complex activates the Arp2/3 complex to induce actin polymerization, facilitating recycling of phagocytic receptors and plasma membrane proteins to the cell surface.

The vacuolar H+-ATPase (V-ATPase), responsible for acidification of the phagosome, is also recruited within minutes of phagocytosis. The V-ATPase appears to be delivered via fusion with lysosomal vesicles recruited by Rab7 and leads to rapid acidification of the nascent phagosome, reaching a pH of as low as 3.5-4 in between 10 and 30 minutes after phagosome formation (Dunn *et al.*, 2018). The phagosome becomes a microbicidal environment, with low pH and of a number of proteases, hydrolases, lysozymes and antimicrobial peptides, which aid killing in conjunction with reactive oxygen species (ROS) generated within the phagosome and the outward export of trace metals to prevent bacterial growth (Dunn *et al.*, 2018). Lysosomal enzymes which act in the

phagosome include cysteine proteases CP-p34 and cathepsin D, as well as lysosomal glycosidases, a-mannosidase and b-glucosidase (Bozzaro, Bucci and Steinert, 2008; Steinert, 2011; Dunn *et al.*, 2018). The phagosome is now late-stage or a mature phagosome, or phagolysosome, and bacterial destruction is achieved in a number of ways. Low pH is in itself, not sufficient to kill bacteria, but works in conjunction with lysosomal enzymes. ROS are known to be critical for bacterial killing in mammalian phagocytes and *Dictyostelium* encodes three catalytic NOX subunits. It remains unclear how essential ROS are for bacterial destruction in *Dictyostelium*, and what function ROS may have outside of this (Dunn *et al.*, 2018). Divalent metals, such as iron, manganese, zinc and copper, are a key source of micronutrients for intracellular bacterial pathogens but may also be toxic. Mammalian macrophages have been shown to use metal deprivation by sequestering metals to kill bacteria in their phagosomes, as well as metal poisoning by pumping toxic metals into the pathogen-containing compartment (Dunn *et al.*, 2018). Both mammalian macrophages and *Dictyostelium* possess the metal ion transporter NRAMP1 which is present on the phagosomal membrane. NRAMP1 uses the proton gradient generated by the V-ATPase to transport manganese and iron out of the phagosome, resulting in a metal-ion depleted environment deleterious to the bacteria; this is known as nutritional immunity (Soldati and Neyrolles, 2012; Lima *et al.*, 2014; Dunn *et al.*, 2018). *Dictyostelium* also synthesize pore-forming peptides, which are able to perforate the membrane of bacteria, and it is proposed these peptides also act against bacteria in the phagosome (Bozzaro, Bucci and Steinert, 2008).

From particle binding and engulfment to this stage in phagocytosis takes approximately 40 minutes. The *Dictyostelium* phagosome will then begin to mature into a postlysosome, with the V-ATPase and lysosomal enzymes retrieved and recycled via the WASH complex activating Arp2/3 and actin polymerization. The postlysosome returns to a neutral pH and acquires vacuolin A and B, markers of the late phase of phagosome

maturation, around 60-90 minutes post-internalization. (Steinert, 2011; Falkenstein and De Lozanne, 2014; Dunn *et al.*, 2018). The actin coat reforms following this, at around 60-180 minutes post-uptake, this vesicle may then fuse with the plasma membrane in a manner similar to exocytosis, allowing expulsion of non-digested material (Dunn *et al.*, 2018) (Fig. 1.8).

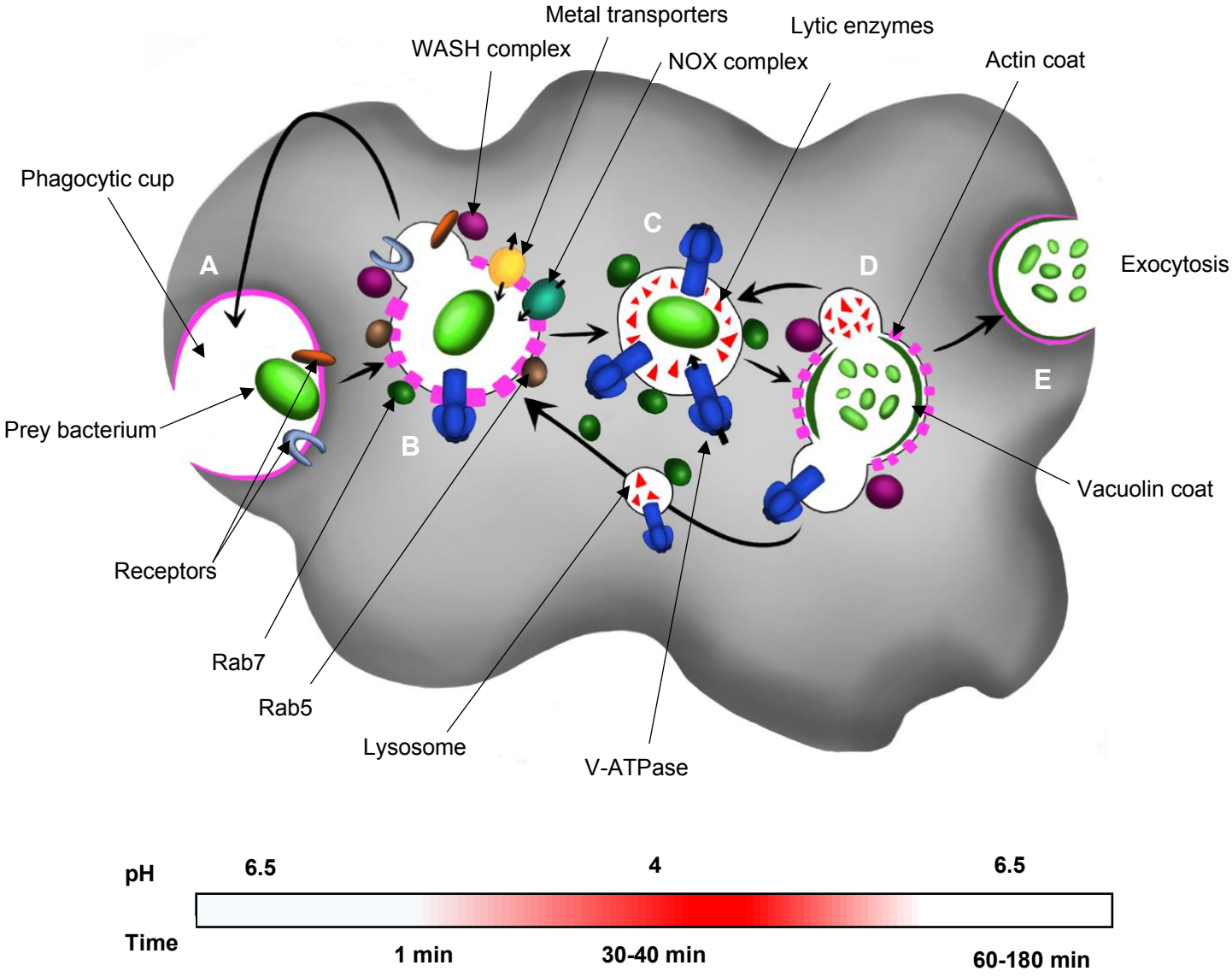
Metal transporters
Lytic enzymes
WASH complex
NOX complex
Actin coat
Phagocytic cup
A
C
D
Exocytosis
B
E
Prey bacterium
Vacuolin coat
Receptors
Rab7
Rab5
Lysosome
V-ATPase
pH
6.5
4
6.5
Time
1 min
30-40 min
60-180 min

Figure 1.8: Phagocytosis in *Dictyostelium.* The amoebae senses folate released by prey bacterium and moves towards it chemotactically. Receptors on the amoebae surface bind to ligands on the surface of the prey bacterium and an actin polymerization is initiated and the phagocytic cup forms **(A)**. The phagocytic cup closes and the bacterium is captured inside an intracellular compartment known as the phagosome **(B)**. The process of phagosome maturation beings, with Rab GTPases, Rab7 and Rab5, sequentially recruiting effectors which control docking and fusion of endocytic compartments with the nascent phagosome. One effector recruited within minutes of formation of the phagosome is the H+-vacuolar ATPase (V-ATPase) which is responsible for acidification of the phagosome. The V-ATPase is delivered by fusion of lysosomal vesicles along with lysosomal enzymes. Acidification is rapid, reaching a pH of as low as 3.5-4 between 10- and 30-minutes post phagosome formation. Metal transporters co-localise with the V-ATPase and efflux metals from the phagosome to the cytosol to restrict metal availability the pathogen, a process known as 'nutritional immunity'. The NADPH oxidase (NOX) complex produces ROS, that together with metal transporters and lysosomal enzymes, create a bactericidal environment. Meanwhile, the phagocytic receptors are recycled to the cell surface via actin polymerization induced by the WASH complex. Nascent phagosomes have an actin coat, which is gradually lost as the phagosome matures **(C)**. Bacteria are destroyed within the mature phagosome. Following destruction phagosomes mature into postlysosome **(D)**. Approximately 40 minutes post creation of the phagosome, the V-ATPase and lysosomal enzymes are recycled via the WASH complex. The phagosome rises to neutral pH and acquires Vacuolin A and B as well as an actin coat. This compartment fuses with the plasma membrane of the cell to allow exocytosis of undigested bacterial material **(E)**. (Figure adapted from Dunn et al., 2018).

Bacterial survival and virulence within *Dictyostelium*

As predation by amoeba is likely a significant source of bacterial mortality, it is probable that bacteria are under a selective pressure to avoid predation by protists and have correspondingly developed mechanisms to circumvent killing by amoeba. The ability to evade or resist predation by amoeba is likely to, in many cases, prelude the development of pathogenicity towards amoeba predators and other eukaryotes (Shi *et al.*, 2021). Several bacterial human pathogens, such as *Legionella, Salmonella,* and *Mycobacterium* species are also pathogenic towards *Dictyostelium* through subversion of phagocytic processes (Bozzaro and Eichinger, 2011). *Dictyostelium* therefore serves as an excellent model by which to examine the interplay of phagocytic host cells with intracellular pathogens.

The mechanisms which bacteria employ to avoid intracellular killing vary. *Mycobacterium marinum* and *Mycobacterium tuberculosis* are able to inhibit phagosome maturation, manipulating it instead into a replication-permissive compartment known as a mycobacterium containing vacuole (MCV). The proliferation of mycobacterium inside the MCV will eventually lead to deformation and rupturing of the phagosome membrane, facilitating bacterial release into the *Dictyostelium* cytosol (Hagedorn and Soldati, 2007; Cardenal-Muñoz *et al.*, 2018; Gueho, Bosmani and Soldati, 2019).

Salmonella typhimurium is able to induce uptake by *Dictyostelium* macropinocytosis via its T3SS. If taken up by phagocytosis, the bacterium is typically transported to lysosomes, however, if taken up via T3SS-driven macropinocytosis, *S. typhimurium* is able to modify the phagosome and create a *Salmonella*-containing vacuole (SCV) which supports bacterial survival and replication (Bozzaro and Eichinger, 2011).

Legionella pneumonphila is similarly able to arrest phagosomal maturation and instead form the *Legionella*-containing vacuole (LCV) in both *Dictyostelium* and macrophages. *L. pneumophila* is therefore able to replicate and grow within the phagocyte and after 48 hours, cell lysis occurs and the bacteria are released (Bozzaro and Eichinger, 2011).

Project Aims and Rational

How does a gene operon involved in nutrient uptake in a non-pathogenic, saprophytic bacterium evolve into a virulence factor aiding cell invasion in one of the world's deadliest human pathogens? Current hypotheses for the emergence of bacterial virulence proposes that it evolved from free-living bacteria seeking to avoid predation by protozoa which utilized them as a food-source. The *mce* operon of *Streptomyces coelicolor* provides a fascinating opportunity to elucidate the mechanisms of virulence evolution in bacteria, with the aims of this study being the characterization of *mce* gene function in relation to nutrient acquisition, amoebae-predation, spore cell wall durability and spore germination.

Chiefly, the main aim of this thesis is to the determine the function of and characterise the role of the *mce* operon of *S. coelicolor.* Specifically:

1) To determine the effect of *mce* operon deletion on the phenotype of *S. coelicolor* and to characterise this, including how this effects spore susceptibility to deleterious agents and spore germination.

2) Characterise the enhanced virulence phenotype previously observed in the protist *Acanthamoeba* in the model protist and model macrophage *Dictyostelium discoideum* and investigate the cell biology of what occurs to *Streptomyces* spores upon predation by amoebae.

3) Determine the localisation of the Mce proteins within the cell, and whether there is potential for some Mce-domaining containing proteins to be secreted.

Outline of this thesis

Chapter 1 of this work is an introduction to Actinobacteria, *Streptomyces* and the bacterium's lifecycle and ecology, the *mce* operon, and the use of amoebae as models for cell biology.

Chapter 2 of this work lists all strains, plasmids, media, techniques, and equipment utilised in this study.

Chapter 3 of this work explores the phenotypic effects of *mce* operon deletion in *S. coelicolor*, including its effect on spore morphology, germination, and susceptibility to various deleterious agents.

Chapter 4 of this work follows examination of *mce* deletion phenotypes by exploring the effect of these phenotypes on interactions with amoeba. Optimisation of amoeba models and spore-amoeba co-culture assays are explored.

Chapter 5 of this work investigates the potential structure, function, and location of the Mce proteins within *S. coelicolor* as well as their possible mechanism of action.

Chapter 6 summarizes and discusses the work presented in this study and contextualises the role of *mce* operon in *Streptomyces*.

Chapter 2: Materials & Methods

Reagents

Analytical grade chemicals and components used in this work were purchased from Sigma-Aldrich, Fisher Scientific, Invitrogen, Melford, New England Biolabs, Merk or Promega unless otherwise stated.

Growth Media

Unless otherwise stated, all media was prepared in Duran bottles and sterilised via autoclave at 121°C, 100 kPa for 15 mins. Any and all heat sensitive media or media components were filter sterilised via 0.22 µm filter. *Dictyostelium* cell culture HL5 media and SM nutrient agar were purchased from Foremedium™. To prepare solid media, agar was added in a concentration of 20g l^{-1} prior to autoclaving. For soft nutrient agar, agar was reduced to 10 g l^{-1}.

Cultivation of Strains

Unless otherwise stated, all *Streptomyces* strains used in this study were cultivated at 30°C and all *E. coli* and *K. aerogenes* strains at 37°C. *K. aerogenes,* when grown in conjunction with *Dictyostelium* amoeba as a food source, was grown at 22°C. The complete list of all bacterial stains used may be found in Table 2.1 and all plasmids in Table 2.2. A list of media and their composition for the cultivation of these strains can be found in Table 2.4. The antibiotics used for plasmid maintenance and their concentration are specified in Table 2.5.

Table 2.1 Bacterial strains used in experimental work

Strain	Description	Genotype	References
E. coli DH5α	*E. coli* K12 derivative	F⁻ φ80*lac*ZΔM15 Δ(*lac*ZYA-*arg*F)U169 *rec*A1 *end* A1 *hsd*R17(r_K^-, m_K^+) *pho*A *sup*E44 λ⁻ *thi*-1 *gyr*A96 *rel*A1	(Grant *et al.*, 1990)
E. coli BL21 (DE3)	*E. coli* BL21 derivative	F⁻ *omp*T *hsd*S_B (r_B^-, m_B^-) *gal dcm* (DE3)	(Studier and Moffatt, 1986)
E. coli ET12567	*E. coli* K12 derivative	*dam13*::*Tn*9, *dcm6*, *hsdM*, *hsdR*, *recF143*, *zij201*::*Tn*10, *galK2*, *galT22*, *ara14*, *lacY1*, *xylS*, *leuB6*, *thi*-1, *tonA31*, *rpsL136*, *hisG4*, *tsx78*, *mtli*, *glnV44*, F-	(MacNeil *et al.*, 1992)
Streptomyces coelicolor M145 A(3)2	Wild type *S. coelicolor*	SCP1⁻ SCP2⁻	(Kieser *et al.*, 2000)
SLC201	*S. coelicolor* ∆mce	M145 Δ*SCO2422:SCO2415*	(Clark, 2011)
SLC202	*S. coelicolor* ∆mce+*mce*	SLC201 pLCS006	(Clark, 2011)
SLC301	*S. coelicolor* M145+*mce*	M145 pLCS006	(Clark, 2011)
M145 mCherry	Wild type *S. coelicolor* expressing mCherry	SCP1⁻ SCP2⁻ , pRed	This study
SLC201 mCherry	*S. coelicolor* ∆mce expressing mCherry	M145 Δ*SCO2422:SCO2415*, pRed	This study
SLC301 mCherry	*S. coelicolor* M145+*mce* expressing mCherry	M145 pLCS006, pRed	This study
Klebsiella aerogenes	K. aerogenes	NeoR	Dictybase

Table 2.2 Plasmids used in experimental work

Plasmid	Description	Antibiotic Marker	References
pRed	Derivative of integrative vector pMS82 encoding a *gap1-mCherry* insertion.	Hygromycin B	(Zacchetti *et al.*, 2016)
pUZ8002	RK2 derivative, non-replicative defective *OriT, tra* transfer protein.	Kanamycin	(Paget *et al.*, 1999)
pLCS001	Supercos derivative 8A2.1.F04 with deletion between BamH1 sites at 22505 and 13639bp	Apramycin	(Clark, 2011)
pLCS006	pLCS004 with ligation of pNRT4 at KpnI site at 34231 bp	Apramycin Ampicillin Kanamycin	Clark, 2011)
pUC57	Cloning vector with MCS.	Ampicillin	(Yanisch-Perron, Vieira and Messing, 1985)
pUC57_N-SCO2421	pUC57 storage vector encoding N-SCO2421	Ampicillin	This study
pUC57_C-SCO2421	pUC57 storage vector encoding C-SCO2421	Ampicillin	This study
pUC57_N-SCO2420	pUC57 storage vector encoding N-SCO2420	Ampicillin	This study
pUC57_C-SCO2420	pUC57 storage vector encoding C-SCO2420	Ampicillin	This study
pUC57_N-MceA	pUC57 storage vector encoding N-MceA	Ampicillin	This study
pUC57_C-MceA	pUC57 storage vector encoding C-MceA	Ampicillin	This study

pT7-7	Expression vector with T7 bacterial promoter	Ampicillin	(Tabor and Richardson, 1992)
pT7-7_N-SCO2421	Expression vector encoding N-SCO2421	Ampicillin	This study
pT7-7_C-SCO2421	Expression vector encoding C-SCO2421	Ampicillin	This study
pT7-7_N-SCO2420	Expression vector encoding N-SCO2420	Ampicillin	This study
pT7-7_C-SCO2420	Expression vector encoding C-SCO2420	Ampicillin	This study
pT7-7_N-MceA	Expression vector encoding N-MceA	Ampicillin	This study
pT7-7 C-MceA	Expression vector encoding C-MceA	Ampicillin	This study
pIJ6902	Chromosomally integrating *PtipA* expression vector with MCS, φC31 int/*attP* and *oriT* RK2.	Apramycin Thiostrepton	(Huang *et al.*, 2005)
pIJ6902_N-SCO2421	Integrating vector containing N-SCO2421	Apramycin Thiostrepton	This study
pIJ6902_C-SCO2421	Integrating vector containing C-SCO2421	Apramycin Thiostrepton	This study
pIJ6902_N-SCO2420	Integrating vector containing N-SCO2421	Apramycin Thiostrepton	This study
pIJ6902_C-SCO2420	Integrating vector containing N-SCO2421	Apramycin Thiostrepton	This study
pIJ6902_N-MceA	Integrating vector containing N-SCO2421	Apramycin Thiostrepton	This study

pIJ6902_C-MceA	Integrating vector containing N-SCO2421	Apramycin Thiostrepton	This study
pDXA/VatM-GFP	*Dictyostelium* expression vector containing VatM-GFP fusion	Ampicillin Hygromycin	(Clarke *et al.*, 2002)
pDEXRH[GFP-TubA]	*Dictyostelium* expression vector containing GFP-α-tubulin fusion	G418	(Neujahr *et al.*, 1998)
pGFP-Golvesin	*Dictyostelium* expression vector containing GFP-golvesin	Neomycin	(Gerisch, G, Luderitz, O, Ruschmann, E, 1967)

Table 2.3 Amoebae strains used in experimental work

DictyBase ID	Strain names	Genotype	Summary	References
DBS0235534	AX2, AX2-214	axeA2, axeB2, axeC2	Axenic wild type	(Watts and Ashworth, 1970)
DBS0235537	AX2-N2-gfp, vat-gfp, ax-2-vat-gfp	axeA2, axeB2, axeC2, vatM-GFP, neoR	Axenic, GFP-α-tubulin producing cells	(Clarke *et al.*, 2002)
DBS0236181	GFP-tubulin, GFP-alpha-tubulin, tubA:GFP	axeA2,axeB2,axeC2,[GFP-tubA],neoR	Axenic, GFP-α-tubulin producing cells	(Neujahr *et al.*, 1998)
DBS0236061	76-2-3, GFP-(N)-Δ(559-579)-golvesin	axeA2,axeB2,axeC2GFP:gol(1-558),[pDEX],neoR	Axenic, C-terminally deleted GFP-(N)-Δ(559-579)-golvesin expressing cells	(Gerisch *et al.*, 2004)

Table 2.4 Media compositions

Name	Composition
LB (Sambrook et al., 1989)	10g tryptone 10g NaCl 5g yeast extract 20g agar Make up to 1 litre with deionised water pH to 7.0
Mannitol soy flour (MS) (Hobbs et al., 1989)	16g soya bean flour 16g d-mannitol 20g agar Make up to 1 litre with tap water pH to 7.2
Yeast extract malt extract (YEME) (Kieser et al., 2000)	3 g yeast extract 5 g peptone 3 g malt extract 10 g glucose 340 g sucrose Make up to 1 litre with deionised water
Nutrient Agar (NA) (Oxoid)(Kieser et al., 2000)	13 g nutrient broth mix (Oxoid) 20 g agar Make up to 1 litre with deionised water

SM Agar (Basu et al., 2013)	10 g glucose
	10 g proteose peptone
	1 g yeast extract
	1 g $MgSO_4 * 7H_2O$ (or 0.5 g $MgSO_4$)
	1.9 g KH_2PO_4
	0.6 g K_2HPO_4
	20g agar
	Make up to 1 litre with deionised water
	Adjust pH to 6.0 - 6.4
HL5 (Axenic medium) (Ashworth and Watts, 1970)	5 g proteose peptone
	5 g neutralised bacteriological peptone
	10 g glucose
	5 g yeast extract
	0.35 g Na2HPO4∗7H2O
	0.35 g KH2PO4
	Make up to 1 litre with deionised water
	Adjust pH to 6.5
	Filter sterilise
GAE medium (Suarez, Barbes and Hardisson, 1980)	0.5 g K2HPO4
	0.5 g MgSO4.7H2O
	0.01 g FeSO4.7H2O
	10 g glucose
	1 g asparagine
	0.5 g yeast extract
	Make up to 1 litre with deionised water

2x YT (Kieser et al., 2000)	16 g tryptone 5 g NaCl 10 g yeast extract Make up to 1 litre with deionised water
Minimal Media (Kieser et al., 2000)	0.5g L-asparagine 0.5g K2HPO4 0.2g MgSO4*7H2O 0.01g FeSO4*7H2O 10g D-mannitol (added after autoclaving) 10g agar Make up to 1L with deionised water
ZY Media (Studier, 2005)	10g Tryptone 5 g Yeast Extract Make up to 925 mL with deionised water

ZYP-5052 (Studier, 2005)	1% N-Z-amine
	0.5% Yeast extract
	25 mM Na_2HPO_4
	25 mM KH_2PO_4
	50 mM NH_4Cl
	5 mM Na_2SO_4
	2 mM $MgSO_4$
	0.5% Glycerol
	0.05% Glucose
	0.2% Lactose

Table 2.5 Buffers and stock solutions

Name	Composition
Sörensen's buffer (Sor) (Gerisch et., 1967)	15mM KH_2PO_4 2mM Na_2HPO_4 pH to 6.0
Solubilisation Buffer	1M Tris Base 5M NaCl Glycerol 100 mL DNase 10 mg/mL 1mM PMSF 750 mL H_2O
PBS(Oxoid)	8.0 g NaCl 0.2 g KCl 1.15 g Na_2HPO_4 0.2 g KH_2PO_4 Make up to 1L in deionised water. pH 7.3
20 X NPS	0.5 M $(NH_4)_2SO_4$ 1M KH_2PO_4 1M Na_2HPO_4
50 X 5052	0.5% (w/v) Glycerol 0.05% (w/v) D-glucose 0.2% (w/v) Lactose

Lysis Buffer A	10 µg/mL
	4 mM PMSF
	5 mg/mL Lysozyme
	2% DDM
	10% Glycerol
IMAC Buffer A	1M Tris (pH 8)
	5M NaCl
	100 mL Glycerol
	Make up to 1L with distilled water
IMAC Buffer B	1M Tris (pH 8)
	5M NaCl
	100 mL Glycerol
	34.04 g Imidazole
	Make up to 1L with distilled water

Table 2.6 Antibiotic concentrations for bacterial culture

Antibiotic	Class	Stock conc. (mg/mL)	Working conc. (ug/mL)	Stock solution solvent
Kanamycin	Aminoglycoside antibiotic	50	50	H_20
Apramycin	Aminoglycoside antibiotic	50	50	H_20
Carbenicillin	β-lactam antibiotic	100	100	H_20
Ampicillin	β-lactam antibiotic	100	100	H_20
Nalidixic acid	DNA gyrase inhibitor antibiotic	25	25	0.1M NaOH
Chloramphenicol	N-dichloroacylphenylpropanoid antibiotic	25	25	96% ETOH
Gentamicin	Aminoglycoside antibiotic	50	50	H_2O

Cultivation of *Streptomyces* on MS

Unless otherwise stated, all *Streptomyces* strains were cultivated on Mannitol-soya flour (MS) agar (see Table 2.4), supplemented with appropriate antibiotic, for 5 - 10 days at 30°C.

Cultivation of *Streptomyces* in Liquid Medium

Liquid culture of *Streptomyces* was performed in YEME medium (see Table 2.3) without sucrose, at 30°C with shaking at 250 rpm. Erlenmeyer conical flasks containing 50 mL YEME and coiled springs to prevent spore clumping were inoculated with approximately 10^8 spores prior to growth for the requisite time.

Creation of *Streptomyces* Spore Stocks

MS agar plates with appropriate antibiotic selection were evenly streaked with spores from a singular colony using a sterile cotton bud and incubated for approximately 9 days at 30°C. Maturity of the spore lawn was observed through the production of grey polyketide spore pigment. Plates were then flooded with 5 mL of 25% glycerol and spores harvested via gentle scaping with a sterile cotton bud. Spore solution was filtered through a 20 mL sterile syringe containing approximately 5 cm of non-absorbent cotton wool to eliminate cell debris. Filtered spores were pipetted into 1.5 mL screw-top vials and preserved either at 20°C for working preparations, or -80°C for longer-term storage.

Cultivation of *E. coli* on Solid Medium

E. coli cells were acquired from a glycerol stock using a sterile loop and streaked for single colonies onto a LB plate containing the appropriate antibiotic selection. Plates were incubated in a static incubator at 37°C for 16-18 hours.

Cultivation of *E. coli* in Liquid Medium

Sterile universals containing aliquots of either 5 or 10 mL of LB broth were inoculated with a single colony of the relevant *E. coli* strain and appropriate concentration of the required antibiotic. Cultures were grown at 37°C, 250 rpm for 16-18 hours.

Creation of *E. coli* Stocks

Overnight cultures (5 mL) of the desired strain were pelleted by centrifugation and resuspended in 2 mL of fresh LB. Glycerol (50%) was added in a proportion of 1:1 to achieve a final glycerol concentration of 25%. Stocks were transferred to screw-top vials and stored at -80°C.

Preparation of Chemically Competent *E. coli* Cells

A single colony of the appropriate *E. coli* strain was used to inoculate 5 mL of LB containing appropriate antibiotics. The culture was grown at 37°C, 250 rpm overnight, following which a 1:50 dilution of the culture was made into 50 mL fresh LB with appropriate antibiotics. Fresh cultures were grown in 250 ml Erlenmeyer flasks at 37°C, 250 rpm until reaching an OD_{600} of 0.4-0.6. Cultures were pelleted by centrifugation at 4000 x *g* for 10 minutes before resuspension and gentle washing twice in 25 mL of ice-cold 0.1 M $CaCl_2$. Following the final wash, the pellet was resuspended in 500 µL of 0.1 M $CaCl_2$ with 15% Glycerol. Aliquots (50 µL) of cell suspension were pipetted into Eppendorf's. Competent cells were used immediately or were flash-frozen in liquid nitrogen and stored at -80°C.

Transformation of *E. coli*

Aliquots (1-50 ng/µL) of donor DNA were mixed with 50 µL of electrocompetent cells in an Eppendorf and incubated on ice for 30 minutes. The mixture was then transferred to

a heat-block and heat-shocked at 42°C for 30 seconds before being immediately placed back on ice for 2 minutes. Fresh LB (450 µL) was added to the Eppendorf and the mixture incubated for an hour at 37°C. Aliquots (50-200 µL) were then pipetted onto a LB agar plate containing the appropriate antibiotic selection and spread using a sterile spreader. The plate was then incubated at 37°C overnight for growth of transformant colonies.

Intergenic Conjugation of Integrating vectors from *E. coli* to *Streptomyces* (Kieser et al., 2000).

The *E. coli* strain ET12567/pUZ8002 was transformed with the appropriate integrating vector and colonies grown overnight on LB agar plates with appropriate antibiotic at 37°C. A single transformant was then used to inoculate 10 mL of LB media containing relevant antibiotics and grown overnight at 37°C at 250 rpm. The overnight was then diluted 1:100 into 50 mL fresh LB and grown in Erlenmeyer flaks to an OD_{600} of 0.4-0.6. Cells were harvested via centrifugation for 15 minutes at 4000 x *g* and pellets washed twice in 10 mL LB without antibiotics. During this period, 500 µL of 2 x YT broth was inoculated with approximately 10^8 *Streptomyces* spores, vortexed briefly, and heat-shocked for 10 minutes at 50°C. Once cool, this 500 µL aliquot was added to 500 µL of washed E12567/pUZ8002 cells, vortexed, and centrifuged for 2 minutes at 11,000 x *g*. The cell pellet was resuspended in residual liquid and spread onto an MS agar plate containing 10 mM $MgCl_2$. Plates were then incubated at 30°C for 14-18 hours. At approximately 16 hours, plates were overlaid with 1 mL sterile H_2O containing 0.5 mg Nalidixic acid and the relevant antibiotics in necessary concentration for the donor plasmid. Plates were then incubated for a further 3 days before colonies were streaked onto a fresh MS plate containing 50 µg/mL Nalidixic acid and the appropriate antibiotic. Colonies which grew were streaked for single colonies onto fresh MS plates containing the appropriate antibiotics and incubated at 30°C. A single colony was then streaked for

a confluent lawn on a fresh MS plate with relevant antibiotic and incubated at 30°C to allow growth for a stock solution.

Restriction Digest

Appropriate amounts of plasmid DNA were mixed with the required buffer and restriction enzymes sourced from Promega. Appropriate buffer and digest conditions were identified using the Promega Restriction Enzyme Tool.
(https://www.promega.co.uk/resources/tools/retool/)

Agarose Gel Electrophoresis

A 1% agarose gel was prepared by adding the appropriate amount of agarose to the required volume of 1 x TAE buffer (40mM Tris-acetate, 1 mM EDTA) and microwaved until dissolved. Ethidium bromide at a final concentration of 100 µg/mL was added to the gel mixture whilst liquid. The gel mixture was then poured into a casting tray and solidified. DNA samples were mixed with gel loading dye (6X, New England Biolabs®) and an appropriate molecular weight marker (1Kb Plus, New England Biolabs®) was loaded into the first and last well. Gels were run using BIO-RAD® PowerPac$^{(TM)}$ Basic Power Supply and horizontal electrophoresis cell in 1 x TAE buffer at 80 V for 120 minutes. Bands were visualised and imaged under UV excitation in a Syngene Bioimaging Ingenius trans-illuminator.

If necessary, gel extraction was carried out using the Bioline Isolate II PCR and Get Kit per manufacturer's instructions. A sterile scalpel was used to extract DNA from the gel after visualisation on a UVP high performance UV transilluminator.

DNA Ligation

DNA ligation was carried out per manufactures instructions using Promega T4 DNA ligase. Briefly, a 1:1 molar ratio of vector to insert DNA was mixed with the appropriate volume of 10X Ligase Buffer and T4 DNA Ligase. The reaction mixture was incubated at 4°C overnight to allow ligation to occur.

Plasmid Mini Prep.

A single colony of the desired *E. coli* strain was used to inoculate 10 mL of LB containing appropriate antibiotic which was then grown overnight at 37°C, 250 rpm. Following this isolation of plasmid DNA was achieved using a Wizard® Plus SV Minipreps DNA Purification Systems (Promega®, cat. # A1330) kit as per manufacturer's instructions. Purity and concentration of the plasmid was analysed via a ThermoFisher Scientific Nanodrop 2000c spectrophotometer.

Germination Assay (Haiser, Yousef and Elliot, 2009)

Germination Assays were adapted from methods described in (Haiser, Yousef and Elliot, 2009). Cellophane discs (10 cm) were washed in distilled water, sandwiched between damp Whatman paper, wrapped in tinfoil, and autoclaved. Sterile cellophane discs were placed on square MS agar plates and flattened with a sterile spreader. A concentration of 5.2×10^9 *Streptomyces* spores were plated on top of the cellophane disc and spread with a sterile spreader. Cellophane was left to dry for 20 minutes in a laminar flow to allow easier imaging. Plates were then incubated at 30°C in a static incubator for 8 hours. At various time-points, portions of the cellophane discs were excised and viewed using a Nikon Eclipse TE2000-S Inverted Microscope equipped with a 100x objective and phase contrast images taken, allowing visualisation of germinated and non-germinated spores. Three different fields of view were photographed and all spores visible counted

and scored by whether or not they had germinated. Germination scoring was carried out on a minimum of 200 spores for each field of view.

Aggregation Assay (Hirsch and Ensign, 1976)**.**

Modified from assays by Hirsch and Ensign, 1976. MS plates were streaked for a lawn using a sterile cotton-bud and grown for 9 days (216 hours) at 30°C. Plates were flooded with 5 mL of sterile distilled water and spores harvested by gentle scraping with a sterile cotton bud. Suspended spore solution was pipetted through a cotton-filtered, sterile syringe into a falcon tube to separate mycelial fragments from spores. The suspension was spun at 4000 x *g* for 10 minutes to pellet the spores. Spores were resuspended in 5 mL of sterile minimal media with mannitol. Suspension (1 mL) was pipetted into a cuvette which was kept sterile via cuvette lid. Cuvettes were incubated at 30°C, 180 rpm. The OD_{600nm} was taken every 20 minutes on a spectrophotometer (Eppendorf Biophotomometer, cat. #6131-01503) without cuvette inversion.

Heat-Kill Assay (Hoskisson, Hobbs and Sharples, 2000).

Heat-Kill technique for *Streptomyces* was modified from (Hoskisson, Hobbs and Sharples, 2000). MS plates were streaked for a lawn using a sterile cotton-bud and grown for 8 days at 30°C. The plates were flooded with 5 mL YEME and spores harvested by gentle scraping with a sterile spreader. The suspended spore solution was filtered through a cotton-filtered syringe into universals to separate spores and mycelia. Spore solution (150 µL) was pipetted into Eppendorf's and incubated at either 60°C, 70°C, 80°C, 90°C or 100°C.

At set time points, spores were vortexed and 10 µL of spore solution removed and diluted down to $1x10^{-8}$ in PBS. A 100 µL aliquot of this solution was spread on nutrient agar

plates which were incubated for 5 days at 30°C. Plates were then counted for colony forming units.

Antibiotic Disc Diffusion Assay

Nutrient agar square plates were overlaid with soft nutrient agar seeded with 10^8 *S. coelicolor* spores. Sterile filter discs approximately 5 mm in width were dropped onto the soft nutrient agar overlay and 5 µL antibiotic of the appropriate concentration was pipetted onto discs. Plates were incubated for 48 hours at 30°C before examination for zones of inhibition.

Permeability Assay (Coldham *et al.*, 2010.)

Permeability Assays were performed based on modified techniques described by Coldham *et al.*, 2010. Flasks containing 50 mL YEME was inoculated with 1 x 10^7 spores and grown at 30°C for 11 hours until slightly branched germlings were apparent. Cultures were harvested via centrifugation at 4000 x *g* for 20 minutes, washed once in PBS and pellets resuspended in PBS to an OD_{600} of 0.1. As a positive control, an aliquot of suspension in Eppendorf's was boiled for 10 minutes at 95°C. Aliquots of suspensions (180 µL), both boiled and non-boiled were added to wells of a Corning Incorporated Costar® 96-well black plate with clear bottom and a final concentration of 2.5 µM ethidium bromide added to cells. In place of ethidium bromide, 20 µL PBS was added to cells to serve as a negative control. Fluorescence was then measured in a FlexStation® 3 Multi-Mode Microplate Reader (Molecular Devices©). Fluorescence was read at an absorption and emission of 515 and 600 nm respectively.

Creation of *Dictyostelium discoideum* Liquid Stocks (Fey et al., 2007)

Dictyostelium spores less than 7 days old were harvested from a single SM agar plate of 9 cm diameter using a sterile plastic loop and suspended in 4.5 mL of cold HL5 media without antibiotic. DMSO (0.5 mL) was added and the suspension mixed well prior to transfer of 0.5 ml aliquots to 1 mL cryotubes for stock. Liquid stocks were frozen for 2 hours at -20°C before being moved to -80°C for long-term storage.

Creation of *Dictyostelium discoideum* Silica Gel Stocks (Fey et al., 2007)

Sterile screw-top glass vials (3 mL) were filled approximately half-full with silica gel (Sigma-Aldrich, product #214426) and baked at 180°C for 90 minutes. The vials were then cooled on ice for 30 minutes. Viable spores were harvested from three 9 cm SM plates with a sterile loop and suspended in 400 µL of cold 5% non-fat milk. Spore-milk solution was pipetted onto the cold silica gel and shaken vigorously for 5-10 seconds. The vial was placed back on ice for 5 minutes prior to long-term storage at -20°C.

Culture of *Dictyostelium discoideum* on Solid Media (Fey et al., 2007)

Dictyostelium were grown on solid SM agar plates. A single colony of *K. aerogenes* was used to inoculate 5 mL LB and grown overnight at 37°C, 250 rpm. *K.* aerogenes overnight culture (250 µl) was spread onto a fresh SM agar plate using a sterile spreader. A sterile 25 mm hypodermic needle was used to remove a portion of frozen *Dictyostelium* HL5 stock which was spread over the bacteria on the agar plate using a sterile spreader. For *Dictyostelium* culture from silica stocks, a few silica gel pieces were scattered across the plate. Alternatively, if *Dictyostelium* fruiting bodies were available, 2-3 spore heads were picked using a sterile pipette tip and carefully streaked onto the plate. Plates were incubated at 22°C in a humid environment until fruiting bodies formed.

Culture of *Dictyostelium discoideum* in HL5 Axenic Liquid Media (Fey et al., 2007)

For grown in axenic suspension, spores from fruiting bodies were harvested using a sterile loop and inoculated into 1 mL of HL5 containing 5 uL Penicillin-Streptomycin (10,000 U/mL, Thermo Fisher Scientific, Gibco™, cat. #15140122) and statically incubated at 22°C for 48 hours. “Hatched” amoebae were detached by gentle pipetting with a blue tip and a 1:20 dilution performed into 5mL fresh HL5 with Pen-Strep in tissue culture flasks. Flasks were again statically incubated at 22°C.

Dictyostelium were allowed to reach a confluency of approximately 2 x 10^6 million cells mL^{-1} before sub-culturing into fresh HL5 inoculated with Pen-Strep, *Dictyostelium* were maintained in exponential phase and split before cells reached a maximum density of 4 x 10^6 cells mL^{-1}. Cultures were continued for a maximum of two-weeks before being discarded.

Cell Count and Viability

Amoebae were detached from the tissue culture flask surface by gentle pipetting with a serological pipette and use of a cell scraper. An aliquot of cell culture was diluted 1:10 with 0.4% Trypan Blue solution and the suspension applied to the grid of a Haemocytometer. Cell count and viability were determined using a light microscope equipped with a 10X objective.

Plaque Assays (Froquet et al., 2009)

Plaque assays were modified from protocols by Froquet *et al*, 2009. Aliquots (2.5 ml) of 80% nutrient broth agar (Oxoid) was inoculated into each well of a 24 well-cell culture plate (Thermo Fisher) and dried for 4 hours under a laminar flow. A normalised density of 1x10^9 *S. coelicolor* spores in 100 uL sterile water was plated onto wells, spread via

plate rotation, and left to dry for 2 hours. During this time exponential *Dictyostelium* cells were harvested and normalised to a cell density of 35 x 10^6 in 1 mL of fresh HL5. A 5 µL aliquot of this cell suspension, containing 175,000 cells, was pipetted directly onto the middle of the well. Spots were left to dry for 10 minutes before plates were wrapped in tinfoil and incubated upside down at 22°C for 48 hours to allow plaques to form.

Dictyostelium Spore Consumption Assays

Exponential phase *Dictyostelium* cells were harvested and pelleted by centrifugation at 500 x *g* for 5 minutes. The pellet was washed in 25 mL Sörensen buffer once, to remove antibiotics, and cells counted. *Dictyostelium* were seeded (1 x 10^6 cells mL^{-1}) into wells of a 6-well cell culture plate (ThermoFisher Scientific Nunclon$^{(TM)}$ Delta Surface). containing 1 mL of either HL5 media or Sörensen buffer and left to adhere for 30 minutes at 22°C. An MOI of 1:100 was created by adding 1 x 10^8 *S. coelicolor* spores to all wells excepting controls. Plates were incubated for 120 minutes to allow spore phagocytosis. Media was removed and cells washed once to remove all exogenous spores. Cells were then incubated in 1 mL of fresh media containing 100 µg/mL gentamicin for 30 minutes to eliminate any remaining exogenous spores. After incubation, *Dictyostelium* were detached from wells and cell suspension spun at 10,600 x *g* for 5 minutes. Pelleted cells were resuspended in 300 µL PBS containing 0.1% Triton-X-100 and incubated for 10 minutes to lyse amoebae. An aliquot of the lysate (30 µL) was mixed with 270 µL clean PBS in a 96-well cell culture plate and diluted to 10^{-4}. Dilutions were spotted (15 µL) onto nutrient agar plates and plates incubated at 30°C until colonies appeared.

Multiplicity of Infection (MOI) Determination

Exponential phase *Dictyostelium* were harvested, centrifuged at 500 x *g* for 5 minutes and washed in clean HL5 before counting. Cells were normalised to a density of 1 x 10^6

mL^{-1} in 1 mL HL5 in 24-well cell culture plates and left to adhere for 30 minutes. Densities of either 1 x 10^7, 1 x 10^8 or 1 x 10^9 mL^{-1} *S. coelicolor* spores were added to create MOIs of 1:10, 1:100 and 1:1000 respectively. Wells containing media and spores only served as negative controls. Plates were spun at 500 x *g* for 10 minutes to bring spores in contract with amoeba before incubation at 22°C for 120 minutes to allow spore phagocytosis. After incubation, media was removed and 1 mL clean HL5 containing 100 µg/mL gentamicin was added to ensure death of all exogenous spores. At 0, 30, 60, 90, 120, 180, 240 minutes and 24 hours post-addition of gentamicin, *Dictyostelium* were detached from wells and the cell suspension spun down at 10,600 x *g* for 5 minutes before resuspension in 300 µL PBS containing 0.1% Triton-X-100. Cell were incubated for 10 minutes before 30 µL aliquots were removed and mixed with 270 µL PBS. Cell lysate was diluted to 10^{-4} and 15 µL aliquots of each dilution spotted on nutrient agar plates at 30°C until colonies appeared.

Intracellular Survival Assays (Arafah *et al.*, 2013)

Intracellular survival assays were adapted from protocols described by Arafah (2013). Exponential phase *Dictyostelium* cells were harvested, washed to remove antibiotic, and 1 x 10^6 ml^{-1} *Dictyostelium* cells seeded into 1mL of HL5 in 24-well cell culture plates. *Dictyostelium* were left to adhere for 30 minutes at 22°C before 1 x 10^8 ml^{-1} *S. coelicolor* spores were added to wells to create an MOI of 1:100. Plates were spun at 22°C at 500 x *g* for 10 minutes and then incubated at 22°C for 2 hours. HL5 in wells was removed and plates washed with fresh HL5. HL5 containing 100 µg/mL gentamicin was then added to wells. At 0, 60, 120, 180, 240, 480 and 960 minutes and 24 hours post-addition of gentamicin, *Dictyostelium* were harvested and lysed by addition of 0.1% Triton-X-100. Lysate was diluted in PBS to 10^{-4} and spotted on nutrient agar for quantification of CFU.

Exocytosis Assays

Exponential phase *Dictyostelium* were harvested from HL5 axenic medium by centrifugation at 500 x *g*, 4°C for 5 minutes. The resultant pellet was washed once in HL5 to remove antibiotics and resuspended in 1mL fresh HL5. *Dictyostelium* were then seeded 100,000 cells into 12-well plates and left to adhere for 20 minutes. *Streptomyces* spores (1×10^7) were then added wells to create an MOI of 1:100. Wells containing only *Streptomyces* spores served as spore-only controls. Media from spore-only controls was immediately removed from wells and transferred to Eppendorf's before suspension was vortexed thoroughly and diluted 1/1000 in Sörensen buffer. The 1/1000 suspension dilution was then plated on nutrient agar. The plate containing spore-*Dictyostelium* suspensions were incubated for 2 hours at 22°C to allow phagocytosis to occur. Following incubation, media was gently pipetted off to remove exogenous spores and replaced with fresh media containing 100ug/mL gentamicin. Plates were placed back in the incubator for a further 30 minutes to allow *Dictyostelium* to re-adhere and allow antibiotic selection. *Dictyostelium* cells were then detached from wells via vigorous pipetting and transferred to Eppendorf's. Eppendorf's were pun for 5 minutes at 500 x *g* and the resultant pellet washed once in sterile Sörensen buffer to remove remaining gentamicin before resuspension in 1 mL Sorensen buffer. The suspension was diluted 1/1000 in Sörensen buffer and plated on nutrient agar plates. Nutrient agar plates were incubated at 30°C until colonies arose and CFU count taken.

Spore Lysozyme Tolerance Assay

Spores (1×10^7) were added to Eppendorf's containing 1 mL Sörensen buffer containing either 0 or 0.5 mg/mL of lysozyme and incubated for 30 minutes at 37°C. Suspensions

were then diluted to 1 x 10^{-4} in Sörensen buffer and 100 µL plated on nutrient agar plates. Plates were incubated at 30°C and CFU quantified.

Extracellular Actinorhodin Production Assay and Cell Dry Weight Determination

Flasks containing coils and 50 mL YEME without antibiotic were inoculated with 1 x 10^6 spores and grown at 30°C, 250 rpm. At select time points, a 1 mL aliquot of culture was removed from the flask and centrifuged at 16,000 x *g* for 10 minutes. An aliquot of the supernatant (500 µL) was mixed in cuvettes containing 500 µL of 1 M NaOH. The absorbance was read at 600_{nm}. The pellet was washed and resuspended in 1 mL YEME, washed twice in distilled water and then transferred onto previously dried and weighed Whatman® glass microfiber filters, with 1 µm pores. A vacuum system used to remove liquid from the filter via a Bruchner funnel and filters and biomass were then dried for 18 hours at 55°C before weighing. The total biomass was determined by subtracting the mass of the filter from the mass of the filter and biomass.

Actinorhodin concentration was calculated using the Lambert-Beer-Law, using the molar extinction coefficient for actinorhodin which is 15,135 m^{-1} cm^{-1}. The actinorhodin production yield was calculated by normalising µM per mg of cell dry weight.

Germling lysozyme tolerance assay

Flasks containing 50 mL YEME without antibiotic were inoculated with 1 x 10^7 spores and grown for 11 hours at 30°C until slightly branched germlings were present. Cultures were harvested by centrifugation at 4000 x *g* for 30 minutes and pellets washed once in Sörensen buffer. Final pellets were resuspended in Sörensen buffer to an OD_{600} of 0.4 and 1 mL of suspension aliquoted into Eppendorf's. Eppendorf's were spun at 11,000 x *g* for 10 minutes and pellets resuspended in Sörensen buffer containing either 0 or 0.5 mg/mL lysozyme. Eppendorf's were incubated at 37°C for 30 minutes. Suspensions

were then diluted to 1 x 10^4 in Sörensen buffer and 100 µL plated on nutrient agar plates. Nutrient agar plates were incubated at 30°C and CFU quantified.

Bacteria and Amoeba Co-culture

Exponential phase *Dictyostelium* were harvested from HL5 axenic media and washed in Sörensen buffer to remove antibiotics. *Dictyostelium* cells were counted and 125,000 cells were seeded into 1 mL of Sörensen buffer in a 35mm low Ibidi µ-dish (Ibidi®) and left to adhere for 30 minutes. *S. coelicolor* spores (1.8 x 10^8 mL^{-1}) were added to produce a MOI of 1:1440. Co-cultures were maintained at 22°C. At various time points, cultures were viewed at 100x magnification in bright-field on a Nikon Eclipse TE-2000-S Microscope. For fluorescence-based co-culture, cells were viewed using 60x magnification on an Olympus 1000FV Confocal Microscope with excitation wavelengths of 488 and 543 nm.

Minimum Inhibitory Concentration Determination

Normalised *S. coelicolor* spores at a density of 1 x 10^7 were added to a 96-well cell culture plate (TPP®, cat. #92096) containing rich or minimal media with decreasing concentrations of the inhibitory test compound. Plates also included wells of the inhibitory compound only and spores only as controls. Plates were incubated in a Microplate Reader (Bio-Tek Multi-Detection Microplate Reader Synergy HT) at 30°C for either 48 or 72 hours and OD readings at 600nm taken every 15 minutes.

Impression Mount Assays (Kieser et al., 2000)

Spores were normalised to a density of 1x10^{10} in 100 µl of sterile distilled water and spread evenly on an MS plate. Plates were incubated at 30°C. At 0, 6, 12, 24, 30, 33, 36, 48, 54 and 60 hours a clean glass 18 mm coverslip (VWR™ cat. #631-01503) was

lightly dropped onto the centre of the plate and gently removed. Coverslips were placed on a slide and viewed in phase contrast using a Nikon Eclipse TE2000-S Inverted Microscope equipped with a 100x objective. Six fields of view were examined for each time point and number of spore chains present recorded.

Induction of His-tag Protein Expression in *E. coli*

Colonies from freshly transformed BL21 (DE3) cells (ThermoFisher ScientificTM, cat. # C600003) were used to inoculate 10 mL overnights. An aliquot of overnight (1 mL) was spun down at 4000 x *g* for 5 minutes as an uninduced control. An aliquot of overnights (500 µL) was used to inoculate 50 mL ZY-5052 autoinduction media in conical flasks. Cultures were grown for 72 hours at 18°C before pelleting by centrifugation at 4000 x *g* for 20 minutes. Pellets were weighed and resuspended in the appropriate amount of BugBuster® Master Mix (Merck Millipore Novagen™) as per manufactures instructions. The serine protease inhibitor PMSF was added to a final concentration of 1 mM. Cell/BugBuster® suspension was incubated at room temperature on a shaking platform for 20 minutes before centrifugation at 16,000 x *g* for 20 minutes at 4°C to remove cell debris. Supernatant was retained for SDS-PAGE analysis.

Lysis of *E. coli* for Protein Detection and Purification

Cells pellets were resuspended in Lysis Buffer A (10 mL for approximately 0.5 g of cell pellet) in 50 mL Falcon tubes. Cell suspension was then mixed on a rotating-wheel for 2 hours at room temperature to break cells. Following cell lysis, the suspension was transferred to 1 mL Eppendorf's and spun at 11,000 x *g* for 30 minutes. The supernatant was transferred to a clean Eppendorf and stored at 4°C or directly mixed with 5 x SDS loading dye and run on an SDS-PAGE gel.

Alternatively, cell pellets were resuspended in solubilisation buffer (10g per 1g of cell pellet) and was passed through a SLM Aminco French® Pressure Cell Press, thrice, at a pressure of 1300 psi. Cell lysate was then spun in a Beckman® Avanti JXN-26 centrifuge at 25,000 x *g* and 4°C. Supernatant was retained and stored at 4°C for later analysis.

Alternatively, for non-membrane proteins, cell pellets were resuspended in Bug Buster® Master Mix with a final concentration of 1 µM PMSF and lysed and then centrifuged as per manufacturer's instructions. The supernatant was then transferred to a clean Eppendorf and stored at 4°C or directly mixed with 5 x SDS loading dye and run on an SDS-PAGE gel.

Immobilised Metal Affinity Chromatography (IMAC)

The supernatant from French® Pressed E.coli lysate, collected by centrifugation at 25,000 x *g*, was loaded onto a IMAC column (HiTrap™ IMAC FF, 1mL), previously equilibrated with IMAC Buffer A (Table 2.4) and loaded with nickel resin, on a ÄKTA™ Pure FPLC system. His-tagged protein was purified in Buffer B (Table 2.4).

Increasing concentrations of imidazole were applied to the IMAC column in order to elute the hexa-histidine-tagged protein of interest and elution fractions with a fraction collector. During the protein purification process, absorbance at 280nm was measured. Following elution, elution fractions were loaded into an SDS-PAGE gel for analysis.

Induction of His-tag Protein Expression in *Streptomyces*

Cultures were set up in 250 ml Erlenmeyer flasks containing 50 ml YEME and a coiled spring were inoculated with approximately 1 x10^8 spores per mL of *Streptomyces* with hexa-histidine-tagged *mce* proteins. Cultures were grown at 30°C, 250rpm for 36 hours.

At this time, to induce expression of histidine-tagged *mce* proteins present on the Thiostrepton-inducible promoter pIJ6902, flasks were inoculated with 5 µg/ml Thiostrepton before continued growth for a further 12 hours. At 48 hours, the cultures were harvested by centrifugation at 4000 x *g* for 30 minutes. Pellets were washed once and resuspended in 10 ml of Buffer A (Table 2.3) containing 0.8 mM PMSF. Resuspended cells were lysed by sonication.

Lysis of *S. coelicolor* for Protein Detection

Cell pellets were resuspended in solubilisation buffer (10g per 1g of cell pellet) and lysed by sonication. Falcon tubes containing cell suspension were placed on ice and sonicated using a Branson Ultrasonics(TM) S-250A Model Sonifier(TM) for 10 seconds intervals until lysed. The suspension was kept cold at all times to prevent protein degradation.

Nickle-bead Protein Purification

Histidine-tag proteins were pulled from suspension and immobilised on HisPur™ Ni-NTA Magnetic Beads (ThermoFisher Scientific™, cat. #8832) as per manufactures instructions (Table 2.7).

Table 2.7 Nickle-bead Protein Purification Reagents

Name	Composition
Equilibrium Buffer	100 mM sodium phosphate 600 mM sodium chloride 30mM Imidazole 0.05% Tween-20 pH 8
Wash Buffer	100 mM sodium phosphate 600 mM sodium chloride 50 mM Imidazole 0.05% Tween-20 pH 8
Elution Buffer	100 mM sodium phosphate 600 mM sodium chloride 500 mM Imidazole pH8

SDS-PAGE

Sample was mixed with appropriate amount of 4X SDS dye and loaded into wells of Novex™ 4-20% Tris-Glycine Mini-Gels (ThermoFisher Scientific™, catalog number: XP04200PK2). Gels were run in 1x running buffer (Table 1.7) for 90 minutes at 120 V.

Coomassie Blue Staining

SDS-PAGE gels were stained in Coomassie Blue for 1 hour prior to de-staining overnight at room temperature, on a shaking-platform. Gel images were taken via an Azure(™) biosystem C200.

Semi-Dry Transfer

PDVF membrane was cut to the size of the SDS-PAGE gel and activated in methanol for 1 minute. The membrane was then equilibrated alongside the SDS-PAGE gel and 6 pieces of Whatman paper in Transfer Buffer (Table 2.7) for 10 minutes. Transfer was performed by sandwiching the membrane and SDS-PAGE gel between the 6 pieces of Whatman paper and placing this on a Biometra Fastblot B44 system (cat. #846-015-200). The semi-dry transfer system was run for approximately 30 minutes at the required current determined by size of the SDS-PAGE gel.

Western Blot

The transferred-membrane was blocked for an hour with shaking at room temperature in 0.01% TBS-T (Table 2.7) containing 5% non-fat milk. Following blocking, the membrane was carefully transferred to a sealed plastic pouch containing 5mL TBS-T with 5% non-fat milk and 1:10,000 primary antibody. The membrane was incubated

overnight at 4°C. Following incubation with primary antibody, the membrane was washed three times for ten minutes each in TBS-T before being placed once more in a fresh sealed plastic pouch containing 5mL TBS-T with 5% milk and 1:10,000 of the secondary antibody. The pouch wrapped in tinfoil to avoid photo-bleaching of the fluorescence tag and incubated at room temperature for four hours prior to visualisation of the membrane on a LI-COR Odyssey® Fluorescence system.

Table 2.8 SDS-Page and Western Blot reagents

Name	Recipe
10X Running Buffer	14.4% Glycine 3% Tris Base, pH 8 1% SDS Make up to 1L with deionised water pH 8.3
Transfer Buffer	1.44% Glycine 0.3% Tris-HCL 0.1% SDS 20 mL methanol Make up to 1L with deionised water
Tris-Buffered Saline (TBS)	50mM Tris 150mM NaCl Make up to 1L with deionised water pH 7.5
TBS-T	0.1% Tween-20 50mM Tris 150mM NaCl
Blocking Solution	0.1% Tween-20 50mM Tris 150mM NaCl 5% (w/v) non-fat milk
5X SDS Loading Dye	50 mM Tris-HCl pH 6.8 2% SDS 10% glycerol 1% β-mercaptoethanol 12.5 mM EDTA 0.02 % bromophenol blue

Chapter 3: Disruption of the *mce* operon in *S. coelicolor* leads to precocious germination and increased susceptibility to deleterious agents

The *mce* operons of some Actinobacteria members, such as *Rhodococcus* and *Mycobacterium*, have been conclusively shown to encode ABC transporter assemblies for importing lipids (Mohn *et al.*, 2008; Pandey and Sassetti, 2008; Nazarova *et al.*, 2019). Evidence also suggests that Mce proteins may have roles extending beyond lipid transport, including in adhesion, invasion, and virulence (Gioffré *et al.*, 2005; Kohwiwattanagun *et al.*, 2007). The function of the *mce* operon in *S. coelicolor* remains undetermined, although from prior research, similarity of the operon to *mce* operons of *Mtb,* and the organism's existence in the highly competitive rhizosphere, a strong case can be made for an ABC transporter assembly which imports sterols. It must also be noted, that given the diverse effects and functions of the *mce* operon copies in *Mtb,* the *mce* operon of *S. coelicolor* may similarly have unpredicted roles in the organism's development, growth, and interaction with other micro-organisms. This chapter aims to investigate phenotypes arising from the disruption of the *mce* operon in an effort to further understand and characterise the function of the Mce proteins in *S. coelicolor.*

The *S. coelicolor* M145 strain functions as a WT proxy in this work and was used as a comparison to an *mce* null strain (Δ*mce*), previously created by Clark (2011). This Δ*mce* strain contains deletions of the first eight genes of the *mce* operon (SCO2422 – SCO2415) (Fig 3.1). Further, to substantiate mutant phenotypes and demonstrate these resulted from Mce protein deletion, a previously created complemented mutant (Δ*mce*+*mce*) was simultaneously tested. This complemented mutant was created via conjugation of the entire *mce* operon, in the vector pLCS006, into the *mce* null mutant

background. The complementing *mce* operon is integrated into an ectopic location at the φC31 *attB* site in the *S. coelicolor* genome (Clark *et al.*, 2013).

An additional copy mutant (M145+mce) was also previously created via conjugation of the *mce* complemented vector pLCS006 into an M145 background, with the additional *mce* operon also introduced ectopically at the φC31 *attB* site (Clark *et al.*, 2013). The resulting strain contains two copies of the *mce* operon (one native, one ectopic) and serves to simulate the existence of multiple *mce* operon copies such as exist in Actinobacteria such as *Mycobacterium*. Investigations of the M145+*mce* strain may potentially provide insights into the function of multiple *mce* operons in Actinobacteria.

The complemented strain, Δ*mce*+*mce*, does not fully complement in all phenotypes

The *mce* operon of *S. coelicolor* is 13.4 kb in size and was re-integrated at an ectopic location in the genome of *mce* null mutant to create the Δ*mce*+*mce* strain. An *mce* complementation vector derived from the cosmid 8A2.1.GO7 containing a Tn*5062* insertion in SCO2423, the gene directly upstream of the *mce* cluster, was used to create both Δ*mce*+*mce* and M145+*mce* strains (Clark, 2011). This allowed the *mce* operon to remain under control of the native promoter. Ultimately, the cosmid was reduced by restriction digest to a 12.9 kb fragment encoding the first 11 genes of the operon and antibiotic selection and was inserted into the ΦC31 *attB* site in the *S. coelicolor* genome of either the Δ*mce* strain (creating the complemented mutant) or M145 (creating the additional copy mutant) via conjugation (Foulston and Bibb, 2010; Clark, 2011; Clark *et al.*, 2013). While the Δ*mce*+*mce* strain is a confirmed complemented mutant and fully sequenced, it nevertheless appears to display select phenotypes more closely resembling that of the Δ*mce* mutant than of WT *S. coelicolor* M145. It is believed this is

due to the ectopic location of the re-introduced *mce* cluster (Clark, 2011). Whilst the *mce* cluster of Δ*mce*+*mce* retains its native promoter, it has been integrated at the ΦC31 *attB* site and is likely expressed non-identically to the native copy due to this difference in chromosomal location. Resultingly, the Δ*mce*+*mce* strain does not behave indistinguishably from the M145 strain and often displays incomplete complementation.

Previously established phenotypes of the Δ*mce* mutant

Various mutant phenotypes of strains (Δ*mce,* Δ*mce*+*mce*, M145+*mce*) have been previously established but not thoroughly analysed. Phenotypes examined include virulence towards protists, resistance to deleterious agents, and plant root colonisation ability (Clark, 2011). As these priorly established phenotypes give rise to further analysis in this work, they are briefly described below.

Spores of the Δ*mce* strains were found to possess an altered spore envelope when viewed under high magnification (10,000x) by scanning electron microscopy. Appendages upon spore chains were indicative of germination in the Δ*mce* mutant whilst absent in the WT M145 strain, thus leading to speculation that the *mce* null mutant may display precocious germination (Clark et al., 2013).

Due to the apparent alteration of the spore envelope, strains were subjected to tolerance assays for SDS and lysozyme, with germlings of the *mce* null mutant shown to demonstrate increased tolerance to both these agents, hypothetically caused by deletions of the *mce* proteins providing more integrity to the cell envelope (Clark et al., 2013).

Deletions of the *mce* operon also resulted in the Δ*mce* mutant demonstrating a hypervirulence phenotype towards the protist *Acanthamoeba polyphaga.* Lysis of the amoeba occurred at approximately 24-hours into co-culture with the Δ*mce* mutant, potentially resulting from precocious germination of spores within the amoeba food vacuole (Clark et al., 2013).

Further, the Δ*mce* strain showed impaired ability to colonise plant roots compared to *S. coelicolor* M145. This was hypothesised to be due to requirement of the Mce proteins in sterol acquisition for bacterial survival in the rhizosphere. This phenotype was fully recovered by complementation as seen with the Δ*mce+mce* strain (Clark et al., 2013).

The following chapter examines and quantifies how sporulation, spore germination and tolerance to deleterious agents in *S. coelicolor* is affected by deletion of the *mce* operon.

A The *mce* operon of *S. coelicolor*

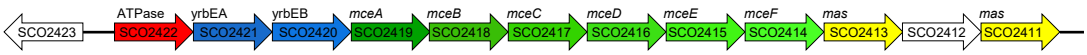

B *mce* null mutant (Δ*mce*)

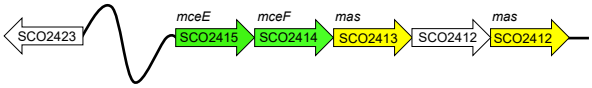

C Complemented vector (pLCS006)

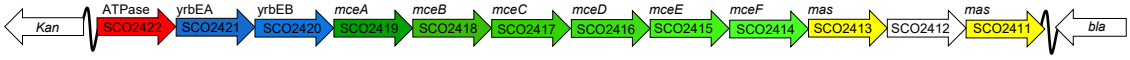

Figure 3.1: Native and mutant operons in *S. coelicolor* (A) The native *mce* operon of *S. coelicolor*, with SCO designations and *Mtb* homologues. **(B)** The *mce* null mutant strain containing a Tn*5062* site and deletions of SCO2422-SCO2414. **(C)** The complemented *mce* operon in pLCS006.

The *mce* operon in *S. coelicolor* encodes a sterol import system

As has been extensively covered in the introduction to this work, the *mce* operons of select Actinobacteria genera have been confirmed to encode sterol importers, and this function may be conserved in *Streptomyces*. Indeed, prior work on the *mce* operon of *S. coelicolor* has indicated involvement of the Mce proteins in sterol import. Expression of the *mce* operon was shown to be abolished in *S. coelicolor* when grown on 0.02% cholesterol, suggesting that this system may act as a high-affinity, low-capacity transporter for sterols, scavenging sterols in conditions of low abundance (Clark, 2011). The *mce* operon also appears necessary for plant root colonisation in a lab-based model, indicating that the *mce* operon aids survival of *Streptomyces* in the rhizosphere, a feat which may be due to utilisation of phytosterols abundant at plant roots (Clark, 2011; Clark *et al.*, 2013)

This study provides further evidence that the *mce* operon of *S. coelicolor* encodes a sterol import system. In media conditions where cholesterol served as a carbon source, growth of the *mce* null mutant was impaired when compared to that of *S. coelicolor* M145 (Fig. 3.2). Deletion of the *mce* operon therefore appears to limit growth of the *mce* null mutant due to a reduced ability to import cholesterol, while *S. coelicolor* M145, containing the native and unmutagenized *mce* operon, shows typical growth in such media. Demonstrating this, specific growth rate of the M145 strain (0.57 h^{-1}) was considerably greater than that of the Δ*mce* mutant (0.09 h^{-1}). Interestingly, the specific growth rates of Δ*mce*+*mce* (0.084 h^{-1}) and M145+*mce* (0.12 h^{-1}) also reflected impaired grow by these strains.

The complemented mutant, Δ*mce*+*mce*, as previously mentioned, often displays incomplete complementation. It is possible that differential expression of the

complemented *mce* operon in this strain limits cholesterol uptake and therefore slows Δ*mce* growth in these conditions. It is less clear why the additional copy mutant, M145+*mce*, shows reduced growth, though this may be explained by expression of the native *mce* operon being impacted by the presence of the ectopic and additional *mce* operon. Potentially, expression of both operons is costly to the bacterium, or alternatively, expression of the native *mce* operon is downregulated due to the presence of the ectopic copy, which, as shown in Δ*mce*+*mce*, may have reduced efficiency in cholesterol importation.

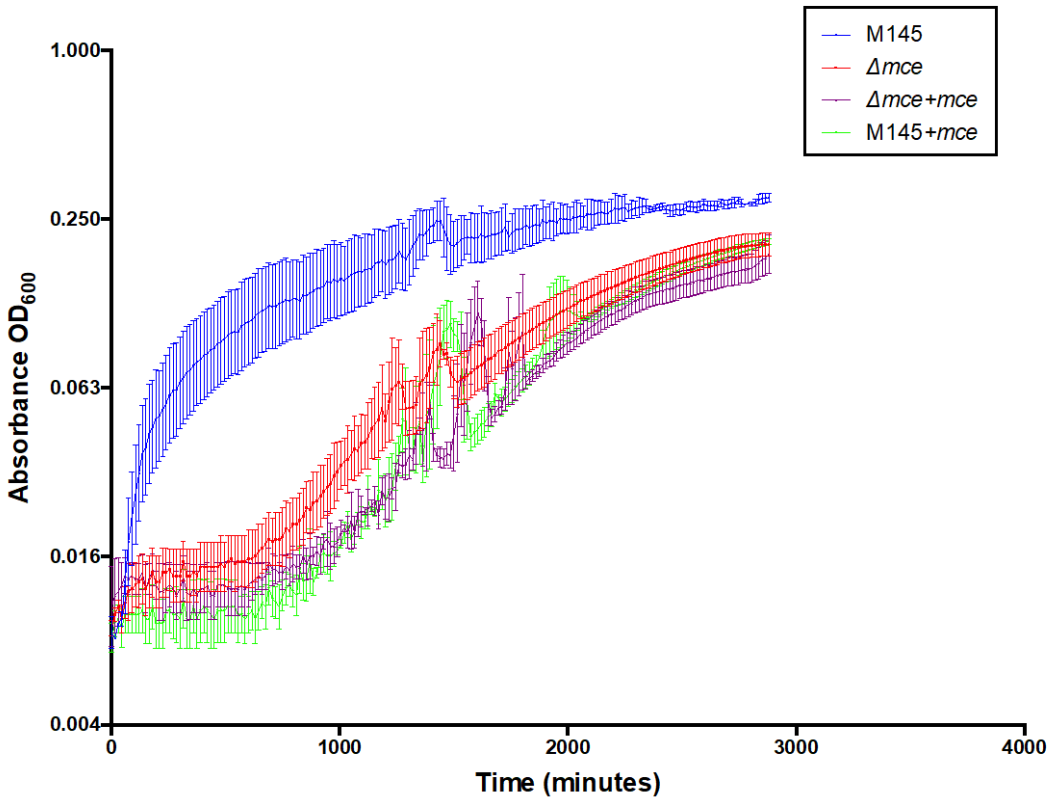

Figure 3.2: Growth of strains in Minimal Media. Growth curve of spores of the M145, Δ*mce*, Δ*mce* +*mce* and M145+*mce* strains in minimal media supplemented with mannitol and addition of 0.193 µg/mL cholesterol. Strains were grown in 96-well plates for a period of 48 hours and absorbance measured at OD_{600}. Multiple comparisons of the growth of the strains via Kruskal-Wallis analysis shows that growth of the *mce*, Δ*mce* +*mce* and M145+*mce* strains are significantly different to that of the M145 strain (****, P< 0.0001) (N=3). Specific growth rate was calculated for M145 (0.57 h^{-1}), Δ*mce* (0.09 h^{-1}), Δ*mce* +*mce* (0.084 h^{-1}), and M145+*mce* (0.12 h^{-1}). Error bars represent standard deviation.

The Δ*mce* mutant displays an altered spore envelope and differential growth to *S. coelicolor* M145

An altered spore envelope phenotype in the *mce* null mutant was previously reported by Clark *et al* (2011, 2013). Scanning electron microscopy (SEM) was used to examine spore chains of the Δ*mce* and *S. coelicolor* M145 strains following identical growth on MS media (Fig. 3.3). Resultant images and analysis showed Δ*mce* spores possessed a "wrinkled" spore coat, with a smaller mean spore diameter, and were prone to collapse (Clark *et al.*, 2013). Furthermore, 'bulges' upon the Δ*mce* spores whilst still on the spore chain appear to be the initiation of germ-tube emergence and implies Δ*mce* spores display a precocious germination phenotype (Clark *et al.*, 2013). Altered cell surface phenotypes have previously and since been observed in response to deletion of Mce proteins. In *E. coli* (K12), a triple *mce* mutant has been found to exhibit cell surface ruffling, potentially caused by disorganisation of the outer membrane (Ekiert *et al.*, 2017). In Actinobacteria, deletion of Mce proteins from *M. smegmatis* results in changes in colony and cell morphology indicative of cell envelope alterations (Klepp *et al.,* 2012). Further, deletions of *mtrAB* results in defective cell walls in *M. avium* and elongated cell shape in *C. glutamicum* (Möker *et al.*, 2004; Cangelosi *et al.*, 2006). The *mtrA*B two-component system is involved in regulation of the *mce* operon in *S. coelicolor* and *M. avium*, with deletions of *mtrA* abolishing expression of the *mce* operon in *S. coelicolor* (Clark *et al.*, 2013). There is therefore a precedent for deletions of Mce proteins causing alterations to the cell envelope.

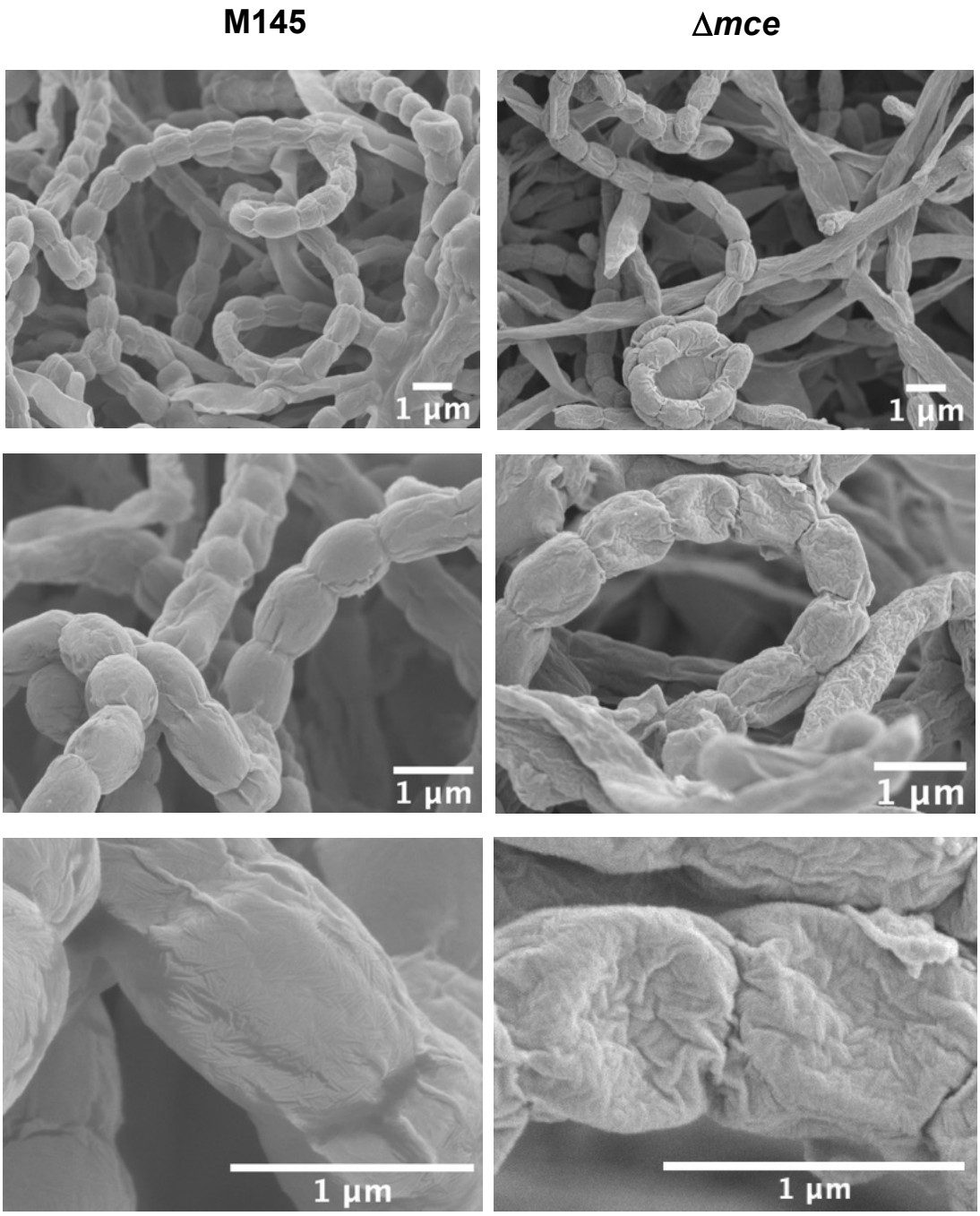

Figure 3.3: Scanning electron microscopy (SEM) images of *S. coelicolor* M145 and Δ*mce* strains grown on MS agar. Spore chains of Δ*mce* showed appendages indicative of precocious germination and 'wrinkled', smaller spores prone to collapse when compared to spores of M145. Images were taken at 10,000x, 20,000x and 60,000x magnification. Images were acquired by Dr Joost Willemse.

In addition to an altered spore coat, the Δ*mce* strain was observed to produce the grey polyketide spore pigment associated with mature spores earlier than M145 *S. coelicolor* (Fig. 3.4). This phenotype was also seen in the complemented mutant, Δ*mce*+*mce,* and the additional copy mutant, M145+*mce*.

When considered alongside the apparent emerging germ-tubes upon spore chains of Δ*mce*, this earlier maturation suggests that the Δ*mce* mutant may exhibit precocious sporulation and germination. Clark *et al* (2011, 2013), has previously proposed a precocious germination phenotype as the mechanism by which the *mce* null mutant displays hypervirulence towards the soil amoebae *Acanthamoeba polyphaga*. Whilst prior germination assays performed by Clark (2011) showed no difference between germination rates of the Δ*mce* and M145 strain, assay sensitivity was technologically limited and was performed in a medium in which precocious germination had not been priorly observed (Clark, 2011).

Figure 3.4: Five days growth of the M145, Δ*mce*, Δ*mce* +*mce* and M145+*mce* strains on MS agar. All strains were streaked in similar fashion and the plate was incubated statically at 30°C. The Δ*mce*, Δ*mce*+*mce* and M145+*mce S. coelicolor* strains show production of the grey polyketide spore pigment earlier than that of the M145 strain.

Δ*mce* spores show increased aggregation in comparison to M145 spores

During routine liquid culture it was observed that spores of the *mce* null mutant appeared to show increased aggregation to those of M145. This was evident as Δ*mce* spores and germlings grouping together and dropping out of suspension in greater quantity and earlier than those of M145.

This phenotype was investigated via aggregation assays carried out in minimal media supplemented with mannitol in cuvettes at 30°C, 180 rpm (Fig. 3.5). Spores were allowed to aggregate and collect at the bottom of the cuvette during the experiment, and cuvettes were not inverted prior to absorbance readings in a spectrometer. Decreases in absorbance were used to indicate increased levels of aggregation in spores.

Resultantly, decreases in absorbance were greater for the Δ*mce* and Δ*mce*+*mce* strains than for M145, indicating increased aggregation in these strains, although a one-way ANOVA finds these differences non-significant ($F_{(3,36)}$= 1.518, *P* = 0.2265 in an ANOVA test). Over the first 80 minutes of the assay, absorbance (600nm) dropped by 76% in the Δ*mce* strain compared to 55% in the M145 strain. The complemented mutant, Δ*mce*+*mce,* displays aggregation at a rate more similar to the *mce* null mutant than M145, dropping in absorbance 69% in the first 80 minutes. However, aggregation in the additional copy mutant, M145+*mce* behaves similarly to in M145, dropping 46% in the first 80 minutes.

Aggregation in germinating spores has been shown to be due to production of extracellular glycans (van Dissel *et al.*, 2015; Zacchetti *et al.*, 2016). It has been

anecdotally noted in this work that plated spores of *S. coelicolor* which have begun to germinate will aggregate, whilst dormant spores do not.

The increased aggregation of Δ*mce* spores may be linked to their altered spore envelope phenotype observed by Clark (2013), as the spore coat provides a hydrophobic and protective sheathe, and therefore, disrupted or damaged spore surfaces may be more adhesive and show increased aggregation. Alternatively, the potential precocious germination of the *mce* spores may result in earlier production of extracellular glycans and thus earlier and increased aggregation.

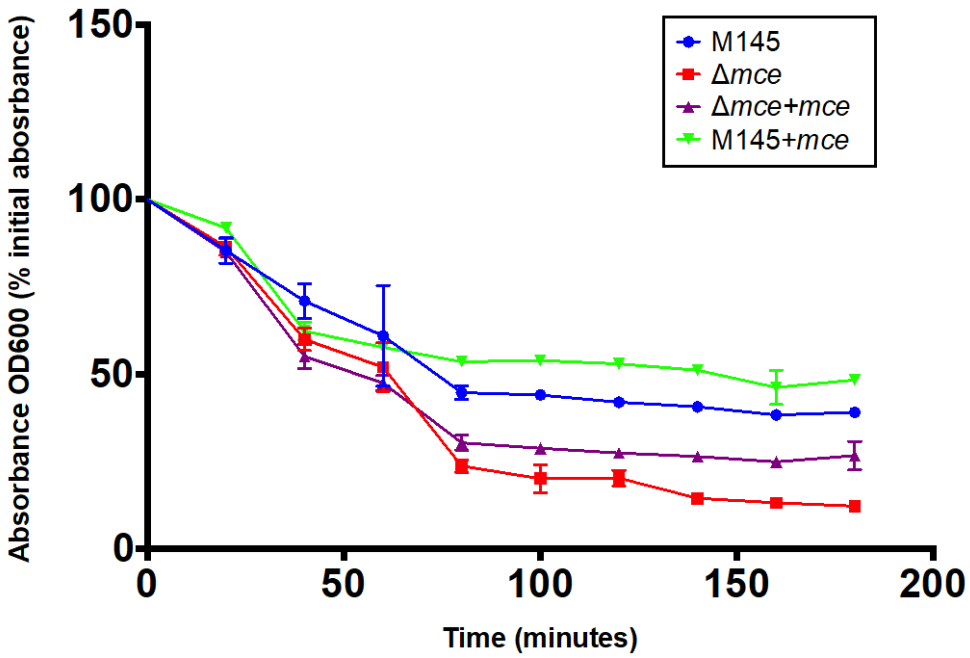

Figure 3.5: Spores of a Δ*mce* mutant show increased aggregation. Aggregation assays were performed in 1mL of minimal media in sterile, sealed cuvettes incubated statically at 30°C. Aggregation was measured via decreases in absorbance at OD_{600}. Graphs show the average of three replicates for each strain. $F_{(3,36)}$= 1.518, *P* = 0.2265 in an ANOVA test. Error bars represent standard deviation.

Precocious sporulation occurs in Δ*mce S. coelicolor*

It was hypothesised that the potential precocious germination phenotype in Δ*mce* spores may also result in earlier spore chain emergence. Impression mount assays were conducted to examine if the Δ*mce* strain displayed precocious sporulation in comparison to M145 *S. coelicolor.* Strains were grown on MS and impression mounts taken at select timepoints for quantification of spore chain number via phase-contrast microscopy. Results show that spore chains emerge earlier in the Δ*mce* and Δ*mce+mce* strains than M145 *S. coelicolor* (Fig. 3.6). The M145+*mce* showed slightly earlier spore chain production when compared to M145, but this was delayed in comparison with the Δ*mce* and Δ*mce+mce* strains. Precocious sporulation therefore occurs in the Δ*mce* strain and is likely a result of precocious germination of spores. The behaviour of the Δ*mce+mce* strain is more similar to that of Δ*mce* than M145, and likely results from the ectopic location of the *mce* cluster in this strain.

The *mce* null mutant does not appear to produce a greater number of spore chains than M145 overall, with spore chain number appearing to equalise in later time points (Fig. 3.7). However, as experimental time progressed, spore chains became more numerous and highly fragmentated which lead to unreliable quantification. For this reason, the experiment was terminated at 60 hours.

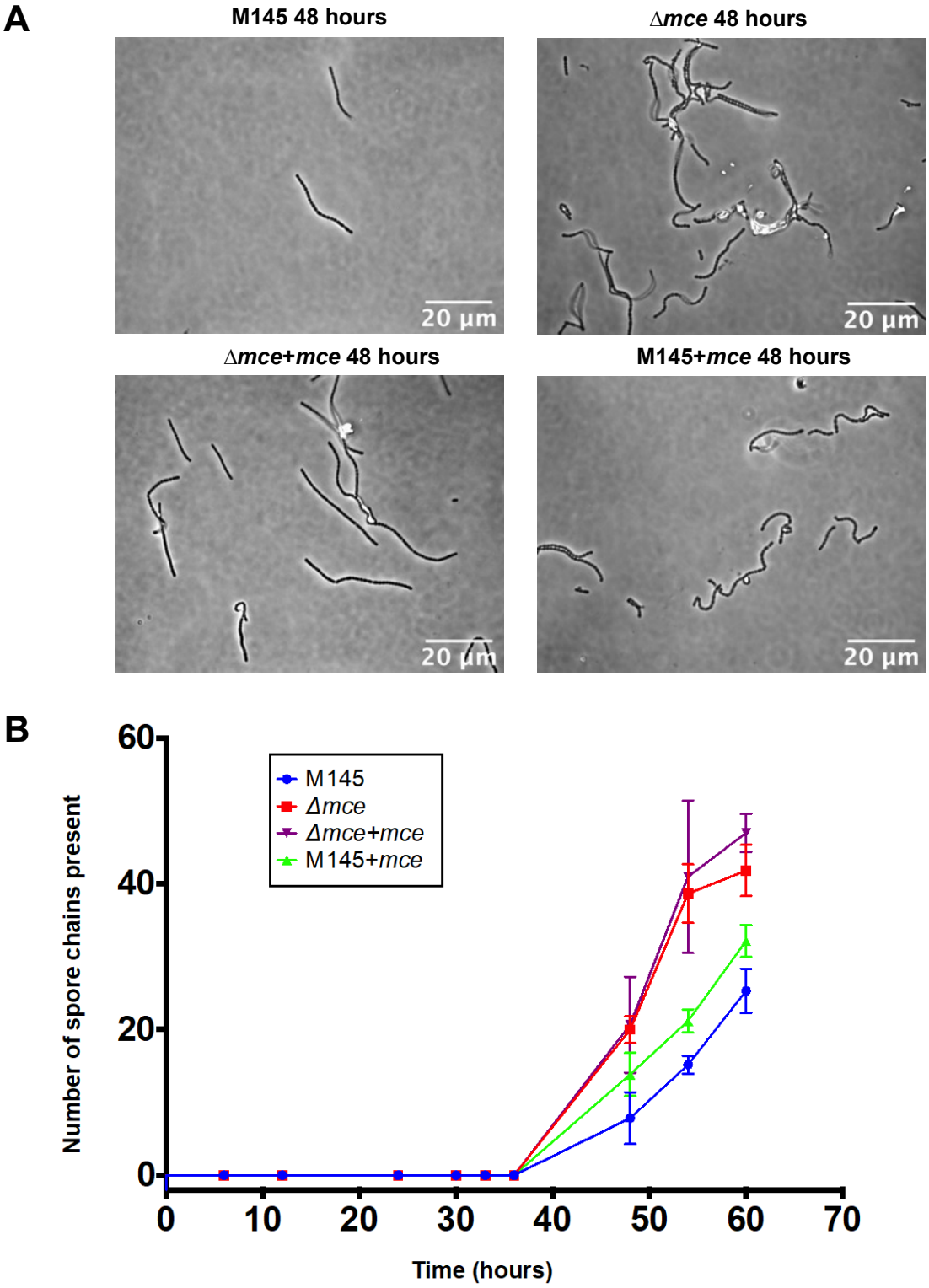

Figure 3.6: Precocious sporulation in the *Δmce* strain. (A) Spore chains from impression mounts of all strains at 48 hours. Images were acquired using an Orca-285 digital camera connected to a Nikon Eclipse TE2000-S microscope equipped with a 100x objective lens and taken in phase contrast. **(B)** Number of spore chains in six fields of view were counted and averaged (N=3). Error bars represent standard deviation.

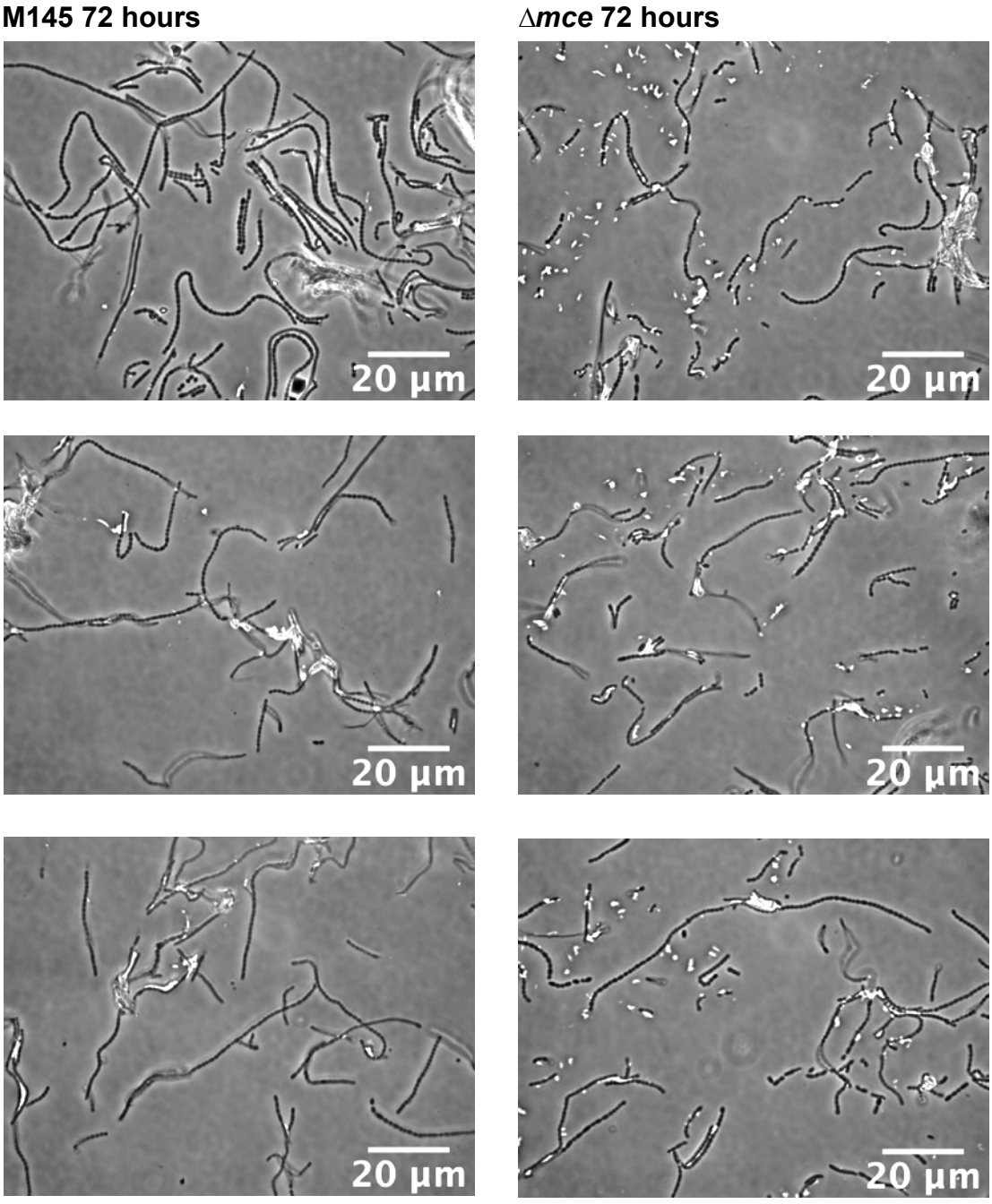

Figure 3.7: Phase contrast images of spore chains from impression mounts of all strains at 72 hours. Spore chains had begun to fragment at this time leading to impeding accurate quantification. Images were acquired using an Orca-285 digital camera connected to a Nikon Eclipse TE2000-S microscope equipped with a 100x objective lens.

The Δ*mce* strain displays a precocious germination phenotype in comparison to WT *S. coelicolor*

Streptomyces spore germination comprises of three stages; darkening, swelling and germ-tube emergence (Hardisson *et al.*, 1978) Darkening involves the reconstruction of the cell wall and results in loss of hydrophobicity, leading to an influx of water into the cell. This continual influx of water causes the spores to swell and enter the second stage of germination in which enzymatic activities of the spore are recovered (Bobek, Šmídová and Čihák, 2017). Swelling of the spore is clearly visible via microscopy when using a 100x objective lens, as is the third stage, when germ tubes emerge by apical tip extension from the spore (Bobek, Šmídová and Čihák, 2017).

Germination assays were performed to directly assess and compare the germination rate of Δ*mce* spores to *S. coelicolor* M145 spores. This assay technique was based on the approach of Haiser *et al* (2009). Briefly, a normalised density of spores was plated on cellophane discs overlaying MS agar plates and grown at 30°C for 7 hours. At select time-points portions of the cellophane discs were excised and viewed on a Nikon Eclipse TE2000-S inverted microscope in phase contrast with a 100x objective lens. This allowed visualisation of spores in various stages: not swollen, swollen, and germinated. Spores were considered to have germinated when an emerging germ tube was clearly visible. This approach had the benefit of using MS medium, on which the differential growth had been observed and on which Δ*mce* spores had been observed to potentially produce germ tubes prematurely upon the spore chain (Clark *et al.*, 2013).

To ensure that assay sample size was sufficient, three fields of view were taken for each strain at each time point, resulting in assessment and scoring of >200 spores per field of view. Use of a self-scoring software was initially employed, however, this was shown to be ineffective at correctly detecting germlings and was thus abandoned in lieu of manual scoring.

At 4 hours, observation through phase contrast microscopy showed the majority of spores of the Δ*mce* strain were visibly swollen, therefore indicating that germination machinery had been switched on and spores were preparing for germination (Fig. 3.8). A small number of Δ*mce* spores also showed early germ tube emergence. Swelling was also apparent in spores of the Δ*mce*+*mce* strain at 3 hours, whilst M145 and M145+*mce* spores showed limited-to-no signs of swelling.

By 6 hours, a clear difference in number and length of germ tubes of Δ*mce* spores to M145 spores can be seen, indicative that Δ*mce* spores had germinated earlier and were further advancing in growth. At 7 hours, spores of the *mce* null mutant have produced germ tubes of considerable length, and by 7.5 hours, Δ*mce* growth had become so dense as to obstruct accurate quantification of germ tube number, leading to termination of the experiment.

Germination assay results showed a clear difference in germination rate of the *mce* null mutant strain in comparison to M145 *S. coelicolor*, confirming that the Δ*mce* strains displays precocious germination (Fig. 3.9). This corroborates previous SEM images in which spores of the *mce* null mutant appeared to be germinating prematurely upon the spore chain. Similarly, this phenotype is likely the mechanism via which the Δ*mce* strain

displays enhanced virulence towards *Acanthamoeba*, with earlier germination resulting in intracellular hyphal growth causing lysis the amoeba (Clark *et al.*, 2013).

It is unclear why loss of the Mce proteins would lead to precocious germination in *S. coelicolor*, though it seems likely this phenotype may be related to the altered spore coat detected via SEM imaging (Clark *et al.*, 2013). Similar phenotypes resulting from deletion of Mce proteins have been demonstrated in other Actinobacteria members, such as altered cell envelopes and defective cell walls seen in *M. smegmatis* and *M .avium* respectively (Möker *et al.*, 2004; Klepp *et al.*, 2012). Such effects likely indicate the localisation of Mce proteins to the cell wall, as has shown to be the case for Mce1 proteins of *Mtb* (Fenn, Wong and Darbari, 2020). The localisation of the Mce proteins in *S. coelicolor* will be examined in depth in Chapter 5 of this work.

Defective cell envelopes have been previously linked with precocious germination in *S. coelicolor*. The deletion of DasA (a sugar-binding component of the chitobiose ABC system) in *S. coelicolor* results in premature germination upon spore chains which is theorised to be the result of weakened cell walls. Scanning electron micrographs of the *dasA* mutant on MS agar show 'unusual branches' which are highly similar to the protrusions seen on ∆*mce* spores with SEM (Colson *et al.*, 2008). A *S. coelicolor lsp* (lipoprotein signal peptidase) mutant was shown to exhibit an altered spore envelope and spores with abnormal size which germinated upon spore chains. This was theorised to be due to the loss of lipoproteins from the cytoplasmic membrane producing pleiotropic phenotypes (Thompson *et al.*, 2010). Furthermore, deletions of MreB, an actin homologue important for cell wall formation and determining cell shape, results in severely compromised spore envelopes. Loss of spore wall consistency was evidenced by irregularly shaped spores which collapsed and were otherwise dented or broken.

These spores were swollen in size compared to WT spores, and showed premature germination on spore chains (Mazza *et al.*, 2006).

Mechanical disruption is a known stimulus leading to germination activation in *Streptomyces* spores, and thus premature germination could be due to defective cell envelopes leaving spores more prone to mechanical damage (Čihák *et al.*, 2017). It is also possible that this defective cell envelope phenotype leaves *Streptomyces* spores in a quasi-dormant, quasi-active state, where they are neither fully dormant, nor fully active as vegetative cells. Break-down of the spore coat, or 'uncoating' occurs relatively early in the germination process, and mutations of cell wall hydrolyses controlling this process have been shown to slow germination (Haiser, Yousef and Elliot, 2009; Bobek, Šmídová and Čihák, 2017). It may be that the *mce* null mutant, with its altered and possibly defective spore wall, exists in a partially dormant, partially activated state and is quicker to germinate due to this fact.

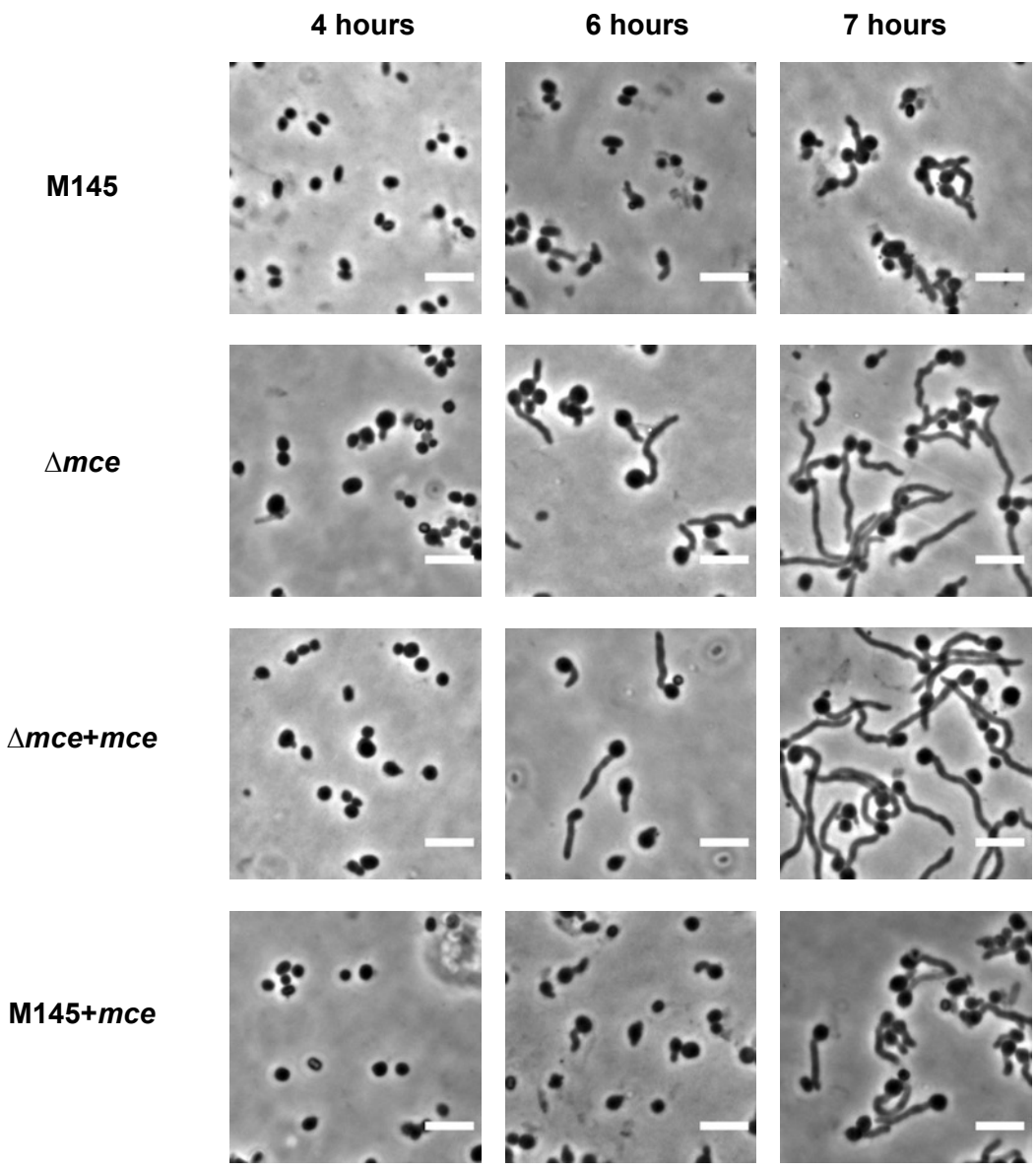

Figure 3.8: Precocious germination of the Δ*mce* strain. Phase contrast images of M145, Δ*mce,* Δ*mce* +*mce* and M145+mce spores excised on cellulose from MS agar plates. Images were taken at 4, 6 and 7 hours into incubation. Images were acquired using an Orca-285 digital camera attached to a Nikon Eclipse TE2000-S inverted microscope equipped with a 100x objective lens. Scale bar represents 5 µm.

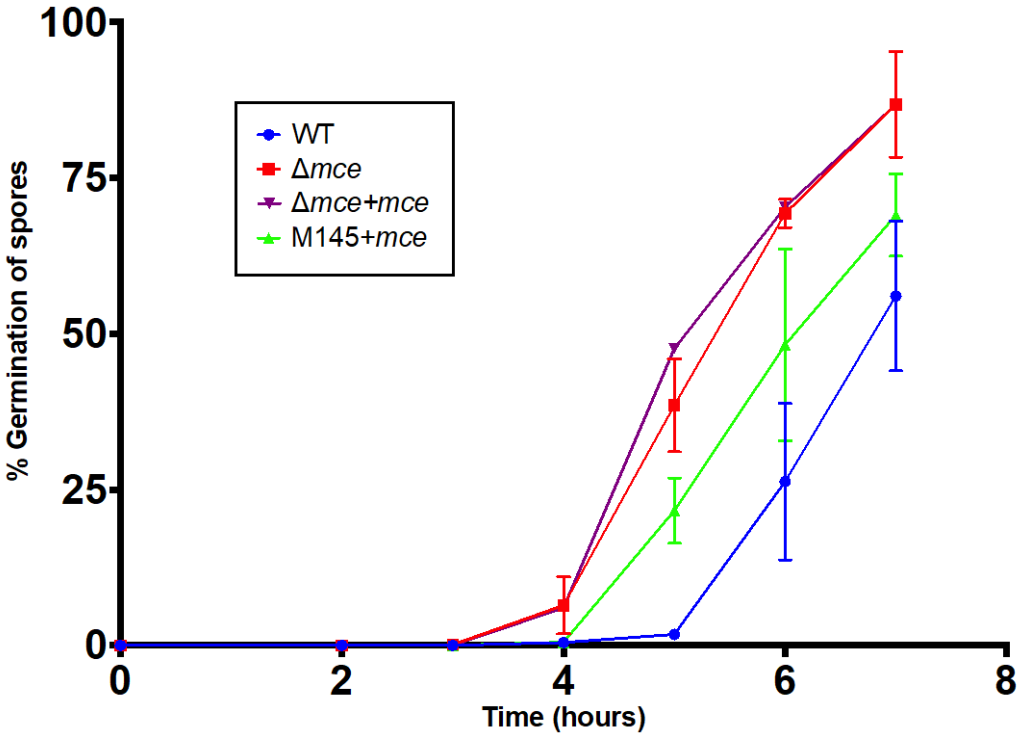

Figure 3.9: Precocious germination of the Δ*mce* strain. Germination assay comparing percentage germination over time of spores of the M145, Δ*mce,* Δ*mce+mce* and M145+*mce* strain. Spores were spread on cellulose discs overlaying MS agar plates and incubated at 30°C. Three fields of view containing >200 spores were scored for evidence of germination (N=3). Error bars represent standard deviation.

The Δ*mce* mutant may overproduce Actinorhodin

Actinorhodin (ACT) is a blue-pigmented antibiotic produced by *S. coelicolor* A3(2), which is capable of undergoing a reversible colour change from blue in alkaline conditions to red in acidic conditions (Nass *et al.*, 2017). Accordingly, ACT is often used a phenotypic marker in *S. coelicolor* research.

It was observed during growth of strains on various media, in both suspension and on solids, that the Δ*mce* mutant appeared to produce ACT in excess and earlier than the M145 strain (Fig. 3.10.A).

To quantify this observation, ACT production assays were performed in YEME, a medium in which *S. coelicolor* shows substantial ACT production (Elibol, 2004). As cell biomass affects actinorhodin production, cell dry weight measurements were also taken and the actinorhodin yield of each strain per gram of cell dry weight (CDW) calculated.

Actinorhodin production, as monitored via absorbance at OD_{600}, was seen in all strains from 40-48 hours into culture (Fig. 3.10.A), with extracellular medium from the Δ*mce* mutant culture displaying substantially higher absorbance than that of the M145 strain.

Results show that the Δ*mce*+*mce* strain appears to produce more ACT than the M145 strain, but less than the *mce* null mutant, again potentially an intermediate phenotype arising from the ectopic *mce* operon. However, interestingly, the M145+*mce* strain produces more ACT than either M145 or Δ*mce*+*mce,* though less than the *mce* null mutant.

CDW was measured at each time-point over the 160 hours that the experiment was run and does not show considerable differences in biomass produced between strains that would give rise to differential actinorhodin production (Fig. 3.10.B)

Following this, actinorhodin yield per gram of CDW was calculated, with the *mce* null mutant showing the greatest ACT production per gram of CDW (Fig. 3.10.C) The M145 strain produced the lowest yield of ACT, with the complemented mutant, Δ*mce*+*mce* producing an ACT amount intermediatory between the *mce* null mutant and M145. Interestingly, it is the M145+*mce* mutant which produces the second greatest yield of ACT.

Although the difference in ACT production seen in the Δ*mce* strain was not found to be statistically significant to that of *S. coelicolor* M145, this is likely a reflection of the small sample number (N=3) and technical issues arising from the assay leading to results which do not reflect the overproduction phenotype seen in media and on plates. Given the clarity of differences observed in ACT production during laboratory growth, this phenotype would benefit from further exploration utilising a far greater sample size, as it appears likely that the Δ*mce* strain does, indeed, overproduce ACT.

(i)

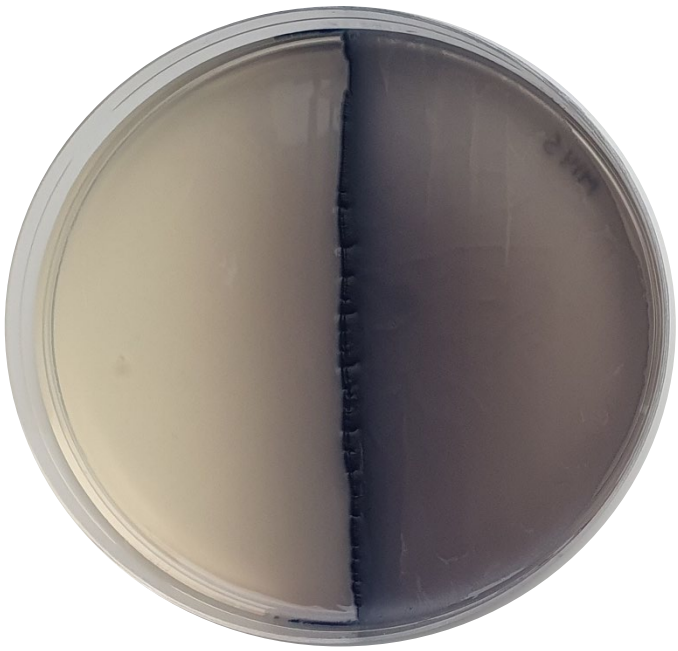

(ii)

Figure 3.10: (A) Growth and ACT production of *S. coelicolor* M145 and Δ*mce* on nutrient agar after ten days incubation. (i) *S. coelicolor* M145 streaked on one half of a nutrient agar plate showing ACT production. **(ii)** *S. coelicolor* Δ*mce* streaked on one half a nutrient agar plate showing ACT production.

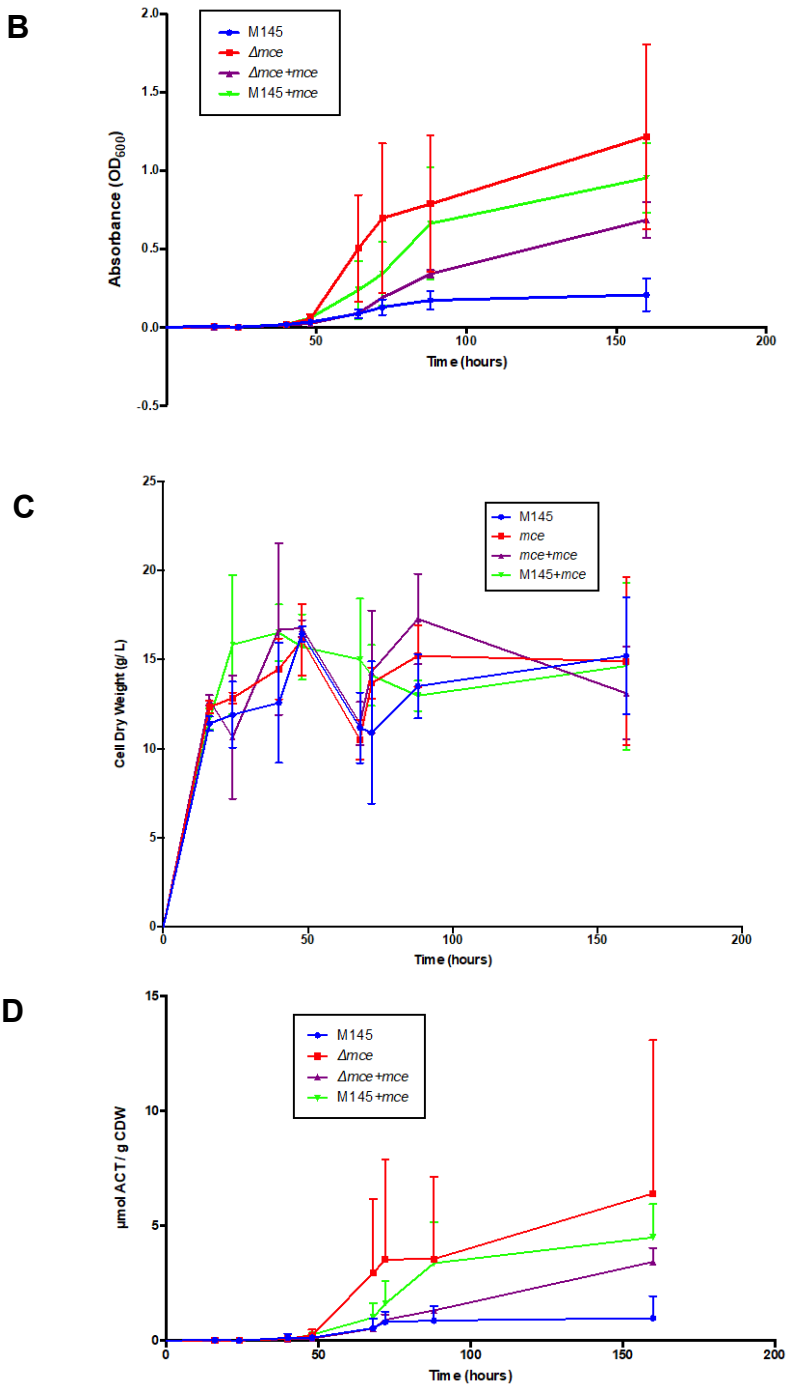

Figure 3.10: Extracellular actinorhodin production of strains. (B) Extracellular actinorhodin production of strains was measured via absorbance at OD_{600} (N=3) over a period of 160 hours. **(C)** Cell dry weight was measured (N=3) for each time point over a period of 160 hours. **(D)** Yield of actinorhodin (µmol) given per gram of CDW for strains over a period of 160 hours. Data was analysed using an Ordinary one-way ANOVA, which found the ACT yield between strains non-significant ($F(3,32)=1.542$, $P=0.2227$) (N=3).

Actinorhodin production, similar to that of other secondary metabolites, is controlled via a complex cascade of regulatory factors (Bruheim *et al.*, 2002). It is closely linked with *Streptomyces* growth, with production in suspension being growth phase dependent and production on solid media coinciding with the formation of aerial hyphae (Bibb, 2005; Hoskisson and Fernández-Martínez, 2018). As was found in this work, ACT production typically becomes evident around 40-48 hours, although culture conditions can greatly impact onset and quantity of ACT production (McArthur and Bibb, 2008; Nieselt *et al.*, 2010). As there is a shift between growth and production phases of growth, accompanied by a series of transcriptomic and proteomic changes, ACT production is thought to usually occur at the onset of stationary phase (Nieselt *et al.*, 2010)

There is no established association between the *mce* operon of *S. coelicolor* and ACT production, however given the current understanding of links between secondary metabolite production and development, it is possible that the overproduction of ACT seen in the *mce* null mutant may be related, in part, to the precocious sporulation and germination phenotype of this strain. Physiological stress has been shown to impact ACT production, as have nutrient limitation and reduced growth opportunities (Bibb, 2005). Expression of secondary metabolites is known to be stimulated in response to biotic and abiotic stressors, and it is possible that the *mce* null mutant, which is under increased stress due to its altered cell envelope, may respond by overproducing ACT (Yoon and Nodwell, 2014).

However, as the M145+*mce* strain germinates and sporulates more slowly than the Δ*mce*+*mce* strain, yet produces more ACT, this may not be the entire explanation. It is possible that the integration of a secondary, ectopic *mce* operon, provides a trigger for greater ACT production in the M145+*mce* strain, potentially due to increased stress on the bacterium. However, given the complexity of secondary metabolism regulation, it may be reductive at this point to speculate further without additional testing.

Δ*mce* spores are more susceptible to heat than M145 spores and do not undergo heat activation

The *Streptomyces* spore envelope serves as a protective layer for the genetic material, being moderately resistant to stressors such as desiccation, heat and physical damage (Sigle *et al.*, 2015; Bobek, Šmídová and Čihák, 2017). Alterations of the spore envelope have accordingly been shown to reduce tolerance to stressors, and uncoating of the spore during germination results in loss of heat resistance (Bobek, Šmídová and Čihák, 2017). It was therefore hypothesised that the altered spore coat and precocious germination phenotype seen in the *mce* null mutant may result in increased heat susceptibility of spores of the Δ*mce* mutant.

To determine whether Δ*mce* spores showed increased susceptibility to heat, heat-kill assays were performed based on the approach by Hoskisson *et al* (2000). Heat-kill assays are able to determine spore heat tolerance via quantification of viable spores, through production of colony forming units (CFU), after exposure to varied temperatures. In this study, a range of temperatures were used to determine overall heat resistance of the *mce* null mutant in comparison to M145.

Streptomyces spores are known to be tolerant of heat up to 50°C, with heating spores for 10 minutes at 50°C a method commonly used to initiate and synchronize spore germination (Kieser *et al.*, 2000). Therefore 50°C was the temperature initially tested in heat-kill assays, with spores of all strains all surviving well at this temperature for considerable periods. Further testing showed that temperatures of 60°C and upwards were capable of killing spores from all strains. Temperatures of 90 and 100°C, at which spore death is exceptionally rapid, were tested to confirm the trends seen in lower temperatures (Fig 3.10).

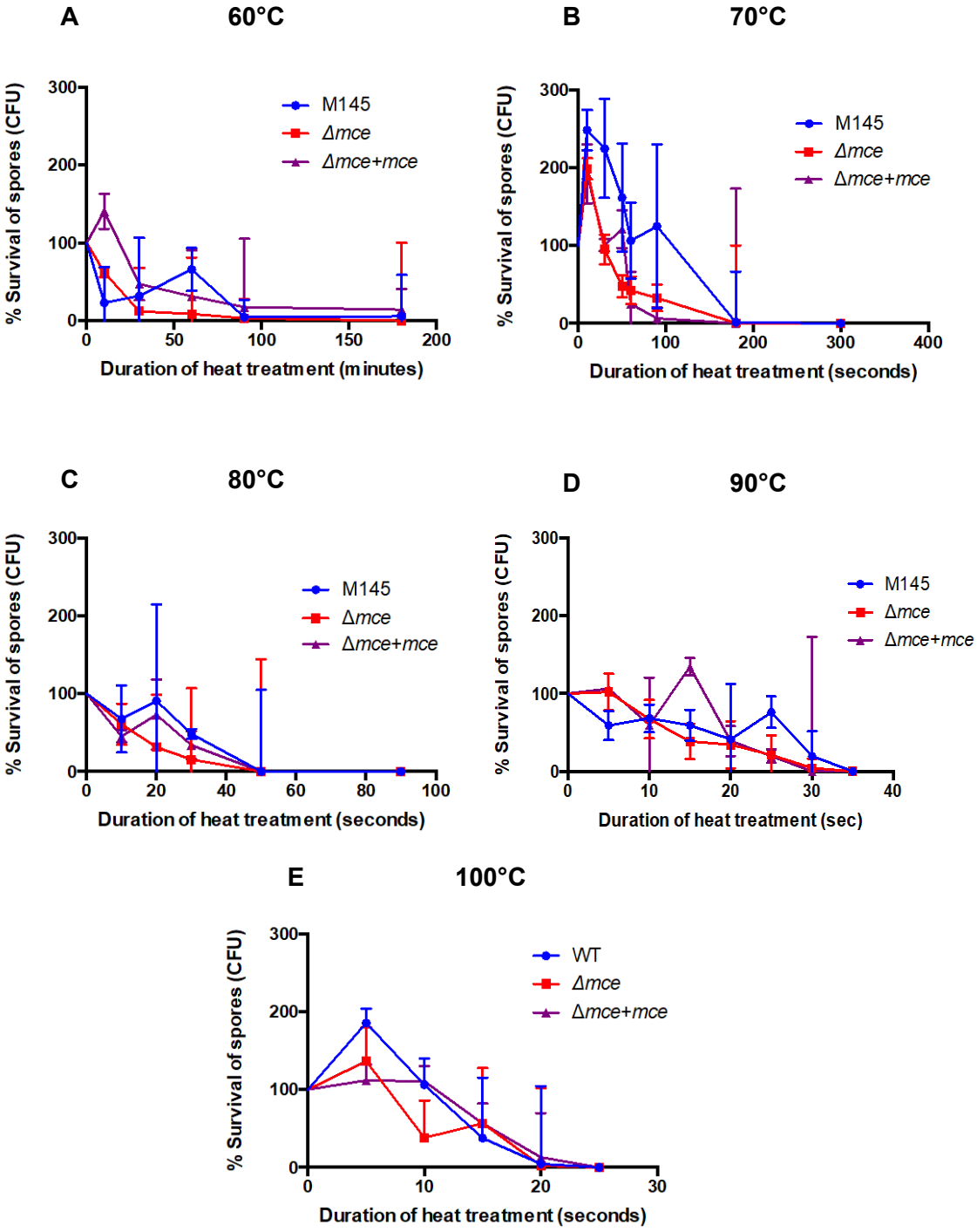

Figure 3.11: Effect of exposure of M145, Δ*mce* and Δ*mce+mce* spores to varying temperatures on colony forming units (CFU). CFU is expressed as a percentage of CFU prior to heat-treatment. **(A)** Percentage CFU after treatment of spores at 60°C for 180 minutes. **(B)** Percentage CFU after treatment of spores at 70°C for 300 seconds. **(C)** Percentage CFU after treatment of spores at 80°C for 90 seconds. **(D)** Percentage CFU after treatment of spores at 90°C for 35 seconds. **(E)** Percentage CFU after treatment of spores at 100°C for 25 seconds (N=3). Error bars represent standard deviation.

The decimal reduction values (D-values) were calculated for each strain, at each temperature, and represent the time taken in minutes to kill 90% of the organisms at the specified temperature (Table 3.1).

D-values are typically calculated as described by Roberts and Hitchins (1969) and involve calculation of the inverse reciprocal of the slope. However, unlike typical heat-kill curves displayed by Gram-negative organisms, data analysis of heat-kills in *Streptomyces* is complicated by the heat-activation phenomenon of *Streptomyces* spores. This is further complicated in the case of the above assays, as the Δ*mce* mutant does not undergo heat-activation whilst both M145 and Δ*mce*+*mce* strains do. The result of activation on M145 and Δ*mce*+*mce* leads to more rapid declines in CFU than is seen in the *mce* null mutant, despite Δ*mce* showing overall lower CFU. This more rapid decline effects the D-values, which are calculated from the average CFU for each strain using D = t / (logN0-logNt), where t represents time.

More considerable differences in D-values between mutant and M145 are seen at lower temperatures; 60°C and 70°C. M145 spores must be heated at 60°C for 70 minutes longer than Δ*mce* spores to reduce CFU 90%. At 70°C, M145 spores must be heated for 17 seconds longer than Δ*mce* spores to reduce CFU 90%. As temperatures increase, D-values are more effected by the rapid fluctuations in CFU. This is particularly true for 90 and 100°C, where samples were taken just seconds apart. The apparent heat-activation of the *mce* null mutant spores at 100°C is likely an artefact of this method being affected by extremely small sampling durations which are prone to error. However, the 90 and 100°C heat-kills serve to confirm the overall trends seen in heat-kills; the increased heat susceptibility of Δ*mce* spores.

Table 3.1: D-values of M145, Δ*mce* and Δ*mce+mce*

D-value	M145	Δ*mce*	Δ*mce+mce*
D_{60} °C	146.04	76.03	212.99
D_{70} °C	1.44	1.27	1.19
D_{80} °C	0.24	0.23	1.07
D_{90} °C	0.71	0.37	0.18
D_{100} °C	0.25	0.21	0.38

Heat-kills show the reduced heat-resistance of the *mce* null mutant spores in comparison to M145 spores clearly, with a partial complementation of the Δ*mce+mce* mutant to M145 *S. coelicolor* spores. Across all temperatures tested, Δ*mce* spores showed increased susceptibility to heat, as exhibited by reduced percentage survival of CFU. Also notable is the absence of heat-activation phenomenon in the *mce* null mutant as compared to M145 and Δ*mce+mce*. This lack of heat-activation is dually indicative; firstly, it further confirms the increased heat-susceptibility of the Δ*mce* spores, with spores continually losing viability upon exposure to heat, rather than undergoing the germination activation. Secondly, it suggests that Δ*mce* spores exist in an intermediary state between 'dormant' and 'active', where they are less heat-resistant than fully dormant spores and more heat-resistant than fully active spores. This spore state and its effect on heat-resistance can be clarified via examination of the heat response of M145 *S. coelicolor* spores. Prior to heat-activation, M145 spores display greater resistance to heat, likely due to their dormancy and intact spore envelope. However, once heat-activation occurs, M145 spores rapidly loose this heat-resistance resulting in more steeply inclining slopes for heat-kills, as germinating and vegetative-cells are considerably more susceptible to heat than their dormant spore counterparts (or semi-dormant spore counterparts) (Haiser, Yousef and Elliot, 2009; Čihák *et al.*, 2017). It is well documented that germination of spores results in loss of heat resistance, thus it is not unexpected that the *mce* null mutant, displaying a precocious germination phenotype, shows reduced tolerance to heat (Bobek, Šmídová and Čihák, 2017).

A further consideration which might affect spore heat-tolerance, and which may be linked to the precocious germination phenotype, is the altered spore coat of *mce* null mutant spores. As mentioned, the Δ*mce* strain produces spores with 'wrinkled' coats which have a smaller mean diameter than M145 spores and are more prone to collapse, as Mce

protein deletion appears to effect the *Streptomyces* cell envelope (Clark *et al.*, 2013). Mutations leading to altered spore walls in *Streptomyces* spores have been previously shown to increase stress sensitivity (McCormick and Flärdh, 2012). Deletions of MreB, as previously mentioned, results in *Streptomyces* spores which possess severely compromised spore envelopes, prone to collapse, denting and breakage due to loss of spore wall consistency. These spores demonstrated increased sensitivity to both heat and SDS (Mazza *et al.*, 2006). Conclusions reached by one study were that deletions of the Mre proteins in *S. coelicolor* resulted in lack of integrity to the cell wall, leading to influx of water and swelling of spores, loss of resistance to deleterious conditions and premature germination (Kleinschnitz, Heichlinger, *et al.*, 2011). It is therefore possible that the reduced heat-resistance of the *mce* null mutant may be due to alterations in the cell wall from deletions of the Mce proteins, conjunctly with the precious germination phenotype of Δ*mce.*

Deletions of the *mce* operon result in increased susceptibility to triclosan in YEME and Minimal Media

In order to determine whether deletion of the *mce* operon effects susceptibility to other stressors and detergents, spores of the Δ*mce* strain were grown in increasing concentrations of triclosan.

Triclosan is an antimicrobial agent which disrupts fatty acid biosynthesis and has been shown to potently inhibit *S. coelicolor* growth (Craney *et al.*, 2012). It was hypothesised that the *mce* null mutant may prove more tolerant of triclosan than the M145 strain, given previously obtained results with SDS and lysozyme (Clark *et al.*, 2013). However, as triclosan is also an inhibitor of fatty acid biosynthesis, it was also considered that the *mce* null mutant might instead show reduced tolerance to triclosan, as the *mce* null mutant is already constrained in its ability to uptake lipids due to deletion of the *mce* operon.

Triclosan testing was originally carried out in YEME rich media and, following a range of concentrations being tested, spores were exposed to 0 – 10 ug/mL triclosan whilst growth was measured over a 48 hour period (Fig. 3.11). Results show that *S. coelicolor* is highly susceptible to killing from even low levels of triclosan, however spores of the Δ*mce* and M145+*mce* strain were considerably more susceptible than M145 and complemented mutant, Δ*mce*+*mce*. A triclosan concentration of 0.625 ug/mL was enough to entirely inhibit growth of Δ*mce* and M145+*mce* spores, whilst spores of M145 and Δ*mce*+*mce* were able to grow to an OD_{600} of approximately 0.2 in a concentration of up to 5 ug/mL triclosan. At a concentration of 10ug/mL triclosan, Δ*mce*+*mce* was again able to grow to an OD_{600} of approximately 0.2, however, the maximum growth spores of M145 were able to achieve were approximately 0.1 OD_{600}. In the absence of triclosan, M145 and Δ*mce* strains demonstrated a specific growth rate of 0.4 h^{-1} and 0.42 h^{-1} respectively, however, upon the addition of triclosan at a concentration of 2.5 ug/mL, the growth of Δ*mce* was entirely abolished and interestingly, the specific growth rate of M145 spores increased to 0.53 h^{-1}, although growth did not achieve the same optical density.

Growth of the Δ*mce* strain was entirely abolished in the presence of triclosan, thus suggesting that deletion of the Δ*mce* operon results in reduced lipid uptake, which, when coupled with the inhibitory effect of triclosan on fatty acid biosynthesis, is prohibitory to cell growth. Interestingly, growth of the M145+*mce* strain is also completely inhibited by the presence of triclosan at 0.625 ug/mL and upwards. Such a result may indicate a less stable, potentially more permeable cell envelope due to the addition of extra Mce proteins. It appears therefore, that if spores of the Δ*mce* strain have increased cell envelope stability that increases tolerance to certain stressors, this advantage is counteracted by inhibition of fatty acid biosynthesis in the absence of the *mce* operon.

The slightly increased growth rate of the M145 strain in 2.5 ug/mL compared to 0 ug/mL triclosan seems to indicate a stress response which seeks to compensate for the presence of triclosan. However, if such a stress response is upregulated in the M145+*mce* and ∆*mce* strain, it is insufficient to rescue bacterial growth.

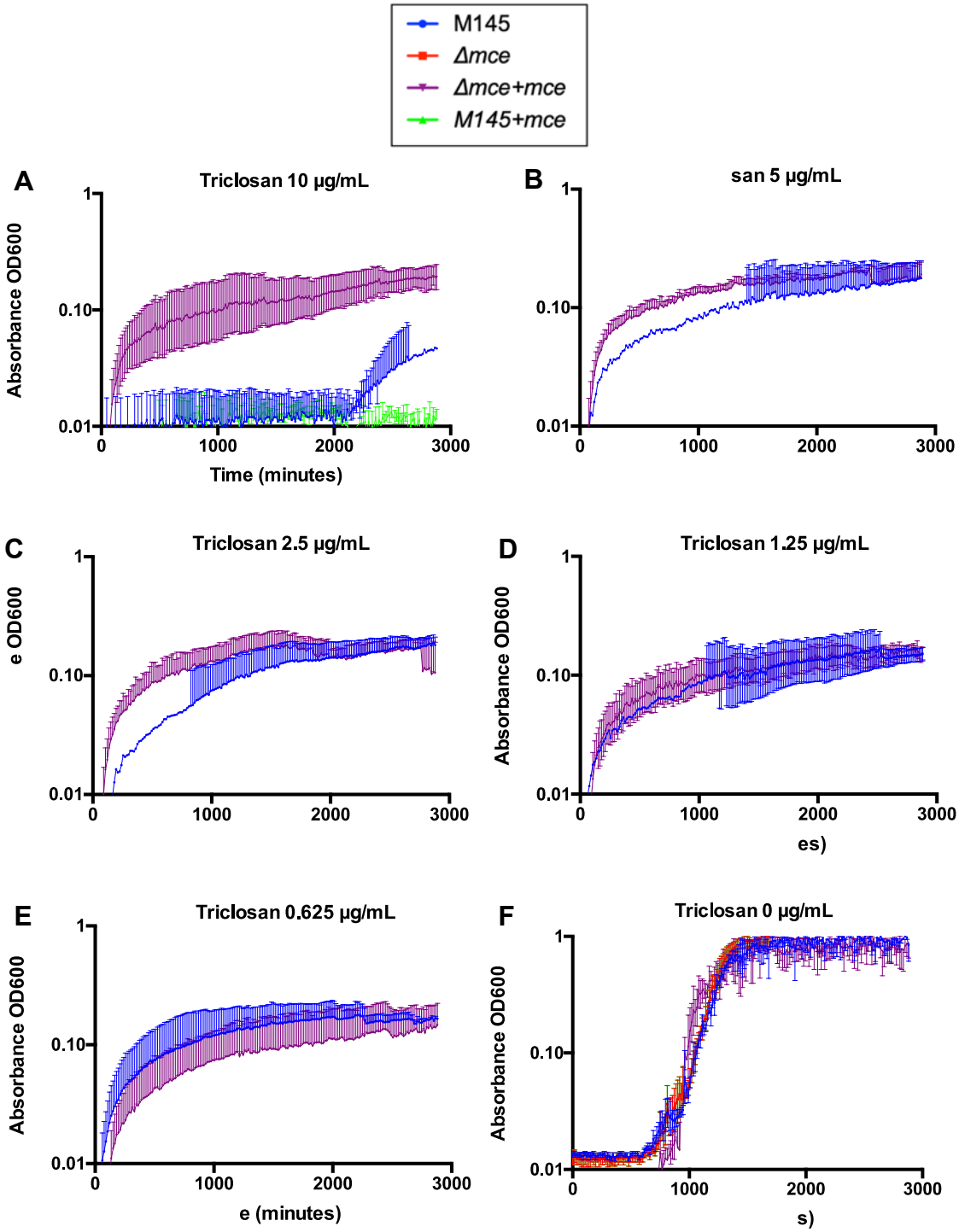

Figure 3.12: Growth curves of M145, Δ*mce,* Δ*mce+mce* and M145+*mce* strains in YEME with decreasing concentrations of Triclosan. Growth was measured by absorbance measurements at 600nm in a microplate reader over a period of 48 hours (N=3). **(A)** Strain growth in YEME with triclosan at a concentration of 10 µg/mL. **(B)** triclosan Strain growth in YEME with triclosan at a concentration of 5 µg/mL. **(C)** Strain growth in YEME with triclosan at a concentration of 2.5 µg/mL.**(D)** Strain growth in YEME with triclosan at a concentration of 1.25 µg/mL. **(E)** Strain growth in YEME with triclosan at a concentration of 0.625 µg/mL **(F)** Strain growth in YEME with triclosan at a concentration of 0 µg/mL. Error bars represent standard deviation.

It was hypothesised that YEME, as a nutrient rich medium, potentially obfuscated the effect of triclosan on spores and thus the experiment was performed in minimal media supplemented with mannitol. Under these nutrient limited conditions, it was possible that *mce* operon expression would be upregulated. A concentration of 2.5 ug/mL triclosan was used, as this appeared to optimally display the difference in survival and growth between M145 and Δ*mce* strains (Fig. 3.12)

It was hypothesised that growth in minimal medium might more strongly activate the *mce* operon of M145, Δ*mce*+*mce* and M145+*mce,* leading to increased growth and accordingly higher absorbance readings, should the *mce* operon be able to compensate for inhibition of lipid biosynthesis. However, growth of strains in minimal media with triclosan were highly similar to those in YEME with triclosan, with spores of M145 and M145+*mce* displaying growth to an OD_{600} of approximately 0.2. However, as minimal media is nutrient poor and bacteria typically display reduced growth rate in this medium compared to growth in YEME (as seen in 0 ug/mL triclosan controls), this itself may signify an increased expression of the *mce* operon which may be providing an advantage.

Interestingly, M145 appeared to show reduced growth in minimal media in the absence of triclosan, with OD_{600} reaching approximately 0.1 - 0.15, compared to 2.0 when in minimal media with triclosan (Fig. 3.12, B). This may possibly be explained by the inhibition of fatty acid biosynthesis resulting in stress responses being triggered to compensate for the presence of triclosan. It is possible that one of these responses may be upregulation of *mce* operon expression, allowing for successful growth of the bacterium in the non-mutagenized M145 strain.

Concurrently, spores of Δ*mce* and Δ*mce+mce* were once again unable to grow in the presence of 2.5 ug/mL triclosan. Both strains grew typically in the absence of triclosan in minimal media (Fig. 3.13). This result is not unexpected, given that a nutrient poor media, combined with an inability to biosynthesis fatty acids, is likely more detrimental to bacterial growth than in a nutrient rich medium. In the case of the M145+*mce* strain, it appears that even with the possibility of increased *mce* expression compensating for fatty acid biosynthesis inhibition, this is not able to offset the deleterious effects of triclosan. This may be due to an increased amount of triclosan permeating the cell wall of the M145+*mce* mutant, more so than with other strains.

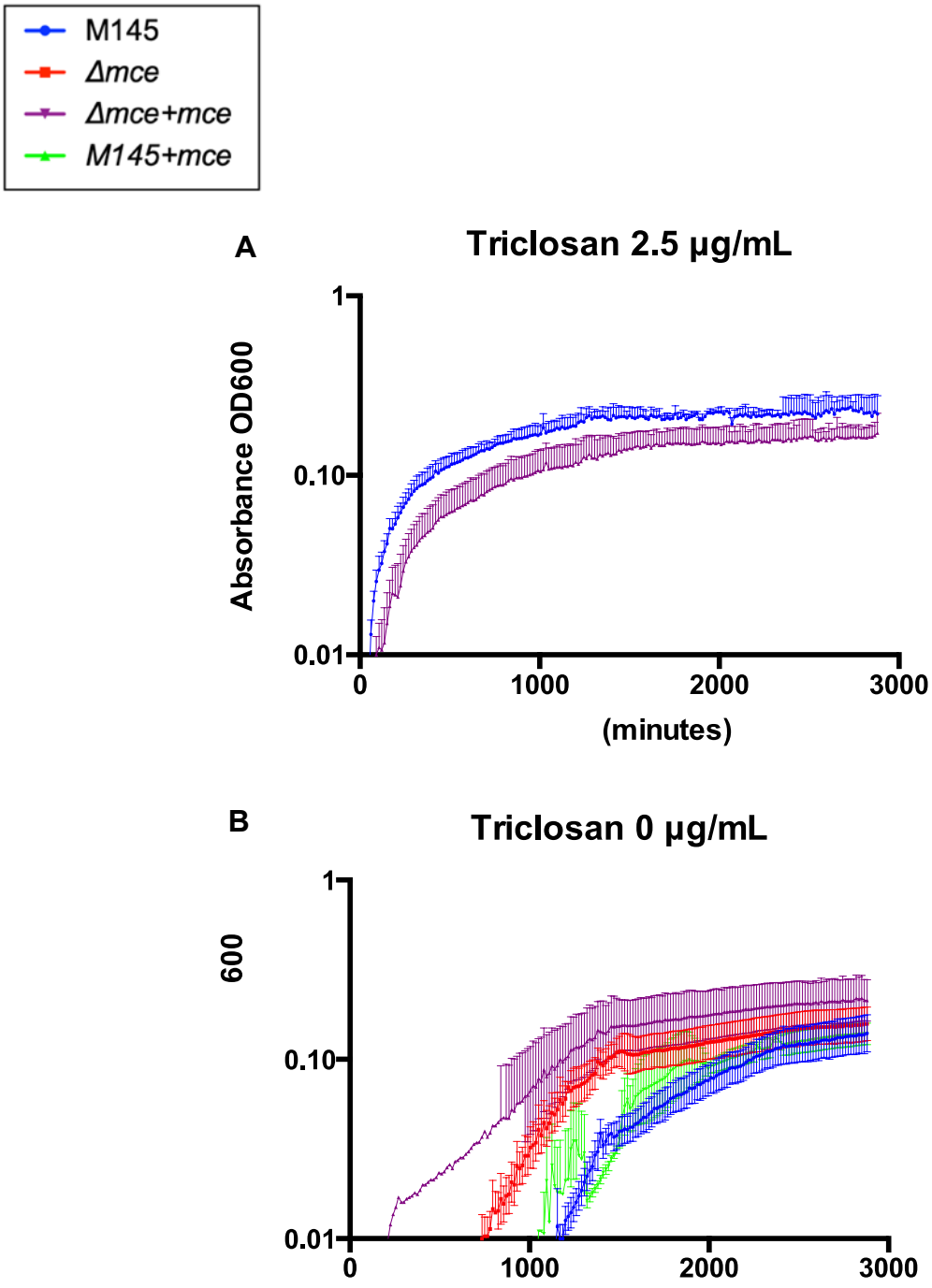

Figure 3.13: Growth curves of M145, Δ*mce*, Δ*mce*+*mce* and M145+*mce* strains in Minimal Media with mannitol and triclosan. Media contained with 0 or 2.5 µg/mL of triclosan. Growth was measured by absorbance measurements at 600nm in a microplate reader over a period of 48 hours. **(A)** Strain growth in Minimal Media with triclosan at a concentration of 2.5 µg/mL. **(B)** Strain growth in YEME with triclosan at a concentration of 0 µg/mL. Error bars represent standard deviation.

Addition of cholesterol does not alter susceptibility of Δ*mce* spores to triclosan

It has been previously shown that the *mce* operon is constitutively expressed during growth on solid YEME medium and that this expression may be abrogated by addition of 0.02 mg/mL cholesterol to the medium (Clark *et al.*, 2013). As priorly discussed, this indicates that the *mce* operon is expressed when cholesterol in the media is low, and serves as a low-capacity, high affinity sterol uptake system. It is therefore likely that in YEME and minimal media, the *mce* operon is active and providing benefit to the bacterium.

The *mce4* operon of *Mycobacterium* and *Rhodoccocus* encodes a sterol importer. Expression of the *mce4* operon is up-regulated 4.0-fold in the presence of cholesterol compared to growth on pyruvate, according to a study by Mohn *et al* (2008). The K_m for cholesterol was found to be 0.6 ± 0.1 μM, which may be approximated to 0.193 μg/mL. This indicates the optimum activity of the *mce4* transporter occurs at this concentration of cholesterol, with the transporter found to be saturated at concentrations of cholesterol above 6 μM.

Transcription of the *mce* operon in *S. coelicolor* appears to be repressed in the presence of high quantities (20 μg/mL), and induced in the presence of low quantities of cholesterol. As highest expression of *mce4* was observed at 0.193 μg/mL cholesterol, this concentration was added to minimal media to determine the effect on *S. coelicolor* strains. It was hypothesised that this concentration of cholesterol in the medium may result in induction or increased expression of the *mce* operon, which may, in turn, translate to increased survival and growth of strains in possession of the *mce* operon in the presence of triclosan. Similarly, the addition of cholesterol to the medium may be

beneficial to restoring growth of M145+*mce* and Δ*mce* strains, should other cholesterol import systems outside of the *mce* system be expressed to compensate.

Results, however, show that the addition of cholesterol did not alter survival and growth of Δ*mce* or M145+*mce* spores in minimal media in the presence of triclosan (Fig. 3.13). This suggests that other cholesterol import systems are unable to compensate for the loss of the Δ*mce* system and that the potentially increased permeability of the M145+*mce* strain cannot be counteracted by increased cholesterol uptake.

M145 and Δ*mce+mce* strains displayed highly similar growth in minimal media with triclosan with and without addition of cholesterol, which indicates that the addition of cholesterol in the presence of triclosan does not greatly benefit the bacterium (Fig. 3.13). However, in media containing both cholesterol and triclosan, the M145 strain displays increased growth over that of all mutants, including Δ*mce+mce* (Fig. 3.13, B). This is easily explained for the Δ*mce* strain, which lacks the functional Mce transport system and thus cannot import and utilise the available cholesterol as efficiently as M145, which contains the non-mutated *mce* operon at the native locus. It is interesting that the complemented mutant, Δ*mce+mce,* does not display a similar level of growth as M145, though perhaps not unexpected. The Δ*mce+mce* mutant, as previously discussed, contains an *mce* operon at an ectopic location, and it is likely that this operon therefore displays differential expression. It is possible that because of this, the Δ*mce+mce* strain is less successful at cholesterol uptake, which hinders its survival in medium containing a fatty acid biosynthesis inhibitor. A further consideration is that Δ*mce+mce* strain in minimal media with cholesterol but without triclosan displays comparably deficient growth to Δ*mce+mce* in minimal media with triclosan, both in the presence and absence of cholesterol. Though this seems to suggest a beneficial role for triclosan in some form,

it is likely a result of other lipid uptake systems being upregulated by the inhibition of fatty acid synthesis and providing a slight advantage in growth.

The increased growth rate of the M145 strain in the presence of cholesterol compared to the *mce* null mutant again suggests that the *mce* operon of *S. coelicolor* imports sterols.

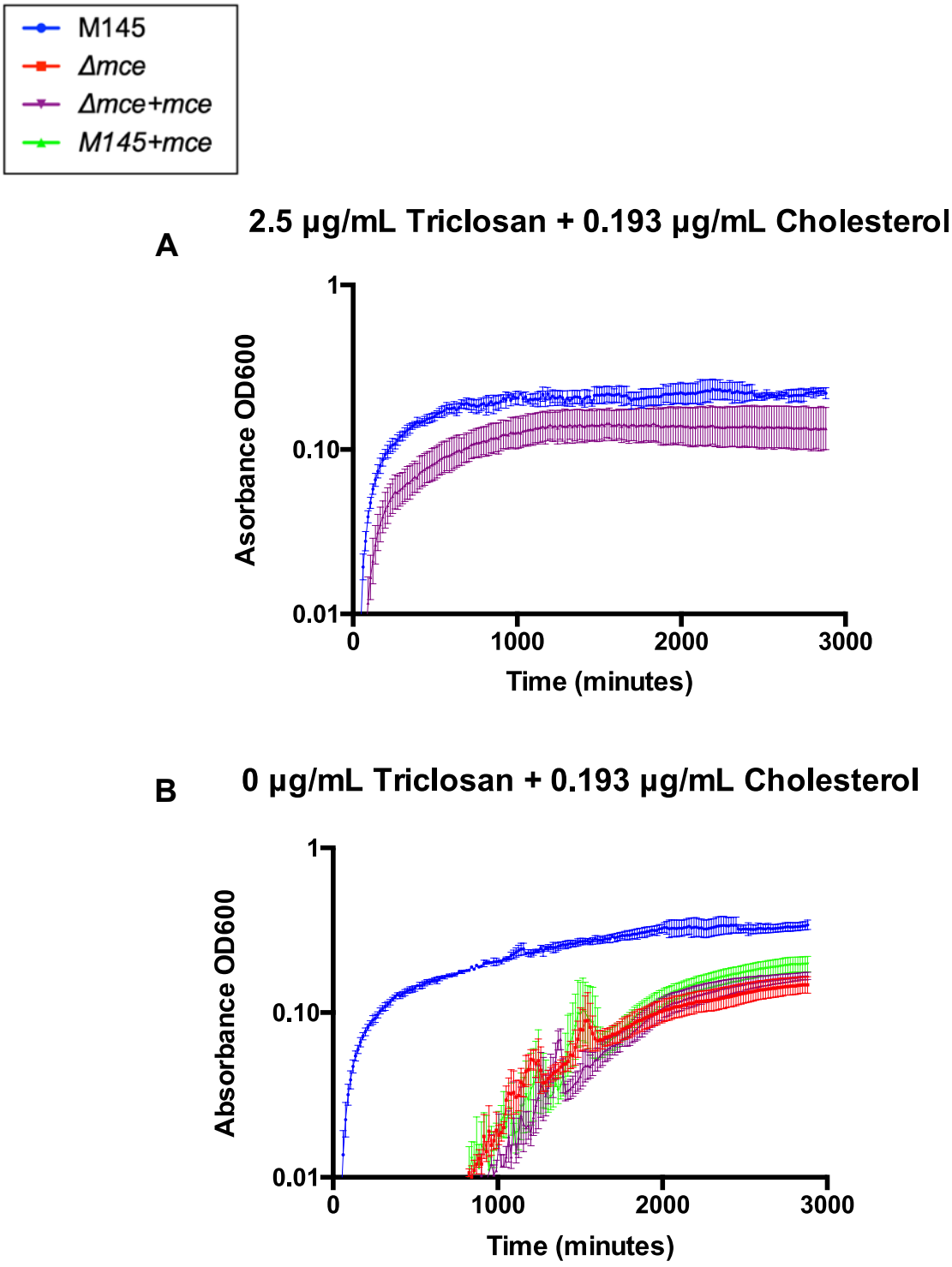

Figure 3.14: Growth curves of M145, Δ*mce*, Δ*mce*+*mce* and M145+*mce* strains in Minimal Media supplemented with mannitol and 0.193 µg/mL of cholesterol. Media contained with 0 or 2.5 µg/mL of triclosan. Growth was measured by absorbance measurements at 600nm in a microplate reader over a period of 48 hours. **(A)** Strain growth in Minimal Media with triclosan at a concentration of 2.5 µg/mL. **(B)** Strain growth in Minimal Media with triclosan at a concentration of 0 µg/mL. Error bars represent standard deviation.

Deletions of the *mce* operon result in increased susceptibility to sulfobetaines in YEME and Minimal Media

Sulfobetaines are a family of zwitterionic detergents which include lauryl sulfobetaine (LSB), myristyl sulfobetaine (MSB) and caprylyl sulfobetaine (CSB). A study by Isom *et al* (2017) in *E. coli* defective in one or more of the three Mce-domain containing proteins, *mlaD, pqiAB* or *yebST*, showed deletions of these proteins increased sensitivity to sulfobetaines due to disturbances in cell envelope homeostasis. Interestingly, sensitivity to LSB varied in severity depending on which of the Mce-domain containing proteins was mutagenized, indicating distinct roles for these proteins in maintenance of cell envelope homeostasis and potentially in substrate specificity. LSB, MSB, and CSB, are similar surfactants with similar structures, but differ in the length of their carbon chains (Fig. 3.14). As the structure of these sulfobetaines is highly similar to that of fatty acids, it has been proposed that the Mce proteins may mistake these detergents as fatty acids and facilitate their import into the cell. Interestingly, Isom *et al* (2017) determined that Mce *E.coli* mutants displayed differing sensitivities to LSB, MSB and CSB, which appears to further confirm a difference in substrate specificity between these Mce-domain containing proteins.

Sensitivity assays to LSB, MSB and CSB were carried out in YEME media over a 48 hour period to access how deletion of the *mce* operon effected bacterial tolerance to these detergents and determine whether sensitivity differed depending on carbon chain length of the detergent (Fig. 3.15 – 3.17).

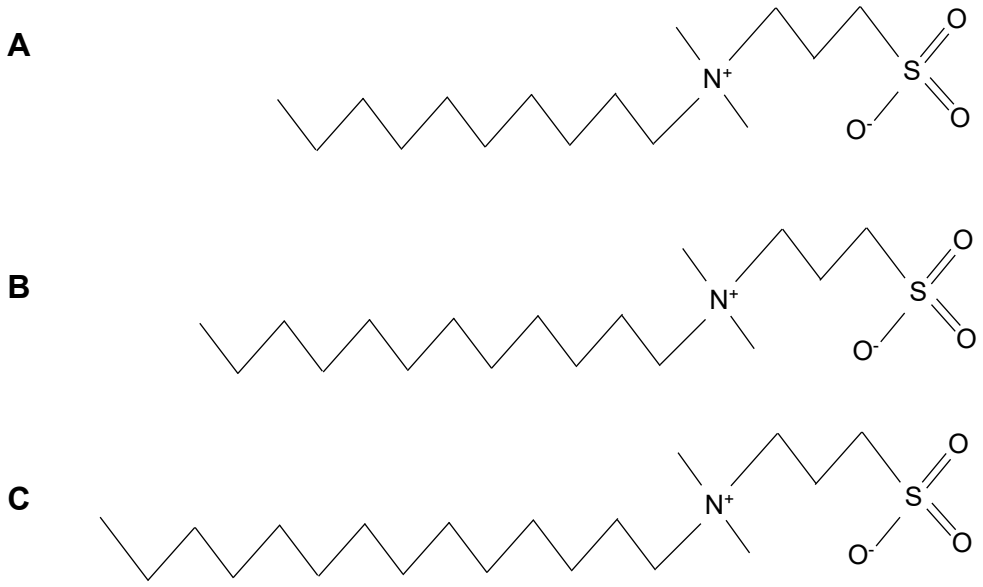

Figure 3.15: Chemical structures of sulfobetaines. (A) caprylyl sulfobetaine, (B) lauryl sulfobetaine, and (C) myristyl sulfobetaine.

Assays demonstrated that all *S. coelicolor* strains were sensitive to LSB, MSB and CSB. In particular the *mce* null mutant and M145+*mce* strain, with concentrations of 0.625% and above resulting in complete inhibition of growth of these mutants (Fig. 3.15 – 3.17). The specific growth rates of M145 and Δ*mce* in the absence of LSB were 0.38 h^{-1} and 0.44 h^{-1} respectively, and whilst specific growth rate of M145 in 2.5% LSB decreased only slightly (0.32 h^{-1}), growth of Δ*mce* was entirely abolished. It is interesting to note that M145 and M145+*mce* strains enter the exponential phase of growth earlier in the presence of the sulfobetaines. This is possibly a result of the detergent nature of the sulfobetaines, as washing spores with a detergent increases germination rate, possibly due to removal of the hydrophobicity of the spore sheath as well as germination inhibitors (Hirsch and Ensign, 1976; Aoki *et al.*, 2007).

The sensitivity of the Δ*mce* strain to LSB mirrors results in *E. coli* Mce mutants (Isom *et al.*, 2017). However, *S. coelicolor* spores of Δ*mce* were also highly sensitive to MSB and CSB across all concentrations tested. Results therefore appear to suggest that the Δ*mce* cell wall integrity may be compromised in some manner, perhaps increasing permeability to detergents. This is interesting, given earlier studies showing increased tolerance of the *mce* null mutant to SDS and lysozyme (Clark *et al.*, 2013). It is possible that the sensitivity of the Δ*mce* strain is not down to decreased cell wall integrity but instead upregulation of other lipid importers with the deletion of the *mce* operon, which may be functioning to import LSB, MSB and CSB inside the cell. Concurrently, it is likely that the sensitivity of M145+*mce* to sulfobetaine detergents, as with triclosan, is caused by a compromised or less integral cell wall due to the existence of multiple mce proteins. It is simultaneously possible that possessing two functioning Mce transporters, which may be aiding uptake of sulfobetaines, may also contribute to the sensitivity of the M145+*mce* strain towards these detergents.

Spores of M145 and Δ*mce*+*mce* displayed similar sensitivity to LSB, MSB and CSB across all concentrations tested, achieving an OD_{600} of approximately 0.2. That M145 and Δ*mce*+*mce* appear more tolerant to sulfobetaines than the *mce* null mutant may be a result of an uncompromised cell wall or possibly - due to the presence of a functional *mce* operon - other distinct lipid importers are not upregulated and so do not increase sulfobetaine intake.

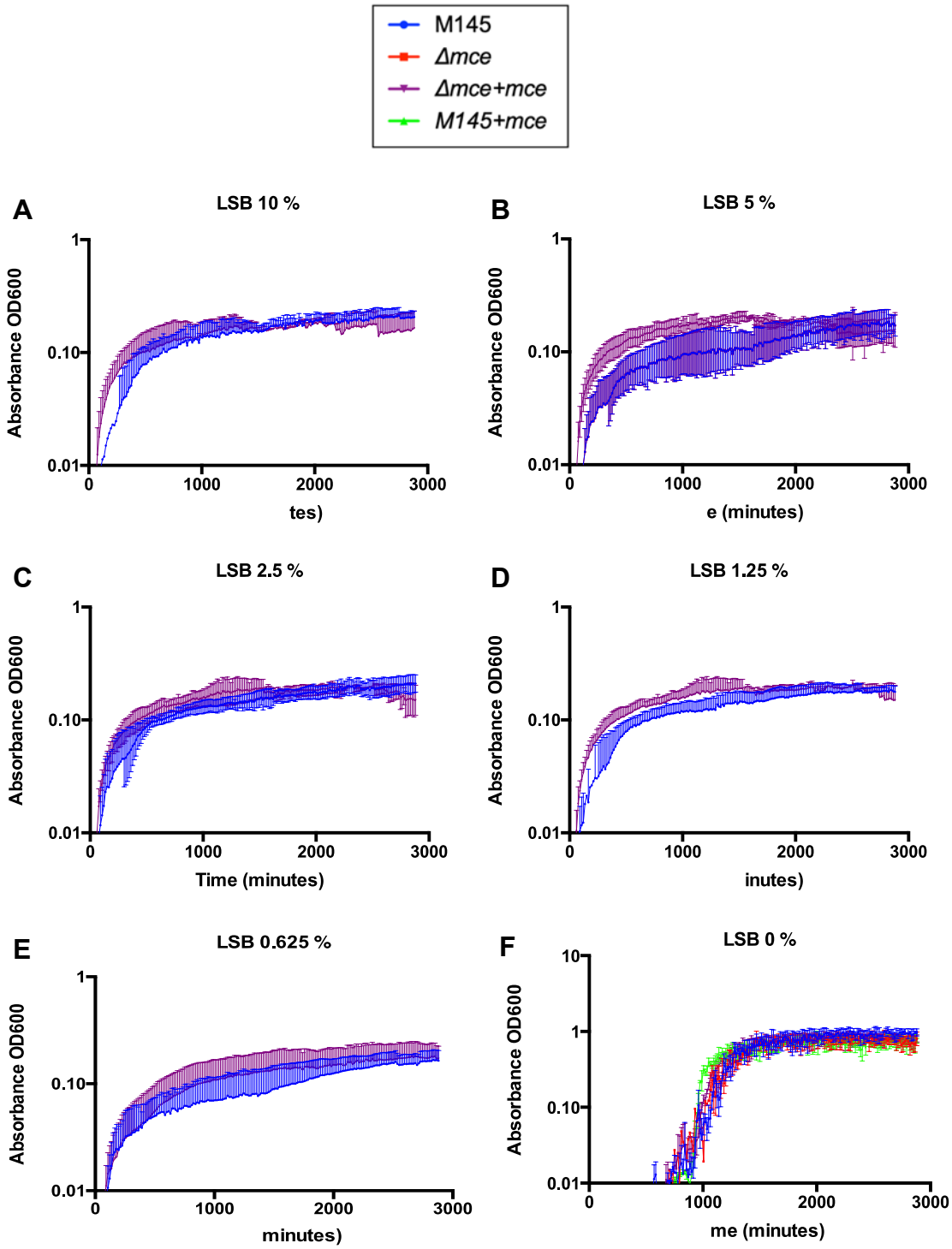

Figure 3.16: Growth curves of M145, Δ*mce*, Δ*mce+mce* and M145+*mce* strains in YEME with decreasing concentrations of LSB. Growth was measured by absorbance measurements at 600nm in a microplate reader over a period of 48 hours. **(A)** Strain growth in YEME with LSB at a concentration of 10%. **(B)** Strain growth in YEME with LSB at a concentration of 5%. **(C)** Strain growth in YEME with LSB at a concentration of 2.5% **(D)** Strain growth in YEME with LSB at a concentration of 1.25 µg/mL. **(E)** Strain growth in YEME with LSB at a concentration of 0.625% **(F)** Strain growth in YEME with LSB at a concentration of 0%. Error bars

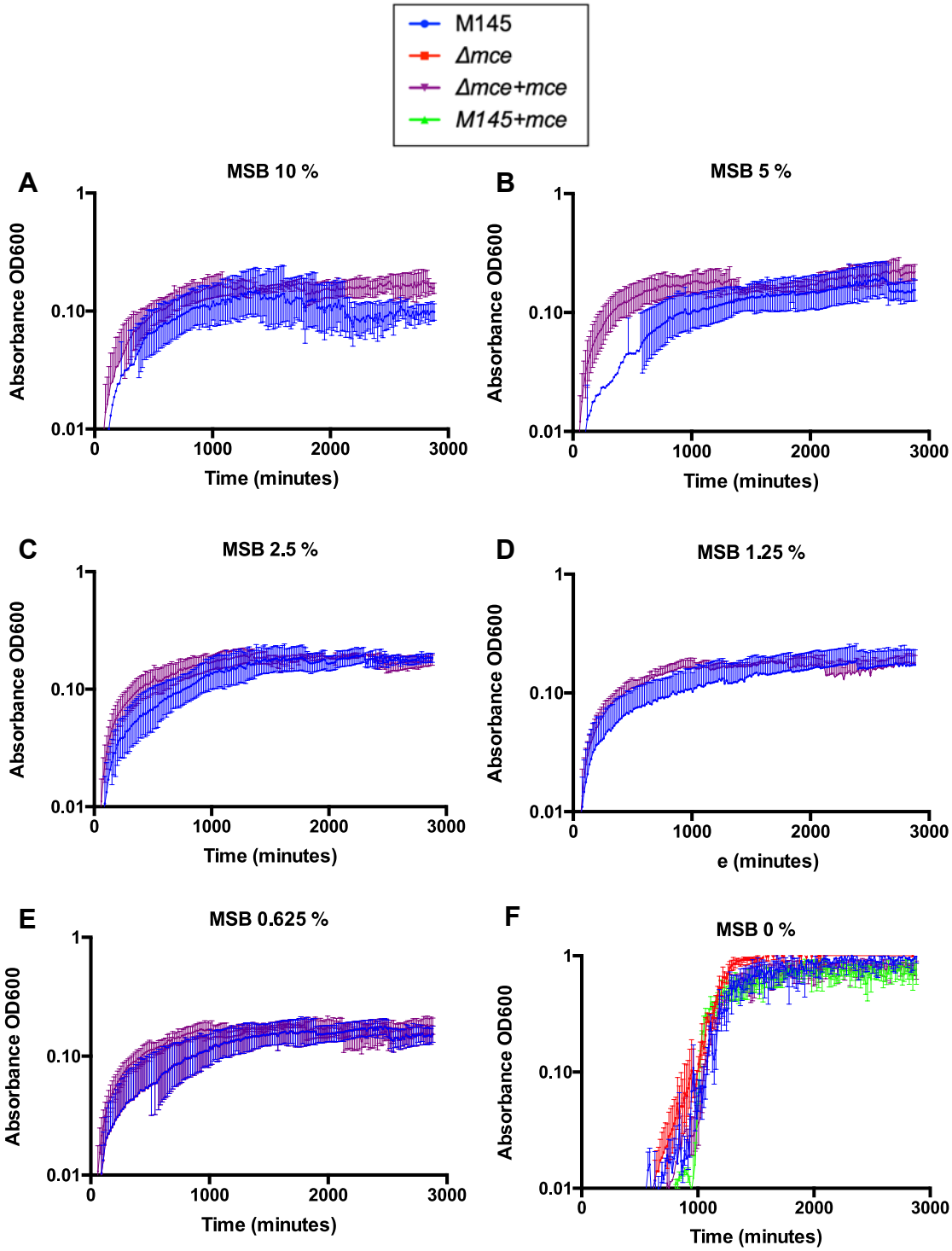

Figure 3.17: Growth curves of M145, Δ*mce*, Δ*mce*+*mce* and M145+*mce* strains in YEME with decreasing concentrations of MSB. Growth was measured by absorbance measurements at 600nm in a microplate reader over a period of 48 hours. **(A)** Strain growth in YEME with MSB at a concentration of 10%. **(B)** Strain growth in YEME with MSB at a concentration of 5%. **(C)** Strain growth in YEME with MSB at a concentration of 2.5% **(D)** Strain growth in YEME with MSB at a concentration of 1.25%. **(E)** Strain growth in YEME with MSB at a concentration of 0.625% **(F)** Strain growth in YEME with 0%. LSB. Error bars represent standard deviation.

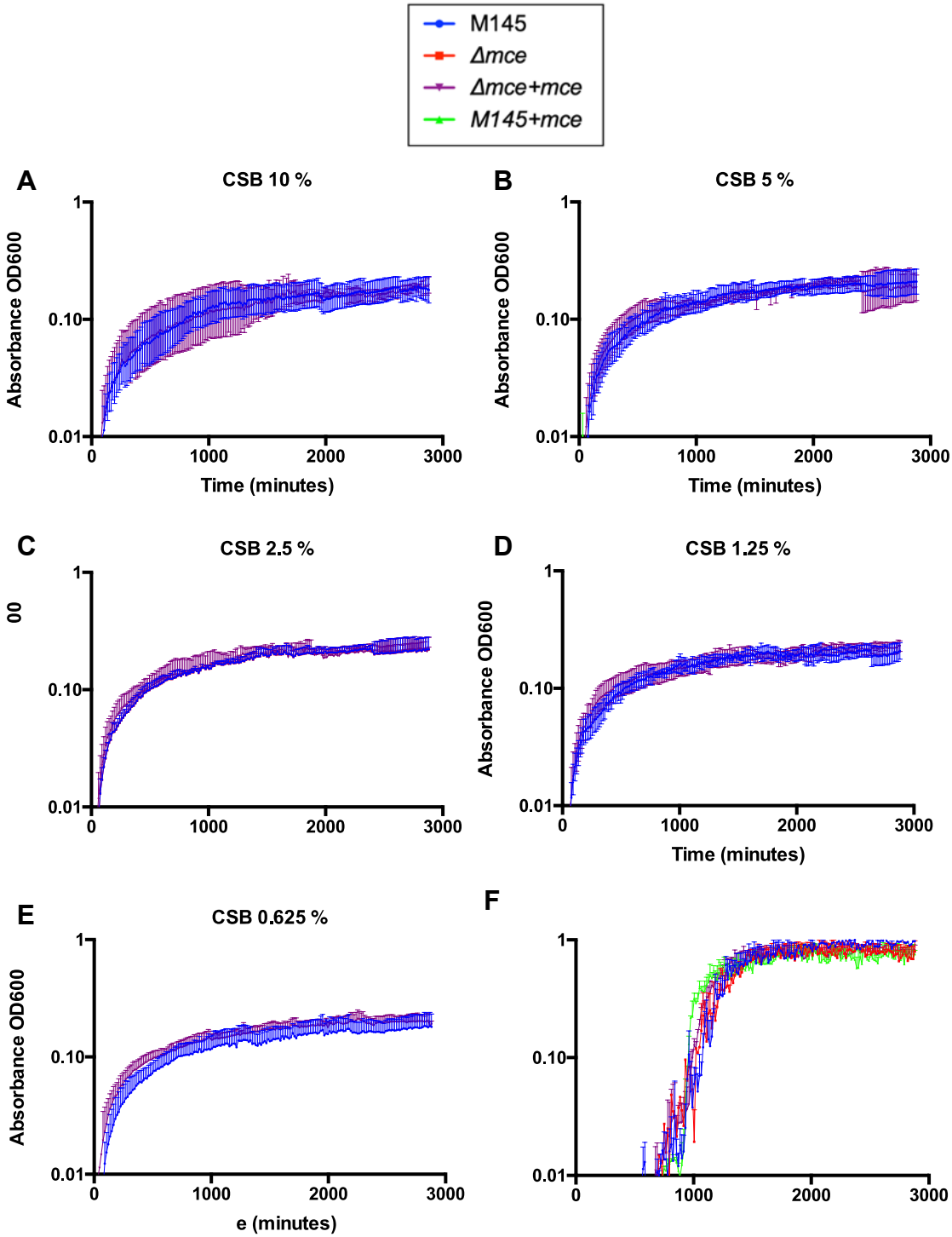

Figure 3.18: Growth curves of M145, Δ*mce,* Δ*mce+mce* and M145+*mce* strains in YEME with decreasing concentrations of CSB. Growth was measured by absorbance measurements at 600nm in a Microplate reader over a period of 48 hours. **(A)** Strain growth in YEME with CSB at a concentration of 10%. **(B)** Strain growth in YEME with CSB at a concentration of 5%. **(C)** Strain growth in YEME with CSB at a concentration of 2.5% **(D)** Strain growth in YEME with CSB at a concentration of 1.25%. **(E)** Strain growth in YEME with CSB at a concentration of 0.625%. **(F)** Strain growth in YEME with LSB at a concentration of 0%. Error bars represent standard deviation.

As with triclosan sensitivity testing, sensitivity assays for sulfobetaines were repeated in minimal media supplemented with mannitol. As strains showed near identical susceptibility to LSB, MSB and CSB, minimal media assays were only performed with LSB. A final concentration of 2.5% LSB was used, as this appeared to be the concentration at which strains show the clearest distinction (Fig. 3.18).

Interestingly, at 0% LSB in minimal media, M145 and Δ*mce*+mce strains displayed reduced growth compared to that in minimal media with 2.5% LSB. It is curious as to why this should be the case, given that deleterious nature of LSB to the organism and may potentially be explained by upregulation of stress responses in the presence of LSB which aid the bacterium's growth, or as previously mentioned, the detergent nature of LSB promoting earlier germination (Hirsch and Ensign, 1976).

The susceptibility of strains to 2.5% LSB in minimal media was highly similar to that displayed in YEME, with spores of M145 and Δ*mce*+mce showing growth to an OD_{600} of approximately 0.2, whilst spores of Δ*mce* and M145+*mce* proved unable to grow in the presence of 2.5% LSB (Fig.3.19).

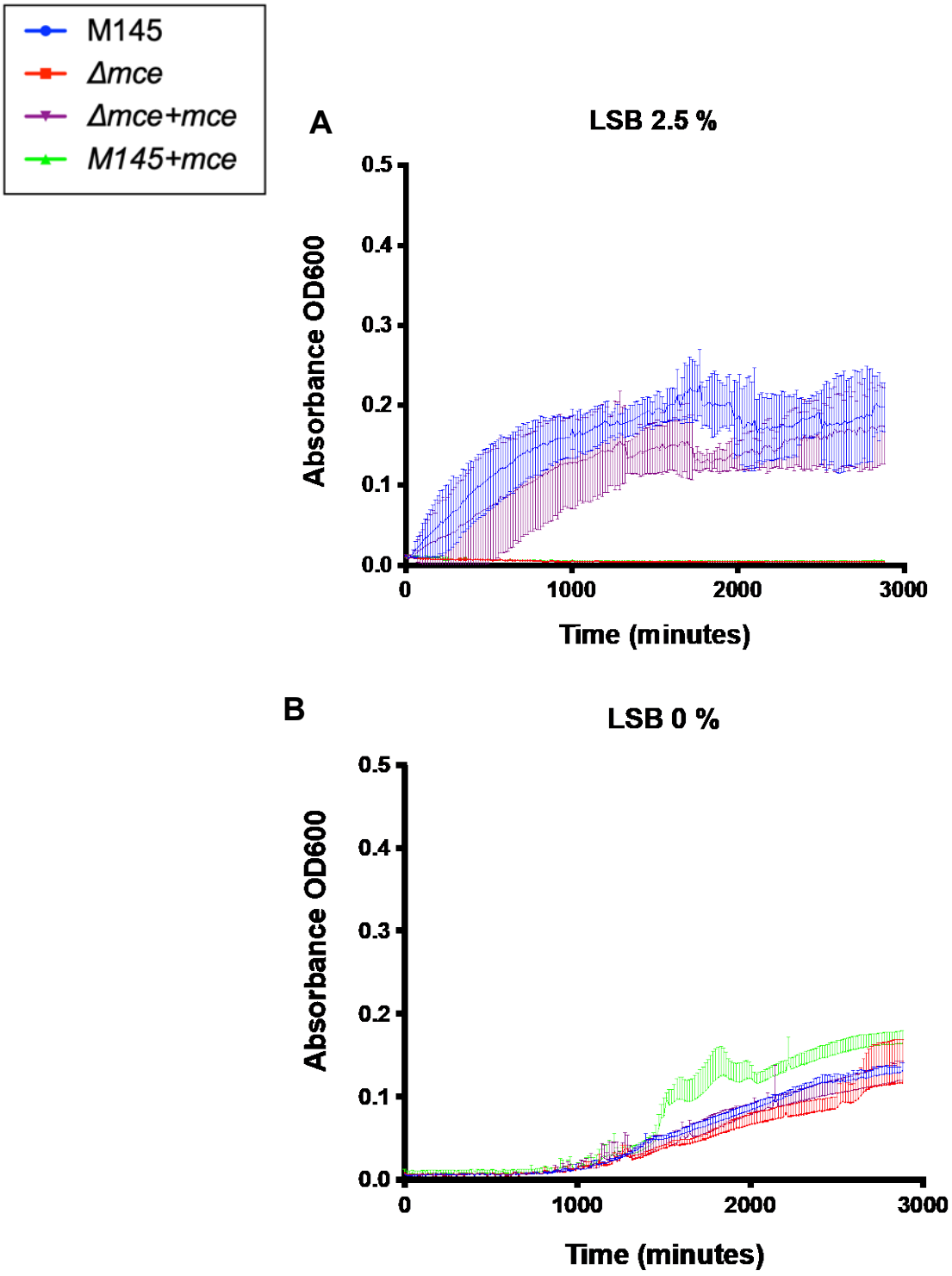

Figure 3.19: Growth curves of M145, Δ*mce,* Δ*mce+mce* and M145+*mce* strains in Minimal Media with mannitol and LSB. Media contained with 0 or 2.5% of LSB. Growth was measured by absorbance measurements at 600nm in a Microplate reader over a period of 48 hours. **(A)** Strain growth in Minimal Media with LSB at a concentration of 2.5%. **(B)** Strain growth in Minimal media with LSB at a concentration of 0%. Error bars represent standard deviation.

The addition of 0.193 µg/mL cholesterol to minimal media with 2.5% LSB had no visible effect on growth of the Δ*mce* or M145+*mce* strains, as both remained unable to grow in the presence of LSB (Fig. 3.19).

Growth of M145 in 2.5% LSB in minimal media was near identical regardless of the absence or presence of cholesterol. Unexpectedly, however, growth of the Δ*mce*+*mce* mutant was reduced in the presence of cholesterol. This complemented mutant, as previously discussed, often displays an intermediary phenotype between M145 and the *mce* null mutant, which may explain this result.

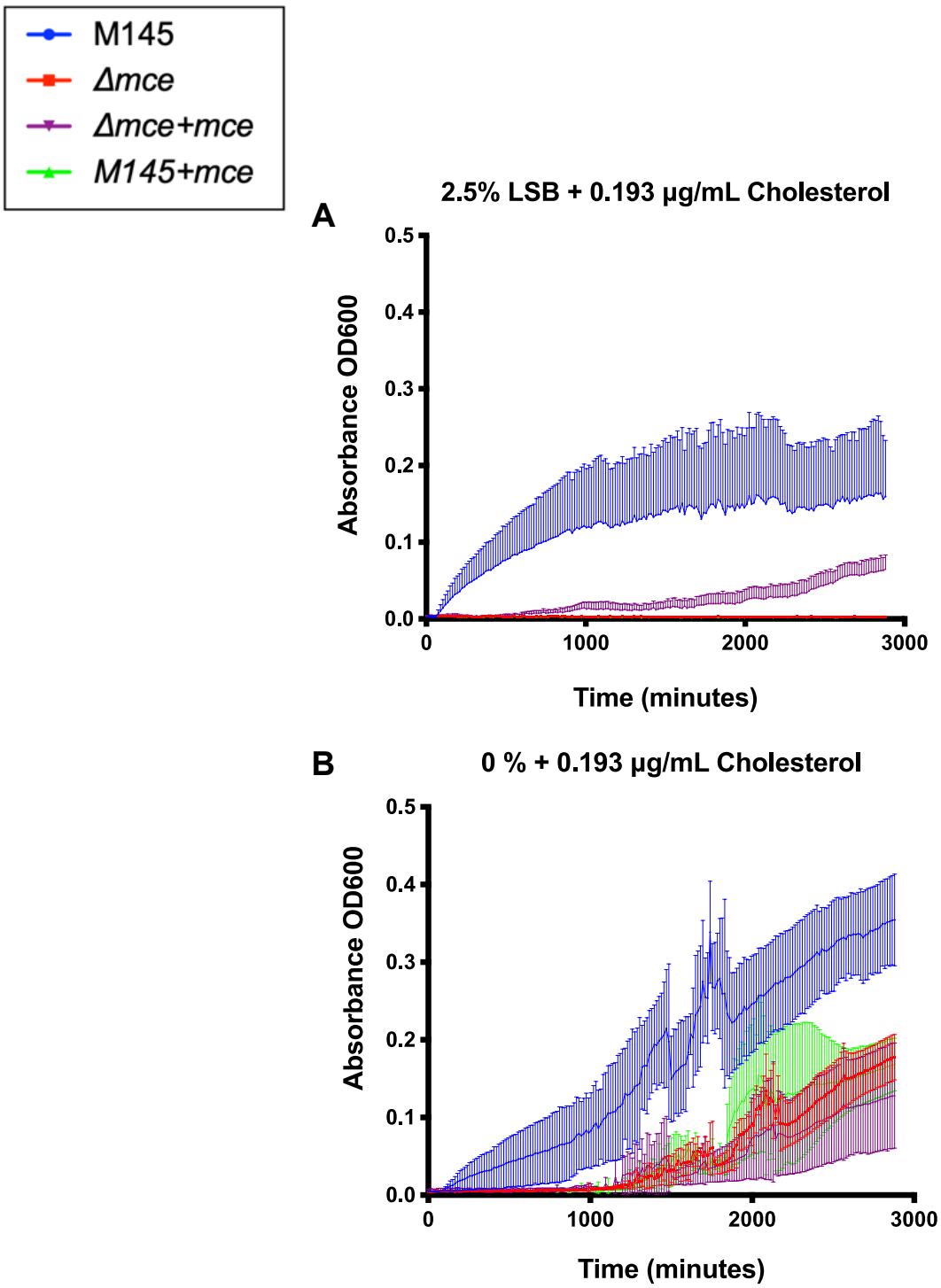

Figure 3.20: Growth curves of M145, Δ*mce*, Δ*mce*+*mce* and M145+*mce* strains in Minimal Media supplemented with mannitol and 0.193 µg/mL of cholesterol. Media contained with 0 or 2.5 % of LSB. Growth was measured by absorbance measurements at 600nm in a Microplate reader over a period of 48 hours. **(A)** Strain growth in Minimal Media with LSB at a concentration of 2.5%. **(B)** Strain growth in Minimal Media with LSB at a concentration of 0%. Error bars represent standard deviation.

The *mce* null mutant shows increased permeability compared to *S. coelicolor* M145

The susceptibility of the Δ*mce* strain to various deleterious agents, such as triclosan and sulfobetaines, suggests that this mutant may possess a compromised cell wall. It is likely that the Mce proteins of *S. coelicolor* are present in the cell wall, therefore deletion of the *mce* operon locus may result in alterations to resistance and permeability of the cell. Similarly, addition of excess Mce proteins within the cell wall, such as may be the case for the M145+*mce* strain, may also have effects on cell permeability.

In order to determine whether the *mce* null mutant displayed increased permeability, a permeability assay was carried out on *S. coelicolor* cells (Fig. 3.20). Germlings, which had just begun to show branching, were used, as these possess cell walls which are newly synthesised and differ from those of dormant spores.

Results show that the *mce* null mutant displays increased permeability in comparison to M145 cells. This may provide clarity as to why the Δ*mce* mutant is more susceptible to sulfobetaines and triclosan, as detergents may be more able to permeate these cell than M145 cells. Interestingly, the M145+*mce* appears to be the most permeable of all mutants, which is not unexpected given the likelihood that insertion of extra proteins disrupts the integrity of the cell wall. This however, poses questions as to why cells of the *mce* null mutant show increased permeability, which may suggest other structural changes.

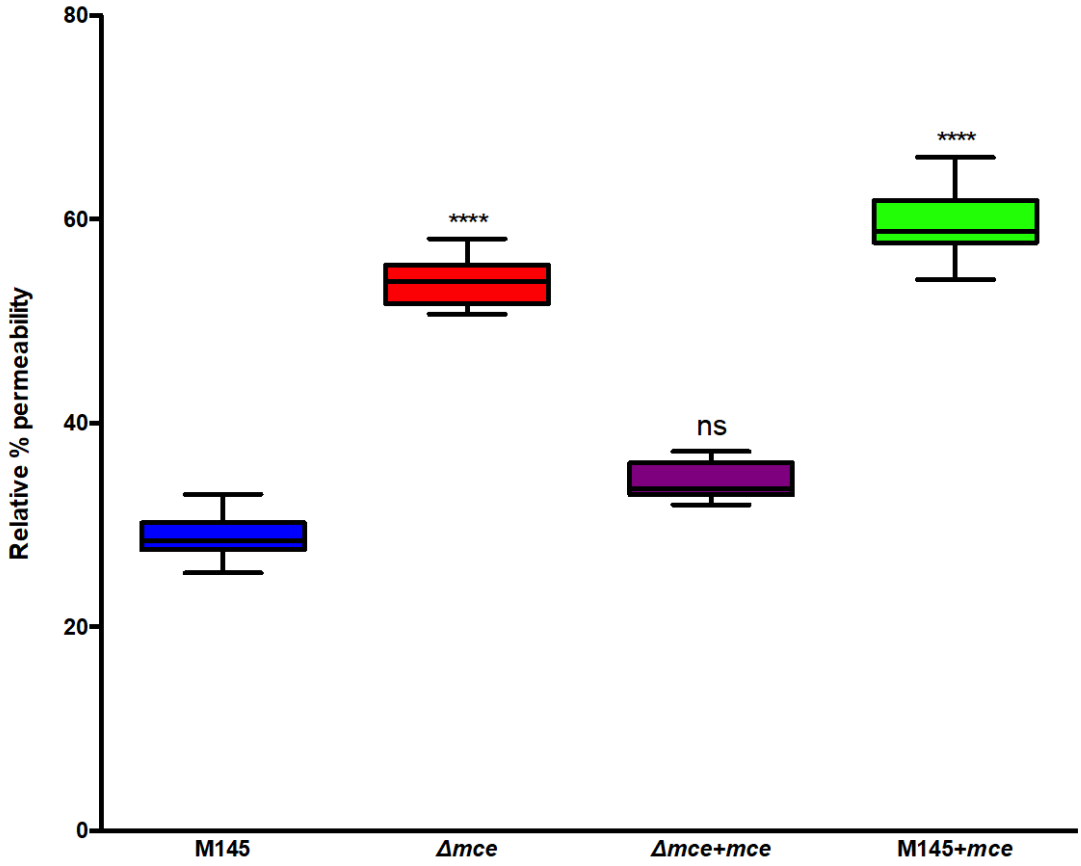

Figure 3.21: Permeability of M145 and mutant *S. coelicolor* germlings. Permeability was measured via accumulation of ethidium bromide within cells detected by levels of fluorescence. Fluorescence was read at an absorption and emission of 515 and 600 nm respectively. Fluorescence of negative controls were subtracted and fluorescence of samples compared relative to positive controls. A Kruskal-Wallis test showed that the *mce* null mutant and M145+*mce* germlings were more permeable than those of M145 in a statistically significant manner (P<0.0001,****) (N=3). Error bars represent standard deviation.

The cell wall thickness of the *mce* null mutant does not differ from that of M145

There is considerable evidence pointing to alterations of the cell wall of the *mce* null mutant, including the increased tolerance to lysozyme, increased cell permeability and physical variation of the spore envelope as seen in SEM images (Clark *et al.*, 2013). It was hypothesised that these alterations of the cell wall may be visible or detectable via changes in cell wall thickness between the Δ*mce* mutant and M145 strain. To determine if cell walls of the *mce* null mutant does indeed differ to those of M145 cells, TEM images of cell walls were measured (Fig. 3.21, A).

Examination of TEM images showed no obvious differences in cell wall physiology. Furthermore, there was no significant differences in width of the cell wall in the Δ*mce* mutant compared to M145 cell walls. Whilst cell wall thickness varied more in the *mce* null mutant, medians of cell wall thickness in Δ*mce* and M145 cells are highly similar (Fig. 3.21, B) Such results suggest that the alterations of the cell envelope in the Δ*mce* mutant does impact the thickness of the cell wall.

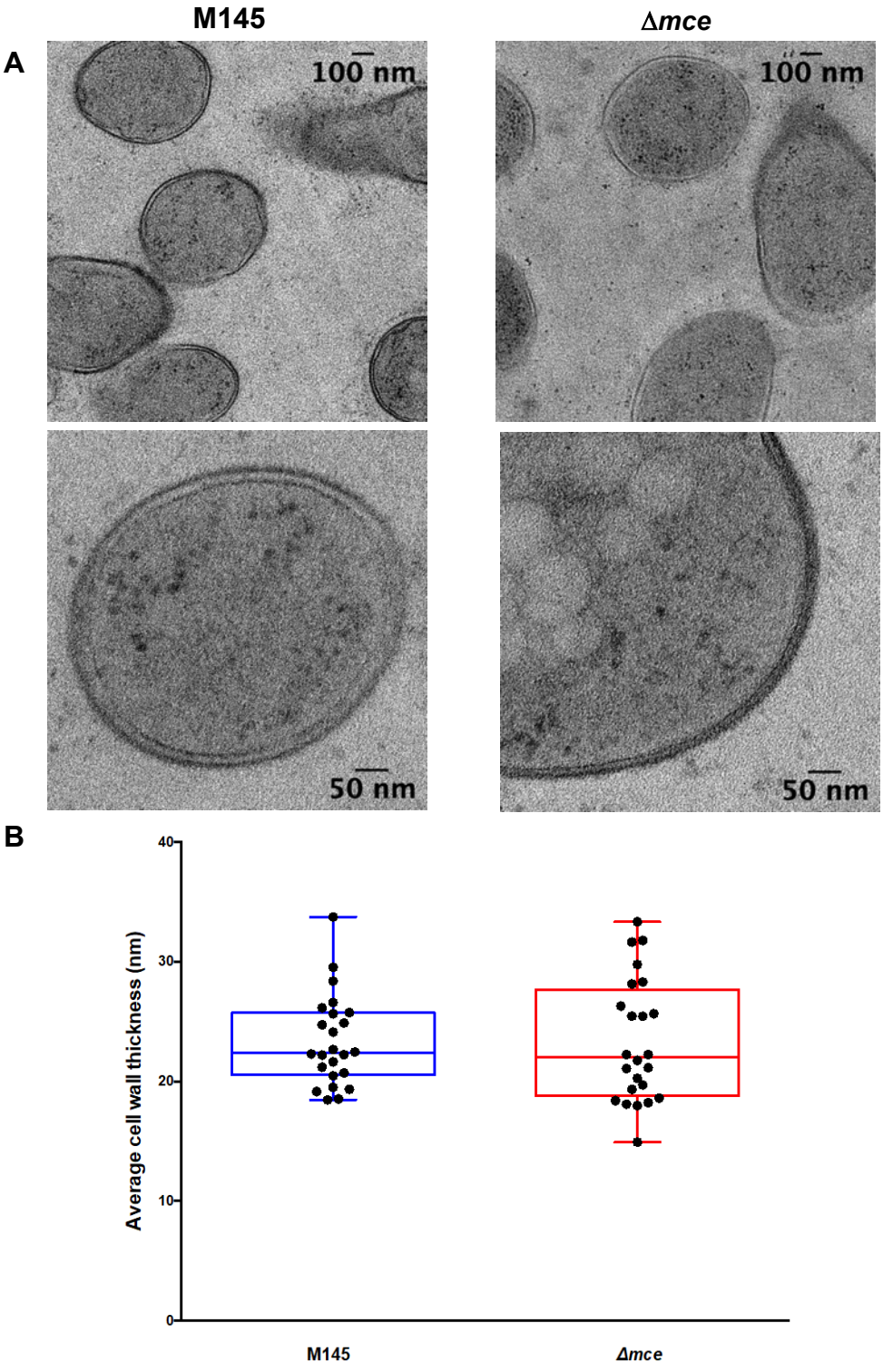

Figure 3.22: Average cell wall thickness of M145 and *mce* null mutant cells compared via TEM images. (A) TEM images taken at the University of Aberdeen by Prof Paul Hoskisson (2013) on a TE microscope at 5000x and 15000x magnification. **(B)** Average cell wall thickness of cell walls of M145 and *mce* null mutant cells measured in TEM images. Mann-Whitney analysis showed no difference in width of cell walls (, P =0.6560 P<0.05) as did Kolmogorov-Smirnov analysis (P=0.6749, P <0.05) (N=24) Error bars represent standard deviation.

Chapter 3: Summary

As previously hypothesised, this study shows that the *mce* operon of *S. coelicolor* likely encodes a sterol import system, as demonstrated by the impaired survival of Δ*mce* compared to M145 in media containing cholesterol. This was not unexpected given previous work by Clark *et al* (2013) and due to the high similarity of the *S. coelicolor mce* operon to those of *Mtb*, two of which have been conclusively characterised as ABC-transporters for lipids (Mohn *et al.*, 2008; Hemati *et al.*, 2019).

The *mce* null mutant of *S. coelicolor* displays differential growth and increased susceptibility to extracellular stressors, such as heat and chemical agents, likely due to alterations in the spore envelope which appear to be caused by deletion of the Mce proteins. Deletion or mutation of Mce proteins have previously been found to alter the cell surface of both *E. coli* and various Actinobacteria, thus this phenotype is not unprecedented (Möker *et al.*, 2004; Cangelosi *et al.*, 2006; Kleinschnitz, Heichlinger, *et al.*, 2011; Ekiert *et al.*, 2017)

The deletion of the *mce* operon in *S. coelicolor* results in precocious germination of spores, potentially due to the altered spore envelope leaving the bacterium in a quasi-dormant state which is simultaneously more prone to mechanical damage. Precocious germination correspondingly means earlier break-down of the spore cell envelope, which may increase spore adhesiveness, and during which extracellular glycans are produced, leading to the increased aggregation of the Δ*mce* mutant compared to the M145 strain.

Precocious germination was determined via germination assays which demonstrate earlier germination of Δ*mce* spores in comparison to those of *S. coelicolor* M145. Spores of the Δ*mce* mutant displayed swelling and germ tube emergence prior to M145 spores

and, at later timepoints, there was notable difference in germ-tube length between Δ*mce* mutant and M145 germlings. Alterations of the spore envelope have previously been associated with precocious germination, supporting the link between these two phenotypes (Colson *et al.*, 2008; Thompson *et al.*, 2010).

Precocious germination also appears to result in precocious sporulation of the *mce* null mutant in comparison with the M145 strain, visualised by earlier emergence of spore chains via impression mount assays. This similarly leads to earlier maturation of spores and results in the production of the grey polyketide spore pigment in the Δ*mce* strain. Similarly, precocious germination may be the cause of the greater and earlier production of ACT pigment in the *mce* null mutant. There are known associations between secondary metabolite production, physiological development, and bacterial stress, the latter two of which are linked to phenotypes seen in the Δ*mce* mutant (Bibb, 2005; Yoon and Nodwell, 2014).

This increased susceptibility of the Δ*mce* mutant to stressors is demonstrated by the strains impaired tolerance to heat and chemical agents.

Heat-kill assays showed Δ*mce* spores to be less resistance to heat than M145 spores, with the complemented strain, Δ*mce*+*mce*, displaying an intermediary phenotype. Heat-activation was similarly seen in M145 and Δ*mce*+*mce* spores, but notably absent from Δ*mce* spores. The absence of both heat-activation and the subsequent rapid loss of heat-tolerance, as can be seen in M145, and to some degree in Δ*mce*+*mce*, is suggestive of a quasi-dormant state for Δ*mce* spores. In this quasi-state, likely due to the defective cell envelope, Δ*mce* spores are more susceptible to heat and therefore show overall lower percentage survival than those of M145. However, because germinated vegetative cells

are far more heat susceptible than dormant spores, once M145 and Δ*mce*+*mce* undergo heat-activation, steeper declines in CFU over time are seen than with Δ*mce*. As Δ*mce* spores are not as resistant to heat as full dormant M145 spores, but are more resistant than germinating spores, this implies that Δ*mce* spores exist in an in-between state of quasi-dormancy.

Whilst previous work has shown the *mce* null mutant to be more tolerant of SDS and lysozyme, potentially due to Mce protein deletion and increased cell wall integrity, this study finds the Δ*mce* strain to be hypersensitive to both triclosan and sulfobetaine in comparison with M145. Hypersensitivity to triclosan is likely a result of the action of triclosan as an inhibitor of fatty acid biosynthesis combined with inability of the Δ*mce* mutant to import cholesterol as efficiently due to deletion of the *mce* operon. The inhibitory effect of the sulfobetaine detergents on the *mce* null mutant may be due in part to upregulation of non-specific fatty acid importers in response to the deletion of the *mce* operon, increasing intake of sulfobetaines compared to the M145 *mce* operon which appears to be a high-affinity sterol transporter. However, as permeability assays also show increased permeability of the *mce* null mutant in comparison with germlings of M145, hypersensitivity to sulfobetaine may be due in part to disruption of the cell envelope in Δ*mce* resulting in a more permeable cell.

Chapter 4: Optimization of *Streptomyces-Dictyostelium* assays and investigation of how *mce* deletions influence spore-amoebae interactions.

Dictyostelium discoideum are efficient bacterivorous soil protists commonly used as model macrophages for the investigation of host-pathogen interactions (Dunn *et al.*, 2018). Like *Streptomyces*, *Dictyostelium* inhabit terrestrial soil in abundance and as such these micro-organisms likely encounter each other in native conditions (Douglas *et al.*, 2013). This makes *Dictyostelium* an ideal model for examining spore-amoeba interactions in a biologically relevant manner. Furthermore, *Dictyostelium* are easily culturable, with a haploid, fully sequenced 34 Mb genome receptive to genetic manipulation. This is advantageous in comparison with the model organism *Acanthamoeba polyphaga*, which has been previously used in the investigation of Δ*mce* mutant and is relatively genetically intractable*. S. coelicolor* has been shown to be virulent towards *Acanthamoeba polyphaga*, with lysis of the amoeba due to intracellular *Streptomyces* hyphal growth (Clark *et al.*, 2013). This amoeba lysis may be seen at approximately 35 hours into co-culture with M145 spores. The Δ*mce* strain displays enhanced virulence towards *Acanthamoeba*, causing lysis of the amoeba at 24 hours in co-culture, likely due to the precocious germination phenotype of the *mce null* mutant as characterised in Chapter 3 of this work (Clark, 2011; Clark *et al.*, 2013). Enhanced virulence of the *mce* null mutant was unexpected, given that *mce* operons are known virulence factors within other Actinobacteria, most notably *Mycobacterium tuberculosis* (Gioffré *et al.*, 2005). Further, such apparent gain of function resulting from gene-knockout is unusual. As bacterial virulence is thought to have arisen from interactions with protists, the increased virulence of the Δ*mce* strain may give insights into the evolution of pathogenic Actinobacteria.

This chapter optimises the methodology for *Streptomyces-Dictyostelium* interactions and investigates the virulence of the *mce* null mutant towards a genus of amoeba other than *Acanthamoeba,* with focus on development and optimisation of spore-amoeba assays. The Δ*mce* strain of *S. coelicolor* exhibits a precocious spore germination phenotype (*Chapter 3)* and a central aim of this chapter is investigating spore-amoeba intracellular interactions to resolve the virulence mechanism of Δ*mce* spores within the phagosome. To this end, M145 and Δ*mce* strains constituently expressing the fluorophore mCherry were cultured with *Dictyostelium* expressing GFP and their extracellular and intracellular interactions visualised by confocal microscopy. Furthermore, as the purpose of multiple *mce* operon copies within Actinobacteria remains unclear, this chapter seeks to determine how multiple *mce* operons may affect *S. coelicolor* virulence towards amoeba. Hence, the additional *mce* copy strain, M145+*mce*, also expressing mCherry, was also co-cultured with GFP-expressing *Dictyostelium*.

Dictyostelium discoideum biology

The size of vegetative *Dictyostelium* amoeba varies greatly, with mean estimates ranging from 10-20 μm in diameter (Fig. 4.1). Accurate measurements are complicated by the amoeba's highly irregular shape, with numerous pseudopodia which have functions in locomotion and in capture and ingestion of prey (Gaudet *et al.*, 2008). *Dictyostelium* amoeba are mononucleate, possessing a plasma membrane but lacking a cell wall, and contain numerous food vacuoles as well as a singular large contractile vacuole approximately 3-4 μm in diameter (Gezelius and Rånby, 1957). *Dictyostelium* amoeba are chemotactic, moving towards and locating prey by sensing the presence of folic acid (Segota *et al.*, 2013). Phagocytosis involves the physical engulfment and degradation of prey micro-organisms in processes which are conserved with the mononuclear phagocytes of mammals (Dunn *et al.*, 2018). As *Dictyostelium* are found naturally in fresh

water and soil, the vegetative amoeba may survive in lightly buffered water as long as a food-source, typically bacteria, is provided. If *Dictyostelium* begin to starve, amoeba will release cAMP signals which lead to aggregation and formation of a multi-cellular psuedoplasmodium (Dunn *et al.*, 2018).

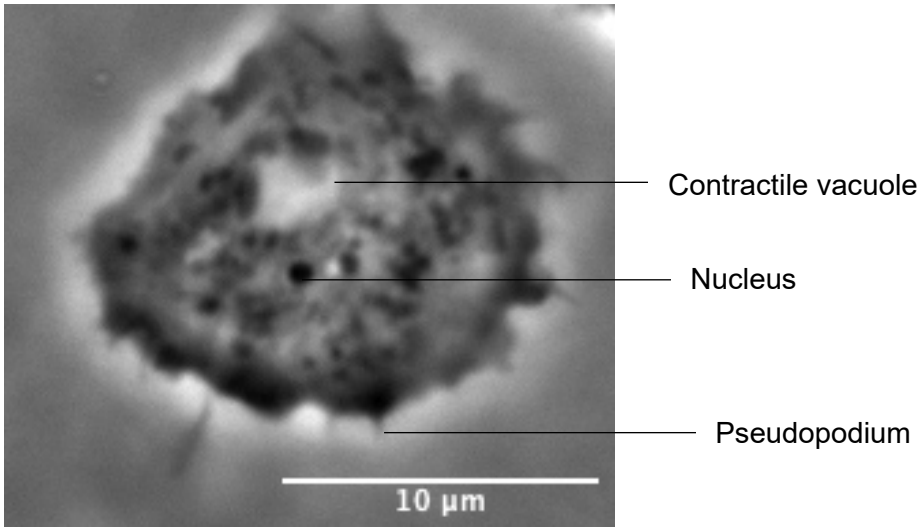

Figure 4.1: Basic *Dictyostelium* amoeba structure. A single *Dictyostelium* amoeba in axenic aqueous suspension, showing nucleus, contractile vacuole, and protruding pseudopodia. The average diameter of a singular *Dictyostelium* amoeba is 10µm, although this varies greatly. Phase contrast image was acquired using an Orca-285 digital camera connected to a Nikon Eclipse TE2000-S microscope equipped with a 100x objective lens.

Dictyostelium and *Streptomyces* interactions

Despite the likelihood that *Dictyostelium* encounters and predates *Streptomyces* in soil, there is little available literature on *Dictyostelium*-*Streptomyces* interactions. Prior work by Hopwood & McQuade (2020, unpublished), demonstrated that the AX4 *Dictyostelium* strain is able to consume and grow upon a number of *Streptomyces* species, including S. *lividans, S. coelicolor* and *S. rimosus.* Other work has found that *Streptomyces luridiscabiei* is consumed by *Dictyostelium*, but is able to avoid digestion, however the mechanism of this remains unexplored (Paquet and Charette, 2016). More recently it has been shown that tunicamycin, a fatty acyl nucleoside antibiotic which is produced by *S. lysosuperificus, S. chartreusis* and *S. clavuligerus*, is capable of interfering with N-glycosylation so as to induce endoplasmic reticulum stress in *Dictyostelium.* The antibiotic effectively inhibits protein glycosylation, cellular growth and development and provokes morphological changes which result in spherically-shaped amoeba (Domínguez-Martín, Hernández-Elvira, *et al.*, 2018; Domínguez-Martín, Ongay-Larios, *et al.*, 2018). By tunicamycin induced interruption of the N-linked glycosylation pathway of *Dictyostelium*, these *Streptomyces* species appear to evade predation (Nasser *et al.*, 2013a). For the purposes of this work, it is notable that *S. coelicolor* does not produce tunicamycin and has no known methods of avoiding *Dictyostelium* predation. This study is unaware of any other existing work on *Dictyostelium*-*S. coelicolor* interactions.

Dictyostelium discoideum actively phagocytoses *Streptomyces* coelicolor spores

Dictyostelium, whilst a common model organism for investigating virulence, has little-to-no prior utilisation with *Streptomyces* spores. Experimental procedures for *Dictyostelium* to investigate phagocytosis, intracellular survival and exocytosis of bacteria have been developed for non-sporulating organisms such as *Legionella* and *Mtb* and thus require optimization for *Streptomyces.* The differences in *Dictyostelium* predation strategies

towards Gram (-) versus Gram (+) bacteria is discussed in more depth in Chapter 1 of this work.

An important consideration is the low metabolic activity and respiration of dormant *Streptomyces* spores, particularly when compared to prey bacteria commonly used for *Dictyostelium*, such as *Klebsiella.* Dormant spores do not produce folate, the main chemoattractant that *Dictyostelium* use to forage for prey, and are non-motile (Sinai *et al.*, 2015). As a result, preliminary testing was needed to determine whether *Dictyostelium* were able to detect, attach to and phagocytose *Streptomyces* spores.

The *Dictyostelium* strain AX2 (DBS0235534, DictyBase), which is an axenic strain derived from AX1 (DBS0237979, DictyBase), the first axenic *Dictyostelium* strain sub-cultured from the non-axenic true WT *Dictyostelium* strain NC-4, was used as a WT proxy in this work. AX2 is the parental strain of all GFP-expressing AX2 derivatives used in this work and therefore fit for this purpose. AX2 is able to grow axenically in HL5 media at 22°C and has a doubling time of 8-12 hours depending on culture conditions and presence of selective drugs (Fey *et al.*, 2007). Whilst 22°C is non-optimum for *Streptomyces*, spores are able to germinate and grow at this temperature, allowing for co-culture with *Dictyostelium* amoeba in both aqueous and solid media.

To confirm that *Dictyostelium* predates *Streptomyces*, spores and amoeba were observed in both rich and minimal media co-culture. *Dictyostelium* amoebae were seen to rapidly physically associate with and phagocytose *Streptomyces* spores (Fig. 4.2A). *Dictyostelium* were also able to clear lawns of freshly plated *Streptomyces* spores on nutrient agar, demonstrating the ability to engulf and destroy spores on solid medium (Fig. 4.2B) When left for extended periods, fruiting bodies are able to form. This strongly suggests that *Dictyostelium* are able to consume singular spores as a food source, with

starvation and the initiation of multicellular development being triggered when the immediate area has been cleared of spores.

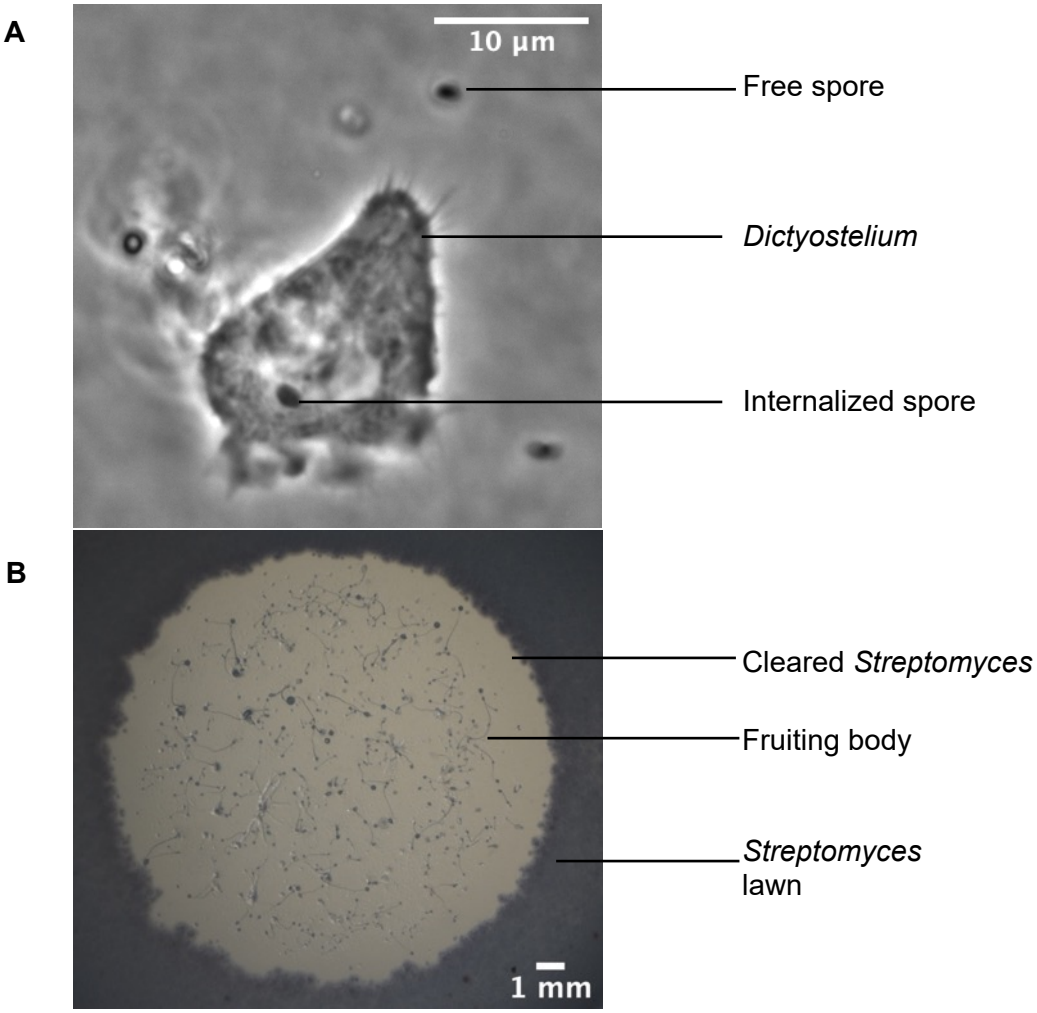

Figure 4.2: *Dictyostelium* in suspension and on solid media with *S. coelicolor*. **(A)** A single *Dictyostelium* amoeba containing an internalised *S. coelicolor* spore, 15 minutes into co-culture in HL5 media, MOI 1:1440. Phase contrast image taken on an Orca-285 digital camera connected to a Nikon Eclipse TE2000-S microscope at 1000x magnification. **(B)** A plaque formed by feeding *Dictyostelium* amoeba on a *S. coelicolor* lawn, 48 hours on nutrient agar at 22°C. Fruiting bodies are apparent within the plaque.

The phenotypes for the GFP-expressing *Dictyostelium* strains used in this work have no documented growth defects on Dictybase (http://www.dictybase.org/) and none were observed during this study. In order to confirm that the GFP-expressing strains displayed no aberrations in phagocytic ability, the spore consumption of the AX2 GFP-expressing derivatives were compared to the AX2 strain in HL5 media. The Vat-gfp *Dictyostelium* strain was omitted from this as prior work has established its ability to phagocytose efficiently (Clarke *et al.*, 2002). Spore consumption across *Dictyostelium* strains over a two-hour period was found to be highly similar with no significant difference across the strains, indicating that all strains could be used in co-culture and virulence assays (Fig. 4.3).

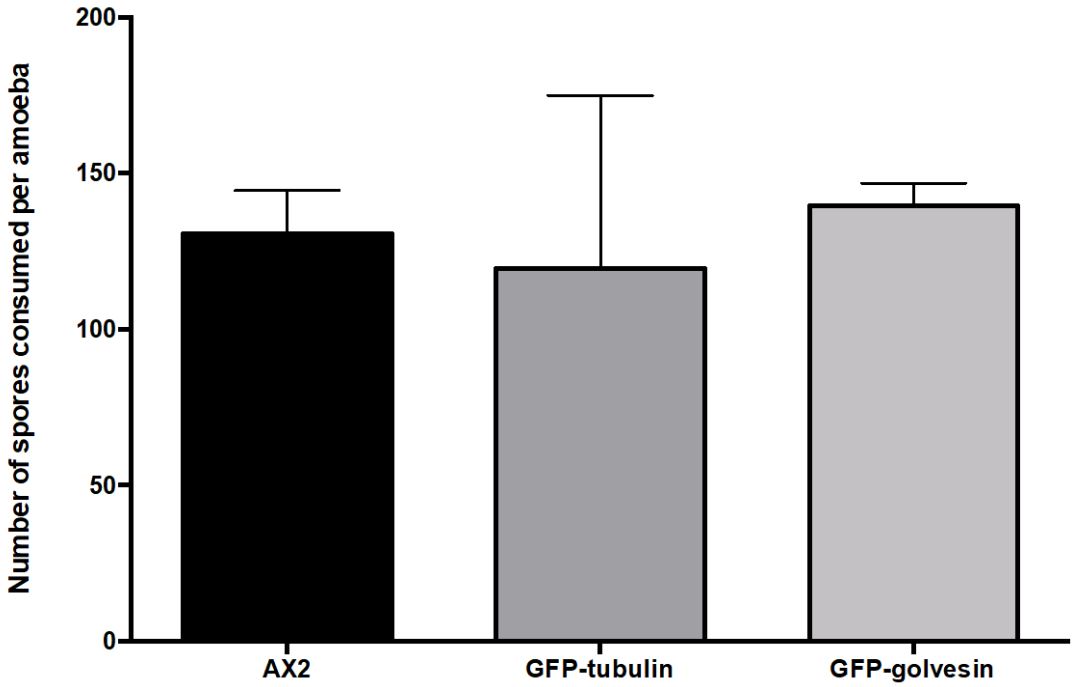

Figure 4.3: Comparisons of number of spores consumed by strains of *Dictyostelium* amoeba in HL5 media at an MOI of 1:100 over two hours. No significant difference was shown between strains with an ordinary one-way ANOVA, P=0.7706. (N=3) Error bars represent standard deviation.

Optimization of plaque assays

Bacterial virulence towards a protist may be reliably determined via the plaque assay technique originally developed in *Dictyostelium* by Froquet *et al* (2008). *Dictyostelium* graze upon non-virulent bacterial lawns, resulting in cleared areas known as phagocytic plaques, but are unable to do so upon virulent bacteria. Plaque formation may therefore be used to determine bacterial pathogenicity towards *Dictyostelium*, with plaque size being inverse to the level of virulence (Froquet *et al.*, 2009).

Dictyostelium plaque assays have been routinely used in the literature to examine the virulence of non-spore forming bacteria such as *Psuedomonas, Leginonella* and *Klebsiella*, however, for the purpose of this work, an important consideration was the practical limitations of the assay when evaluating the virulence of spore-forming bacteria. It has been observed that *Dictyostelium* are unable to form plaques on *S. cerevisiae* or *M. smegmatis*, likely due to an inability to efficiently ingest and digest these organisms rather than being an indication of bacterial virulence (Froquet *et al.*, 2009). Whilst spore consumption assays confirmed the ability of *Dictyostelium* to ingest *S. coelicolor* spores in aqueous media (Fig. 4.3), it was noted that *Dictyostelium* were unable to form plaques on established lawns of *Streptomyces* which had reached multicellular stages of development. It is therefore likely that *Dictyostelium* are able to consume free unicellular spores, but unable to graze upon mycelial spore chains.

Froquet *et al* 2008 observed that varying the number of bacteria used to create the lawn does not appear to greatly impact bacterial virulence towards *Dictyostelium,* but varying media nutrient content can significantly change the outcome of the assay (Froquet *et al.*, 2009). For this reason, a range of media concentrations were tested to determine optimum nutrient content. Optimization of the assay also included determination of the

correct ratio of *Dictyostelium* cells to *Streptomyces* spores. A further issue was encountered with identifying the ideal length of plate incubation for optimum plaque formation, as growing *S. coelicolor* begins to produce actinorhodin pigment which obscures phagocytic plaques.

Plaque assays were performed in 24-well cell culture plates (TPP®, Cat. #Z707791-126EA), enabling a number of conditions to be varied simultaneously. Nutrient broth concentration was altered (100%, 80%, 50% and 20%) to vary the growth rate of *S. coelicolor* lawns. Density of amoebae spotted onto the *S. coelicolor* lawn was varied to allow determination of number of *Dictyostelium* required for optimum plaque formation. *Dictyostelium* amoeba less than a week old were harvested in exponential phase and cells were viewed using a Nikon Eclipse TE2000-S inverted microscope with 100X objective to ensure cells were healthy and motile, before a representative portion was diluted in tryphan blue (0.4%) and counted.

Plaque assays were used to determine if the Δ*mce* strain showed enhanced virulence towards *Dictyostelium* amoebae compared with S. coelicolor M145. The additional *mce* copy strain, M145+*mce*, was also examined for enhanced virulence. In previous work *Acanthamoeba polyphaga* plaque assays examining these strains had been performed at ranges of 1000-10,000 amoebae to 5 x 10^6 *S. coelicolor* spores per well. Plaque assays performed with *Dictyostelium* in this work therefore initially utilised identical parameters across a range of nutrient agar concentrations (100%, 80%, 50% and 20%). However, a density of 1 x 10^8 spores per well was found to produce a thin and 'patchy' lawn across media concentrations and therefore spore density was increased to 1 x 10^9, resulting in an evenly distributed and solid lawn of bacteria that allowed for easier visualisation of plaques. However, a density of 10,000 *Dictyostelium* spotted onto these

lawns was unable to produce plaques, even upon M145 spores. The density of *Dictyostelium* cells per spot was then increased to 40,000 cells on 100% nutrient agar, with subsequent 1:10 dilutions of amoebae as nutrient concentration decreased. However, clear plaques were still unable to form on M145 spores using 40,000 *Dictyostelium* cells per well (Fig. 4.4).

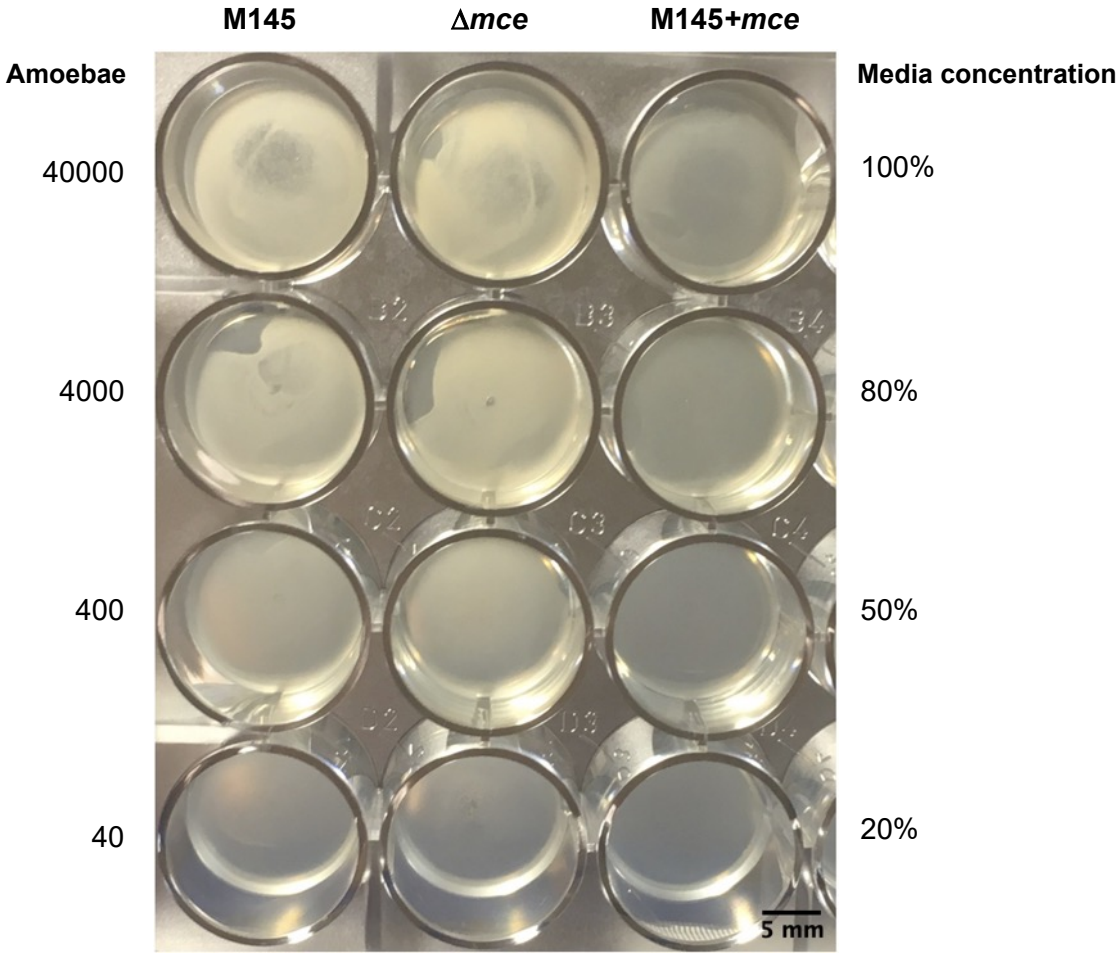

Figure 4.4: A preliminary plaque assay performed with M145, Δ*mce* and M145+*mce* strains on varied concentrations of nutrient agar. A density of 1 x 10^9 spores were used to create the bacterial lawns. An initial density of 40,000 *Dictyostelium* cells were used, with subsequent 1:10 dilutions as media concentration decreased. Clear plaques were unable to form at any cell density and at any media concentration.

As establishing an appropriate number of *Dictyostelium* for plaque formation proved challenging, a large number of *Dictyostelium* at 350,000 cell per well was tested on 100% nutrient agar and shown to produce completely cleared plaques (Fig. 4.5.A). This was therefore regarded as an upper limit for number of *Dictyostelium* cells required. On 80% nutrient agar, 350,000 *Dictyostelium* cells also produced visible plaques whilst maintaining good *Streptomyces* growth, though these retained some colonies within the cleared plaque area (Fig. 4.5.B). As it was theoretically possible that a high number of *amoebae* might serve to mask any virulence the *mce* null mutant displayed towards *Dictyostelium*, half this number of *Dictyostelium* (175,000) cells per well was tested on 80% nutrient agar to determine if *Dictyostelium* number might be reduced further. *Dictyostelium* in a quantity of 175,000 cells per well was found to produce plaques with visible demarcation between edges of plaque and *Streptomyces* lawns. Interestingly, *Dictyostelium* did not completely clear the plaque area of *Streptomyces* colonies under these conditions. It was noted that as total plaque area appeared to remain fairly consistent between the *Streptomyces* M145 and Δ*mce* strains, these remaining colonies could prove useful in assessing possible differences in virulence (Fig. 4.5.C). After further testing, optimum assay conditions were confirmed to be 175,000 *Dictyostelium* cells spotted onto a lawn of 1×10^9 *Streptomyces* spores on 80% nutrient broth agar. This combination produced confluent lawns of *Streptomyces* and clearly visible *Dictyostelium* plaques by 48 hours into incubation (Fig. 4.6).

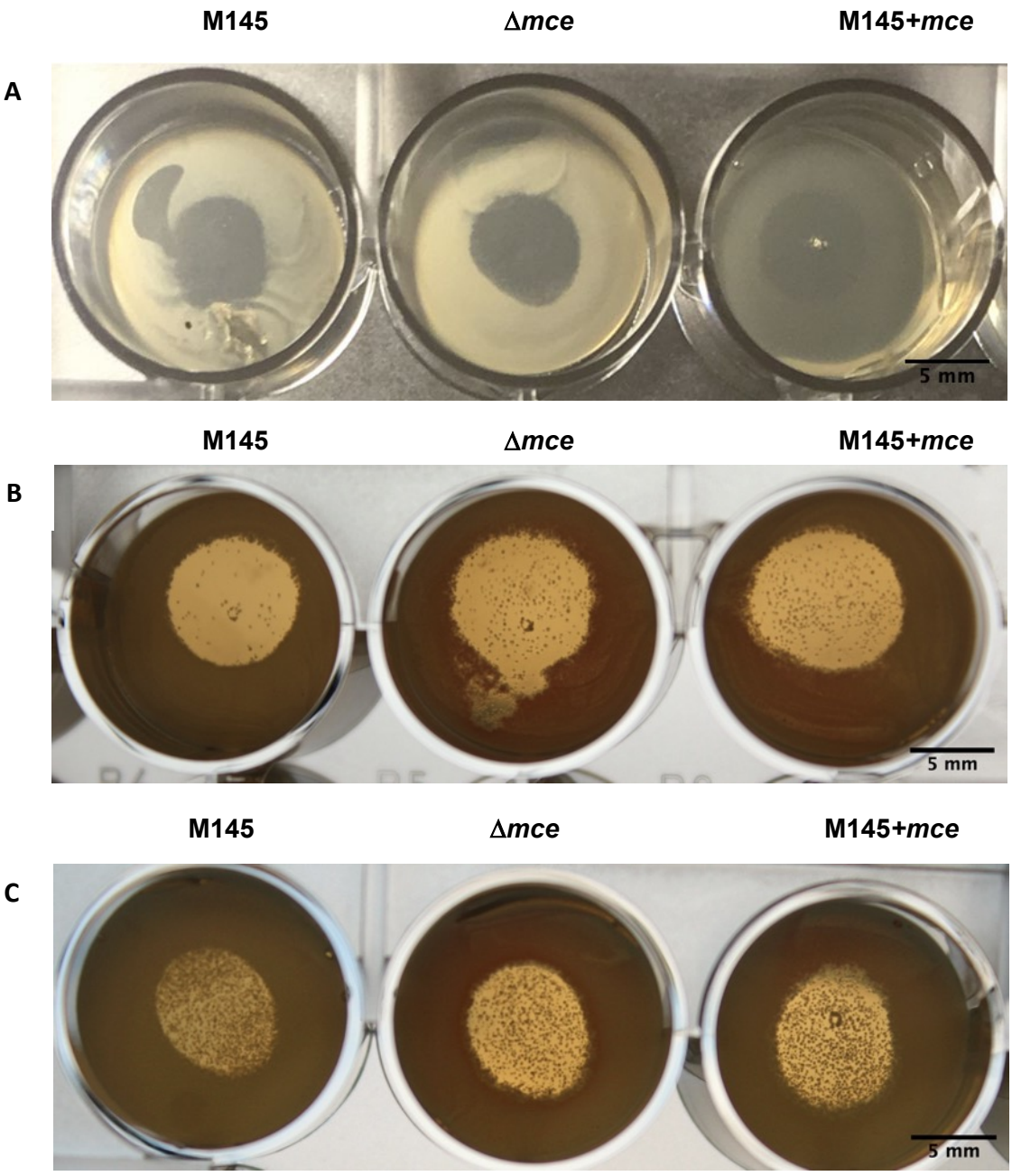

Figure 4.5: Optimisation of *Dictyostelium* – *S. coelicolor* plaque assays. (A) A preliminary plaque assay performed with M145, Δ*mce* and M145+*mce* strains using 350,000 *Dictyostelium* and 1x10^9 spores per well, on 100% nutrient agar. Similarly sized plaques were able to form on all bacterial strains. **(B)** 175,000 *Dictyostelium* cells and 1 x 10^9 spores per well on 100% nutrient agar. 175,000 *Dictyostelium* were sufficient to form large plaques on all bacterial strains. **(C)** 175,000 *Dictyostelium* cells and 1 x 10^9 spores per well on 80% nutrient agar formed plaques on all bacterial strains whilst retaining some *Streptomyces* colonies within the plaque area.

M145

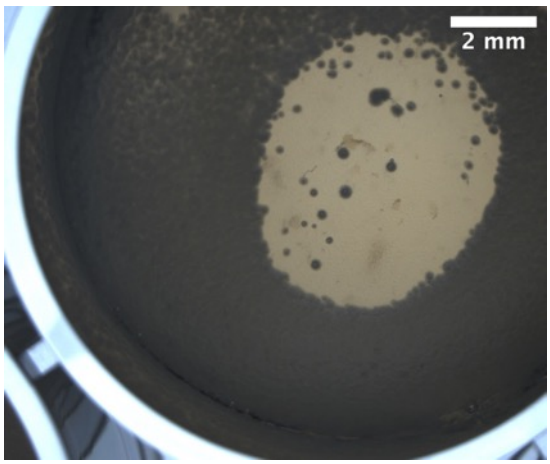

Δ*mce*

M145 +*mce*

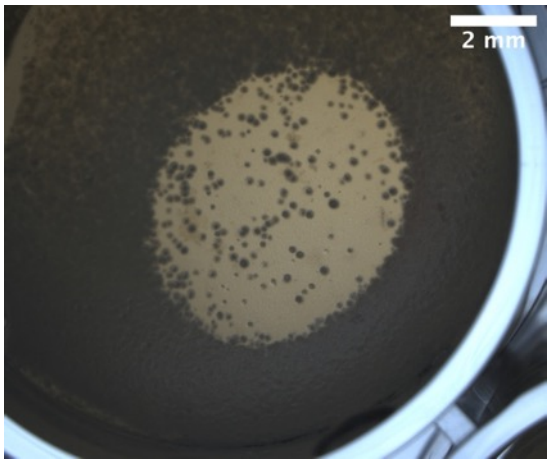

Figure 4.6: 175,000 *Dictyostelium* cells spotted onto 1 x 10^9 *Streptomyces* spores on 80% nutrient broth agar. Lawns and plaques were visualised at 48 hours. Stereo light micrographs taken at 11.25 x magnification on a SMZ1500 stereomicroscope using a DF 33UX264 CMOS camera system.

Optimum incubation time for plaque assays was found to be 48 hours. At 24 hours, *Streptomyces* lawns and plaques begin to be visible but are not fully formed. At 48 hours, lawns and plaques are clearly visible and defined. Past 48 hours *Streptomyces* strains, particularly the Δ*mce* strain, begin to produce pigments which obscure results.

Acutely accurate spore quantification was also found to be critical for plaque assays. Incorrectly quantified spores led to obfuscation of plaque assay results by increasing the number of *Streptomyces* colonies left within the plaque and slightly decreasing plaque area. One such incidence of this occurred when a new spore stock solution of the M145+*mce* strain was used and abruptly increased *Streptomyces* colonies remaining inside the amoeba plaque (Fig. 4.7). Once the spore stock had been re-quantified correctly, this phenotype was shown to be due to higher spore density rather than increased virulence (Fig. 4.8).

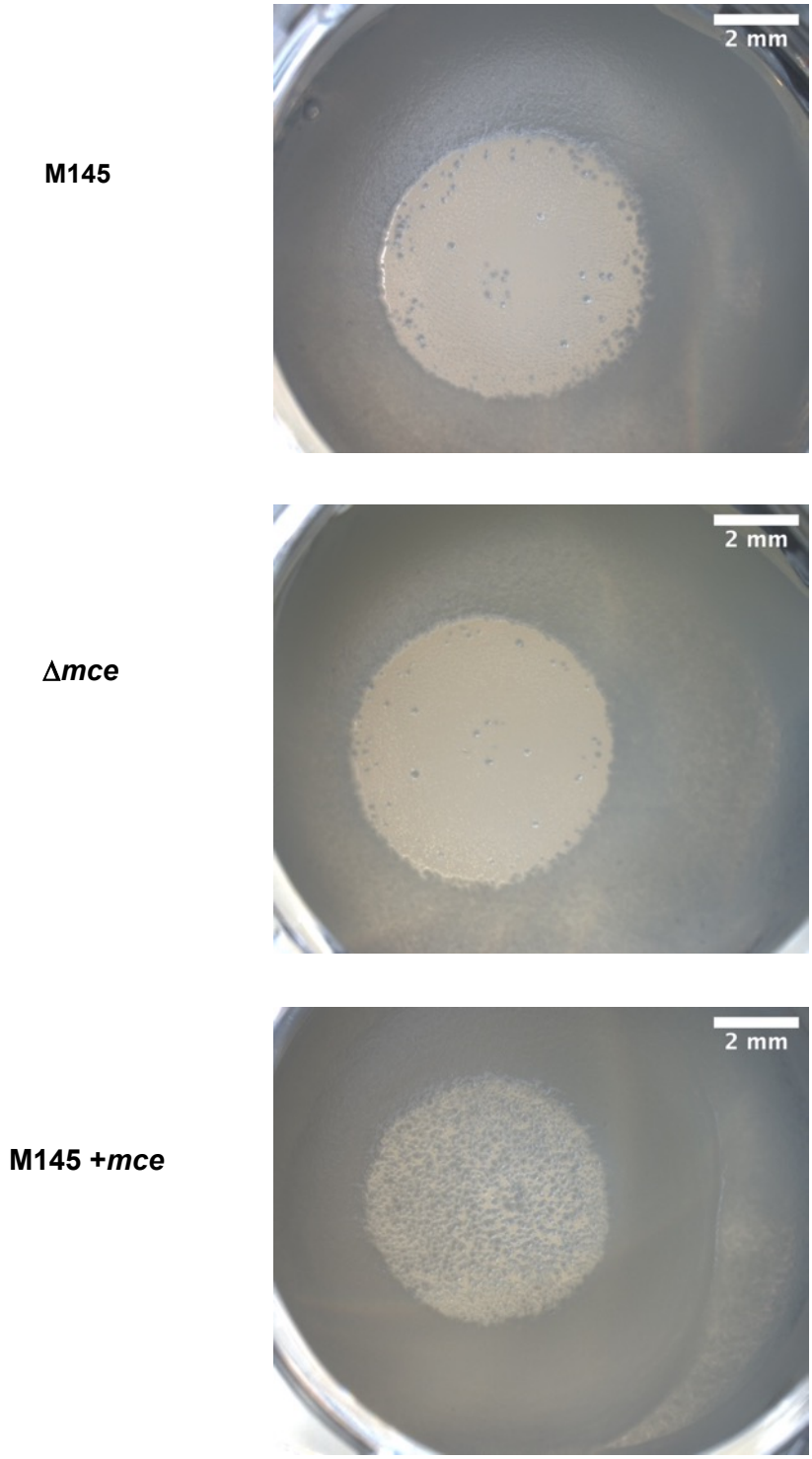

Figure 4.7: 175,000 *Dictyostelium* cells spotted onto 1 x 10^9 *Streptomyces* spores on 80% nutrient broth agar. Lawns and plaques were visualised at 48 hours. Stereo light micrographs taken at 11.25 x magnification on a SMZ1500 stereomicroscope using a DF 33UX264 CMOS camera system. A new and incorrectly quantified stock of M145+*mce* was used, which resulted in smaller, less

M145

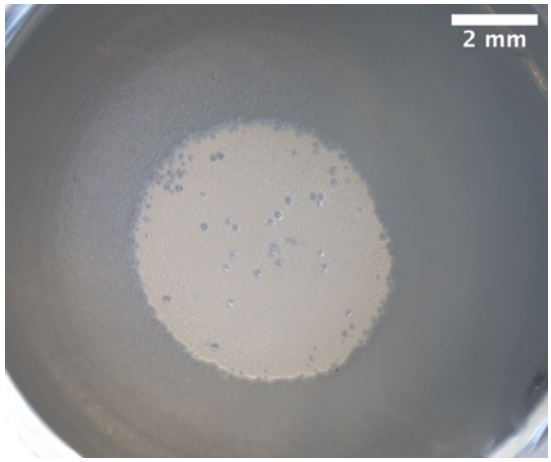

Δ*mce*

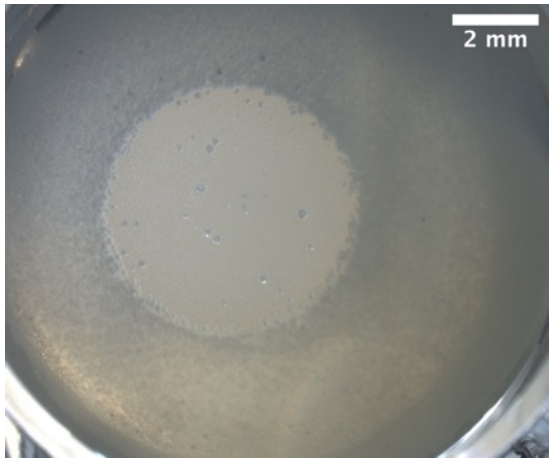

M145 +*mce*

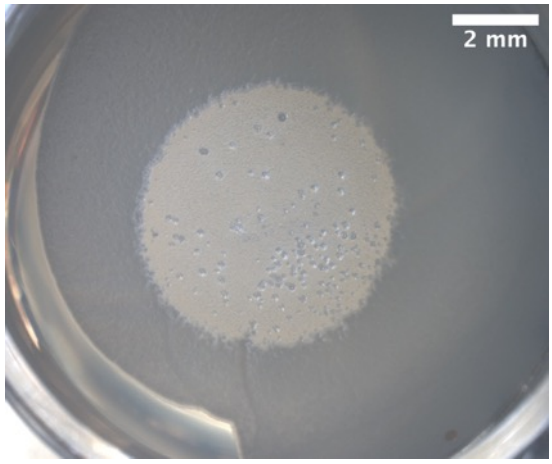

Figure: 4.8 175,000 *Dictyostelium* cells spotted onto 1 x 10^9 *Streptomyces* spores on 80% nutrient broth agar. Lawns and plaques were visualised at 48 hours. Stereo light micrographs taken at 11.25 x magnification on a SMZ1500 stereomicroscope using a DF 33UX264 CMOS camera system. A new and correctly quantified spore stock of M15+*mce* was used, resolving earlier issues.

A further complication encountered with plaque assays was obtaining clear photographs of the plate which retained enough clarity and detail to visualise the plaques and remaining *Streptomyces* colonies. A number of different approaches were trialled. Photographing plates against a black background in an illuminated lightbox (Rmeet Portable Studio) was attempted and showed plaque area in adequate details (Fig. 4.9.A). However, this method resulted in a loss of definition to *Streptomyces* colonies remaining within the plaque.

Plates were also photographed using a DFK 33UX264 camera connected to a SMZ1500 stereomicroscope, which produced the clearest definition and provided the most detailed photographs (Fig. 4.9.B). However, in order to bring the plaque colonies into focus, a portion of lawn had to be sacrificed from the image.

Illuminating plates on a UVP High Performance UV transilluminator for photography was attempted but again lacked clarity and definition, despite the use of a Nikon D3500 SLR with Nikkor 50mm lens (Fig. 4.9.C).

Photographing the plates whilst aloft allowed light to illuminate the plaques and internal colonies and provided the most detailed photographs whilst capturing the entire well. It was also found that increasing the volume of nutrient broth agar in wells from 1 mL to 2.5 mL allowed for better photography of plaques.

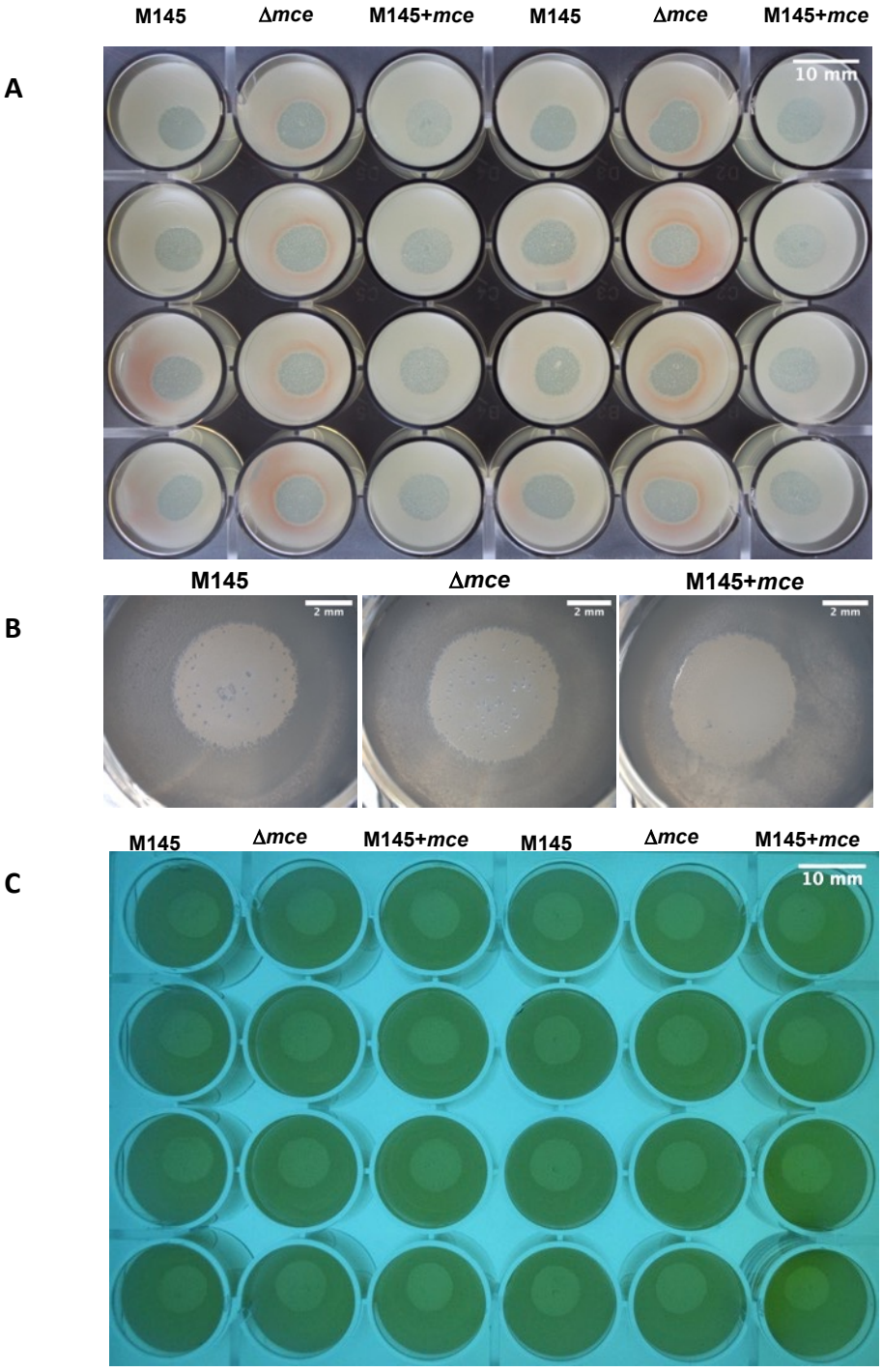

Figure 4.9: Photographing plaque assays. **(A)** 175,000 *Dictyostelium* cells spotted onto 1 x 10^9 *Streptomyces* spores on 80% nutrient broth agar after incubation for 48 hours. Photograph taken using Nikon D3500 SLR with Nikkor 50 mm lens with the plate against a black background. **(B)** 175,000 *Dictyostelium* cells spotted onto 1 x 10^9 *Streptomyces* spores on 80% nutrient broth agar. Lawns and plaques were visualised at 48 hours. Stereo light micrographs taken at 11.25 x magnification on a SMZ1500 stereomicroscope using a DF 33UX264 CMOS camera system. **(C)** 175,000 *Dictyostelium* cells spotted onto 1 x 10^9 *Streptomyces* spores on 80% nutrient broth agar. Lawns and plaques were visualised at 48 hours. Photograph taken using a Nikon D3500 SLR with Nikkor 50 mm lens with the plate illuminated by a UV-transilluminator.

The *S. coelicolor* Δ*mce* strain is not virulent towards *Dictyostelium discoideum* in plaque assays

Following optimisation of the assay technique a number of plaque assays were performed to assess possible virulence of the *mce* null mutant towards *Dictyostelium*. Nutrient broth agar (2.5 mL) at a concentration of 80% was added to 24-well tissue culture plates before addition of 1 x 10^9 *Streptomyces* spores. *Dictyostelium* (175,000 cells per well) were spotted in a 5 µL aliquot directly onto the freshly plated spores and plates incubated for 48 hours. Assays were repeated across a number of days with multiple replicates for each *Streptomyces* strain. A difference in plaque size between strains, as had been apparent with *Acanthamoeba*, was never visualised (Fig. 4.10, Fig. 4.11).

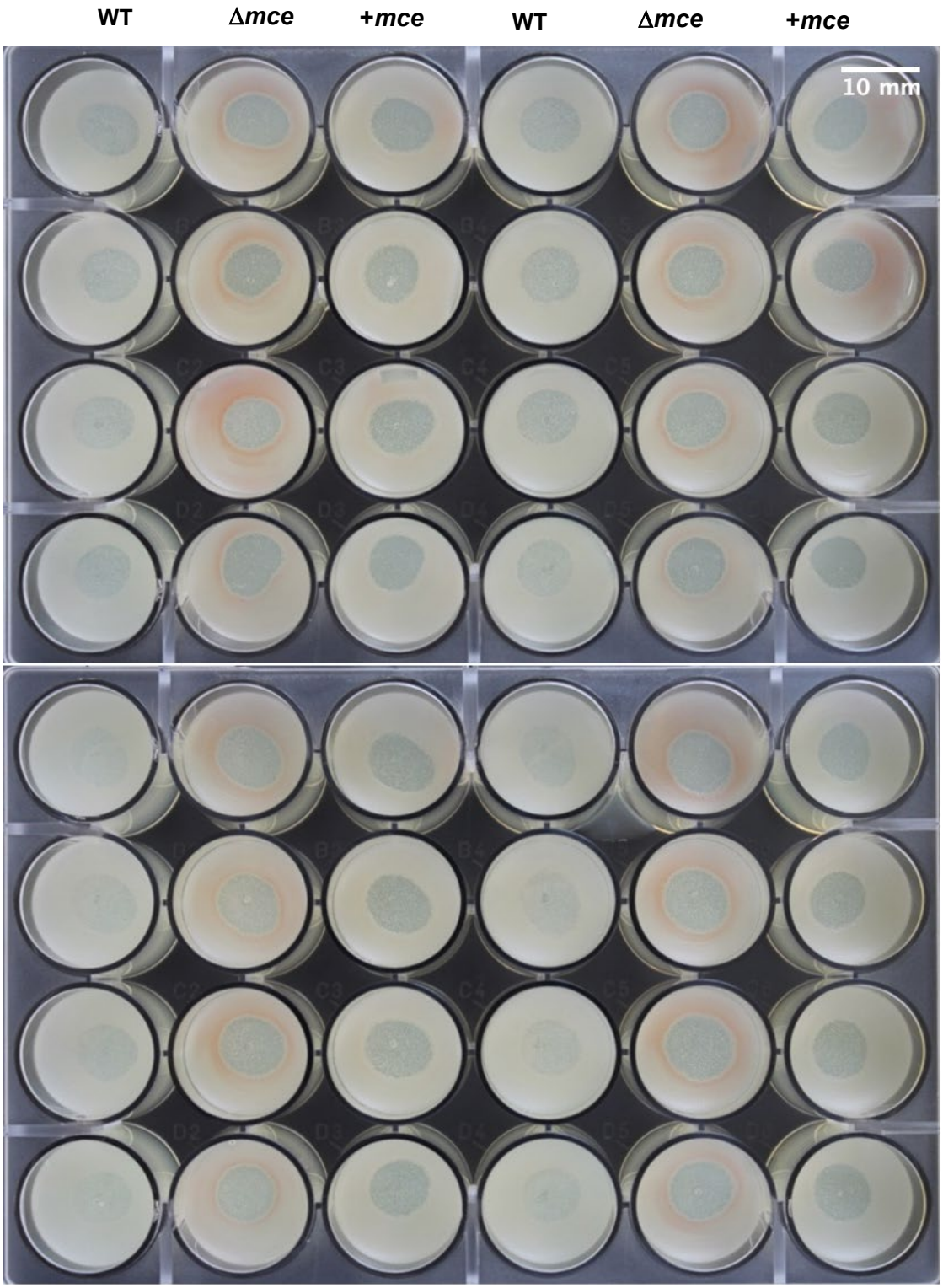

Figure 4.10: *Dictyostelium – S .coelciolor* plaque assays with replicates. Two replicates of 175,000 *Dictyostelium* cells spotted onto 1 x 10^9 *Streptomyces* spores on 80% nutrient broth agar after incubation for 48 hours. Photograph taken using a Canon EOS 1200D camera with the plate against a black background.

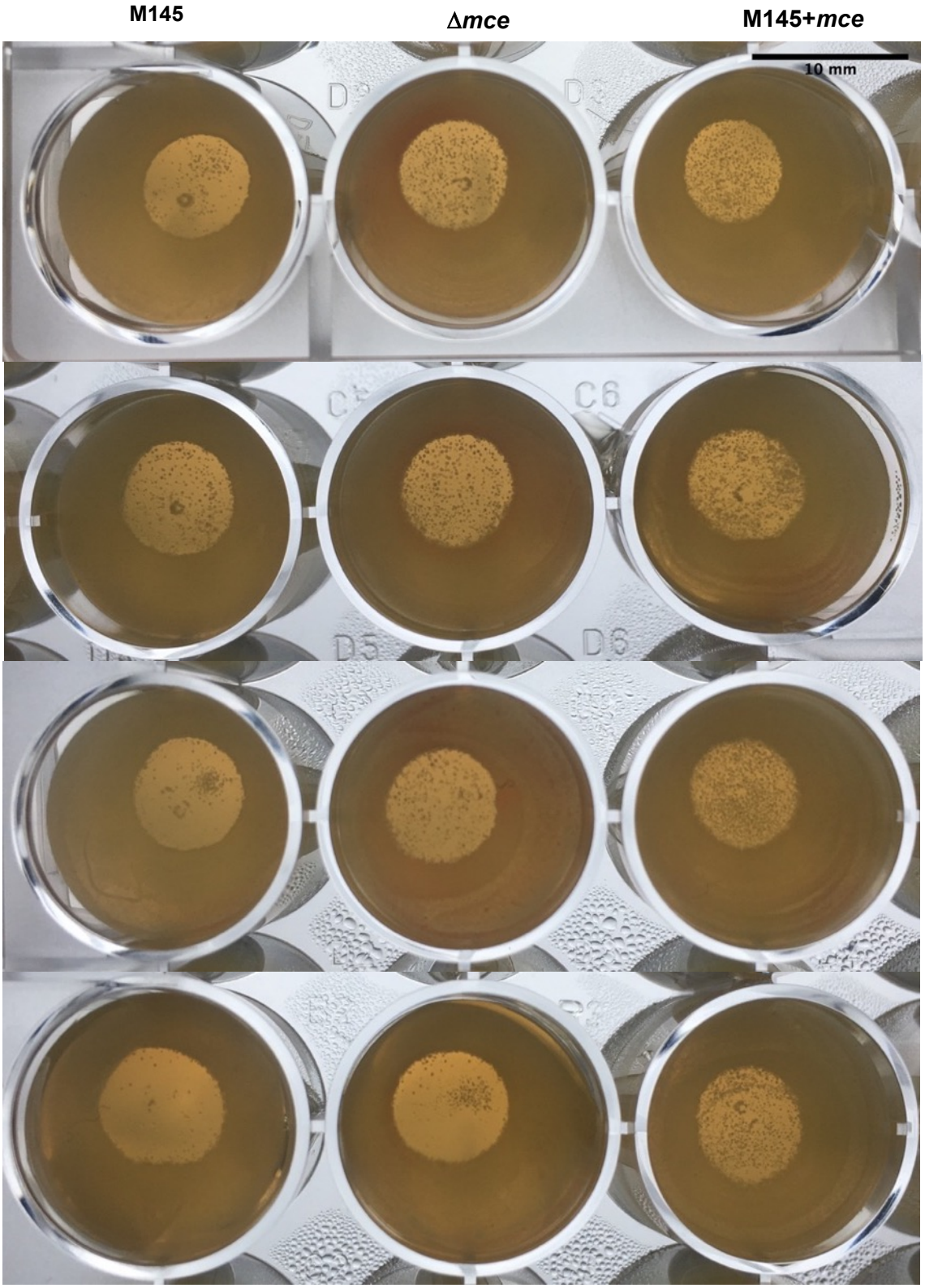

Figure 4.11: No virulence observed in *Dictyostelium* – *S. coelicolor* plaque assays. 175,000 *Dictyostelium* cells spotted onto 1 x 10^9 *Streptomyces* spores on 80% nutrient broth agar after incubation for 48 hours. Photograph taken using a Canon EOS 1200D camera.

Previous worked showed *Acanthamoeba* were unable to form clear plaques upon lawns of the *mce* null mutant, which demonstrated the virulence of the Δ*mce* strain towards this amoeba. Plaque formation by *Acanthamoeba* upon lawns of the M145+*mce* strain were also enhanced, suggesting that the virulence phenotype was dose-dependent (Clark, 2011). *Dictyostelium*, however, were able to form similar and clear plaques on M145, Δ*mce* and M145+*mce* strains. To determine whether plaque size differed between strains, plaque areas were measured in ImageJ for each of the plaques in Fig. 4.11 and data analysed (Fig. 4.12). An ordinary one-way ANOVA was performed on results and found no difference in plaque area on lawns of M145, Δ*mce* or M145+*mce* (P = 0.4033).

It was noted that the number of phagocytosed colonies appeared to be greater within plaques on lawns of the Δ*mce* strain (Fig. 4.10). This could be indicative of *Dictyostelium* lysis, leading to reduced phagocytosis, which in turn may be due to enhanced virulence of the Δ*mce* strain compared to *S. coelicolor* M145. In order to ascertain if the incidence of colonies within plaques was higher for the *mce* null mutant, colonies were counted using ImageJ and a cell colony counter software (Liam Rooney, 2019, unpublished) (Fig. 4.11). A one-way ANOVA found no difference in within-plaque CFU between strains (P=0.6690). An unpaired t-test was used to compare intra-plaque colonies of the M145 strain with the *mce* null mutant and found no difference (P=0.1852). Similarly, an unpaired t-test comparing CFU within M145 and the M145+*mce* strain plaques found no difference (P=0.0890) between strains. Non-parametric Mann-Whiney tests comparing intra-plaque colonies between strains again found no difference in CFU between M145 and the Δ*mce* strain (P=0.2000) or M145 and the M145+*mce* strain (P=0.1000). The Δ*mce* strain therefore appears to be avirulent towards *Dictyostelium* in plaque assays, unlike the phenotype observed with *Acanthamoeba* (Clark *et al.*, 2013).

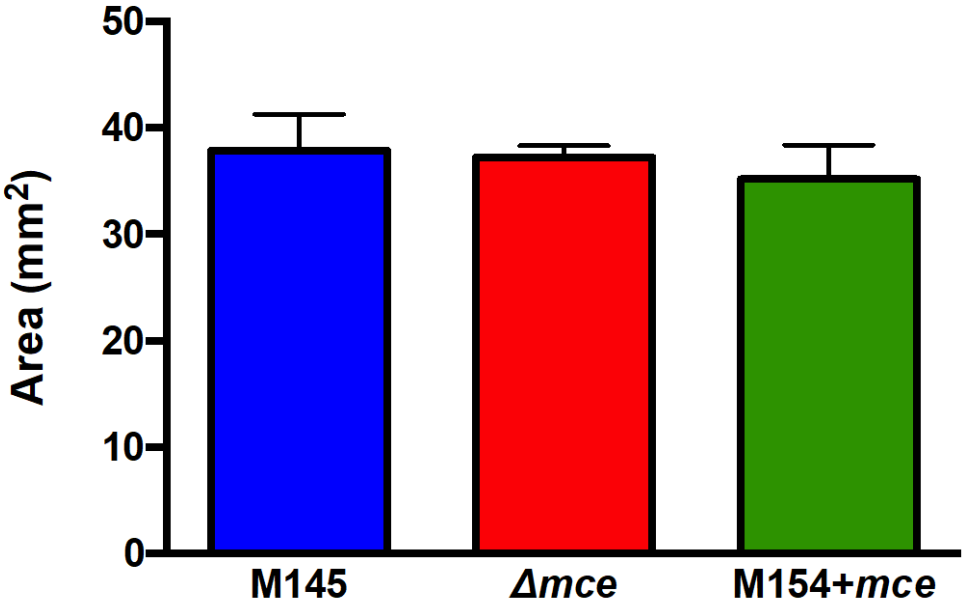

Figure 4.12: Comparisons of mean plaque area (mm^2) of plaques on lawns of M145, Δ*mce* and M145+*mce* strains. An ordinary one-way ANOVA found no difference in mean plaque areas between strains (P = 0.4033) (N=4). Error bars represent standard deviation.

‘

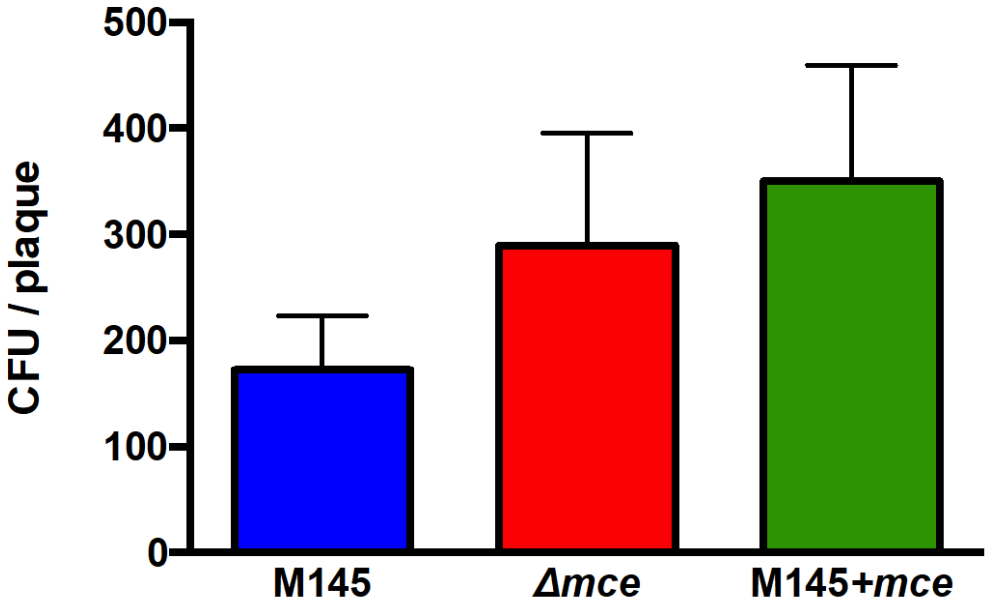

Figure 4.13: Comparisons of CFU within *Dictyostelium* plaques on lawns of M145, Δ*mce* and M145+*mce* strains. A one-way ANOVA found no difference in within-plaque CFU between strains (P=0.6690) (N=3). Error bars represent standard deviation.

Development of *Dictyostelium* – *Streptomyces* co-culture

Preliminary co-culture experiments were performed in nutrient rich HL5, the standard growth medium for axenic *Dictyostelium* strains. *Dictyostelium* grow well and are able to phagocytose efficiently in this medium (Rosel *et al.*, 2012; T. D. Williams and Kay, 2018). Spores of *S. coelicolor* were also observed to germinate well in HL5. Co-culture phase contrast images were acquired with an Orca-285 digital camera attached to a Nikon Eclipse TE2000-S inverted microscope equipped with 20X and 100X objectives. All images are of live, unfixed, and highly motile cells.

Early development of co-culture technique aimed to determine the correct density of *Dictyostelium* to *Streptomyces* spores, as well as optimize imaging methods and co-culture time-points. Spores of the *mce* null mutant had displayed enhanced virulence towards *Acanthamoeba* at approximately 24 hours in prior work, thus initially co-cultures were observed for a 24-hour time period. Varied densities of AX2-214 *Dictyostelium* ($1x10^6$, 500,000, 250,000 or 125,000 cells per mL) were examined to determine optimum density for imaging (Fig. 4.14.A). A quantity of 125,000 cells per mL was found to allow for clear imaging of individual amoeba and manageable growth within the 24-hours the co-culture was observed. An amount of 1.8×10^8 Δ*mce* spores per mL was trialled and found to be suitable for observing spore-amoeba dynamics (Fig. 4.14.B). This produced a MOI of 1:1440. Co-culture experiments were carried out in Ibidi µ-Dishes (Ibidi®, Cat. # 81156) with a 3.5 cm^2 growth area and an ibidi Polymer coverslip bottom which facilitates imaging. Dishes were filled with 1mL of HL5 containing the correct density of amoeba to spores and maintained at 22°C in a static incubator for the duration of the experiment.

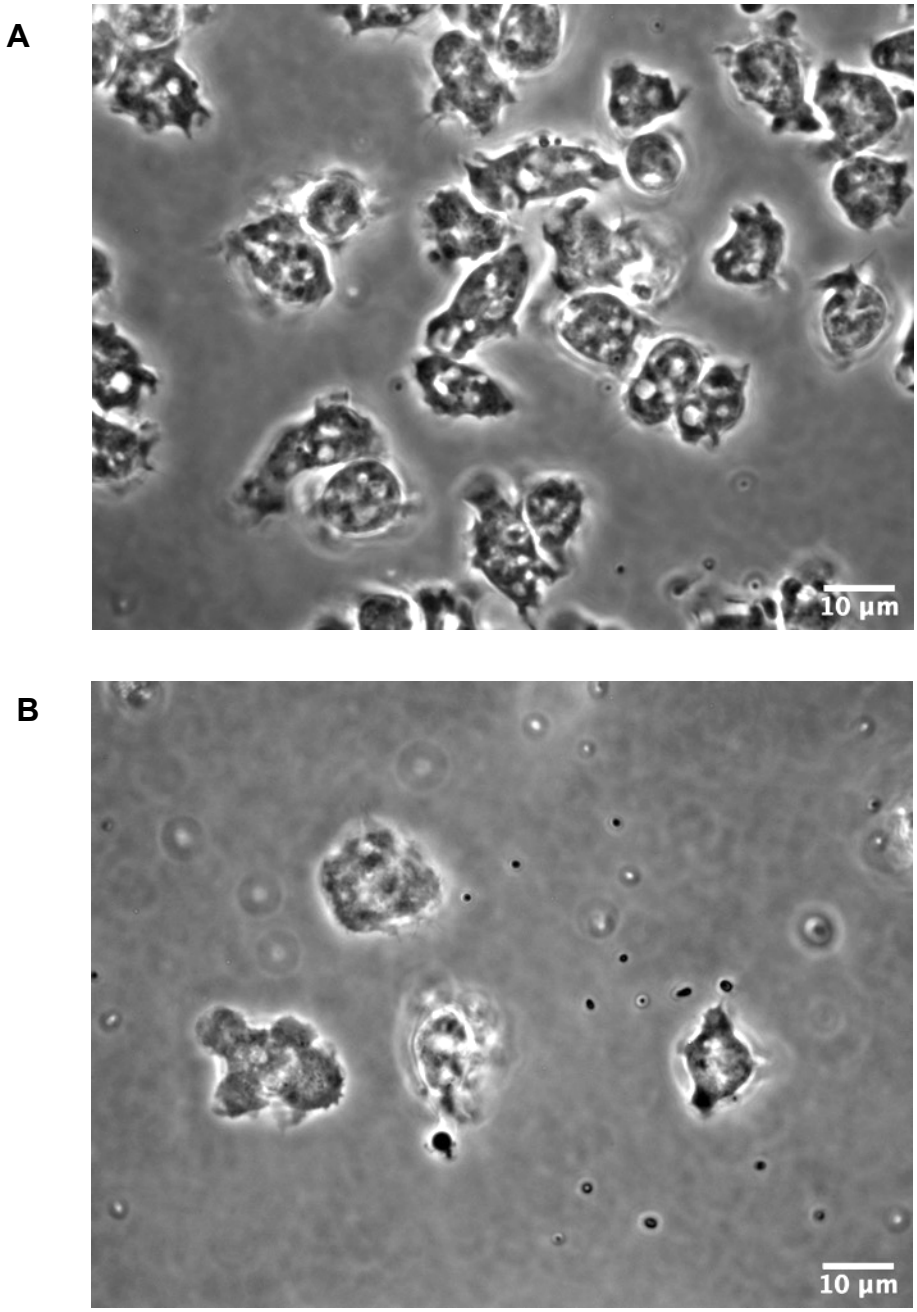

Figure 4.14: Co-culture of *Streptomyces* spores with *Dictyostelium* in 1mL HL5 medium in Ibidi® dishes. Densities of 500,000 **(A)** and 125,000 **(B)** *Dictyostelium* cells per mL were examined. A density of 125,000 amoebae with 1.8 x 10^8 spores per mL was found to the optimum for observing spore-amoebae interactions. Phase contrast images were acquired using an Orca-285 digital camera attached to a Nikon Eclipse TE2000-S Inverted microscope with a 100X objective.

Co-cultures were imaged at 0, 1, 5, 8 and 24-hours post-spore addition. Prior experiments with *Acanthamoeba* and *S. coelicolor* spores were conducted at a MOI of 1:1, however the *Dictyostelium* model appears to be more active in spore consumption and requires a higher spore-to-amoebae MOI. This was observed in the first hour of co-culture, where a number of phagocytosed spores were already apparent within the amoeba (Fig. 4.15). Physical association of *Dictyostelium* and spores occurred almost instantly, with *Dictyostelium* seen to use pseudopodia to attach to spores for phagocytosis. *Dictyostelium* were also highly mobile and travelled across the substratum whilst attaching to and phagocytosing spores at a rapid rate. There was no observable difference in attachment and uptake of Δ*mce* spores to M145 spores by *Dictyostelium* during observation of co-culture.

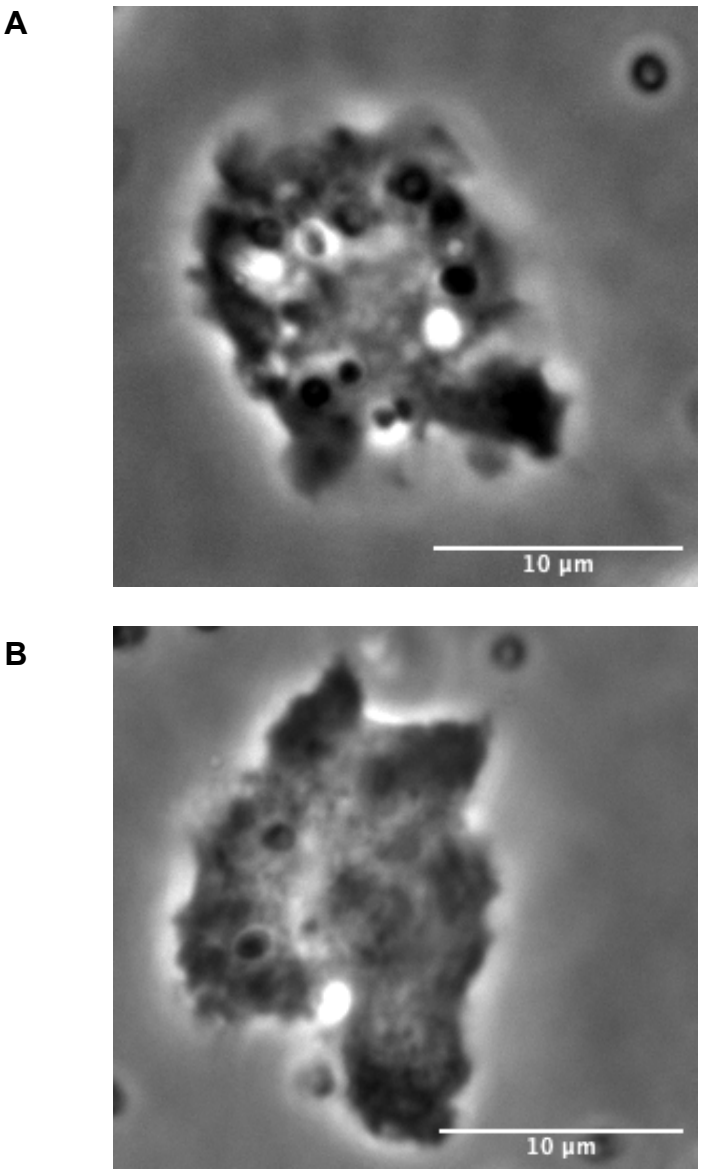

Figure 4.15: Co-culture of *Dictyostelium* and *S. coelicolor* spores at 1-hour in HL5 media. (A) A single *Dictyostelium* amoeba at 1-hour post spore addition. A number of *S. coelicolor* spores are identifiable intracellularly, indicating phagocytosis has occurred. **(B)** A *Dictyostelium* amoeba with two internalised *Streptomyces* spores visible intracellularly at 1-hour into co-culture. Co-culture in 1mL HL5 with 125,000 *Dictyostelium* and $1.8x10^9$ spores. Phase contrast images were acquired using an Orca-285 digital camera attached to a Nikon Eclipse TE2000-S Inverted microscope with a 100X objective

At 5 hours in co-culture, further spore consumption by amoeba and an increase in *Dictyostelium* cell numbers was apparent (Fig. 4.16.A). At 8 hours, number of *Dictyostelium* cells had again increased, with further phagocytosis of spores occurring. *Dictyostelium* cells retained their amoeboid shape with pseudopodia and were seen to be actively motile and feeding. Free spores in the medium had decreased and uptake into amoeba was evident (Fig. 4.16.B).

Typically, phagosomes appeared to conform tightly to the size of the spore at a rapid rate following uptake. Occasionally, distinct internalised spores could be visualised in phagosomes which contained a larger volume of liquid to result in a spacious compartment, a phenomenon which has been previously seen in *Dictyostelium* with yeast (Clarke *et al.*, 2002). Such a spacious phagosome containing an intracellular spore may be seen in Fig. 4.16.B. These phagosomes appeared to be in a transient state, as their size rapidly resolved to fit the spore tightly.

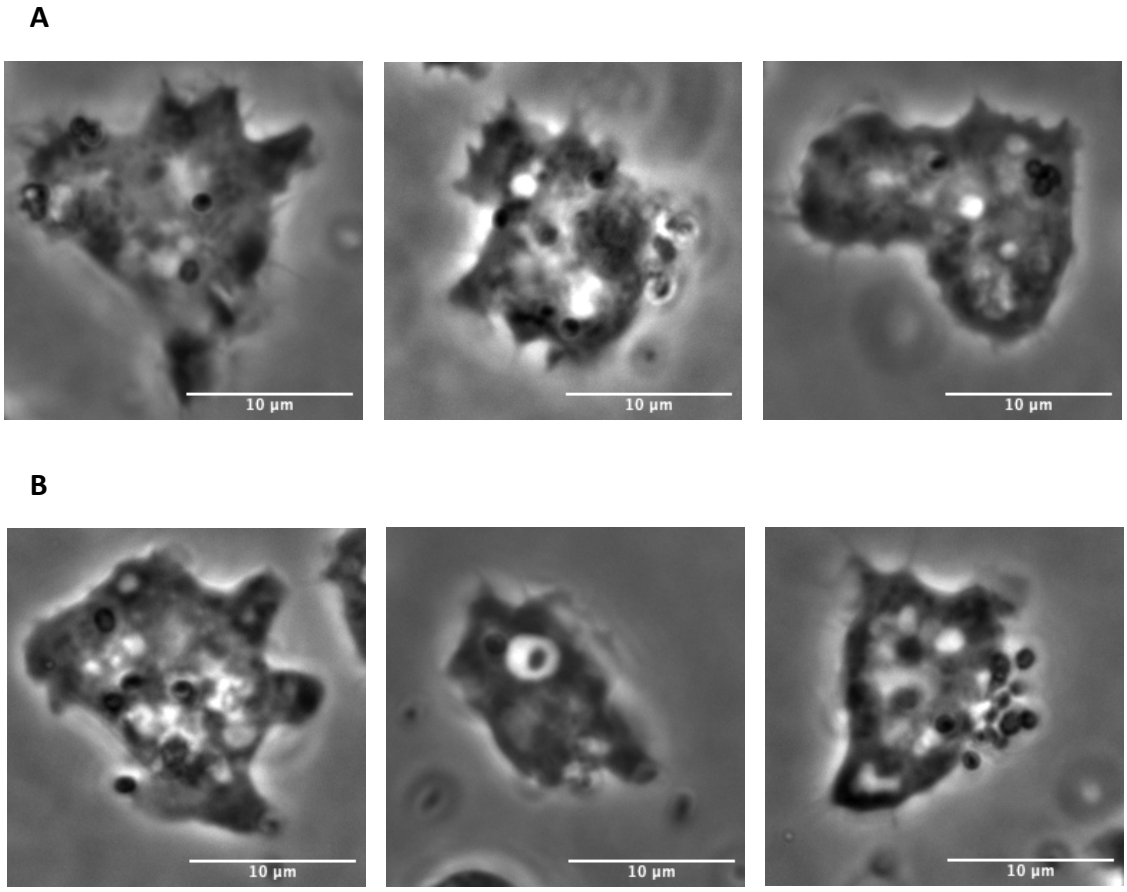

Figure 4.16: Co-culture of *S. coelicolor* spores in HL5 suspension with *Dictyostelium* amoeba. (A) Individual amoeba 5 hours into co-culture showing association and phagocytosis with *Streptomyces* spores. **(B)** Individual amoeba 8 hours into co-culture with internalised *Streptomyces* spores. Increased numbers of lysosomes indicate attempted degradation spores is occurring.

At 24 hours density of amoeba had increased significantly and few free spores were visible (Fig 4.17.A). Internalised spores were evident within amoeba, however no lysis of *Dictyostelium* was visualised. Spores which remained inside amoeba at 24 hours without signs of germination may be nonviable, as not all spores in a population will germinate. It is also possible that the internal conditions of the amoeba have rendered the spores nonviable or are inhibitory towards germination (Fig. 4.17.B).

Floating mycelial clumps of both M145 and the *mce* null mutant were also apparent, demonstrating the germination and growth of spores occurred within the 24-hours of co-culture (Fig. 4.17.C). This mycelium did not appear to be associated with lysed amoeba as observed with *Acanthamoeba* by Clark *et al* (2013).

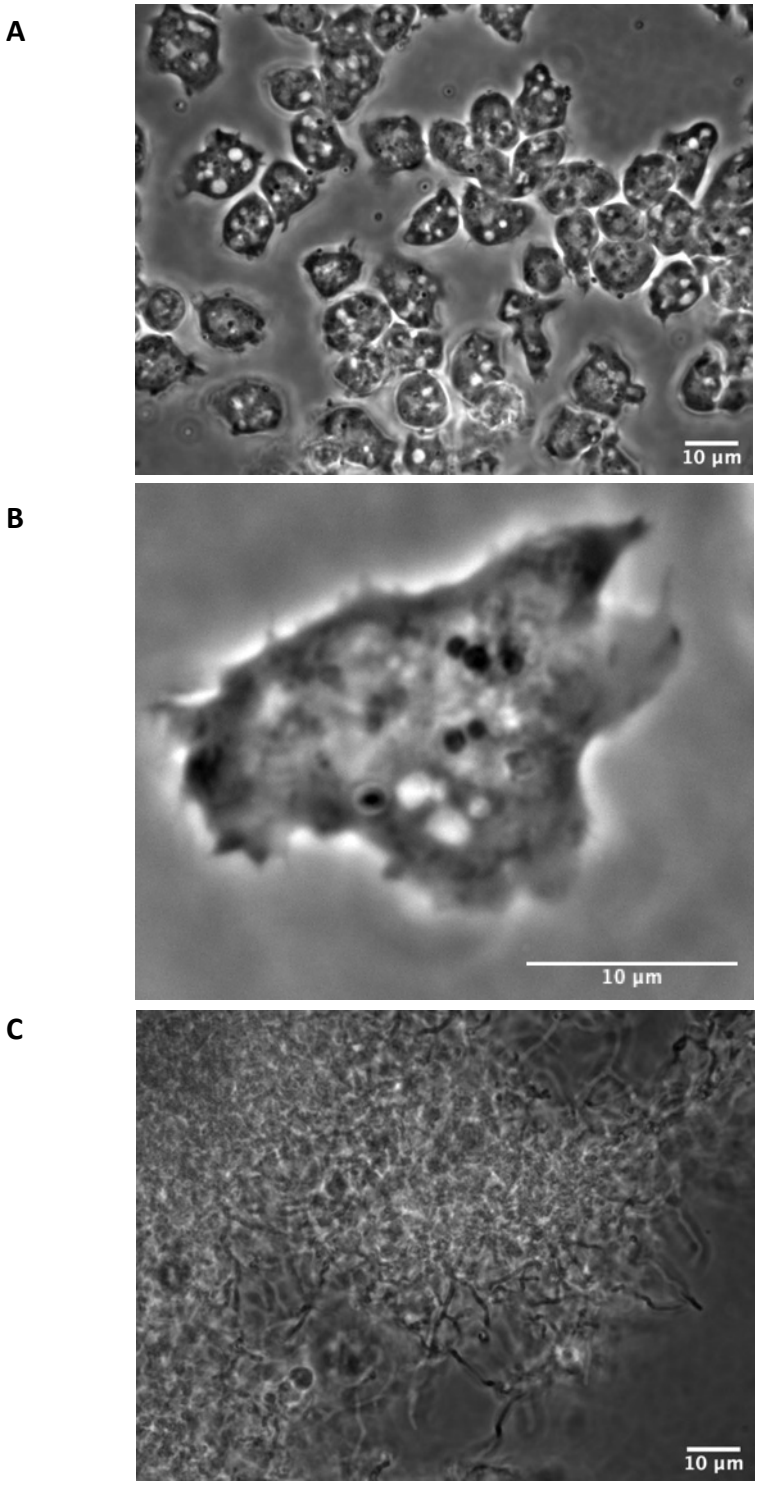

Figure 4.17 No virulence of *S. coelicolor* spores towards *Dictyostelium* amoeba observed at 24-hrs into co-culture. (A) 24 hours into co-culture in HL5 a clear increase in *Dictyostelium* cells is apparent, with fewer free spores visible in the aqueous medium. **(B)** Amoeba in co-culture remained healthy with internalised, non-germinating spores. **(C)** A proportion of spores had germinated in HL5 medium within 24 hours to produce dense floating mycelium.

Determination of optimum co-culture experimental media

Dictyostelium within the environment grows essentially in fresh water and soil, surviving through phagocytosis of prey bacteria. Axenic HL5 medium is able to support growth of axenic strains of *Dictyostelium* in the absence of bacteria, with amoeba performing macropinocytosis to acquire nutrients. Growth of *Dictyostelium* in HL5 has a number of benefits, including eliminating the necessity of separating amoeba from food-source bacteria, a time-consuming process. As HL5 is a nutrient rich medium, it also prevents starvation from initiating the onset of *Dictyostelium* development, a process during which vegetative amoeba stop feeding and begin to aggregate. Further essential for co-culture experiments, *Dictyostelium* retain the ability to phagocytose bacteria very efficiently in HL5 medium, as phagocytosis is the preferred feeding method of these amoeba (T. D. Williams and Kay, 2018). However, for the purpose of co-culture experiments, HL5 media also presents a number of disadvantages compared to more physiological buffers such Sörensen's (Sor) buffer. Sor buffer is essentially buffered water, meaning it is a more biologically relevant medium to study predation. HL5, as a rich medium, is likely to increase germination rate in *Streptomyces*, a factor which may affect pathogenicity of the bacteria if virulence is due to precocious germination. HL5 is also highly autofluorescent, making it unsuitable for fluorescence-based co-culture (Fig. 4.18)

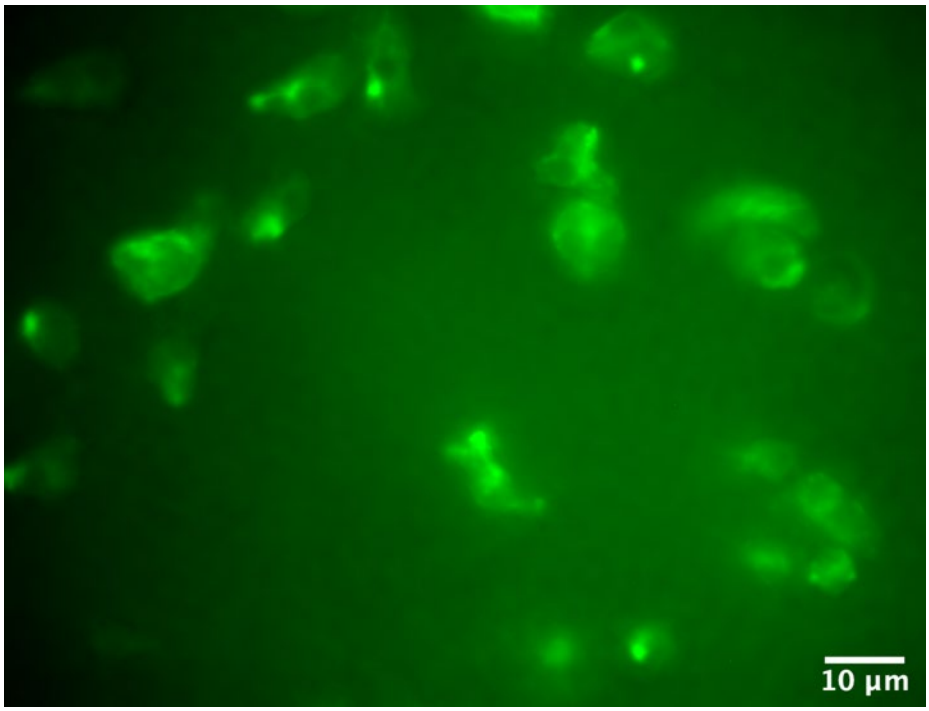

Figure 4.18: Autofluorescence of HL5 media. AX2-n2-GFP in HL5 medium under fluorescence illumination using the FITC filter on a Nikon Eclipse TE2000-S microscope and 100X objective lens. HL5 medium was strongly autoflourescent and caused autofluorescence of *Dictyostelium* cells. The V-ATPase of *Dictyostelium* appears brighter within autoflourescent cells.

Sor buffer was chosen for co-culture experiments as a buffer more reflective of the nutrient limited soil conditions encountered by *Dictyostelium.* It has the benefit of being non-fluorescent, and *Dictyostelium* are able to survive and phagocytose well in this medium when provided with bacterial prey. As Sor lacks a carbon source, results of co-culture experiments performed in this medium are more comparable to those from previous work with *Acanthamoeba*, performed in Page's Amoeba Saline (Clark *et al.*, 2013).

Co-culture experiments were repeated in Sor buffer. Notably, although growth of *Dictyostelium* was reduced in Sor buffer compared to HL5 medium, aggregation of *Dictyostelium* in higher concentrations was seen to occur. In Sor buffer containing 1.8 x 10^8 *Streptomyces* spores per mL, *Dictyostelium* at concentrations of 250,000 cells per mL or higher were seen to aggregate at 14 hours. This occurred in the presence of both M145 and Δ*mce* spores, with aggregation being more severe with increasing density of *Dictyostelium* (Fig. 4.19.A). At 16 hours, aggregation had increased further, and fruiting bodies could be visualised within the medium (Fig 4.19.B). *Dictyostelium* aggregation is the first step in development which is triggered by starvation of single-celled amoeba. This suggests that at higher concentrations of amoebae, the number of spores present is insufficient to keep amoebae from starvation in Sor buffer. It is possible that this is due to low folate production by *Streptomyces* spores, particularly whilst dormant, resulting in initiation of starvation protocols in *Dictyostelium* whilst in high cell density, as amoeba are unable to sense bacterial prey in the medium. At lower densities, such as 125,000 *Dictyostelium* cells to 1.8 x 10^8 *Streptomyces* spores per mL, no aggregation occurred for the duration of co-culture. Aggregation as seen in co-culture is therefore density dependent and may be exacerbated by the chemical inactivity of *Streptomyces* spores.

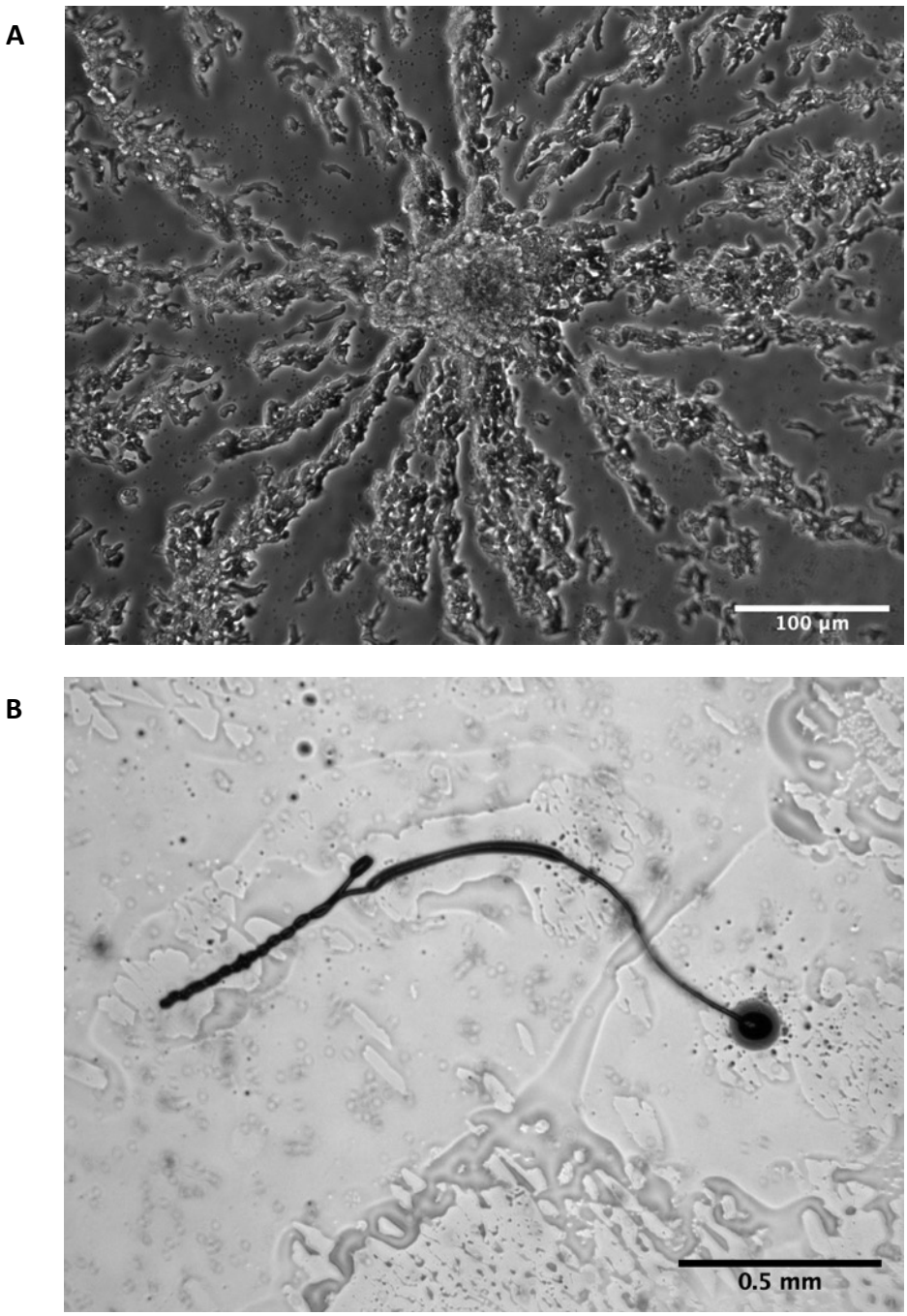

Figure 4.19: Morphological development in *Dictyostelium* co-culture. (A) 500,000 *Dictyostelium* in 1mL Sor buffer aggregating at 16 hours in co-culture. Phase contrast image was acquired using an Orca-285 digital camera attached to a Nikon Eclipse TE2000-S Inverted microscope with a 20X objective. **(B)** A fully formed fruiting body visualised at 16 hours into co-culture of *Streptomyces* and *Dictyostelium* in Sor buffer. Phase contrast image was acquired using an Orca-285 digital camera attached to a Nikon Eclipse TE2000-S Inverted microscope with a 4X objective.

No *Streptomyces*-induced lysis of *Dictyostelium* is seen in co-culture with spores of Δ*mce* mutant or M145

Following optimisation, co-culture experiments were performed with the AX2-N2-gfp *Dictyostelium* strain. AX2-N2-gfp was used in phase contrast co-culture experiments to ensure consistency across phase contrast and fluorescent co-culture. Co-culture was carried out in 1 mL Sor buffer with no external carbon source in Ibidi-dishes with a polymer coverslip bottom for cell imaging. Phase contrast images of co-culture experiments were acquired using an Orca-285 digital camera attached to a Nikon Eclipse TE2000-S microscope equipped with a 100X objective.

Co-cultures in Sor buffer were observed at 0, 1, 5, 8, 14, 16, 20, 24 and 40 hours (Fig. 4.20). *Dictyostelium* were seen to rapidly phagocytose *Streptomyces* spores in Sor buffer and continued to feed for the duration of the experiment. Healthy *Dictyostelium* could be seen at 24 hours actively phagocytosing remaining spores in the co-culture medium (Fig. 4.21.A)

Mycelial growth of the *mce* null mutant strain was visualised by 16 hours in Sor buffer (Fig. 4.21.B) but was not seen for the M145 strain. However, this may be due to the difficulty of locating floating mycelium within the culture. The presence of dense mycelium at 16 hours indicates that spores of the Δ*mce* strain had germinated some hours earlier in the medium. Amoeba lysis due to precocious spore germination would therefore be predicted to begin occurring prior to this time; although it is possible the intracellular environment of the amoeba may slow germination in phagocytosed spores. However, no *Dictyostelium* lysis due to intracellular spore germination was observed for the duration of the experiment.

Although spore germination occurred, it did not appear that *Streptomyces* were utilising the *Dictyostelium* as a carbon source, since no association of amoeba with mycelium was observed. Though this may have been due to density of the mycelium obscuring amoeba or complete break-down of lysed amoeba, it is more likely that spore germination was enabled by intracellular stores of trehalose and polyphosphates, particularly as spores were seen to germinate in Sor buffer without amoeba present (Ranada and Vining, 1993; Bobek, Šmídová and Čihák, 2017)

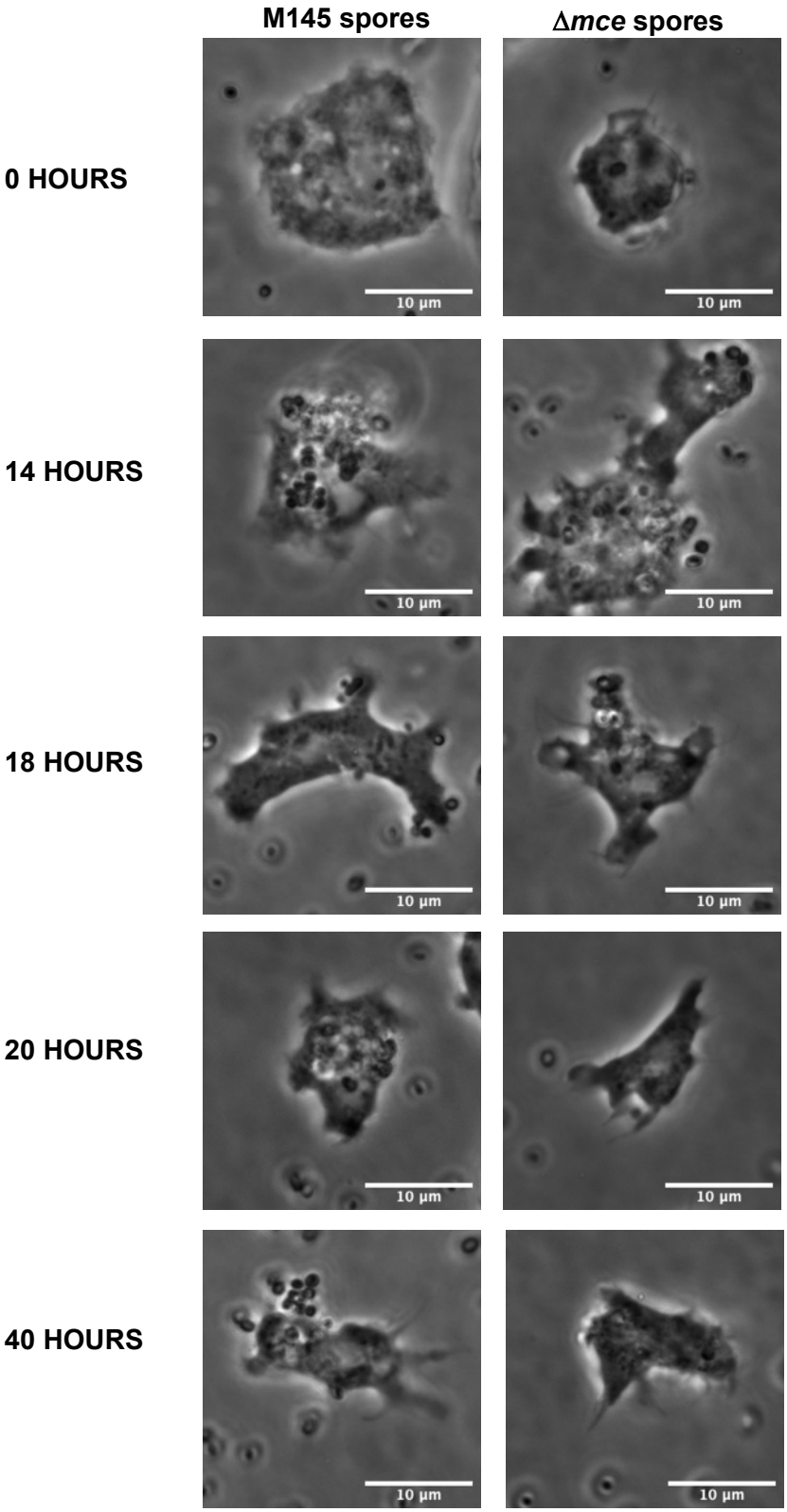

Figure 4.20: 40-hr co-culture in Sor buffer. 125,000 AX2-N2-gfp *Dictyostelium* with 1.8 x 10^8 M145 or Δ*mce* spores in 1mL Sor buffer over a period of 40 hours. Phase contrast images were acquired using an Orca-285 digital camera attached to a Nikon Eclipse TE2000-S Inverted microscope with a 100X objective.

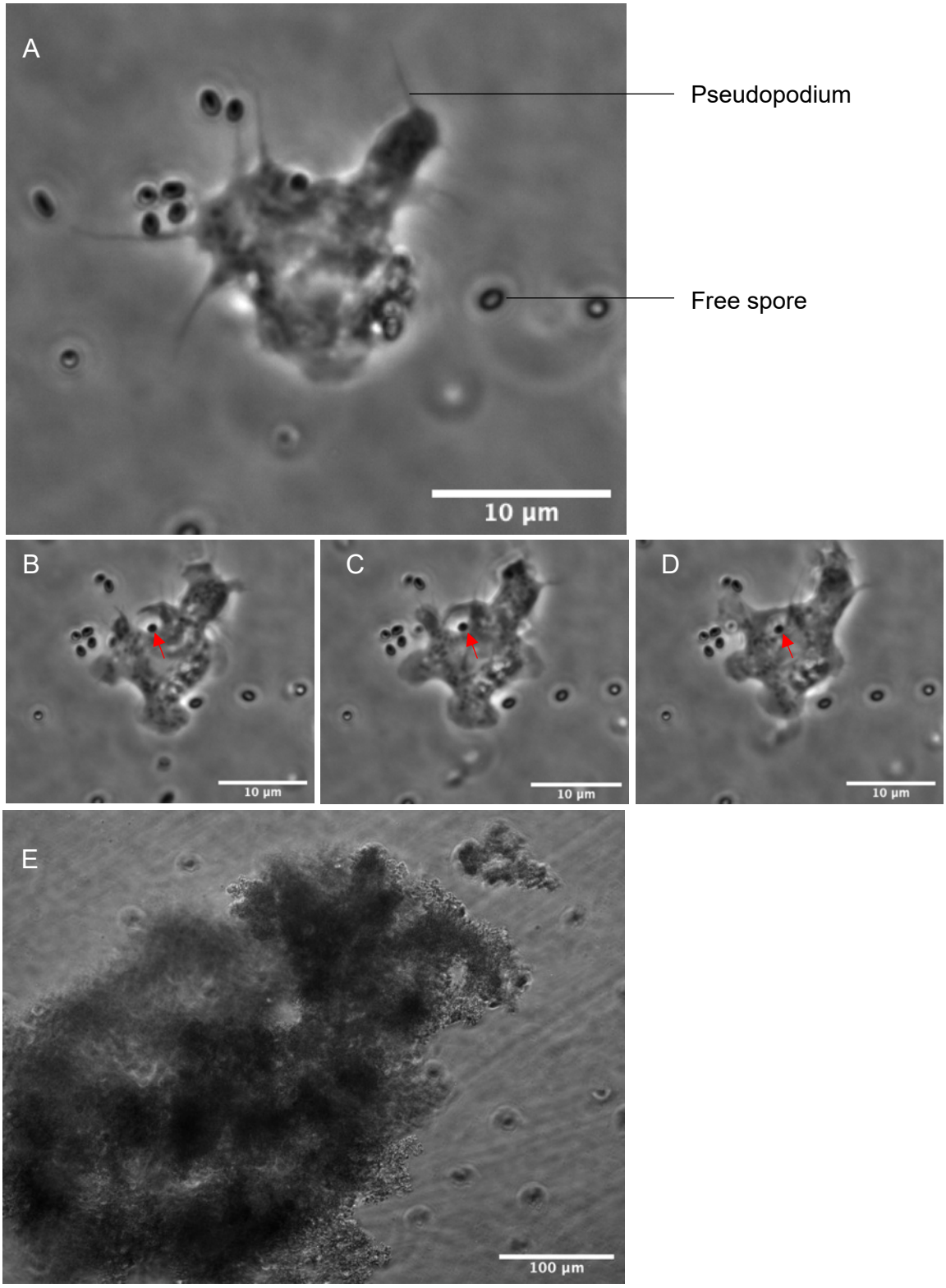

Figure 4.21: Co-culture observations in Sor buffer. (A) A *Dictyostelium* amoeba at 24 hours in Sor co-culture, using pseudopodia to attach to spores. **(B – D)** Phagocytosis of a spore at 24 hours with visualisation of formation of the phagocytic cup and eventual engulfment of the spore. A period of 17 seconds passes between **B** and **D. (E)** Mycelial growth of the *mce* null mutant at 16 hours in Sor buffer during co-culture.

Creation of mCherry::Δ*mce* and M145 strains for co-culture

Fluorescent co-culture required use of both spores and *Dictyostelium* expressing distinct fluorophores. *Dictyostelium* expressing GFP-fusions were purchased from DictyBase (http://www.dictybase.org/). Strains of M145, Δ*mce* and M145+*mce* expressing the fluorophore mCherry were originally created using a modified pIJ8655 plasmid encoding mCherry under control of the ermEp promoter but produced too poor a fluorescent signal to be viable in co-culture experiments. For this reason, strains were transformed with the modified plasmid pMS82, encoding mCherry under control of the *S. coelicolor* gap1 promoter. This plasmid, named PRed, was created by Zacchetti *et* al (Zacchetti *et al.*, 2016) (Fig. 4.22). pRed plasmids were conjugated into WT, Δ*mce* and M145+*mce* and observed under a fluorescence microscope and found to emit a strong and stable fluorescent signal.

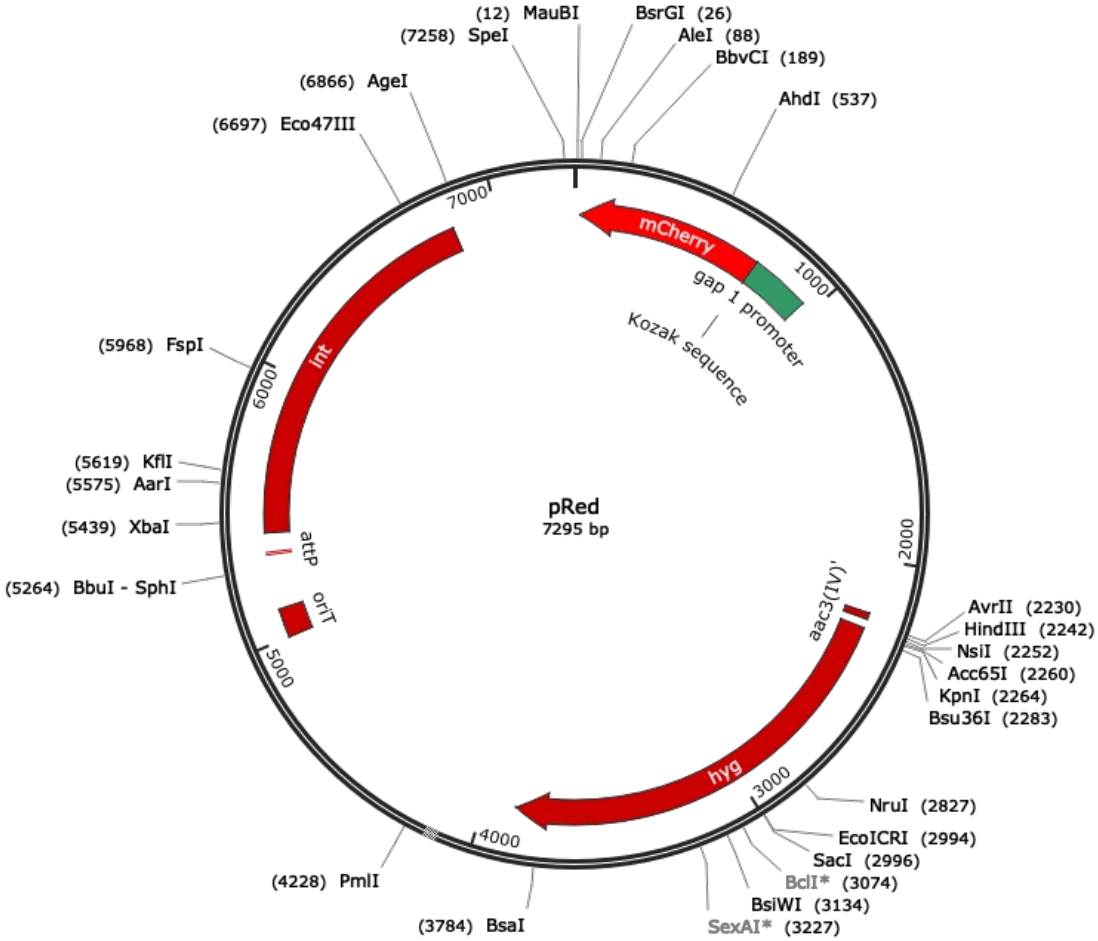

Figure 4.22: The pRed plasmid. The plasmid contains the gene encoding the flurophore *mCherry* under the control of the *gap1* promoter from *Streptomyces*.

Spores of the Δ*mce* mutant and *S. coelicolor* M145 rapidly co-localise with the V-ATPase of *Dictyostelium*.

In order to observe the intracellular interactions of the *Streptomyces* spores within the *Dictyostelium* amoebae, the AX2-N2-gfp *Dictyostelium* strain was used in conjunction with mCherry expressing *Streptomyces*. The AX2-N2-gfp strain expresses the fusion protein VatM-GFP, with the GFP moiety located on the C-terminus of VatM, the 100kDa transmembrane subunit of the vacuolar H^+-ATPase (V-ATPase) (Clarke *et al.*, 2002). In *Dictyostelium* the V-ATPase is responsible for acidifying the phagolysosome and is recruited to the phagosome within minutes of bacterial internalisation. *Dictyostelium* expressing VatM-GFP were utilised in co-culture experiments allowing for visualization of the internal interactions of the spores with the phagolysosome.

Co-culture was set up in Sor buffer as priorly described and observed over a 40-hour period. Microscopy was performed with an Olympus 1000FV confocal laser scanning microscope equipped with a 60X objective. Confocal fluorescence images were captured using excitation at 488 nm and 543 nm simultaneously with a Red He-Ne and a Melles-Griot Argon-ion laser. Cultures were observed and images taken at 0, 2, 12, 16, 18, 20, 24 and 40 hours.

Rapid co-localisation of the GFP-tagged V-ATPase with *Streptomyces* spores was seen from approximately 5 minutes onwards (Fig. 23). This was indicative of internalisation of the spores into the *Dictyostelium* and presence within phagosomes. High numbers of spores were found associated with and within phagosomes at any one time. No preferential association of either M145 or Δ*mce* spores with phagosomes was observed. *Dictyostelium* continued to associate with and phagocytose spores for the length of experiment, with localisation of phagosomes and spores still apparent at 40 hours. No apparent internal germination of either M145 or Δ*mce* spores was seen inside the

Dictyostelium at any time-point. Germination of Δ*mce* spores had clearly occurred by 16 hours, observed as a floating mycelial mass at the culture surface. M145 spores were seen to have produced a floating mycelium by 40 hours.

An issue encountered with the Olympus FV1000 microscope was a lack of phase contrast imaging available on this system, which prevented overlay of phase contrast and confocal images to provide greater detail to amoeba structures. This made distinguishing between V-ATPase localisation in the membrane of phagosomes, endosomes and the contractile vacuole highly difficult. The VatM-GFP fusions has been shown to be delivered by endosomal vesicles to newly formed phagosomes within 1-2 minute of prey uptake, with endosomes clustering at the phagosome membrane (Clarke *et al.*, 2002). As the localisation of the VatM-GFP to the phagosome via endosomes occurs so rapidly following uptake, it is reasonable to assume the GFP signal observed originates from the membrane of the phagosome or closely clustered endosomes and spore interaction with these is evident. The contractile vacuole does not cluster with the phagosome but may be distinguished in some images via the absence of GFP within its lumen. As no amoeba lysis was observed due to *Streptomyces* intracellular growth, attempts to define and visualise intracellular amoeba structures via staining and microscopy were not warranted.

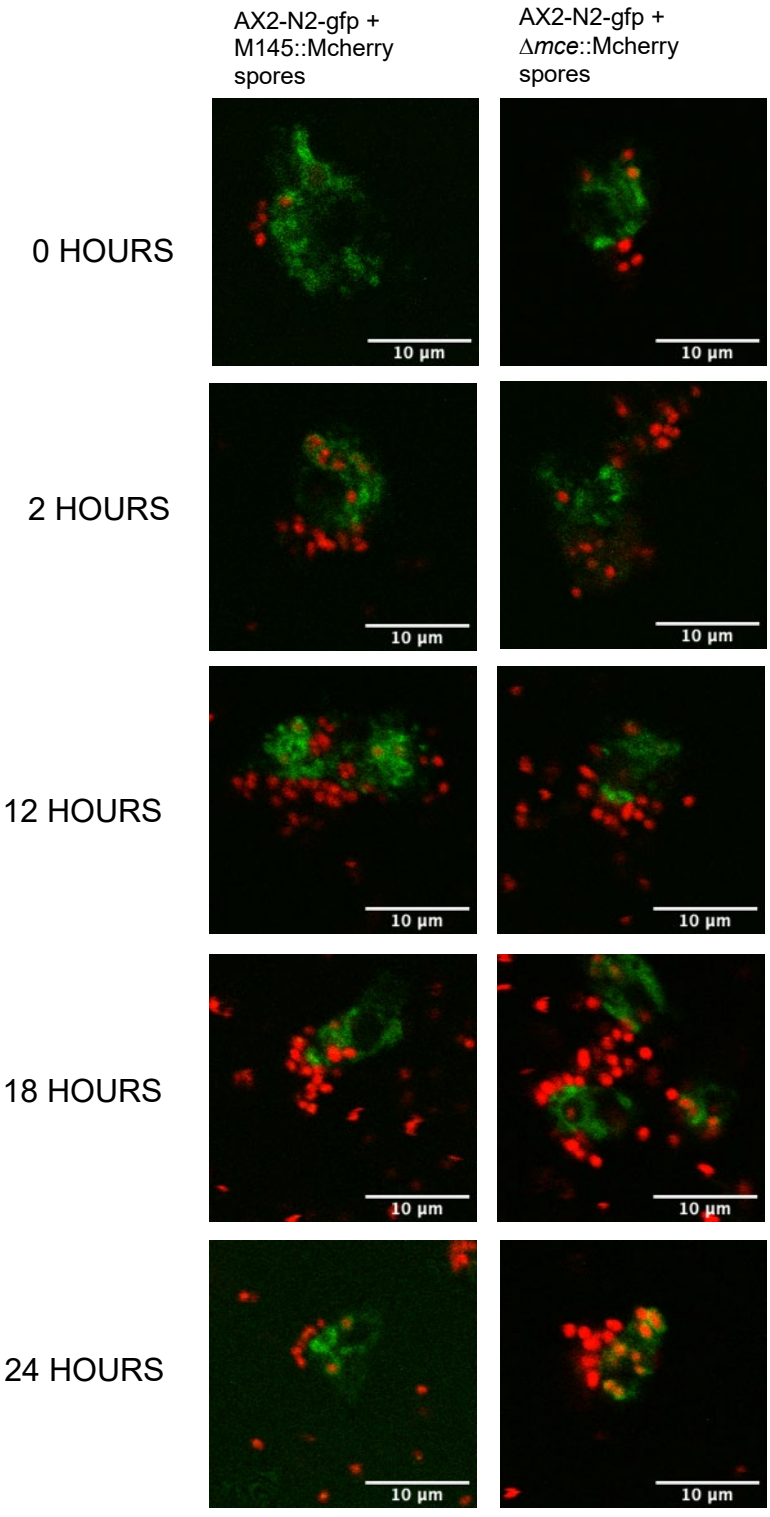

Figure 4.23: 125,000 AX2-VatM *Dictyostelium* with 1.8 x 10^8 WT or *mce* null spores in 1mL Sor buffer. Images were taken using a Olympus FV1000 confocal microscope with a 60X objective, using a Red He-Ne and a Melles-Griot Argon-ion laser at excitation of 488nm and 534 simultaneously.

Dictyostelium associate with and phagocytose *Streptomyces* spores rapidly, with no *Dictyostelium* lysis observed as a result

Imaging of the AX2-N2-gfp *Dictyostelium* strain proved challenging due a lack of detail in distinct structures of the amoeba. This issue was compounded by the absence of phase contrast imaging available on the Olympus FV1000 confocal microscope used, which prevented visualisation of the amoeba cell membrane, contractile vacuole and pseudopodia. To circumvent this issue and allow visualisation of the entire amoebae and its interaction with *Streptomyces* spores, the axenic *Dictyostelium* strain AX2-GFP-tubA was used; this strain contains GFP fusions to alpha-tubulin. *Streptomyces* spores expressing mCherry red fluorescent protein were again used for fluorescent co-culture, as previously described. Co-culture was shortened to a length of 24 hours as no prior lysis had been observed at 40 hours. As well as spores of M145 and the *mce* null mutant strain, the additional copy mutant M145+*mce* was tested in co-culture to determine if this strain showed enhanced virulence towards *Dictyostelium* (Fig.4.24).

Dictyostelium were seen to rapidly associate with spores, with uptake of spores seen within 5-10 minutes of addition. Spores appeared to be “caught” by the *Dictyostelium* and often associated in a crescent-moon shape around the *Dictyostelium* cell surface, likely interacting with phagocytic cell-surface receptors required for prey-binding and internalisation. Spores appeared to be internalised in multiples, with phagocytosis continuing over the 24-hour period the cultures were observed. No *Dictyostelium* lysis was observed in association with either M145 or *mce* null mutant spores at any time.

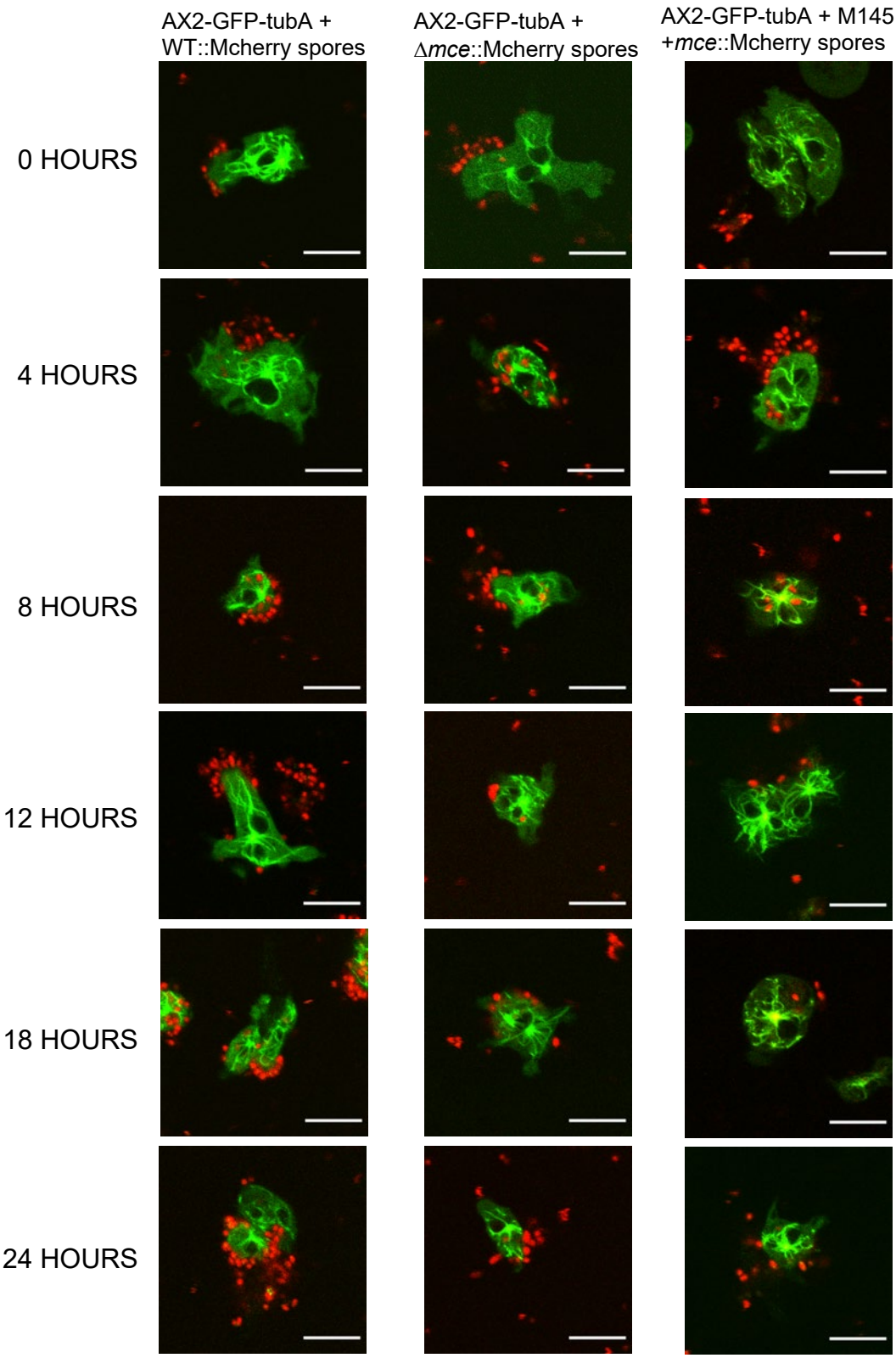

Figure 4.24: 125,000 GF AX2-GFP-tubA *Dictyostelium* with 1.8 x 10^8 M145, Δ*mce*, or M145+*mce* spores expressing mCherry, in 1mL Sor buffer. Images were taken using an Olympus FV1000 confocal microscope with a 60X objective, using a Red He-Ne and a Melles-Griot Argon-ion laser at excitation of 488nm and 534 simultaneously. Scale bar represents 10μm.

Development of Intracellular survival assays

As this work has established that *Dictyostelium* predates *S. coelicolor* and efficiently phagocytoses spores, a further aim was to investigate the intracellular interactions of these organisms. It has been previously shown that the *mce* null mutant displays increased tolerance to SDS and lysozyme compared to M145 (Clark *et al.*, 2013). Clark proposes that this increased tolerance may aid the survival of spores of the Δ*mce* strain intracellularly, as lysozymes aids killing and degradation of bacteria within amoeba (Clark, 2011). In order to determine whether *mce* null mutant spores showed enhanced survival within *Dictyostelium*, an intracellular survival assay was developed, relying on similar principles to gentamicin protection assays. This assay sought to determine how long spores were able to survive post-internalisation in *Dictyostelium* and whether this survival differed between spores of M145 and Δ*mce* strains.

Intracellular survival assays as performed in this study were adapted based on protocols for monitoring infection of *Dictyostelium* with Mycobacteria (Arafah *et al.*, 2013). CFU quantification was used to assess bacterial survival post-internalisation and over-time. *Dictyostelium* were seeded into 24-well tissue culture plates (TPP®) and incubated with M145 spores for two hours to allow spore internalisation. External spores were removed by washes and addition of gentamicin to the medium. At various timepoints, amoebae were detached from wells, lysed and lysate plated for CFU quantification. As *Dictyostelium* has been shown to phagocytose spores efficiently in HL5, assays were performed in this medium, which allowed higher densities of *Dictyostelium* to be used without the issue of amoeba aggregation. Higher densities of *Dictyostelium* were found to be useful due to loss of cells in washing steps.

The correct MOI, or number of *S. coelicolor* spores added per one *Dictyostelium* cell, for the assay first had to be determined. MOIs of 1:10, 1:100 and 1:1000 were trialled (Fig. 4.25). High levels of spores (MOI 1:1000) were found to produce significant fluctuations in CFU early in the experiment which would lead to difficulty in examining intracellular survival of spores. Conversely, an MOI of 1:10 produced a very low spore count, which reduced ease of quantification of CFU. Furthermore, considering the ratio of *Dictyostelium* amoeba to *Streptomyces* spores in the environment, a 1:100 MOI is likely more biologically relevant. An MOI of 1:100 gave effective results, producing an easily quantifiable number of CFU and avoiding CFU variation seen with an MOI of 1:1000.

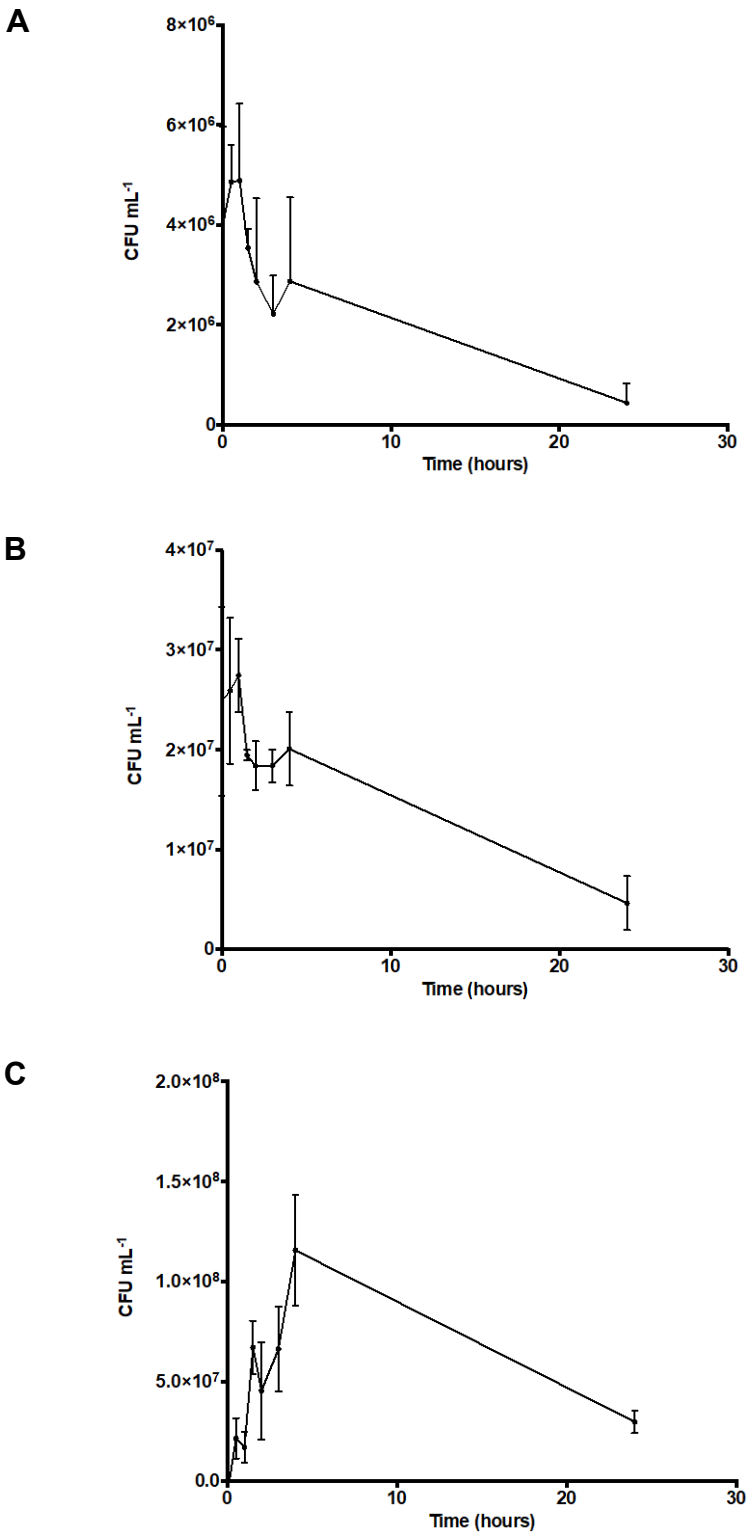

Figure 4.25: MOI determination. (A) Intracellular survival of M145 spores inside *Dictyostelium* amoeba over a 24-hour period, MOI 1:10. **(B)** Intracellular survival of M145 spores inside *Dictyostelium* amoeba over a 24 hour period, MOI 1:100. **(C)** Intracellular survival of M145 spores inside *Dictyostelium* amoeba over a 24-hour period, MOI 1:1000. For all MOIs N=3.

Spores of the Δ*mce* strain show increased intracellular survival compared to M145

Intracellular assays were carried out with all strains at an MOI of 1:100. Unexpected variation in CFU across the course of the experiment is likely due to error introduced by the difficulty of removing all external spores as well as loss of *Dictyostelium* cells during detachment and washing.

Overall, the Δ*mce* strain showed markedly higher CFU counts post-internalisation when compared to M145 *S. coelicolor* spores, indicating that Δ*mce* spores show increased intracellular survival within *Dictyostelium* (Fig 4.26). It seems likely that is due to the enhanced resistance of Δ*mce* spores to lysozyme, a major enzyme utilised by amoebae for intracellular killing of micro-organisims (Clark, 2011). By contrast, it appears *S. coelicolor* M145 spores are quickly ingested and undergo degredation, resulting in sharply decreasing CFU as time of co-incubation increases. At 8 hours post-internalisation, no M145 spores were viable, whilst CFU of Δ*mce* spores remained high. CFU counts of the additonal copy M145+*mce* spores appears more similar to that of M145 spores, indicating there is little to no advantage to intracellular survival of *Streptomyces* spores with additional *mce* operon copies.

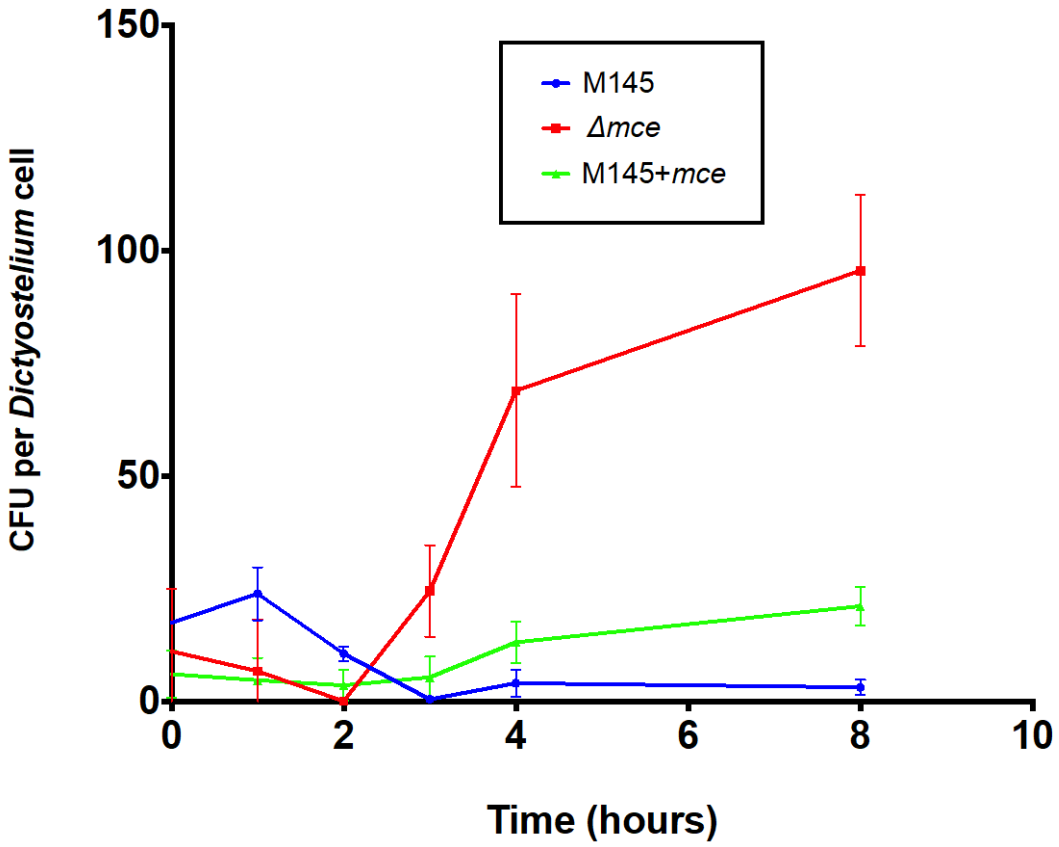

Figure 4.26: Intracellular survival of spores of the M145, Δ*mce* and M145+*mce* strains over a 8-hour period in *Dictyostelium* amoeba. Intracellular survival was measured by quantifying CFU of strains after internalization and indicates that Δ*mce* spores show enhanced intracellular surival compared to spores of M145 or and M145+*mce* strains (N=3). Error bars represent standard deviation.

The *mce* null mutant does not show cross-resistance to gentamicin

It was hypothesised that the higher CFU of Δ*mce* spores observed in intracellular survival assays may be due to increased gentamicin resistance caused by cross-resistance from the apramycin resistance gene in the *mce* null mutant. To determine this, the gentamicin MIC was determined for all three strains in HL5 suspension. Gentamicin MIC assays were performed in HL5 in 96-well plates using a Microplate reader (Bio-Tek Multi-Detection Microplate Reader Synergy HT) for 24 hours. MIC assays showed that 12.5 µg/mL of gentamicin in HL5 media was sufficient to inhibit growth of all strains (Fig 4.27.A). Minimum inhibitory concentration of gentamicin in HL5 for Δ*mce* and M145+*mce* was 6.25 µg/mL (Fig 4.27.B). Growth of the Δ*mce* and M145+*mce* strain was seen at concentrations ≤ 3.125 µg/mL (Fig 4.27.C), however the 100 µg/mL gentamicin used in the intracellular survival assays far surpasses these concentrations. Higher CFU results in intracellular survival assays are therefore not due gentamicin resistance in the *mce* null mutant.

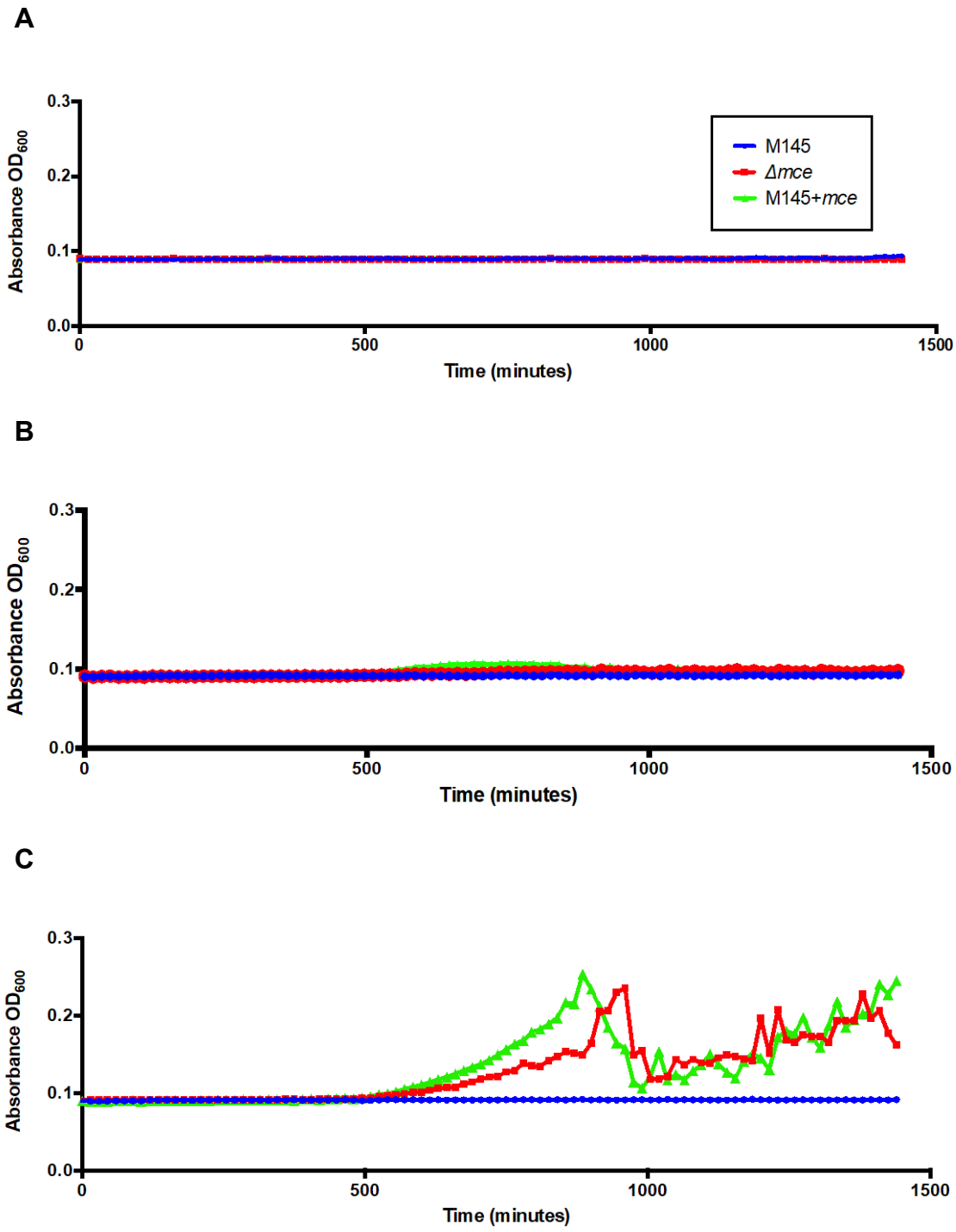

Figure 4.27 Growth of spores in HL5 with varied concentrations of gentamicin was measured in a Microplate reader over 24 hours. (A) Concentrations of 12.5 µg/mL of gentamicin in HL5 media was sufficient to inhibit growth of all strains. **(B)** Concentrations of 6.25 µg/mL of gentamicin in HL5 media was found to be the MIC for gentamicin for all strains in HL5. **(C)** At concentrations of 3.125 µg/mL and lower, Δ*mce* and M145+*mce* strains showed some growth; M145 did not (N=3).

The *mce* null mutant may show increased spore viability following exocytosis from *Dictyostelium*

The intracellular survival assay method used in this study is based on a robust protocol developed for *Dictyostelium* and utilises concepts of gentamicin-protection assays. However, *Streptomyces* spores behave distinctively from the intracellular pathogenic organisms priorly examined with this method in the literature, and therefore this method may not be entirely suited to examining intracellular survival of *Streptomyces* spores. It is unclear how or why there is an increase in number of spores for all strains, particularly the *mce* mutant intracellularlly, when *Streptomyces* do not undergo reproduction. It was therefore considered that this protocol, whilst an established method for testing intracellular survival of pathogens, may not be suitable for measuring spore intracellular survival. As such, an alternative method for analysing intracellular survial of spores was therefore employed. This method measured the exocytosis of *Streptomyces* spores from *Dictyostelium* following uptake and quantified the viability of spores following internalisation.

Results show that spores of the Δ*mce*, Δ*mce*+*mce* and M145+*mce* strains all proved more viable post-exocytosis compared to spores of M145 *S.coelicolor* (Fig. 4.38). Although these results were found to be non statistically significant, sample size was N=3 and has likely impacted the statistical analysis, leading to a type II error skewing the the results. It appears likely that the *mce* null mutant does indeed show increased resistance, and the experiment should be repeated with a larger sample size to confirm this.

Increased intracellular survival of the *mce* null mutant is likely linked to the spores increased resistance to lyzosyme, as previously reported (Clark *et al.*, 2013). Lyzosyme is responsible for enzymatically cleaving glycosidic linkages in the peptidoglycan of

bacterial cell walls and is utilised in *Dictyostelium* to destory bacterial prey (Oliver and Wells, 2015; Dunn *et al.*, 2018). *Streptomyces*, as Gram-positive bacteria, possess peptidogyclan walls of considerable thickness. The Mce proteins are believed to function as an ABC transporter in *S. coelicolor,* and may localise to the cell wall (Clark *et al.*, 2013). Deletion of the Mce proteins may therefore lead to increased inegrity of the cell wall, resulting in increased lysozyme resistance which enables Δ*mce* spores to withstand intracellular killing for increased periods compared to M145 spores. That the complemented mutant behaves similar to the mutant is likely due to the ectopic nature of the complemented *mce* operon.

The spores showing greatest survival following phagocytosis appears to be those of the M145+*mce* strain, this is interesting given that this mutant had two copies of the *mce* operon and therefore potentially more proteins in the cell wall. There is therefore likely another mechanism, aside lysozyme tolerance which acts upon intracellular spore survival.

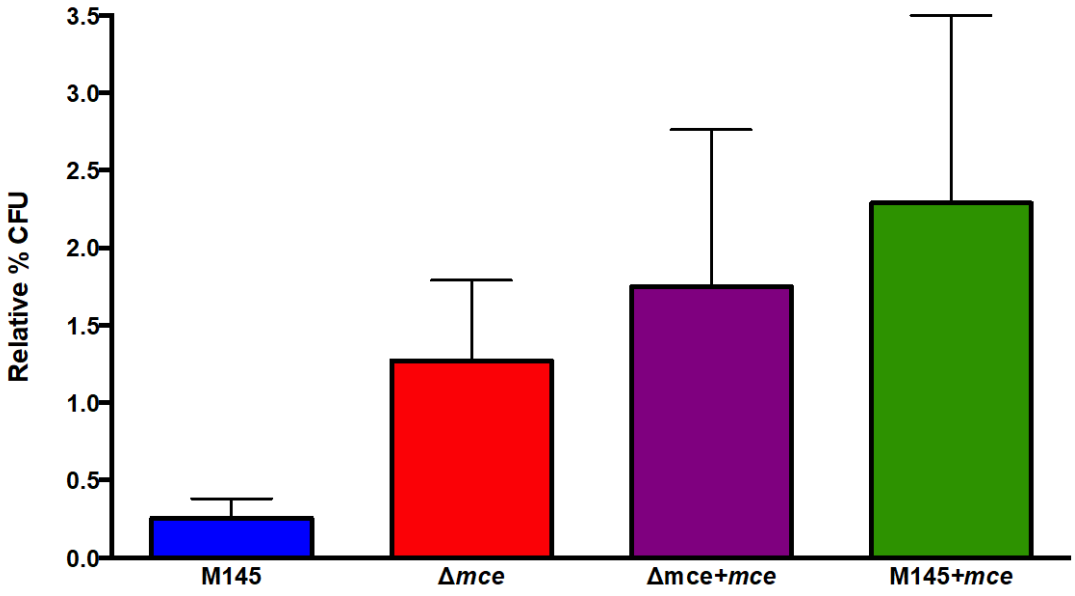

Figure 4.28: CFU of strains post-internalisation into *Dictyostelium*, following exocytosis. Relative percentage CFU was calculated as a percentage survival relative to a 0-hour time-point spore-only control. An Ordinary one-way ANOVA showed no difference between CFU of strains post-internalisation ($F(3, 7) = 1.262$, $P = 0.3587$) (N=3). Error bars represent standard deviation.

The mce null mutant may show increased lysozyme resistance compared to M145 spores

As mentioned, the Δ*mce* strain was previously identified to show increased tolerance to 0.5 mg/mL lysozyme compared to the M145 strain. Lysozyme susceptbility was previously tested via plate spot assays (Clark *et al.*, 2013). However, as lysozyme resistance was determined via strain growth, this manner of testing examined lysozyme tolerance in germlings rather than in spores. As *Dictyostelium* internalise *S. coelicolor* spores, spore lysozyme susceptbility assays were performed alongside germling susceptbility assays in suspension. As co-culture assays examining *S. coelicolor* spore and *Dictyostelium* interaction had been performed in Sor Buffer, this media was used for lysozyme resistance assays.

Interestingly, the results of the spore tolerance to 0.5 mg/mL lysozyme in Sor buffer show an identical trend to results from exocyotsis assays. *S. coelicolor* M145 spores are the least tolerant to lysozyme, while Δ*mce* spores are more tolerant than M145 spores, but less tolerant than Δ*mce*+*mce*. As with results from exocytosis assays, the spores showing greatest tolerance to lysozyme are those of M145+*mce*. Although results did not show a statistically significant difference in lysozyme tolerance of spores between strains, this may be reflective of the small sample size used impacting the statisical analysis.

Results from lysozyme susceptibility assays performed with germings show a very distinct trend than that of spores, with germlings of M145, Δ*mce* and Δ*mce*+*mce* showing similar and relatively low tolerance to lysozyme in comparison with M145+*mce*. The differences in tolerance between M145 and Δ*mce*+*mce* was found to be statisitically signficant ($P = 0.0003$). There was no difference found between germling lysozyme tolerance in M145 and Δ*mce* strains.

It is interesting to consider that both spores and germlings of M145+*mce* appear to show the greatest resistance to lysozyme, given prior findings by Clark (2013) that deletion of the Mce proteins appeared to increase tolerance to lysozyme. It was unexpected, then, that a strain containing the greatest number of Mce proteins would prove more tolerant to lysozyme than either the *mce null* mutant or M145.

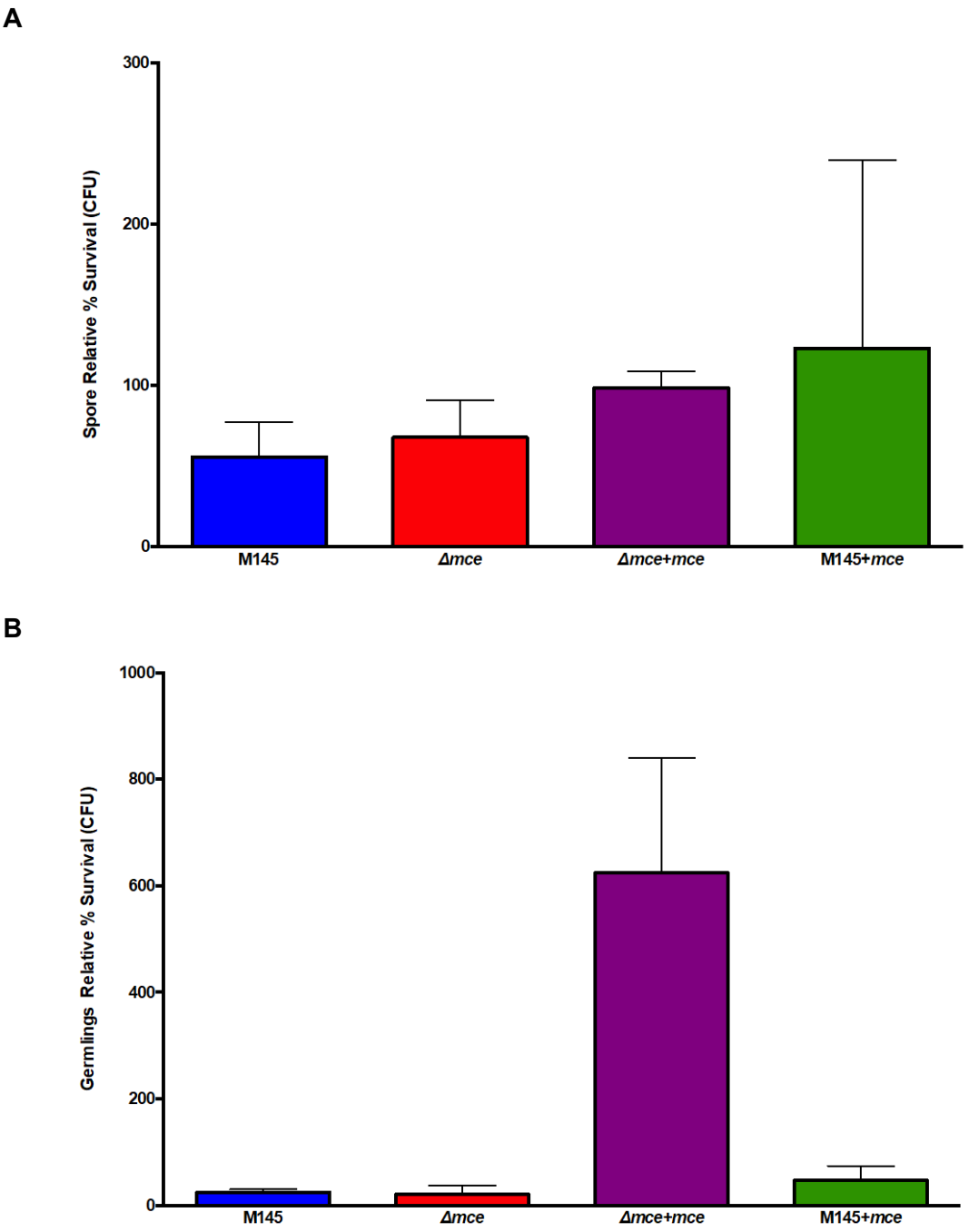

Figure 4.29: *S. coelicolor* strains tolerance to lysozyme. (A) Percentage survival of spores (CFU) exposed to lysozyme, relative to non-lysozyme treated control. An ordinary one-way ANOVA found no statistical significant difference between strains F (3, 8) = 0.7536, P = 0.5505. **(B)** Percentage survival of germlings (CFU) exposed to lysozyme, relative to non-lysozyme treated control. An ordinary one-way ANOVA found there was a statistically significant difference in germling survival in Δ*mce*+*mce* compared to M145 (F (3, 8) = 22.27, P = 0.0003) (N=3). Error bars represent standard deviation.

Chapter 4: Summary

Acanthamoeba and *Dictyostelium*, whilst both being bacterivorous protists which exist in similar environments, are nonetheless phylogenetically distinct organisms with vastly different foraging strategies. It is therefore perhaps unsurprising that their interaction with *S. coelicolor* differs so substantially (Kuburich, Adhikari and Hadwiger, 2016). *Acanthamoeba* vary from 25 to 40 μm in size, significantly larger than the average size of *Dictyostelium* at 10 μm. *Acanthamoeba* locomotion is slow, whilst motility in *Dictyostelium* is rapid and chemotactic (Marciano-Cabral and Cabral, 2003). Furthermore, *Dictyostelium* are capable of bacterial discrimination and modulation of predation behaviour and phagocytic responses depending on prey bacteria; particularly bacteria with pathogenic potential (Nasser *et al.*, 2013; Shi *et al.*, 2020). *Streptomyces* presents an interesting quandary to *Dictyostelium*, as some species of this genera appear as an ideal food source, whilst others are indigestible or even virulent (Clark *et al.*, 2013; Paquet and Charette, 2016).

Dictyostelium are able to rapidly and efficiently phagocytose *S. coelicolor* spores both on solid and in aqueous medium. As *Streptomyces* spores prior to germination are largely dormant, *Dictyostelium* likely encounter spores through random movement, with phagocytosis being triggered from the physical association of the phagocytic receptors of amoeba with spores. It has been observed that *Dictyostelium* will phagocytose polystyrene beads upon physical association, therefore internalisation of dormant spores is not unexpected (Williams and Kay, 2018; Bodinier *et al.*, 2021).

Unlike in *Acanthamoeba polyphaga*, however, phagocytosis of *S. coelicolor* M145 or Δ*mce* spores did not lead to lysis of the *Dictyostelium* due to intracellular germination and hyphal growth or otherwise. This is likely due to the differences in feeding and

phagocytotic processes between these two amoebae. *Acanthamoeba* were only seen to phagocytose spores 8-12 hours into co-culture, with M145 spores remaining in food vacuoles for a further 12 hours prior to germination, whereas *Dictyostelium* appear to associate with and phagocytose spores within minutes (Clark *et al.*, 2013). This rapid rate of phagocytosis appears to occlude germination from occurring and thus prevents lysis of the *Dictyostelium* due to hyphal growth. Spores of the Δ*mce* strain, despite undergoing precocious germination, are similarly avirulent in *Dictyostelium*. Results of both plaque assays and co-culture assays in suspension confirm this result.

The Δ*mce* strain, despite a lack of pathogenicity towards *Dictyostelium*, shows enhanced intracellular survival inside *Dictyostelium* compared to M145 spores. This may be a result of increased lysozyme tolerance slowing degradation of the bacterium inside the food vacuole. This potentially increased tolerance to lysozyme has previously been theorised to be due to increased integrity of the cell wall of the *mce* null mutant due to deletion of the Mce proteins, which are likely located within the cell wall. However, results from both spore and germling lysozyme tolerance assays indicate that the additional copy strain, M145+*mce* shows enhanced tolerance to lysozyme over that of the *mce* null mutant, which is a counterintuitive result based upon this hypothesis. It is indicative of more complex interplay between the cell envelope of *Streptomyces* and the Mce proteins which will likely require definitive characterisation of the Mce proteins location and function within the *Streptomyces* cell.

Chapter 5: Structural investigation and detection of the Mce proteins of *Streptomyces coelicolor*.

All current available evidence suggests that the *mce* operon of *Streptomyces coelicolor* encodes an ABC importer for sterols. However, the cellular localisation of this transport system, including both putative permeases and Mce-domain containing proteins, remains unknown in *Streptomyces*, as does the function and mechanism of substrate transport by the Mce-domain containing proteins.

Prokaryotic ABC transporters are comprised of integral membrane proteins which, together with associated substrate binding proteins (SBPs), form ATP-binding cassette (ABC) transporters which couple ATP-hydrolysis to the import or export of substrates across biological membranes (Rees, Johnson and Lewinson, 2009). SBPs act to recognize and bind to the substrate, facilitating substrate delivery to the permease component of the transporter. In Gram-negative bacteria, SBP are typically found in the periplasmic space, whilst in Gram-positive bacteria, SBPs are usually lipoproteins anchored to the outer surface of the cell membrane by linkage to a lipid moiety (Maqbool *et al.*, 2015). The Mce-domain containing proteins are believed to function as the SBPs of the Mce ABC transporter assembly in Actinobacteria and, as such, they are likely secreted and may either remain membrane associated or be free in the extracellular milieu. It is currently unknown how the six Mce proteins may interact once secreted. It is possible they may co-localise at the outer-face of the transporter or the that the lipobox signal on some homologues of the MceE proteins (though seemingly absent in *S. coelicolor*) may act as a nucleation point for the assembly of the Mce protein-substrate complex at the membrane.

It has been shown that the Mce-domain containing proteins of the Gram-negative *E. coli* K12 are located in the periplasm and function to shuttle lipids between the inner and outer membranes of the bacterium, maintaining outer membrane homeostasis (Ekiert *et al.*, 2017). Gram-positive bacteria, including *S. coelicolor*, lack an outer membrane or any structure that could be considered a pseudo-outer membrane, such as in *Mycobacterium*. Thus, it is likely that Gram-positive and Gram-negative Mce proteins are distinct in location and mechanism, though may share some functional similarities such as the ability to bind hydrophobic substrates.

All six of the Mce1 proteins of *M. tuberculosis* have shown to localise to the cell envelope (Chitale *et al.*, 2001; Stavrum *et al.*, 2012; Zaychikova and Danilenko, 2020). It is possible that the *S. coelicolor* Mce proteins are similarly located, given the altered cell envelope phenotype observed in the *Streptomyces mce* null mutant, i.e., wrinkled spores, increased susceptibility to deleterious agents, etc. The cellular location of the *S. coelicolor* Mce proteins and whether the Mce-domain containing proteins are lipid-anchored or freely secreted remains unclear. Further, Gram-positive ABC transporters typically possess only a singular SBP and six SBP is therefore highly unusual and may indicate non-redundant functions among the Mce-domain containing proteins. For example, the individual Mce-domain containing proteins may each function to transport a distinct substrate, or they may form a complex to together bind to a singular larger substrate (Rice, Park and Pinkett, 2014).

Predicted location and structure of the *S. coelicolor* Mce transporter assembly

The known structure of the *mce* operon of *S. coelicolor* includes SCO2422, the first gene of the operon and a putative ABC-transporter ATP-binding protein. SCO2422 is 1032 bp (343 aa) in size and encodes a 36.7 kDa protein predicted to form the cytoplasmic

nucleotide binding domains of the ABC transporter. SCO2422 contains an ATP-binding site motif A (P-loop) and the conserved ABC transporter signature motif (LSGGQ).

Downstream of SCO2422 are SCO2421 and SCO2420, genes encoding putative integral membrane proteins thought to form the transmembrane permease components of the ABC transporter system. SCO2421 and SCO2420 are 765 and 807 base pairs in size respectively. SCO2421 contains six conserved protein domains; PLN03100, a provisional permease subunit of ER-derived-lipid transporter, PIG-L; an N-acetylglucosaminyl phosphatidylinositol de-N-acetylase which catalyses a step in GPI biosynthesis, LmbE; an N-acetylglucosaminyl deacetylase involved in carbohydrate transport and metabolism, [pfam Family: pfram02405], a permease domain, TIGR00056; a subfamily of ABC transporter permease subunits, and COG0767 MlaE, the ABC-type transporter Mla which maintains outer membrane lipid asymmetry in *E. coli* (Isom *et al.*, 2020). SCO2420 also shares conserved protein domains with TIGR00056, PLN03100; provisional permease subunit of ER-derived-lipid transporter, [pfam Family: pfram02405] and MlaE. This bioinformatic analysis suggests that these two open reading frames comprise the transmembrane components of the ABC transporter.

To further address this, sequence alignments were carried out using LALIGN (https://embnet.vital-it.ch/software/LALIGN_form.html). SCO2421 is a 26.5 kDa protein which shares 50.8% identity (87.2% similar) in a 242 aa homologous region with the *Mtb* Mce protein Rv3501c, (MTV023.08c) also known as *yrbE4A* which is part of the mce4 operon. SCO2420 is a 28.5 kDa protein which shares 51.7% identity (85.1% similar) in a 261 aa homologous region with *Mtb* Mce protein Rv3499c (MTV023.07c), also known as *yrbE4B.*

The amino acid sequences of SCO2421 and SCO2420 were examined using TMpred (Dellaire, Farrall and Bickmore, 2003). TMpred predicts that SCO2421 contains 5 possible transmembrane helices, with a probable cytoplasmic N-terminal and extracellular C-terminus. Likewise, SCO2420 is predicted to contain 6 transmembrane helices, with both N and C-terminus located inside the cell (Fig. 5.1). 'Typical' ABC transporters contain a total of 12 transmembrane helices, though this varies with transporter class. Sequence alignment of SCO2421 and SCO2420 gives a 30.0% identity (70% similar) in a 190 aa homologous region. Given the predicted structural differences between SCO2420 and SCO2421 it appears that the Mce ABC transporter of *S. coelicolor* may be a heterodimeric half-transporter (Hürlimann *et al.*, 2016).

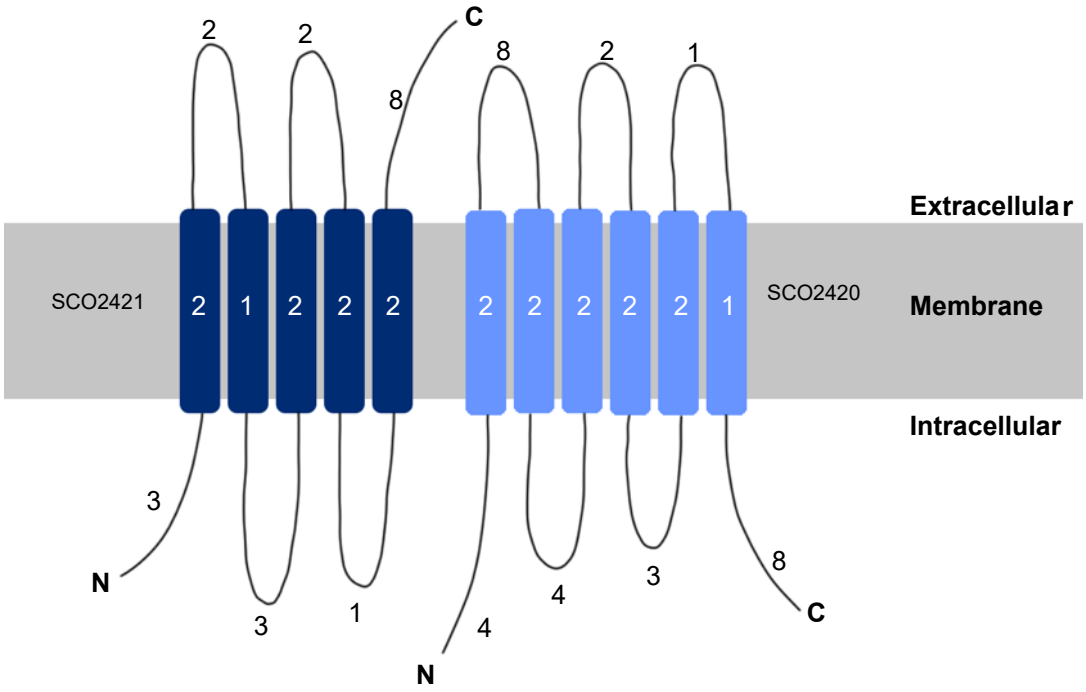

Figure 5.1: Predicted structure and orientation of SCO2421 and SCO2420 proteins in the membrane. SCO2421 and SCO2420 are both putative ABC-transporter integral membrane proteins containing possible hydrophobic membrane spanning regions. TMpred predicts 5 transmembrane helices in SCO2421 and 6 transmembrane helices in SCO2420. It is predicted that the N-terminus of SCO2421 is intracellular, whilst the C-terminus is extracellular. Both the N-terminus and C-terminus of SCO2420 are predicted to be intracellular. Length of both inside and outside helices in amino acids is annotated.

The Mce-domain containing proteins of *Streptomyces coelicolor*

Further analysis of the *mce* operon in *S. coelicolor* indicates that SCO2419 (MceA) is a possible secreted Mce-domain containing protein, encoded directly downstream of SCO2420. *MceA* is the first of the Mce-domain containing genes in the operon and encodes a protein 44 kDa in size which shares a 32.5% identity (59.6% similar) in a 366 aa homologous region with the *Mtb* protein Mce3A, found in the *mce3* operon.

SCO2418 (MceB) is the downstream encoded Mce-domain containing protein and is 37.3 kDa in size, sharing a 37.6% identity (68.2% similar) in a 343 aa homologous region with the *Mtb* protein, Mce3B, of the *mce3* operon of *Mtb*. SCO2417 (MceC) is 37.4 kDa in size and shares a 33.3% identity (66.9% similar) in a 369 aa homologous region with Mce3C of the *mce3* operon in *Mtb.* SCO2416 (MceD) is 35.4 kDa in size and shares a 32.9% identity (67.7% similar) in a 319 aa homologous region with Mce3D of the *mce3* operon of *Mtb.* SCO2415 (MceE) is 42.7 kDa in size and shares 38.0% identity (67.8% similar) in 171 aa homologous region with Mce2E of the *mce2* operon of *Mtb.* SCO2414 (MceF) is 44 kDa in size and shares 30.4% identity (59.0% similar) in 437 aa homologous region with Mce3F of the *mce3* operon of *Mtb*.

Interestingly, the most similarity between the *mce* operon of *S. coelicolor* and those of *Mtb* is found in the *mce3* operon. The *mce3* operon is present in *Mtb* but is absent from the genomes of *M. leprae*, *M. bovis* BCG*, M smegmatis,* and *M. microti* (Zaychikova and Danilenko, 2020). A definitive role for the *mce*3 operon in *Mycobacterium* has still to be determined, however, it has been shown that Mce3A and Mce3E are involved in invasion (El-Shazly *et al.*, 2007). Mce3C also appears to play a role in adhesion and penetration of macrophages, by interacting with β2 integrins of the host (Zhang *et al.*, 2018). Furthermore, Mce3A, D and E are capable of eliciting an antibody response in humans

during infection, demonstrating that the *mce3* operon in *Mtb* has a role in virulence (Hemati *et al.*, 2019)

Properties of the Mce proteins

Typically, substrate binding proteins of ABC importers contain a characteristic lipobox motif (LA(S)G(A)C) with a conserved cysteine residue which is modified to anchor the protein to the cell membrane (Zückert, 2014b). The *M. tuberculosis* proteins Mce1E, Mce3E and Mce4E all contain a lipobox motif, but it is apparently absent in all the *S. coelicolor* mce-domain containing proteins, which may suggest these proteins are not associated with the cell membrane. It is interesting to consider that the MceE protein of *S. coelicolor* is most similar to the MceE2 of *Mtb* which is the sole MceE protein of *Mtb* to not contain a lipobox motif.

Amino acid sequences of all Mce-domain containing proteins of *S. coelicolor* were examined using SignalP 5.0 (Almagro Armenteros *et al.*, 2019) to gain further insight into whether the Mce-domain proteins possess characteristic secretion signal peptides (Table 5.1).

Table 5.1: Signal sequences in Mce proteins of *S. coelicolor.* Possible signal sequences within Mce-domain containing proteins predicted using SignalP 5.0. The probability of existing signal sequence is shown. The highest probability and most likely signal sequence are underlined. Three types of signal sequences may be detected via SignalP, a Sec signal peptide, a Lipoprotein signal peptide, or a Tat signal peptide. If no signal peptide is detected the highest probability is found in 'none'.

Protein	Signal peptide (Sec/SPI)	TAT signal peptide (Tat/SPI)	Lipoprotein signal peptide (Sec/SPII)	None
SCO2419 (MceA)	0.1611	0.0221	0.045	<u>0.7717</u>
SCO2418 (MceB)	<u>0.6554</u>	0.0928	0.0667	0.1851
SCO2417 (MceC)	0.0624	0.0017	0.007	<u>0.9289</u>
SCO2416 (MceD)	0.279	<u>0.6879</u>	0.0262	0.0068
SCO2415 (MceE)	<u>0.549</u>	0.0769	0.155	0.2191
SCO2414 (MceF)	<u>0.622</u>	0.0029	0.0101	0.365

SignalP 5.0 software predicts the presence of signal peptides and the location of their cleavage sites in protein amino acid sequences. It can discriminate between three types of signal peptides, including Sec/SPI ("standard" secretory signal peptides transported by the Sec translocon and cleaved by Signal Peptidase I, *Lep*), Sec/SPII (lipoprotein signal peptides transported by the Sec translocon and cleaved by Signal Peptidase II, *Lsp*) and Tat/SPI (Tat signal peptides transported by the Tat translocon and cleaved by Signal Peptidase I, *Lep)*. Whilst StrepDB (Bentley *et al.*, 2002) predicts that all Mce-domain containing proteins of *S. coelicolor* contain possible N-terminal signal peptide sequences, SignalP 5.0 only identifies potential signal sequences in SCO2418, SCO2416, SCO2415 and SCO2414. Of these, SignalP 5.0 predicts that the signal sequence in SCO2418, SCO2415, and SC2414 are Sec/SPI sequences, whilst SCO2416 is Tat/SPI. There are no detectable signal sequences in SCO2419 or SCO2417.

The amino acid sequences of Mce-domain containing proteins of *S. coelicolor* were further examined using LipoP 1.0 (Juncker *et al.*, 2003). This server was created to produce predications of lipoproteins in protein sequences and can discriminate between lipoprotein signal peptides, other signal peptides and N-terminal membrane helices. Although LipoP 1.0 was originally designed for Gram-negative bacteria sequences, evidence suggests that it offers good performance in Gram-positive bacteria also (Rahman *et al.*, 2008). LipoP 1.0 does not predict any lipoprotein signal peptides in any of the Mce-domain containing proteins of *S. coelicolor*. It does, however, predict a signal peptide in SCO2417, SCO2416, SCO2415 and SCO2414.

The absence of a lipobox motif with conserved cysteine residue in the MceE protein of *S. coelicolor* is somewhat atypical when considered against MceE proteins of other

Actinobacteria, which characteristically contain a lipobox motif with conserved cysteine residue indicating they are likely lipoproteins anchored to the cell membrane (Table 5.2). Most *Streptomyces* species possess MceE proteins which lack a lipobox motif, with the exception of *S. avermitilis*, a non-pathogenic soil bacterium known best for its production of secondary metabolites with anthelmintic activity. As previously mentioned, three of the four MceE proteins of *M. tuberculosis* possess a lipobox motif with conserved cysteine. Only Mce2E of *Mtb* lacks the motif, and therefore is unlikely to be a lipoprotein. This protein has previously been shown to be a virulence factor with multiple functions, including regulating the host immunresponses by suppressing TNF and IL-6 in macrophages and promoting epithelial cell proliferation. Interestingly, Mce2E has therefore been proposed to be secreted into host cells, a role which would eliminate the necessity for a lipobox motif (Qiang *et al.*, 2019). It is therefore potentially worthwhile to consider that the MceE protein of *S. coelicolor* shares the closest homology with the Mce2E protein of *Mtb* (38.0% identity, 67.8% similar), with all indications that it is a secreted protein. As such, it is possible that even within copies of the *Mtb* operons, Mce proteins may display distinct localization and properties. In *S. coelicolor*, it remains to be elucidated where the Mce proteins localize, and whether the proteins act as a complex to bind a single substrate or bind multiple substrates individually.

Table 5.2: Lipobox motifs of Actinobacteria MceE proteins. The first 40 amino acid sequence of the MceE proteins of various Actinobacteria. LipoP 1.0 was used to identify potential lipoprotein signal peptides (underlined) and the conserved cysteine residue (red) which is the target of acylation and will become the new N-terminal of

M. tuberculosis H37Rv Mce1E	MMSVLARMRVMRHRAWQGLVLLVLALLLSSCGWRGISNVA
M. tuberculosis H37Rv Mce2E	MRCGVSAGSANGKPNRWTLRCGVSAGHRGSVFLLAVLLAP
M. tuberculosis H37Rv Mce3E	MRIGLTLVMIAAVVASCGWRGLNSLPLPGTQGNGPGSFAV
M. tuberculosis H37Rv Mce4E	MNRIWLRAIILTASSALLAGCQFGGLNSLPLPGTAGHGEG
S. coelicolor A3(2) M145 MceE	MKRATLPRGRVAGLTAGSLAAVGLALALTLGGVSVVPSGF
S. avermitilis ATCC 31267 MceE	MNALRKVGAVAWAAVGSLLLSGCEFNGWYDVQLPGGAAAD
R. jostii RHA1 MceE	MTKHTRVRRGGIAAVAITLSLTLTGCEWEGLNSLPLPGTE
N. farcinica IFM 10152 Mce1E	MRRARRTATVLALGVSLTLGLTACEWDGLNSLPMPGAEGT
N. farcinica IFM 10152 Mce2E	MRVPAGRVLRRLFLAPLLTGTIALAGCAFDPSAVPVPGNS
N. farcinica IFM 10152 Mce3E	MSVFAPSEAGRGARRWRIGALALVLVVAGCGFDPSDHTLP
N. farcinica IFM 10152 Mce4E	MRAARIAVAALSLAVLTGTTGCAVTVDNVPLPKPGIGGPG
N. farcinica IFM 10152 Mce5E	MRMRLPATRMLAAVAIAATAALVGSCSADGIYSVPLPGGA
N. farcinica IFM 10152 Mce6E	MTNRMRIKARRALIALAAVTAVGTTSGCGLTVEDLPLPKP
S. albidoflavus MceE	MKRVPHLGRTAAAGIGGVLALGLGFTLALGAFAEAAPSFE
S. lividans MceE	MAGLTAGSLAAVGLALALTLGGVSVVPSGFDGIEDLPLPG
S. venezuelae MceE	MRRATLPSRKAAGAGAVGVIAVGLGLAVILGATPANPFRF

Creation of hexa-histidine tagged Mce proteins

To allow detection and localisation of Mce proteins, histidine tagged constructs of SCO2419 (Mce-domain containing protein, MceA), and SCO2421 and SCO2420 (integral membrane components of the ABC transporter) were created. The hexa-histidine tag facilitates protein localisation via Western Blot, via interactions between histidines and anti-6x His antibodies. An N-terminal and C-terminal his-tagged version of each gene was created. From here on, N-terminal his-tagged *mceA* will be referred to as *N-mceA*, C-terminal his-tagged *mceA* as *mceA-C*, N-terminal his-tagged SCO2420 as N-SCO2420 and C-terminal his-tagged SCO2420 as SCO2420-C. SCO2421 is referred to as either N-SCO2421 (N-terminal his-tagged) or SCO2421-C (C-terminal his-tagged) (Fig. 5.2.A).

Nucleotide sequences for these proteins were obtained from StrepDB (http://strepdb.streptomyces.org.uk/) and modified to include six histidines as the his-tag. The his-tag was extended via a poly-linker, ensuring it remained flexible to facilitate purification. To allow easy subcloning into expression vectors, restriction enzyme sites were added to either side of the sequence, allowing it to be easily excised from and ligated into *E. coli* and *Streptomyces* plasmids (Fig. 5.2.B). *Streptomyces* pIJ6902 plasmids encoding the constructs were conjugated into the M145 background and *E. coli* expression vector pT7-7 encoding the constructs were transformed into BL21 (DE3) and C43 (DE3). This would enable overexpression in *Streptomyces* and expression and purification from *E. coli*. Prior to conjugation and transformation, all constructs were confirmed to be correct via restriction digest (Fig. 5.3A, 5.3.B).

As secreted proteins are recognised by a signal sequence in their N-terminus domain, his-tagging of the N-terminus will result in cleavage of the his-tag if the protein is

secreted. The signal sequence is approximately 16-30 amino acids residues long and is recognised by secretion machinery which direct it to the Sec secretion pathway. Signal peptide sequences are composed of a positively charged n-region, a hydrophobic h-region and a site where recognition and cleavage by signal peptidases occurs known as the c-region. The cleavage sites can be predicted by SignalP 5.0. Although SignalP does not predict a signal peptide in SCO2419, if present, the stretch of 23 amino acid residues at the N-terminus should contain most or all of the signal sequence. In construction of N-MceA, these 23 amino acids were removed. This will resultingly prevent secretion of N-MceA, should it be a secreted protein and trap it within the cytoplasm, allowing this protein construct to be used as a negative control for examining secretion of the MceA protein.

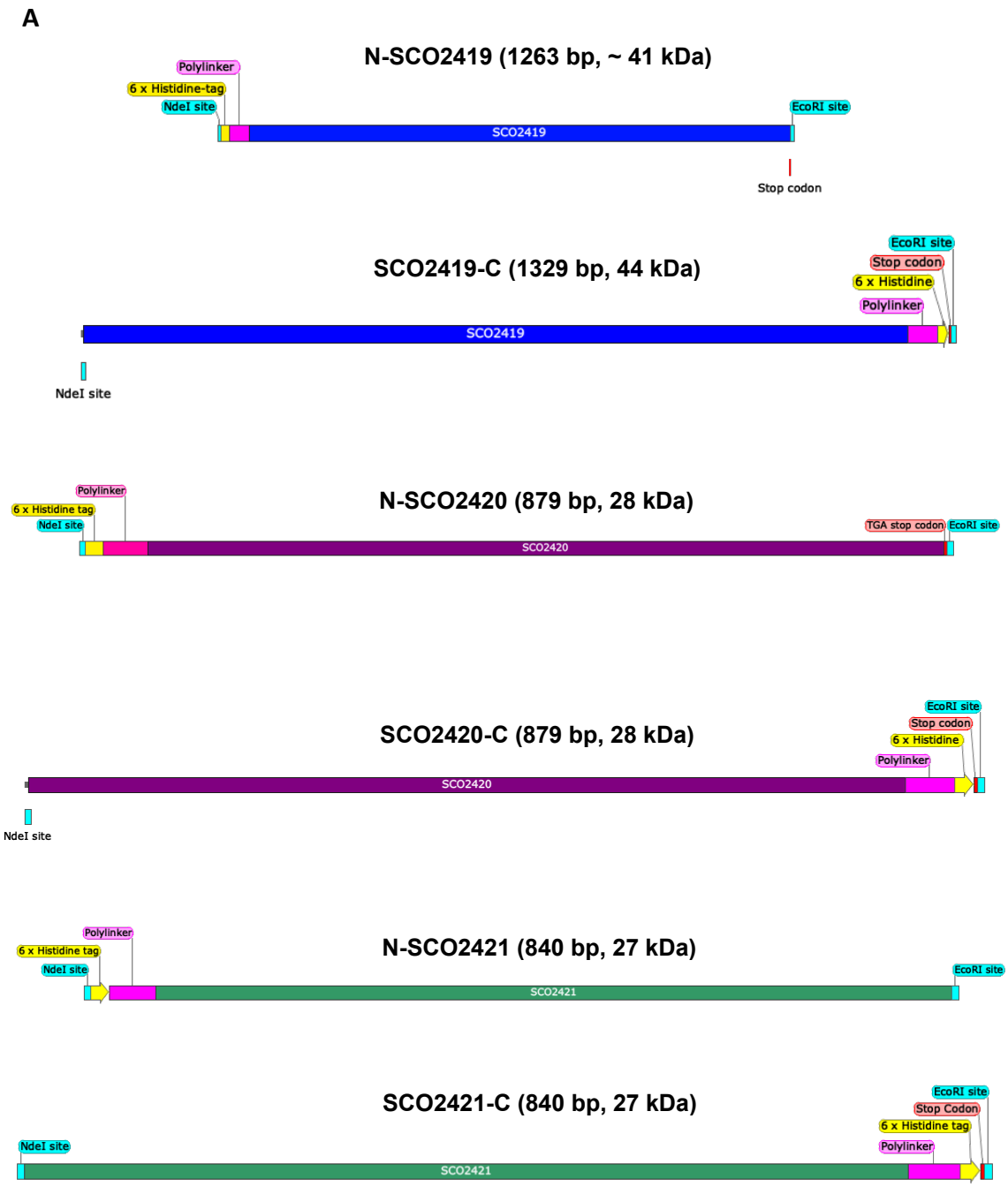

Figure 5.2: His-tagged constructs of *mce* genes of *S. coelicolor* (A) His-tagged gene constructs of SCO2419 (*mceA*) and the two putative permeases of the *mce* operon, SCO2421 and SCO2420. N-SCO2419 (*N-mceA*) is his-tagged on the N-terminus and has the first 23 amino acids, encoding a possible signal sequence, of its sequenced removed. SCO2419-C (*mceA-C)* is his-tagged on the C-terminus. The putative permease protein SCO2420 sequence was his-tagged on either the N or C-terminus, as was the sequence of putative permease protein SCO2421.

B

1

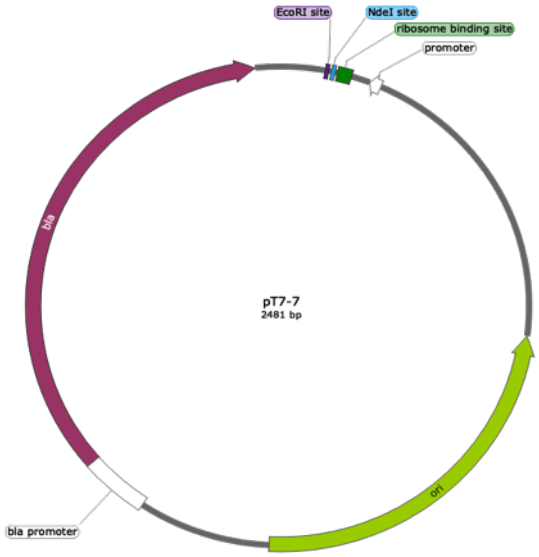

2

Figure 5.2: Expression vectors for His-tagged constructs. (B) Expression vectors into which the his-tagged constructs were ligated between the EcoRI and NdeI sites. Each of the his-tagged constructs were ligated either into **(B1)** the *E. coli* expression vector, pT7-7 for expression in *E. coli*, or **(B2)** the *Streptomyces*

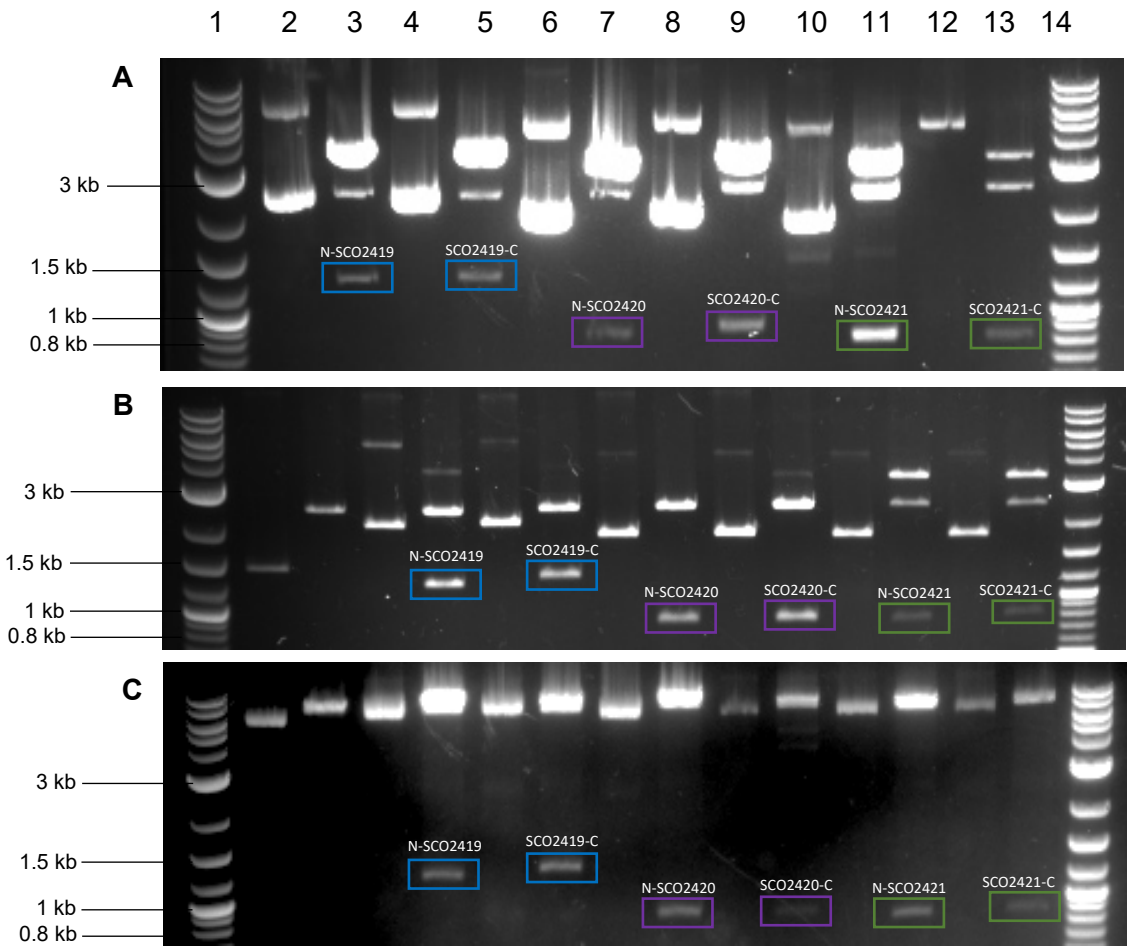

Figure 5.3: Confirmation of his-tag constructs transformation into expression vectors. (A) His-tagged DNA sequences were cut from the storage vector pUC57 via EcoRI and NdeI restriction enzymes. Non-digested and digested DNA was run on a gel electrophoresis alongside the New England Bioline 1kb Plus DNA ladder. All constructs were found to be present in the digested DNA at the expected sizes. N-SCO2419 is 1263 bp in size, SCO24219-C is 1329 bp in size. N-SCO2420 and NSCO2420-C are both 879 bp in size. N-SCO2421 and SCO2421-C are both 840 bp in size. **(B)** After cloning into pT7-7, presence of constructs within the vector were confirmed by restriction digest of pT7-7 with EcoRI and NdeI. All constructs were present in the digested DNA at the expected sizes. **(C)** After cloning in pIJ6902, presence of constructs within the vector were confirmed by restriction digest of pIJ6902 with EcoRI and NdeI. All constructs were present in the digested DNA at the expected sizes.

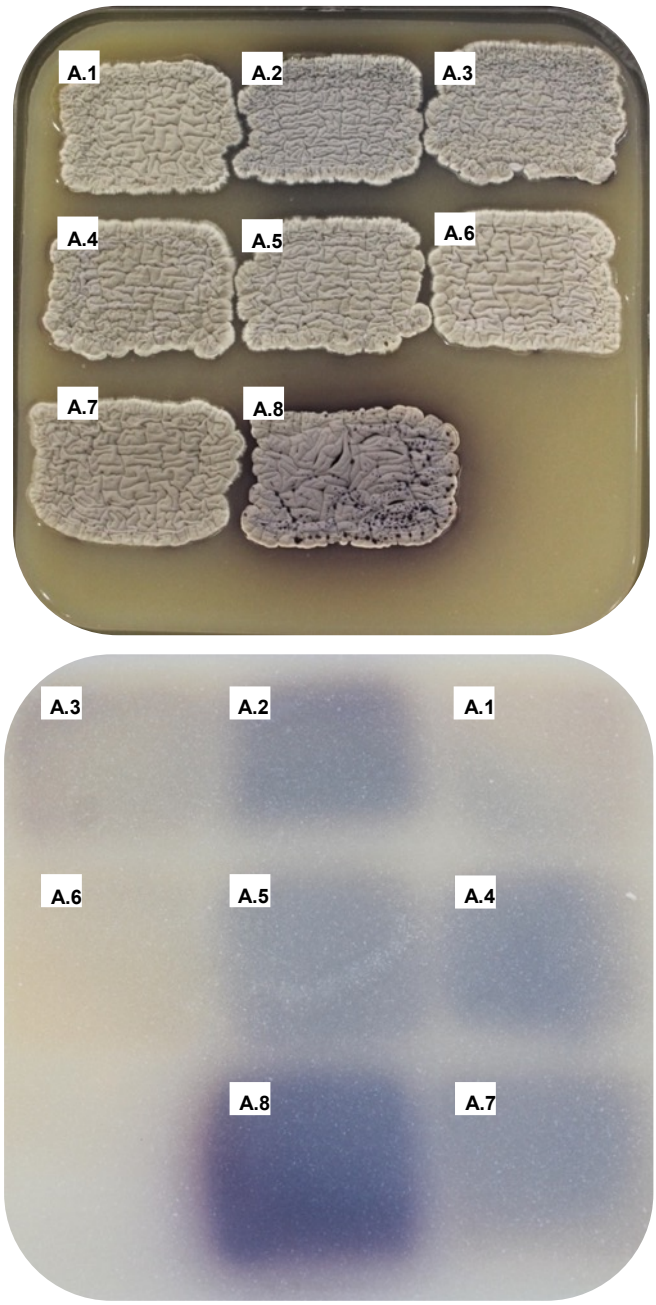

Figure 5.4: Growth of *mce* his-tagged strains of *S. coelicolor*. *S. coelicolor* strains containing the pIJ6902 vector with one of the four histidine-tagged *mce* genes were patched onto MS agar and grown for 7 days at 30°C. **A.1** M145, **A.2** N-MceA, **A.3** NmceA-C, **A.4** N-SCO2420, **A.5** SCO2420-C, **A.6** N-SCO2421, **A.7** NSCO2421, **A.8** Δ*mce*. All his-tagged strains displayed normal growth. N-mceA, N-SCO2420, SCO2420-C and SCO2421-C appear to show increased actinorhodin production in comparison to M145.

Optimising his-tagged protein overexpression and detection by Western Blot in *Escherichia coli*

Vectors (pT7-7) encoding genes for his-tagged Mce proteins were transformed into chemically competent *E. coli* for protein expression. *E. coli* were initially used for expression of native *S. coelicolor* proteins due to the robust, established protocols for expression that are available for *E. coli*, and the relative ease of protein expression in *E. coli* hosts compared to *Streptomyces*. The *E. coli* strains BL21 (DE3) and C43 (DE3) were utilised for protein expression. Both strains contain the λDE3 lysogen which carries the gene encoding T7 RNA polymerase under control of the lacUV5 promoter, the expression of which may be induced by IPTG. Therefore, strains containing DE3 are capable of expressing recombinant genes cloned downstream of a T7 promoter. BL21 (DE3) may be unable to express proteins due to toxicity, a problem that is particular with membrane proteins, which SCO2420 and SCO2421 are believed to be. For this reason, the C43 (DE3) cell line was also used. The cell line C41 (DE3) is a strain derived from BL21 (DE3) which contains mutations conferring resistance to cell death from expression of some recombinant toxic proteins. C43 (DE3) is further derived from C41 (DE3) and is further resistant to a range of other toxic proteins (Dumon-Seignovert, Cariot and Vuillard, 2004).

E. coli cultures were not induced with IPTG. Instead, ZYP-5052, an autoinduction media based on Studier (2005), was used for both BL21 and C43 cell lines, both due to ease of this method and that yields of target proteins obtained are typically several-fold higher than those with IPTG induction (Studier, 2005). Cultures were originally grown at 25 and 37°C for protein expression, but higher temperatures were abandoned in favour of growth at 18°C, 250 rpm, when his-tagged proteins were not detected by Western Blot. Lower temperatures are believed to encourage correct protein folding and therefore prevent formation of inclusion bodies (Vera *et al.*, 2007).

Cultures were harvested at a range of times in an effort to determine the optimum growth time for protein production and biomass cultivation. C43 cultures outgrew BL21 growth rates, leading to harvesting of C43 cultures at 24 hours into culture and harvesting of BL21 cultures at 72 hours.

Initially, cell lysis was performed by either use of a French® Pressure Cell Press or use of BugBuster™ Master Mix, per manufacture's instructions. BugBuster Master Mix™ was found to be ideal for lysing smaller amounts of culture whilst French® Press allowed breakage of a larger biomass. Following both methods, cell lysate was centrifuged at 4°C, and aliquots of the resultant supernatant boiled with 5X SDS loading dye for 10 minutes at 95°C. Only samples containing secreted proteins were boiled, while potential membrane proteins were not denatured prior to SDS-PAGE analysis. A portion of supernatant was also mixed with HisPur™ Ni-NTA Magnetic Beads and his-tagged proteins purified as per manufactures instructions before being mixed with 5X SDS loading dye and loaded, without boiling, onto an SDS-PAGE gel.

Proteins in samples were then separated by SDS-PAGE. Followingly, SDS-PAGE gels were stained with Coomassie for visualisation of total protein content (Fig. 5.4.A) or transferred to a PDVF membrane prior to Western Blotting to detect the presence of his-tagged target proteins (Fig. 5.4B).

From cells lysed with BugBuster™, two bands indicating his-tagged protein expression were detected via Western Blot. Both bands originate from the MceA-C induced whole cell lysate supernatant sample; the first band, in lane 8, from unpurified supernatant, and the second band, in lane 9, from supernatant purified on nickel-beads prior to loading. Therefore, the cell line BL21 (DE3) is able to express MceA-C when cultured at 18°C, 250 rpm for 24 hours. Noticeably, the band from the sample of uninduced MceA-C culture

is absent, demonstrating that the induction media is successful at producing protein expression in induced cultures. Nickle-bead purification appears to increase the concentration of MceA-C in the loaded sample, as the band produced on the Western Blot (Fig. 5.4.B, lane 9) appears brighter than that of unpurified MceA-C (Fig. 5.4.B, land 8). However, nickel-beads were unsuccessful at entirely purifying MceA-C from the sample, as other non-target proteins clearly remain visible via SDS-PAGE (Fig. 5.4.A, lane 9).

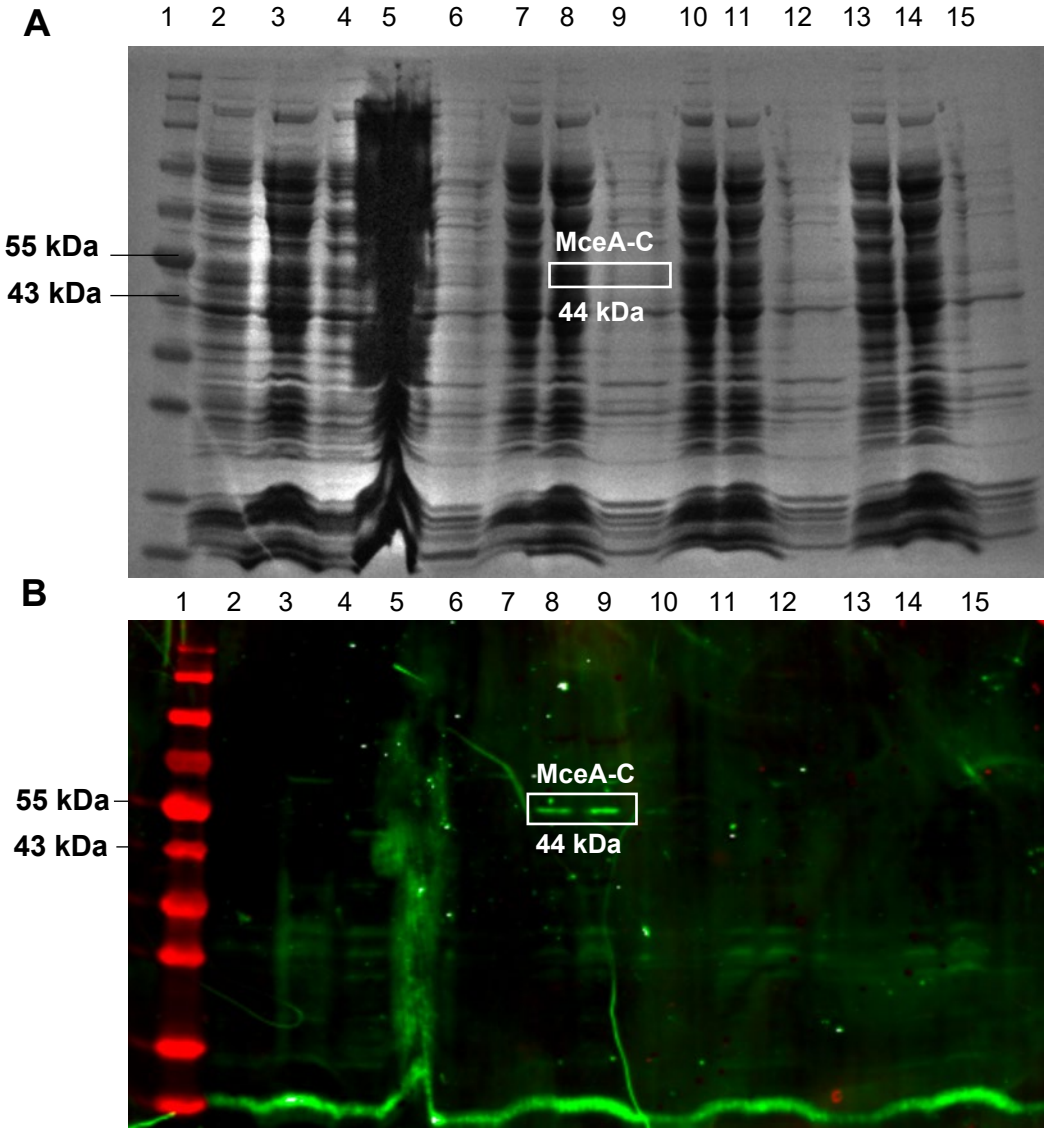

Figure 5.5: Detection of MceA-C in BL21. SDS-PAGE gels were either stained with Coomassie Brilliant Blue **(A)** or transferred to a PDVF membrane for Western Blotting **(B)**. Gels show whole cell lysate supernatant of BL21 cells (Bug Busted™) containing the empty pT7-7 plasmid or the pT7-7 plasmid with his-tagged constructs, from both induced and uninduced cultures. His-tagged proteins were further concentrated from the whole cell lysate via nickel-bead purification. Lanes were loaded as follows: **(1)** Blue Prestained Protein Standard, Broad Range (11-240 kDa) (NEB# P7706), **(2)** pT7-7 uninduced, **(3)** pT7-7 induced, **(4)** N-MceA uninduced, **(5)** N-MceA induced, **(6)** N-MceA induced and purified, **(7)** MceA-C uninduced, **(8)** MceA-C induced, **(9)** MceA-C induced and purified, **(10)** N-SCO2420 uninduced, **(11)** N-SCO2420 induced, **(12)** N-SCO2420 induced and purified, **(13)** SCO2420-C uninduced, **(14)** SCO2420-C induced, **(15)** SCO2420-C induced and purified. Western blotting shows the presence of MceA-C protein in the induced MceA-C culture sample and the induced MceA-C culture sample which was nickel-bead purified.

To confirm that the band produced in the above blot was indeed MceA-C, BL21 (DE3) and C43 (DE3) cells were again transformed with appropriate his-tagged construct DNA and cells cultured as previously, prior to lysis with BugBuster™ Master mix®. Supernatants of lysate from the N-terminally his-tagged and C-terminally his-tagged MceA cultures were run on an SDS-PAGE gel and blotted for alongside cultures from the empty pT7-7 vector as a control.

No bands were detected from C43 cell lysate. The sole band observed in BL21 cells was from the sample supernatant originating from induced BL21 MceA-C cultures, and confirms the expression of MceA-C protein (Fig. 5.6.B, lane 7). The absence of N-MceA and presence of MceA-C may reveal the potential information about the processing of these proteins, due to potential loss of the his-tag from cleavage. As priorly described, should secretion machinery cleave the N-terminal signal sequence in N-MceA to prepare the protein for secretion, the hexa-histidine tag would be lost. Conversely, even with cleavage of the signal sequence in MceA-C, the C-terminal his-tag is preserved. Therefore, it is possible that the presence of C-MceA, but not N-MceA may indicate that these proteins are secreted proteins. Alternatively, the lack of N-MceA protein detected even within the cytoplasm could point to protein mis-folding occurring due to the removed 23 amino acids from the beginning of the protein sequence, leaving N-MceA to be targeted to the proteosome and destroyed.

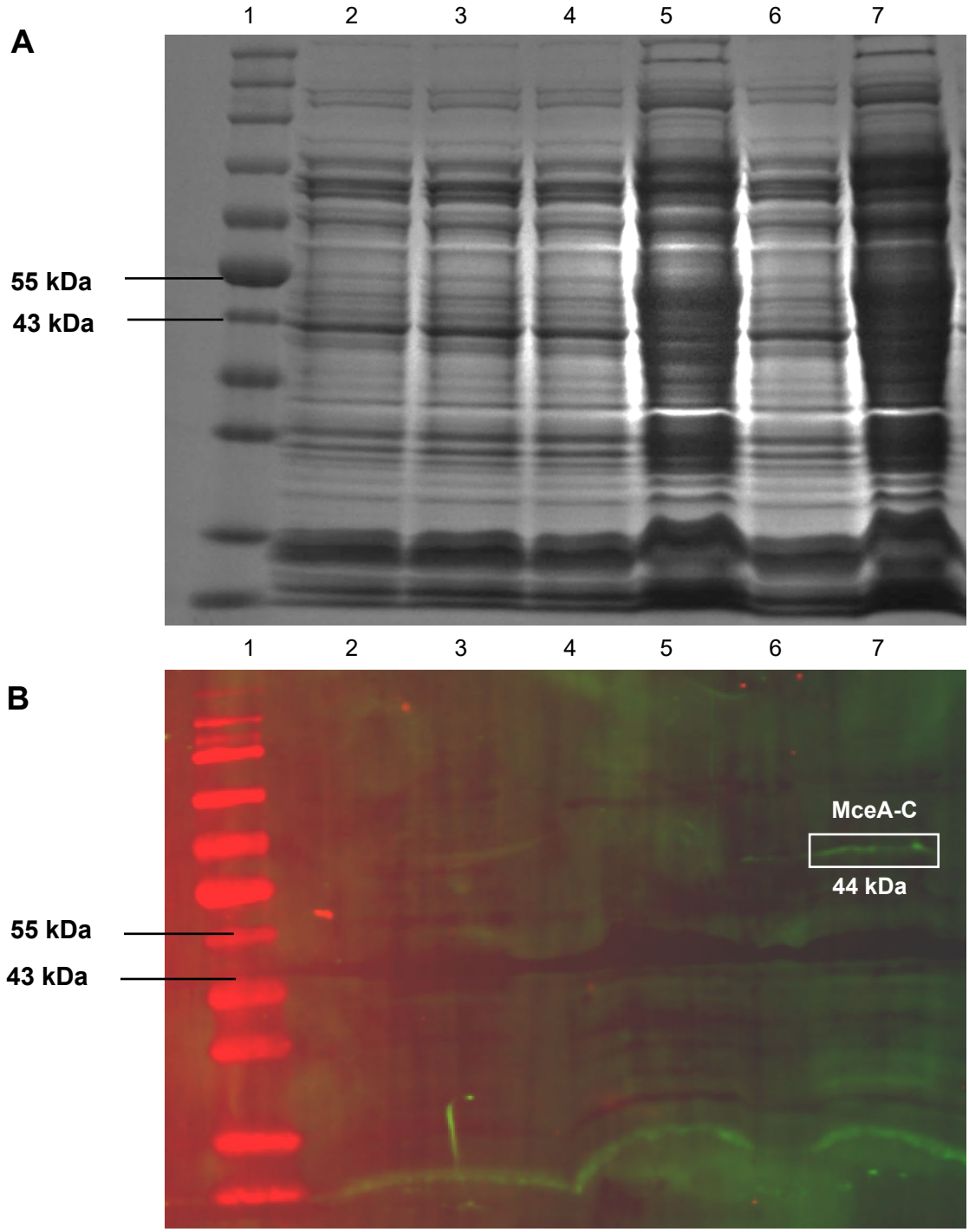

Figure 5.6: Immunoblot of BL21 lysate. SDS-PAGE gels were either stained with Coomassie Brilliant Blue **(A)** or transferred to a PDVF membrane for Western Blotting **(B)**. Gels show whole cell lysate supernatant of BL21 cells (Bug Busted™) containing the empty pT7-7 plasmid or the pT7-7 plasmid with his-tagged constructs, from both induced and uninduced cultures. Lanes were loaded as follows: **(1)** Blue Prestained Protein Standard, Broad Range (11-240 kDa) (NEB# P7706), **(2)** pT7-7 uninduced, **(3)** pT7-7 induced, **(4)** pT7-7 N-MceA uninduced, **(5)** pT7-7 N-MceA induced, **(6)** pT7-7 MceA-C uninduced, **(7)** pT7-7 MceA-C induced. The Western Blot shows the presence of MceA-C protein in the induced MceA-C culture whole cell lysate (lane 7).

As SCO2421 and SCO2420 are putative membrane proteins, it was considered that their absence in supernatant of the whole cell lysate during Western Blot analysis may be due to lysis methods. Membrane proteins have distinct physiological properties to secreted proteins and require specialised lysis techniques (Williamson *et al.*, 2020). Sonication is known to be detrimental to membrane proteins and BugBuster(TM) MasterMix® similarly failed to produce any detectable SCO2421 or SCO2420 expression. For this reason, an alternative method of lysis using the Lysis Buffer A, containing lysozyme, was utilised on both C43 and BL21 cells. This method has been specifically developed for membrane proteins (Dias Mirandela *et al.*, 2018). A concentration of 0.7 µg/mL purified his-tagged Rhesus protein, RH50 H324E, was also loaded onto gels as a positive control.

Following SDS-PAGE and Western Blot as previously described, in BL21 cells there was no detectable expression of MceA proteins (Fig. 5.7). The Rhesus protein positive control can be clearly identified in both Coomassie gel and Western blot (Fig. 5.7, lane 11).

However, a band indicating the presence of SCO2421-C was observed in the sample originating from the BL21 SCO2421-C induced culture (Fig. 5.7.B, lane 9). N-SCO2421 was not detected, potentially again due to cleavage of the signal sequence resulting in misfolding and subsequent targeting to the proteosome.

Expression of SCO2420-C was also not detected, perhaps surprising considering the similarity between SCO2420 and SCO2421 and their likely co-localisation in the membrane. This result may hint at subtle differences between these two proteins. As previously mentioned, TMPred predicts the C-terminus is intracellular in SCO2420 but extracellular in SCO2421 and alignment of their amino acid sequences suggest potential structural differences.

As no his-tagged protein expression had been detected at any point or with any method in samples originating from C43 (DE3) cells, this cell line was abandoned and remaining expression experiments were conducted solely in the BL21 (DE3) cell line.

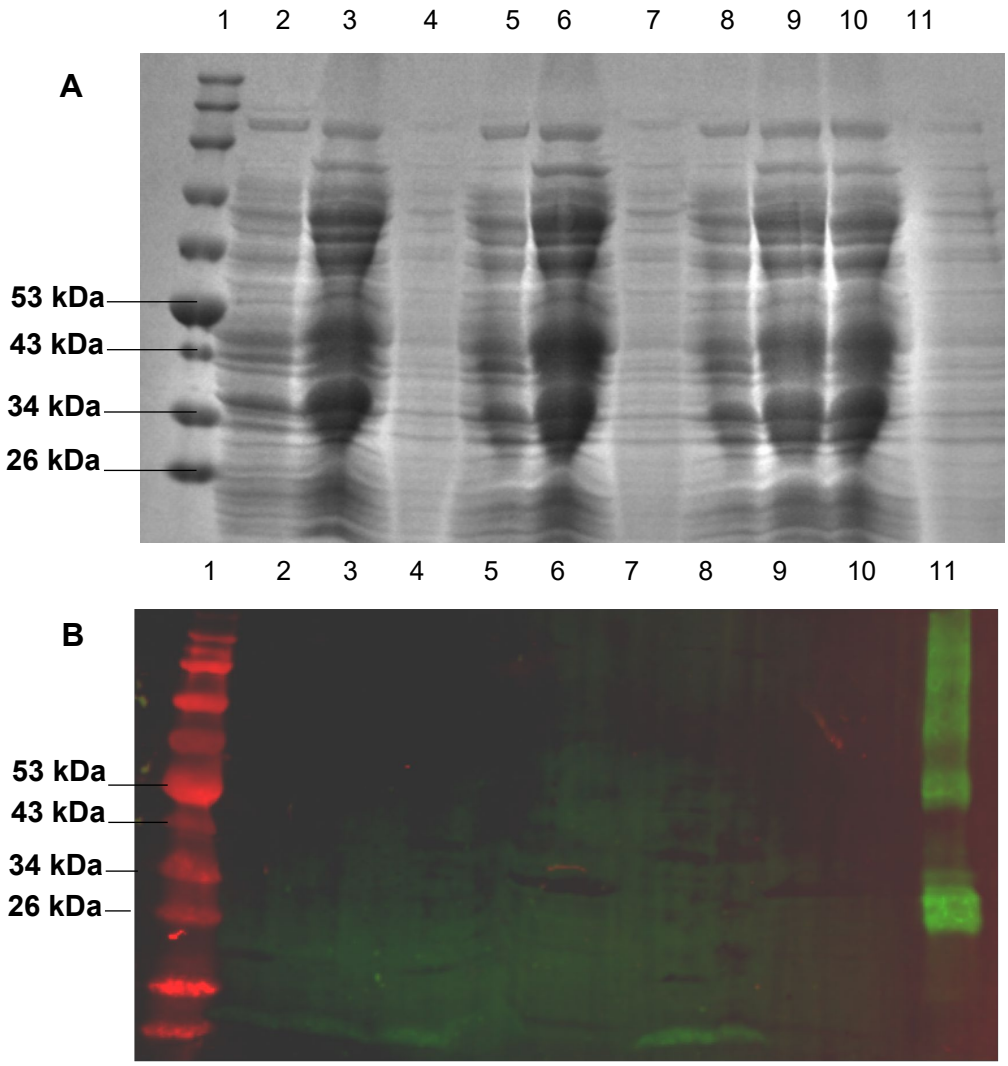

Figure 5.7: Immunoblotting results following BL21 cell lysate and processing with membrane specific techniques. SDS-PAGE gels were either stained with Coomassie Brilliant Blue **(A)** or transferred to a PDVF membrane for Western Blotting **(B)**. Gels show supernatant of whole cell lysate of BL21 cells, lysed with Lysis buffer A, containing the empty pT7-7 plasmid or the pT7-7 plasmid with his-tagged constructs, from both induced and uninduced cultures. The extracellular growth media of N-MceA and MceA-C induced cultures was treated with 10% TCA to precipitate extracellular proteins. Protein precipitants were loaded alongside whole cell lysate samples. The lanes of gels **A** and **B** were loaded as follows: **(1)** Blue Prestained Protein Standard, Broad Range (11-240 kDa) (NEB# P7706), **(2)** pT7-7 uninduced, **(3)** pT7-7 induced, **(4)** pT7-7 induced precipitated, **(5)** pT7-7 N-MceA uninduced, **(6)** pT7-7 N-MceA induced, **(7)** pT7-7 N-MceA induced and precipitated, **(8)** pT7-7 MceA-C uninduced, **(9)** pT7-7 MceA-C induced, **(10)** pT7-7 MceA-C induced and precipitated **(11)** RH50 H324E.

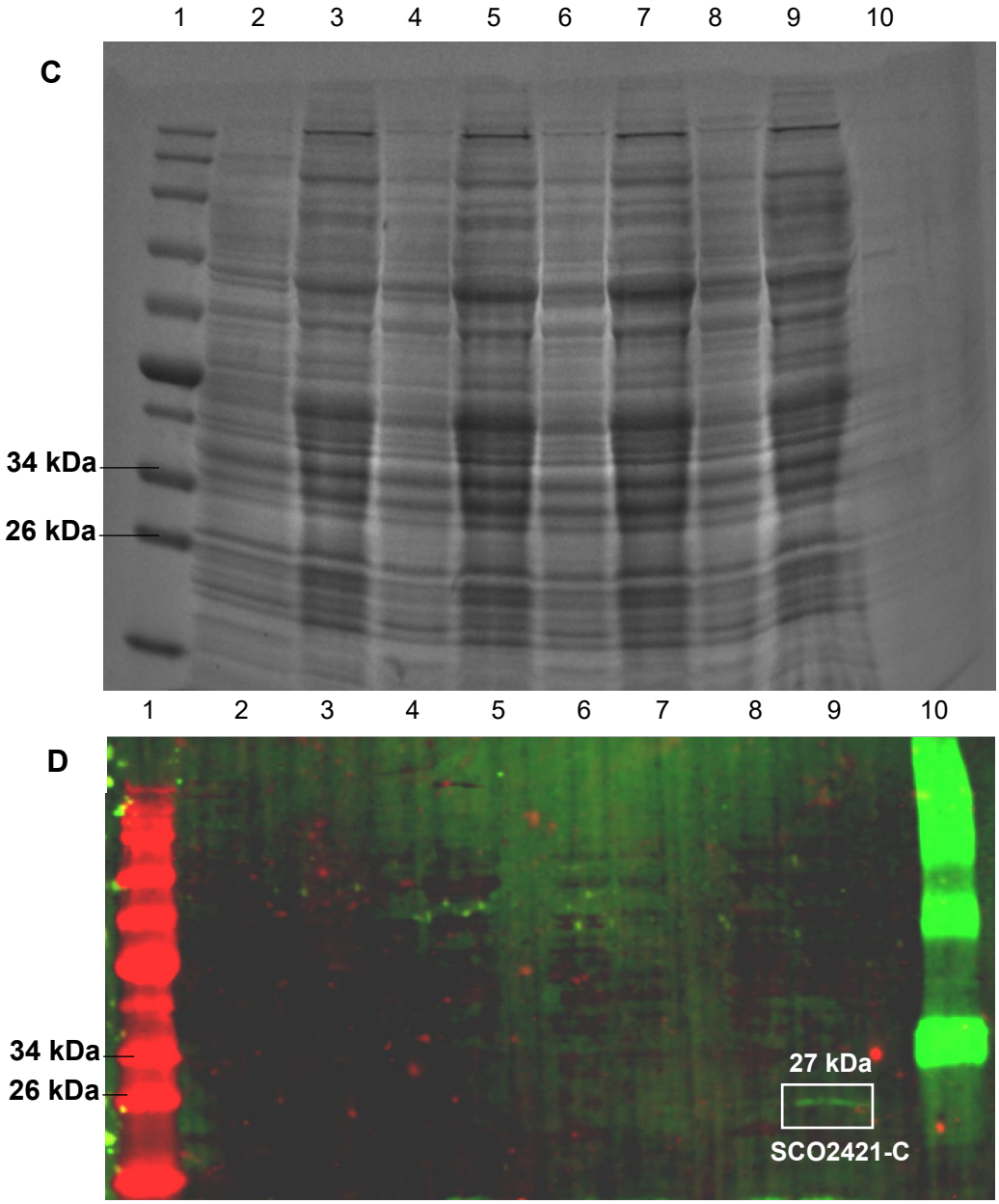

Figure 5.7: Immunoblotting results following BL21 cell lysate and processing with membrane specific techniques. The lanes of gels **C** and **D** were loaded as follows: **(1)** Blue Prestained Protein Standard, Broad Range (11-240 kDa) (NEB# P7706), **(2)** pT7-7 N-SCO2420 uninduced **(3)** pT7-7 N-SCO2420 induced, **(4)** pT7-7 SCO2420- C uninduced **(5)** pT7-7 SCO2420-C induced, **(6)** pT7-7 N-SCO2421 uninduced, **(7)** pT7-7 N-SCO2421 induced, **(8)** pT7-7 SCO2421-C uninduced, **(9)** pT7-7 SCO2421-C induced, **(10)** RH50 H324E. Western blotting **(D)** shows the presence of SCO2421-C protein in the induced SCO2421-C culture whole cell lysate **(Lane 9)**.

As using Lysis Buffer A to lyse BL21 cells resulted in the detection of SCO2421-C, further sample preparation was performed via this method.

As, based on bioinformatic analysis, some or all of the Mce-domain containing proteins may be secreted proteins, it is possible that they may be detectable in the extracellular growth media of the culture. As such, extracellular growth media was mixed with 5X loading dye, boiled, and loaded onto SDS-gels. However, this failed to produce any visible indications of the target protein, potentially due to his-tagged proteins being below detectable levels. Therefore, proteins present in the extracellular growth media were concentrated using TCA precipitation prior to loading on an SDS-PAGE gel. TCA precipitated extracellular growth media was loaded alongside samples of supernatant from whole protein lysate and Coomassie and Western Blot analysis subsequently performed (Fig. 5.8, Fig 5.9).

Whilst bands of the correct size for MceA (44 kDa) were present in the TCA precipitated growth media sample on the Coomassie stained gel (Fig. 5.8.A), these were not detected on the Western Blot (Fig. 5.8.B). The C-SCO2421 protein was again detected in the sample originating from the induced whole cell lysate (Fig. 5.9.B, lane 13), though there was no indication of the presence of N-SCO2420. All MceA proteins were absent in the Western Blot analysis, including within samples of supernatant of whole cell lysate of induced cultures which had previously contained bands (Fig. 5.8.B).

TCA precipitation was also attempted with the whole cell lysate of cultures of all his-tagged strains, but no protein was detected as a result (data not shown).

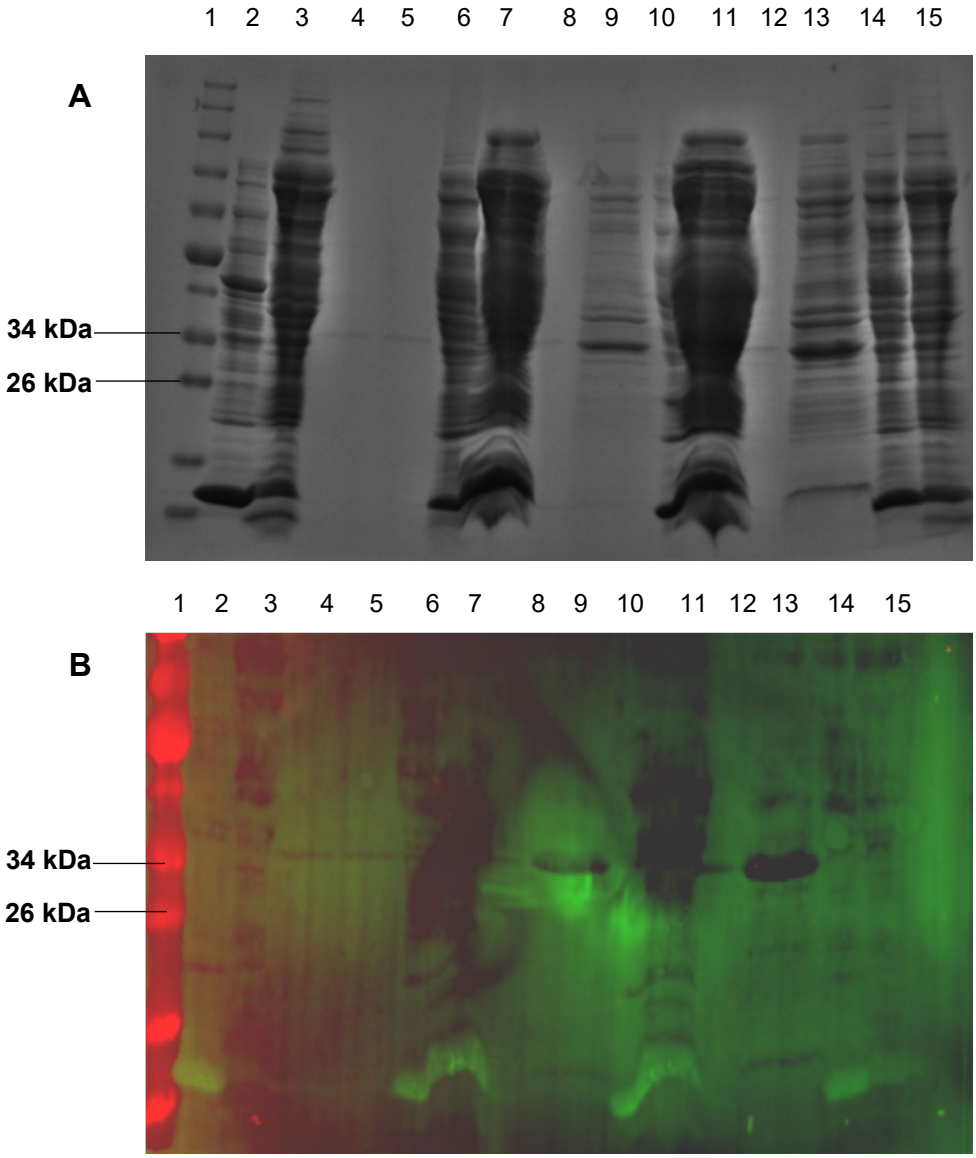

Figure 5.8: Immunoblotting with TCA precipitated samples. SDS-PAGE gels were either stained with Coomassie Brilliant Blue **(A)** or transferred to a PDVF membrane for Western Blotting **(B)**. Gels show whole cell lysate of BL21 cells, lysed with Lysis buffer A, containing the empty pT7-7 plasmid or the pT7-7 plasmid with his-tagged constructs, from both induced and uninduced cultures. The extracellular growth media of all cultures was treated with 10% TCA to precipitate extracellular proteins. Protein precipitants were loaded alongside whole cell lysate samples. Lanes of gels **A** and **B** were loaded as follows: **(1)** Blue Prestained Protein Standard, Broad Range (11-240 kDa) (NEB# P7706), **(2)** pT7-7 uninduced, **(3)** pT7-7 induced, **(4)** pT7-7 uninduced and precipitated, **(5)** pT7-7 induced and precipitated, **(6)** pT7-7 N-MceA uninduced, **(7)** pT7-7 N-MceA induced, **(8)** N-MceA uninduced and precipitated, **(9)** N-MceA induced and precipitated, **(10)** pT7-7 MceA-C uninduced, **(11)** pT7-7 MceA-C induced, **(12)** pT7-7 uninduced and precipitated, **(13)** pT7-7 MceA-C induced and precipitated, **(14)** pT7-7 N-SCO2420 uninduced, **(15)** pT7-7 N-SCO2420 induced.

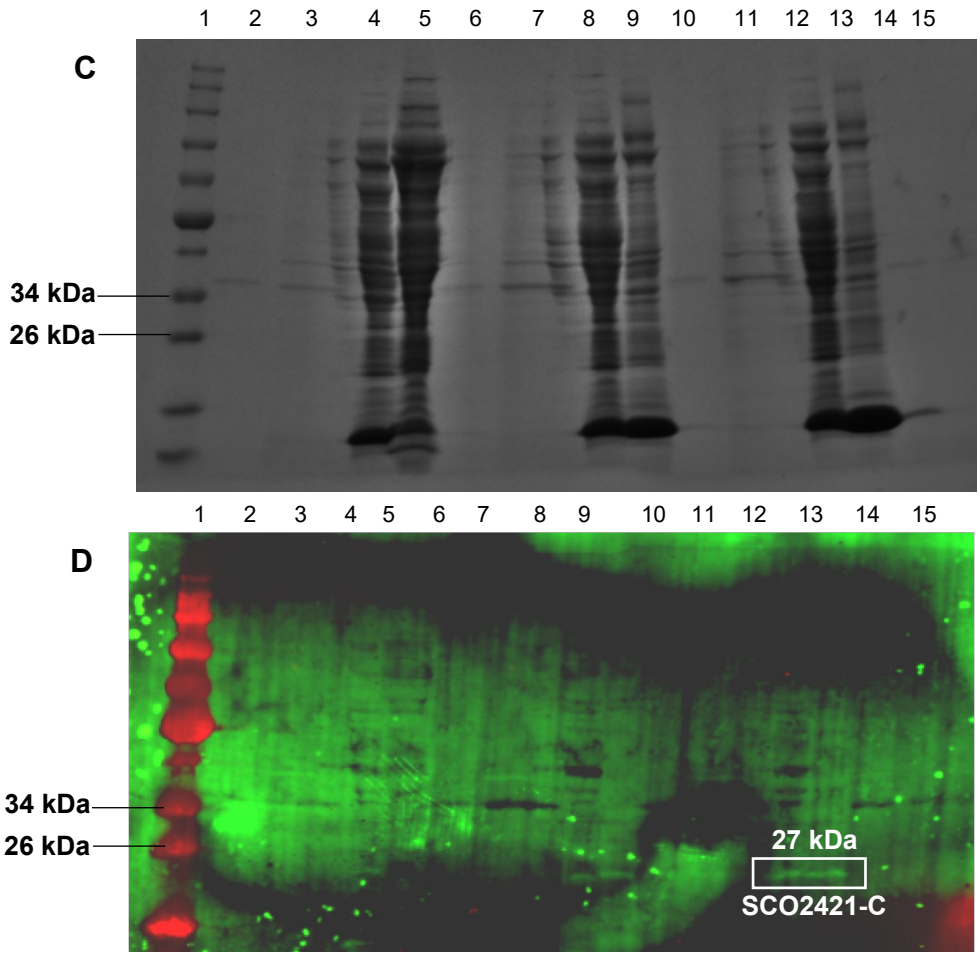

Figure 5.9: Immunoblotting with TCA precipitated samples. SDS-PAGE gels were either stained with Coomassie Brilliant Blue **(A)** or transferred to a PDVF membrane for Western Blotting **(B)**. Lanes of gels **C** and **D** were loaded as follows: **(1)** Blue Prestained Protein Standard, Broad Range (11-240 kDa) (NEB# P7706), **(2)** pT7-7 N-SCO2420 uninduced and precipitated, **(3)** pT7-7 N-SCO2420 induced and precipitated, **(4)** pT7-7 SCO2420-C uninduced, **(5)** pT7-7 SCO2420-C induced, **(6)** pT7-7 SCO2420-C uninduced and precipitated, **(7)** pT7-7 induced and precipitated, **(8)** pT7-7 N-SCO2421 uninduced, **(9)** pT7-7 N-SCO2421 induced, **(10)** pT7-7 N-SCO2421 uninduced and precipitated, **(11)** pT7-7 N-SCO2421 induced and precipitated, **(12)** pT7-7 SCO2421-C uninduced, **(13)** pT7-7 SCO2421-C induced, **(14)** pT7-7 SCO2421-C uninduced and precipitated, **(15)** SCO2421-C induced and precipitated. Western blotting **(D)** shows the presence of SCO2421-C protein in the induced SCO2421-C culture whole cell lysate **(Lane 13)**.

The use of Lysis Buffer A and the lysis method described for membrane proteins appeared to be prohibitive to the detection of the MceA-C protein, which had previously been detected in whole cell lysate samples of induced cultures.

As MceA-C expression had been observed most consistently with BugBuster™ Master Mix® and associated sample preparation protocol, this method was employed in analysis of BL21 N-MceA and MceA-C induced and uninduced cultures.

Three distinct BL21 N-Mce and MceA-C transformants were cultured in induction only and cultures lysed as priorly described via BugBuster™ MasterMix® prior to mixing with 5X SDS loading-dye, boiling and loading onto SDS-PAGE gels. Extracellular media of each culture was TCA precipitated, mixed with 5X SDS loading dye without boiling and loaded alongside. Gels were subsequently analysed via Coomassie straining and Western Blot (Fig. 5.10).

Expression of MceA-C was again detectable in all induced whole cell lysate samples (5.10, lanes 7, 9 & 11). However, no MceA-C protein was detected in TCA precipitated extracellular growth media. N-MceA was not detected in either whole cell lysate or extracellular growth media samples.

The absence of MceA-C in the TCA precipitated extracellular growth media does preclude the MceA protein of *S. coelicolor* being a secreted protein. It is instead likely absent due to the *E. coli* secretion machinery being incapable of secreting a *S. coelicolor* secrete protein, as the *S. coelicolor* protein signal sequence is atypical for *E. coli*.

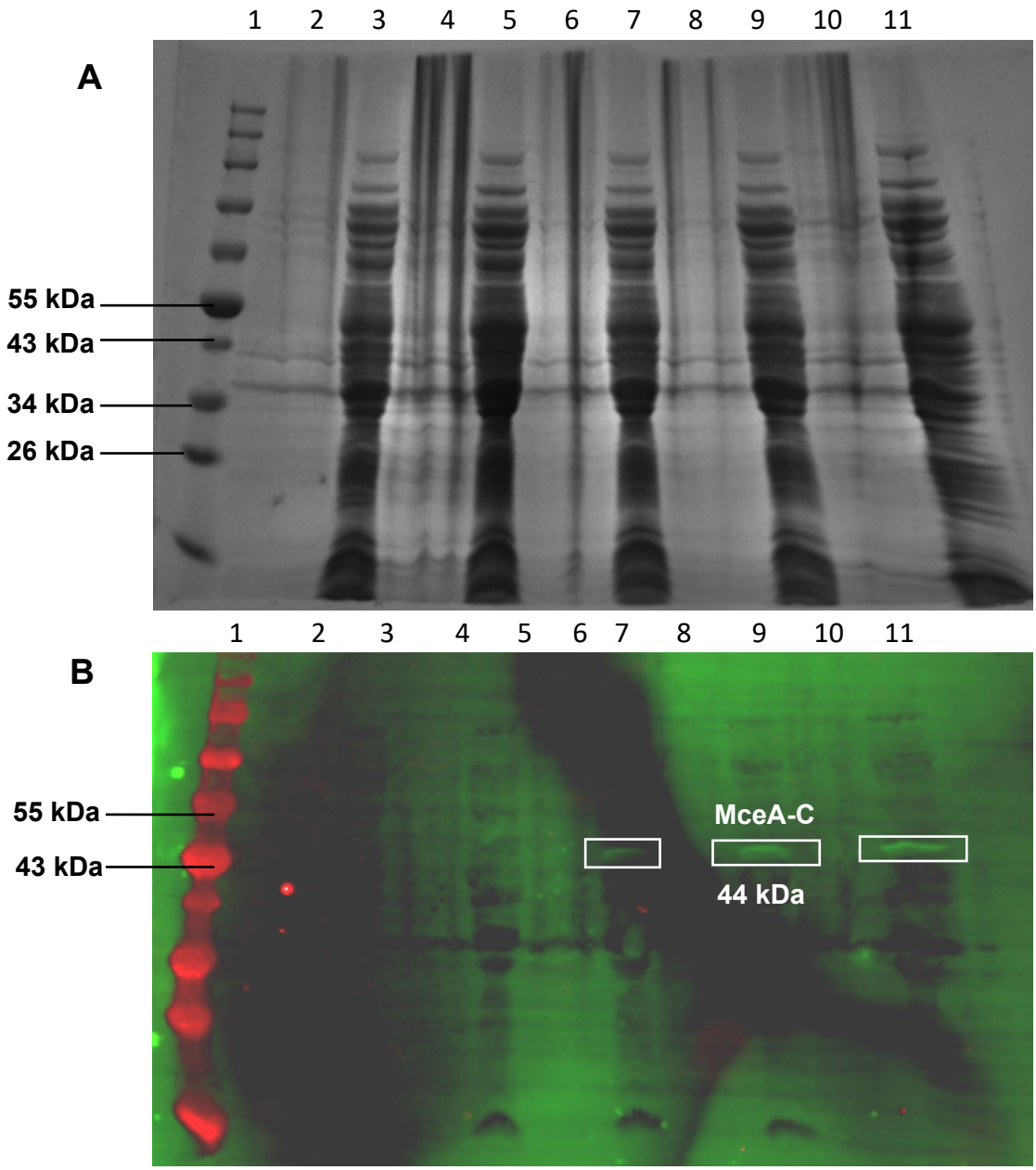

Figure 5.10: Confirmation of MceA-C detection. SDS-PAGE gels were either stained with Coomassie Brilliant Blue **(A)** or transferred to a PDVF membrane for Western Blotting **(B)**. Gels show whole cell lysate supernatant of BL21 cells (Bug Busted™) containing the empty pT7-7 plasmid or the pT7-7 plasmid with his-tagged constructs, from both induced and uninduced cultures. The extracellular growth media of all cultures was treated with 10% TCA to precipitate extracellular proteins. Protein precipitants were loaded alongside whole cell lysate samples. Gel lanes loaded as follows: **(1)** Blue Prestained Protein Standard, Broad Range (11-240 kDa) (NEB# P7706), **(2)** pT7-7 induced and precipitated, **(3)** pT7-7 induced, **(4)** pT7-7 N-MceA induced and precipitated, **(5)** pT7-7 N-MceA induced, **(6)** pT7-7 MceA-C 1, induced and precipitated, **(7)** pT7-7 MceA-C 1 induced**, (8)** pT7-7 MceA-C 2, induced and precipitated, **(9)** pT7-7 MceA-C 2 induced, **(10)** pT7-7 Mce-C 3 induced and precipitated, **(11)** pT7-7 MceA-C 3 induced. The MceA-C protein is present in unprecipitated and induced whole cell lysate samples and visible in the Western Blot (**B)** in Lanes **7**, **9** and **11.**

Purification of C-terminal his-tagged MceA from *Escherichia coli*

Large scale (1 L) induced BL21 C-MceA cultures were grown and harvested as previously described. Pelleted cells were resuspended in solubilisation buffer (Table 2.5), lysed via French® Press and spun at 25,000 x g in a centrifuge. The C-MceA protein in the resultant supernatant was protein purified by IMAC using an ÄKTA Pure system. Supernatant was loaded onto a Histrap column loaded with nickel, to which the hexa-histidine-tagged MceA-C protein is able to bind.

Imidazole was applied to the column in increasing concentrations, as it acts as a competitive inhibitor by binding to the nickel with higher affinity, to cause elution of the histidine-tagged protein.

Considerable amounts of protein were present in the supernatant, as can be seen from the high absorbance during the loading stage (Fig. 5.11). The initial peak indicates the beginning of the wash step and, resultantly, the detachment of non-his-tagged proteins which were loosely bound to the nickel column. Shortly following the initiation of elution, a smaller secondary peak indicates the presence of MceA-C within the eluted fractions.

Eluted fractions of interest were identified by the position of the MceA-C peak and were fractions 6-8.

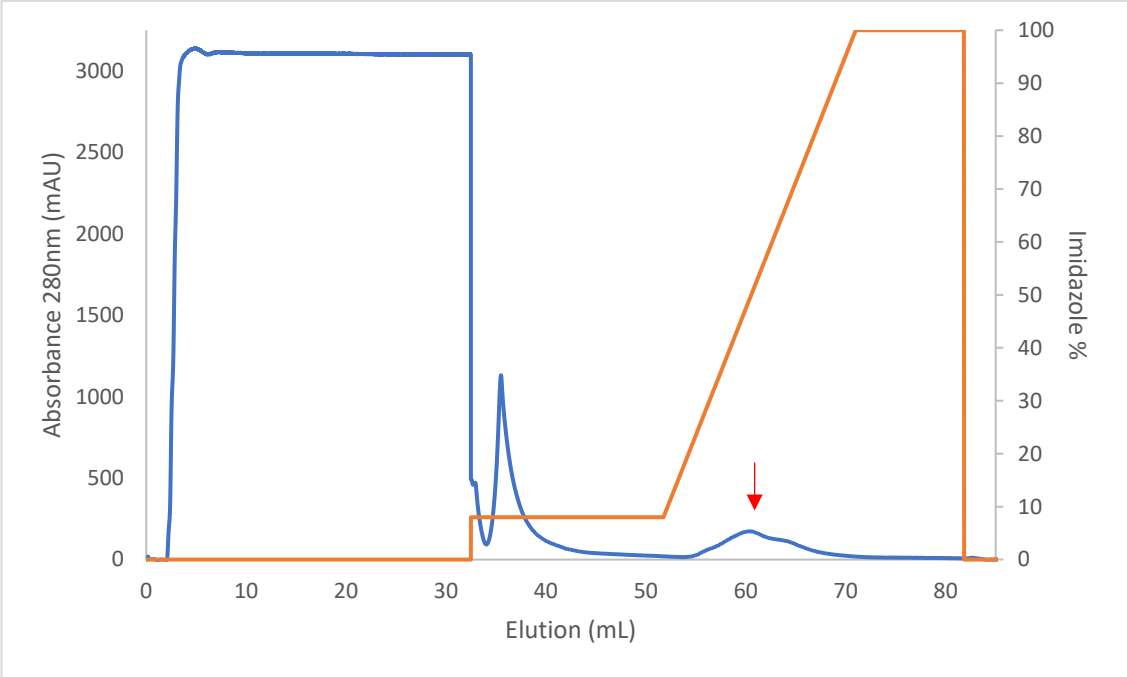

Figure 5.11: Purification of MceA-C by IMAC. $A280_{nm}$ (blue), imidazole concentration (orange). Arrow (red) indicates peak likely caused by MceA-C in the elution.

Eluted fractions were then analysed via SDS-PAGE (Fig. 5.11.A). The resultant gel displays a large number of bands within the elution fractions, indicating the presence of many other proteins. Therefore C-MceA has not been absolutely purified. Following Western Blot analysis, a band was present in fraction 6 at approximately 28 kDa (Fig. 5.11.B, lane 6). As MceA-C is 44 kDa in size, the presence of this band suggests that either anomalous migration of MceA-C has occurred within the gel, or that proteolysis has occurred and a fragment of the MceA-C protein has been cleaved and lost. Proteolysis may occur during protein purification, even with the addition of proteases inhibitiors such as PMSF, as it is impossible to remove all proteases present in a chromatography sample (Walls and Loughran, 2017). Proteolysis is also more prone to occur if the protein possesses an open structure, with an exposed sequence that proteases are capable of accessing (Walls and Loughran, 2017).

Further analysis was conducted on fraction 6 by boiling for ten minutes at 95ºC to ensure denaturation of the protein. The boiled sample was loaded next to an un-boiled sample to compare. Un-boiled fraction 6 was also mixed with 0.193 µg/mL cholesterol for analysis. It was hypothesised that should MceA-C bind to the cholesterol, it may do so in a complex with other MceA-C proteins, which would be reflected in band size detectable by Western Blotting. A 1/000 dilution of 0.000193 µg/mL cholesterol was also mixed with fraction 6, as the *mce* operon is believed to function as a high-affinity sterol transporter. The concentration of 0.193 µg/mL cholesterol was used as this concentration has been shown to provoke optimal transcription of the *mce4* operon in Actinobacteria (Mohn *et al.*, 2008).

MceA-C was detectable in the un-boiled fraction 6, as expected (Fig. 5.13.B, lane 4). MceA-C is detectable at 44 kDa in the sample of fraction 6 mixed with 0.193 µg/mL cholesterol (Fig. 5.13.B, lane 7) as is a smaller band at approximately 18 kDa, again suggestive that proteolysis of the MceA-C protein has occurred during purification.

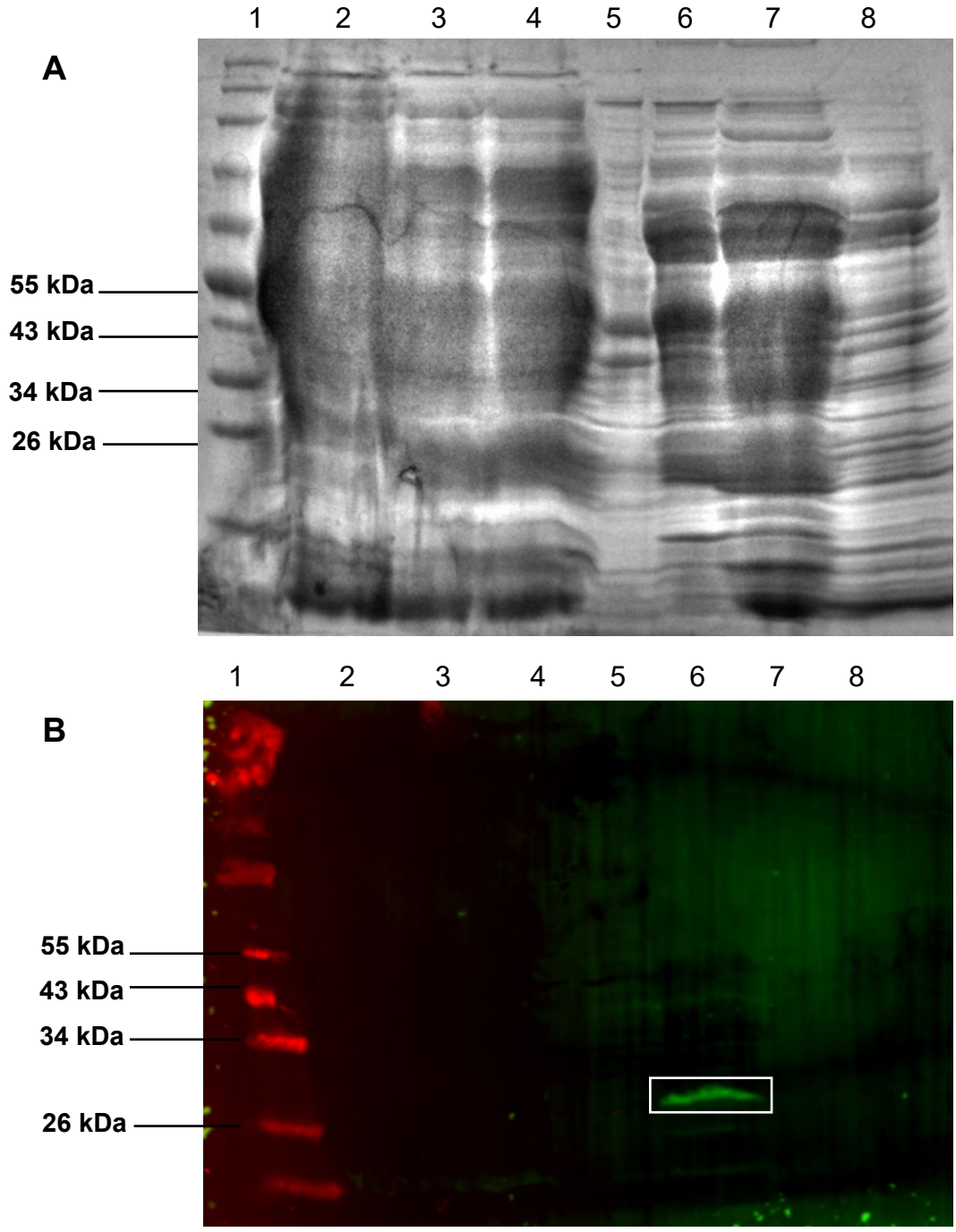

Figure 5.12: Immunoblotting following IMAC purification of MceA-C. SDS-PAGE gels were either stained with Coomassie Brilliant Blue **(A)** or transferred to a PDVF membrane for Western Blotting **(B)**. Gels lanes were loaded as follows: **(1)** ladder, **(2)** whole cell lysate, **(3)** flow through, **(4)** wash, **(5)** fraction 5, **(6)** fraction 6, **(7)** fraction 7, **(8)** fraction 8. A band at approximately 28kDa is visible in lane 6, in purified fraction 6.

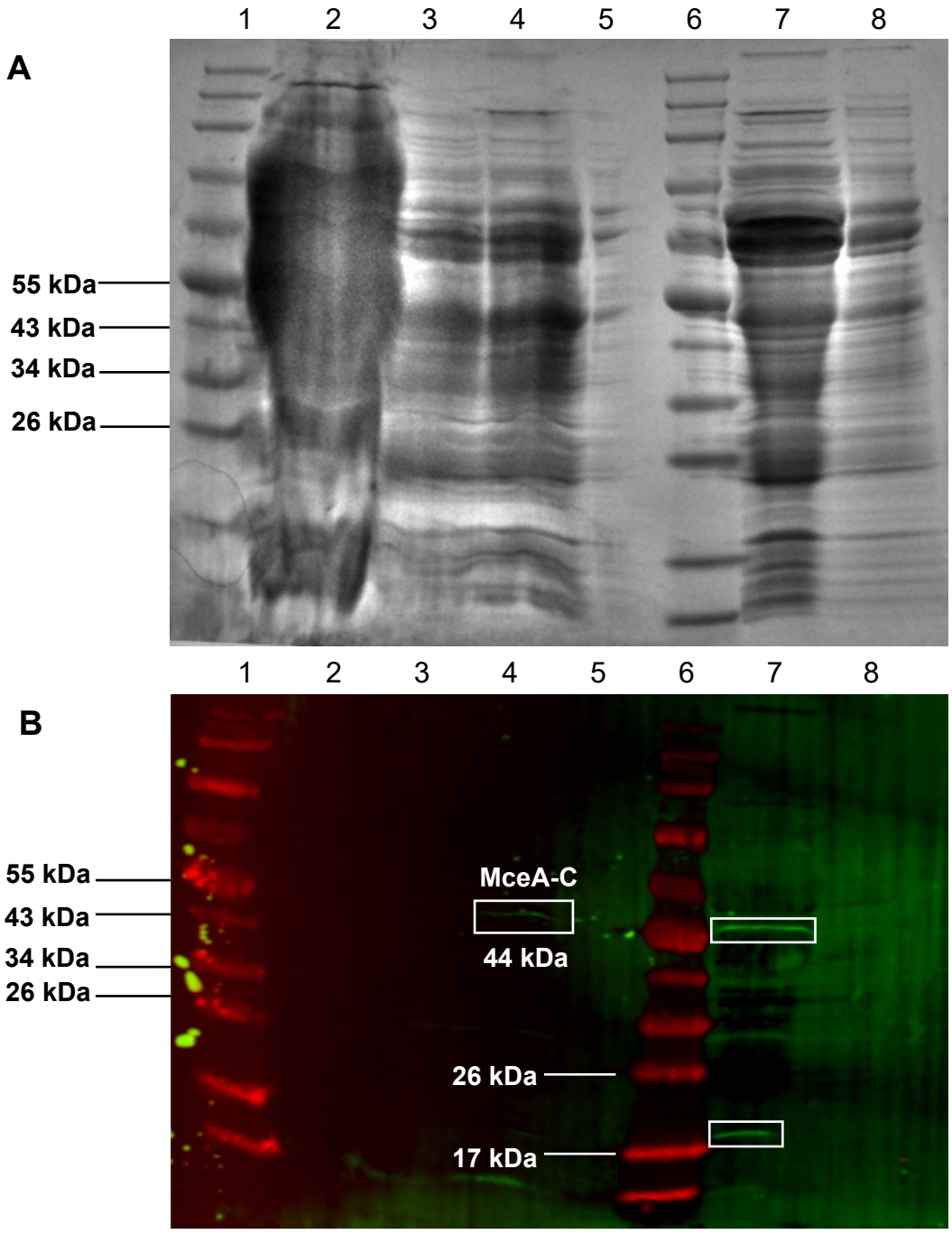

Figure 5.13: Immunoblotting following IMAC purification of MceA-C. SDS-PAGE gels were either stained with Coomassie Brilliant Blue **(A)** or transferred to a PDVF membrane for Western Blotting **(B)**. Gel lanes were loaded as follows: (1) ladder, (2) whole cell lysate, (3) fraction 6, boiled, (4) fraction 6, unboiled, (5) empty, (6) ladder, (7) fraction 6 + 0.193 µg/mL cholesterol, (8) fraction 6 + 0.000193 µg/mL cholesterol.

Optimising his-tagged protein overexpression and detection by Western Blot in *Streptomyces coelicolor*

Overexpression of Mce protein in *S. coelicolor* was attempted with C-terminally his-tagged MceA and SCO2421 proteins, as these had shown expression in BL21. These proteins were expressed from a thiostrepton inducible promoter (*tipA*) encoded in pIJ6902 vector (Huang *et al.*, 2005). A final concentration of 5 ug/mL thiostrepton was added to *S. coelicolor* cultures at exponential phase. Cultures were grown for a further 24-hours before harvesting to allow induction and expression of his-tagged proteins. Whole cell lysate was then sonicated as previously described and samples loaded on an SDS-PAGE gel. Coomassie staining showed lysis of *S. coelicolor* cells and presence of protein in the whole cell lysate. However, no Mce protein band was detected in the Western Blot analysis, likely indicating a lack of his-tagged protein expression (data not shown). It was hypothesised that the thiostrepton concentration for induction could be optimised to increase expression, therefore a range of thiostrepton concentrations were trialled with the his-tagged protein MceA-C and cultures harvested and processed as previously described.

Presence of the MceA-C protein was not visible in by SDS-PAGE or Western Blot analysis at any of the tested thiostrepton concentrations (Fig. 5.10).

To determine whether MceA-C was being expressed, produced and was present in the extracellular media rather than the whole cell lysate, the thiostrepton gradient was repeated and TCA precipitation was performed on both extracellular growth media and whole cell lysate of cultures. No C-MceA was observed for any concentration of thiostrepton in either whole cell lysate or extracellular growth media (data not shown).

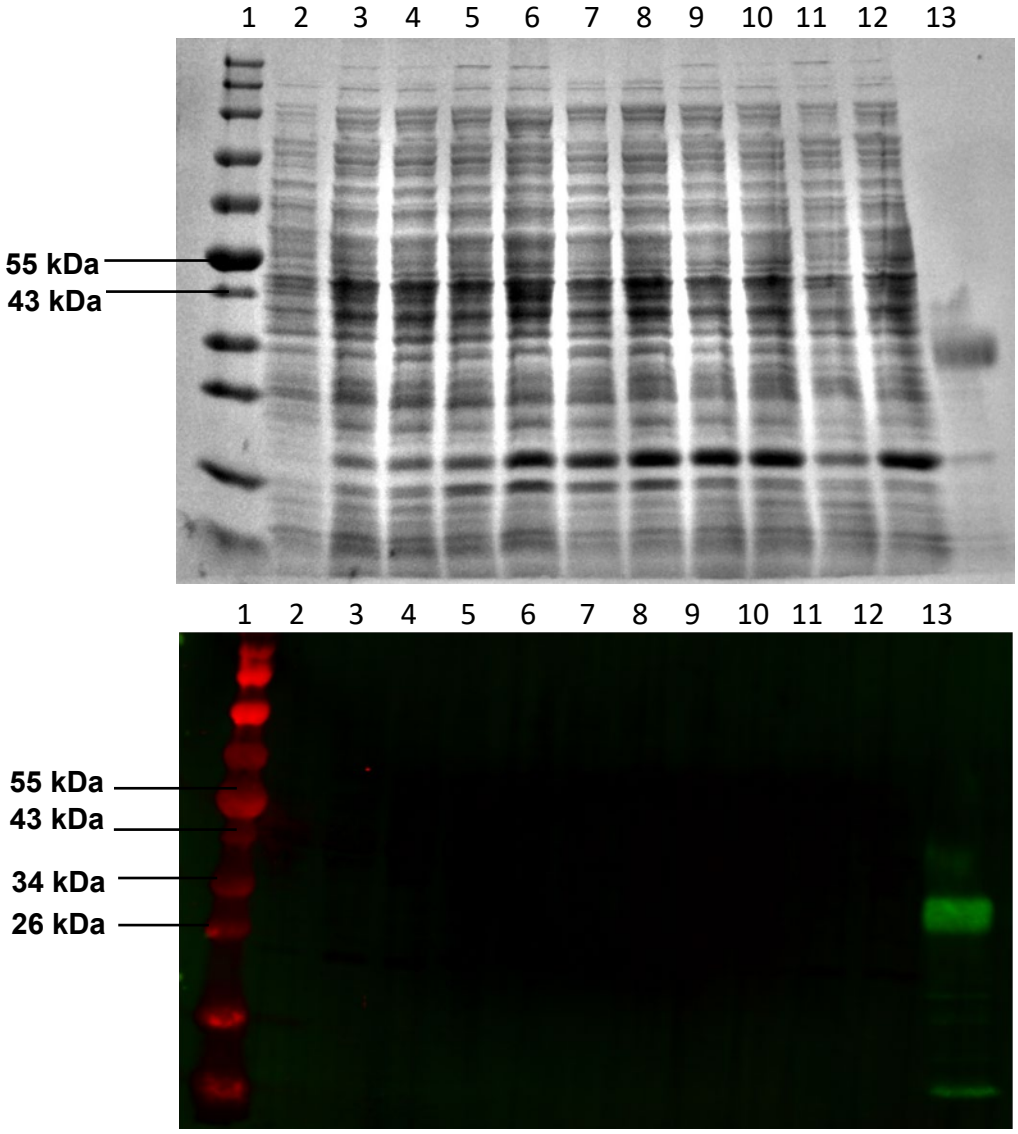

Figure 5.14: No detection of his-tagged Mce proteins in *S. coelicolor* with different concentrations of thiostrepton. SDS-PAGE gels were either stained with Coomassie Brilliant Blue **(A)** or transferred to a PDVF membrane for Western Blotting **(B)**. Gels show whole cell lysate of *S. coelicolor* (sonicated), containing the pIJ6902 plasmid encoding the his-tagged gene construct MceA-C, from cultures induced with a range (0-10µg/mL of Thiostrepton. Gel lanes were loaded as follows: **(1)** Blue Prestained Protein Standard, Broad Range (11-240 kDa) (NEB# P7706), **(2)** 0 µg/mL thiostrepton, **(3)** 1 µg/mL thiostrepton, **(4)** 2 µg/mL thiostrepton, **(5)** 4 µg/mL thiostrepton, **(6)** 4 µg/mL thiostrepton, **(7)** 5 µg/mL thiostrepton, **(8)** 6 µg/mL thiostrepton, **(9)** 7 µg/mL thiostrepton, **(10)** 8 µg/mL thiostrepton, **(11)** 9 µg/mL thiostrepton, **(12)** 10 µg/mL thiostrepton, **(13)** RH50 H324E

Potential of AI systems in predicting Mce protein structure

A number of bioinformatic approaches to predicting protein structure exist, including AlphaFold, a recent AI system which makes predictions of protein structure from the amino acid sequence (Jumper *et al.*, 2020). Although the predicted structures of the Mce proteins of *S. coelicolor* are not available on the systems current database, predicted structures of the *M. tuberculosis* Mce proteins are. The predicted structure of the *E. coli* K12 MlaD protein, the structure of which has been solved experimentally by Ekiert *et al* (2017), is also available on the system.

The AlphaFold AI predicts the structure of the MlaD protein structure (Fig. 5.11.A) with varying degrees of confidence. The system is able to predict the β-barrel of the MlaD protein but is less accurate in regard to the α-helices in the remaining structure. It is possible to compare this predicted structure to the structure of MlaD predicted via X-ray crystallography and electron microscopy (Fig. 5.11.B) (Ekiert *et al.*, 2017). The latter predicts the MlaD protein is anchored to the inner membrane via a single N-terminal TM helix, with the Mce-domain of the protein located in the periplasm. The core Mce-domain is composed of a seven-stranded β-barrel fold of approximately 100 residues. It is this domain which is predicted with the highest confidence in the AlphaFold model.

Experimentally determining the structure of MlaD allowed for understanding of how the protein assembles into a homo-hexameric ring (Fig. 5.11.B), with a central solvent-accessible channel lined with hydrophobic residues (Ekiert *et al.*, 2017).

It is possible that AlphaFold and other AI systems may be useful in predicting the structure of the Mce proteins of *S. coelicolor*, with a reasonable degree of accuracy. However, such models should be confirmed experimentally, as limitations exist.

To further explore the structural aspects of the *S. coelicolor* Mce proteins, the MceA amino acid sequence was run through the homology modelling software, Phyre2, along

with the MlaD amino acid sequence, to validate the structure obtained (Kelley *et al.*, 2015). The structure obtained for MlaD is very close to that obtained experimentally by Ekiert (2017) (Fig. 5.15 B,C) and from AlphaFold (Fig. 5.16.A). Running MceA from *S. coelicolor* through Phyre2 resulted in a predicted structure that contains three antiparallel-beta sheets, similar to those in MlaD, but with an incomplete Beta-barrel like structure (Figure 5.16.B). The Phyre2 model used homology to Mce4 from *M. tuberculosis* (PDB. 7AI3) and several MlaD structures (PDB: 6XBD, 7CHA, 6IC4) to build its structural model, but could only model 27% of the protein at 99% accuracy, with the remaining parts of the protein being modelled at approximately 90% accuracy. The unstructured loop regions are reminiscent of those predicted for MlaD by AlphaFold (Fig.5.15.B, C) reflecting the difficulty in predicted such structures (Hameduh *et al.*, 2020).

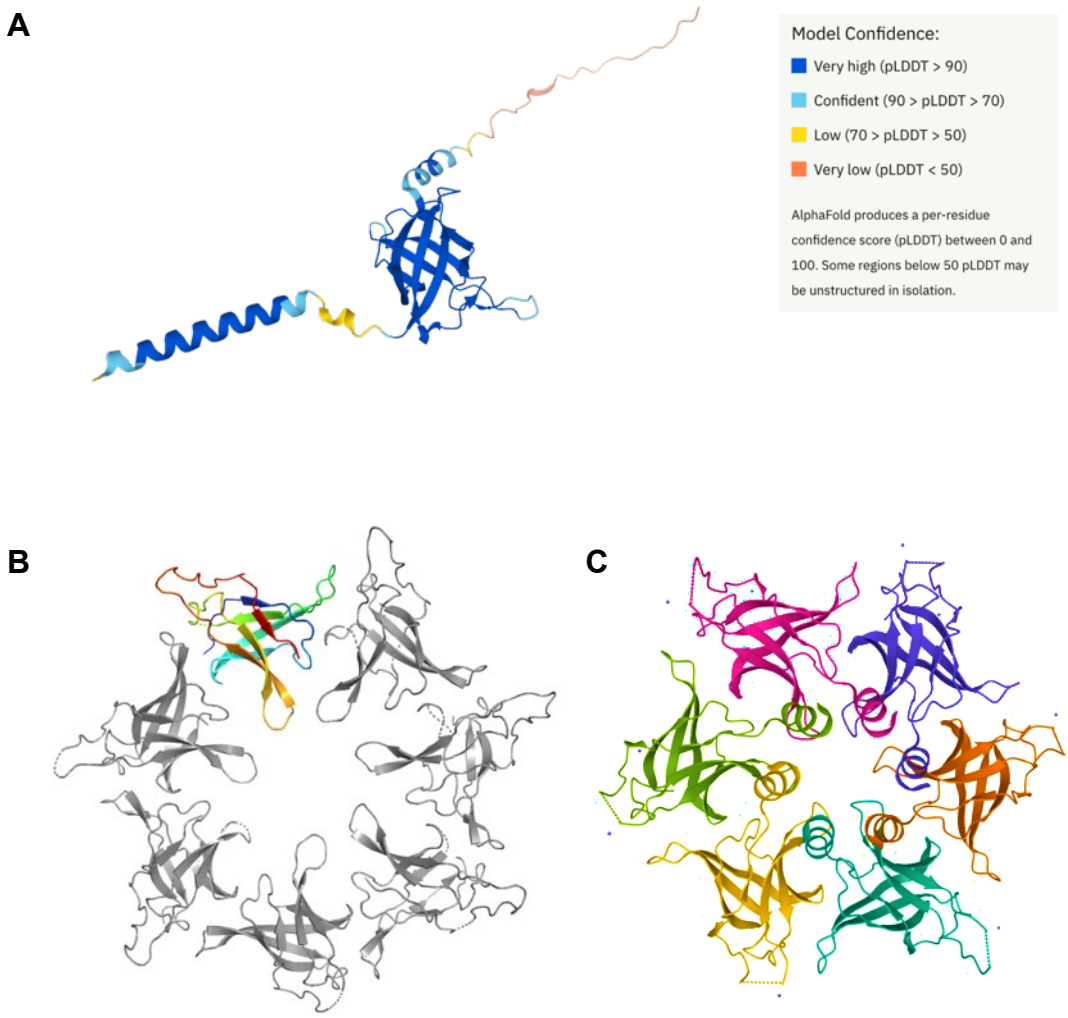

Figure 5.15: Predicted and experimentally determined structure of MlaD. (A) The structure of the MlaD protein of *E. coli* K12 as predicted by the AI system, Alphafold. **(B)** The structure of the MlaD as demonstrated via X-ray crystallography and electronic microscopy (colour). **(C)** The MlaD homo-hexameric ring assembly. Figures made with PyMol (https://pymol.org/2/).

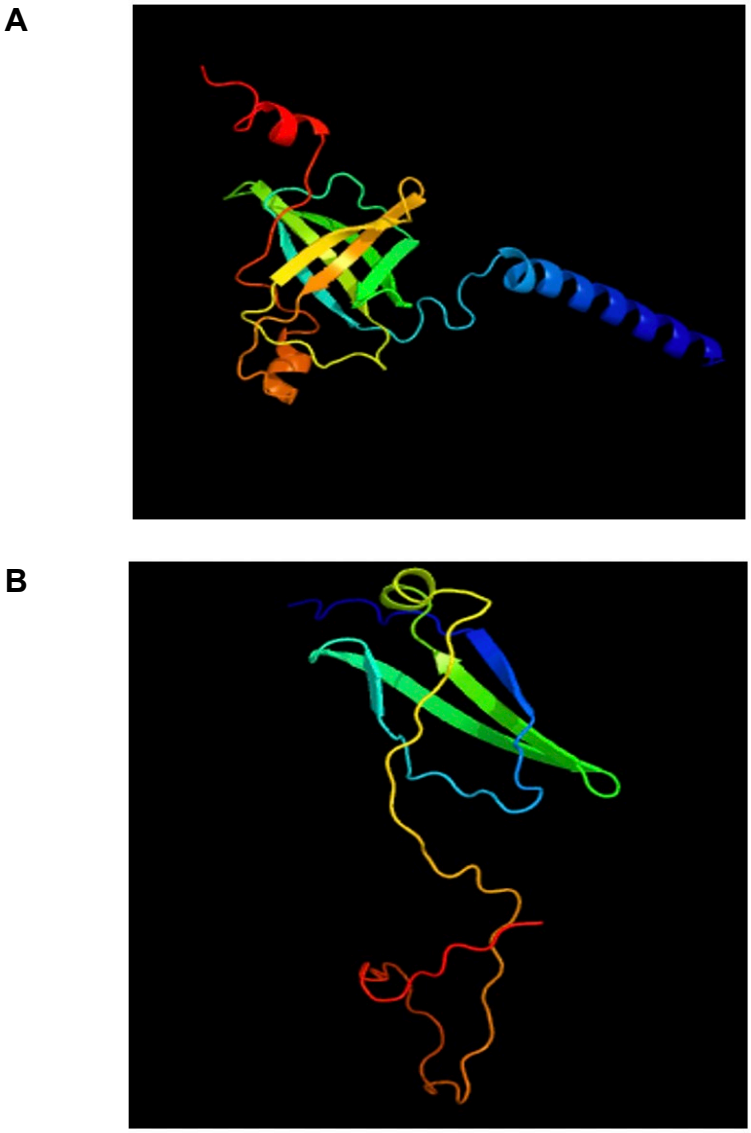

Figure 5.16: Structural models of Mce domain containing proteins (A) MlaD from *E. coli* modelled with Phyre2 to validate the algorithm **(B)** MceA from *Streptomyces coelicolor,* modelled with Phyre2.

Chapter 5: Summary

Evidence from this study strongly indicates that the Mce proteins of *S. coelicolor* form an ABC transporter assembly for sterols and that the Mce-domain containing proteins may potentially be the substrate binding proteins of this assembly. As the structure of the Mce proteins of Gram-positive bacteria have not, as of yet, been experimentally solved, any structural predictions must rely to some degree upon bioinformatics.

Given that TMpred predicts SCO2421 and SCO2420 to contain 5 and 6 transmembrane helices respectively, these proteins are highly likely to be membrane proteins which form the transmembrane domains of the transporter. Further bioinformatic analysis predicts SCO2421 to have a cytoplasmic N-terminus and extracellular C-terminus, whilst SCO2420 is orientated with both N and C-terminus inside the cell.

The Mce-domain containing proteins, which are hypothesised to function as the substrate binding proteins of the transporter, share high sequence similarity with their homologues of the *mce3* operon of *M. tuberculosis*. The exception to this is MceE which shares closest identity with the MceE2 protein of *M. tuberculosis*. This is interesting given that MceE proteins of Actinobacteria typically contain a lipobox motif with a conserved cystine residue to allow anchorage to the cell membrane, and the Mce2E protein is the only of the MceE proteins of *M. tuberculosis* not to encode a lipobox motif (Hemati *et al.*, 2019). Analysis of the amino acid sequence of MceE in *S. coelicolor* does not provide a clear lipobox motif or conserved cystine residue.

In an effort to further characterise the *S.coelicolor* Mce proteins, hexa-histidine-tagged Mce proteins that could be expressed in *S. coelicolor* and *E. coli* were created as part of this study.

MceA-C and SCO2421-C were both detected via Western Blot in the whole cell lysate of *E. coli* BL21 (DE3) cells. N-terminally his-tagged constructs were not found to be present in the whole cell lysate, which may imply that protein cleavage for secretion results in the loss of the his-tag, providing evidence for secretion of these proteins. Alternatively, in the case of N-SCO2419, the deletion of 23-amino acid in its sequence may result in targeted destruction of the protein by cellular machinery.

Whilst MceA-C was easily detected from cells lysed with BugBuster™ Master Mix, SCO2421-C was only detected when membrane protein specific techniques and reagents were applied. Given the predicted transmembrane domains of SCO2421, this strongly re-enforces the likelihood that SCO2421 is a membrane protein and part of the transmembrane domains of the ABC-transporter. It is interesting that even with membrane protein methods, SCO2420 was not detected at any point in the whole cell lysate. This could potentially be due to unknown properties of the SCO2420 protein and may suggest structural differences in SCO2420 to SCO2421.

Purification of MceA-C from *E. coli* also showed limited success, with the resultant fraction containing other non-target proteins. Therefore, in future, cobalt, and not nickel could be utilised in IMAC, as cobalt has a higher level of specificity to the his-tag. Further polishing steps should also be undertaken on fractions found to contain MceA-C via Western Blot, including size exclusion chromatography (SEC), to eliminate non-target proteins.

Western Blot analysis of fraction 6 was able to detect MceA-C, however the proteins appear to run at an anomalous mass, resulting in bands at 27kDa and 18kDa. Gel shifting, also called anomalous SDS-PAGE migration, of proteins can occur, potentially due to detergent binding, although it is more common with membrane proteins (Rath *et*

al., 2009) and could reflect the nature of the hydrophobic binding capabilities of MceA. The smaller band is likely the result of proteolysis, as some proteins exhibit greater susceptibilities to cleavage (Ahmad *et al.*, 2012; Pham *et al.*, 2014).

Chapter 6: Discussion

Discovered in 1993 as a virulence factor in *Mycobacterium tuberculosis (Mtb)*, the *mce* locus facilitates invasion of mammalian cells and was accordingly named the mammalian cell entry operon. Tuberculosis (TB) has long reigned as the leading cause of mortality worldwide from a single infectious disease, killing an estimated 1.66 million in 2020, and has only recently been overtaken by COVID-19 (Glaziou, 2020; Koegelenberg, Schoch and Lange, 2021). SARS-CoV-2 has thrown into stark relief the danger of highly infectious respiratory diseases and the crucial urgency of developing novel therapeutic treatments and effective vaccines.

Currently, the only licenced vaccine for TB is the Bacillus Calmette–Guérin (BCG) vaccine which was first introduced in 1921 and is now a century old. The BCG has limited effectiveness which is highly dependent on geographical region and does not always protect individuals against TB infection (Farajnia, Ansarin and Sahebi, 2019). Furthermore, strains of *Mtb* show extensive drug-resistance, and it is estimated that in the next 35 years, drug-resistant TB will kill approximately 75 million people (Allué-Guardia, García and Torrelles, 2021). Undoubtably, TB is therefore a public health crisis which urgently requires novel therapeutic solutions.

The *mce* operons of *Mtb,* now known to be involved in not only host cell invasion, but transport of cholesterol and other lipids, present promising potential targets for vaccine development (Hemati *et al.*, 2019; Zaychikova and Danilenko, 2020). Cholesterol is an essential carbon and energy source for *Mtb* and the bacterium owes its ability to persist for prolonged periods within host cells to its capacity to import and utilise host cell cholesterol (Hemati *et al.*, 2019). The *mce4* operon encodes a sterol importer and its deletion results in attenuation of *Mtb* inside macrophages (Zhang and Xie, 2011; Khan

et al., 2016). As all Actinobacteria operons have evolved from a singular ancestral operon, and as bacterial pathogenicity towards humans is thought to have emerged from the interplay of bacteria and protists, it is likely that the original role of the ancestral *mce* operon was in environmental nutrient acquisition and its virulence function arose due to selective pressure applied by predation by amoeba (Casali and Riley, 2007; Clark *et al.*, 2013). It is unsurprisingly then, that *mce* operons exist in many saprophytic, non-pathogenic Actinobacteria, such as *Streptomyces coelicolor,* where they may perform their original function and import nutrients to aid bacterial survival in highly competitive environments.

Our understanding of the evolution of such systems, from nutrient acquisition to key virulence factors within a deadly pathogen, is critical for comprehension of how infectious human diseases arise and allows us to target essential systems for the development of better therapeutics and more effective vaccines. The study of the *mce* operon of *S. coelicolor* gives us insight into this non-virulent to virulent pathway.

The mce operon of *S. coelicolor* encodes a sterol importer, with Mce proteins likely localised within the bacterium cell wall.

The sole *mce* operon of *S. coelicolor* has been hypothesised to encode an ABC importer for sterols due to evidence pre-existing this work, as well as its similarity to *mce* operons of *Mtb.* Clark (2013) demonstrated that transcription of the *S. coelicolor mce* operon is repressed in high-cholesterol media, indicating that it may encode a high-affinity, low-capacity transporter which functions to scavenge sterols. *Streptomyces* typically reside in the rhizosphere, the plant-root interface of the soil, where nutrients such as phytosterols are rich. Accordingly, the rhizosphere is also a highly competitive environment and *Streptomyces* has evolved numerous mechanisms to out-compete surrounding micro-organisms, including production of antimicrobial secondary metabolites and highly efficient nutrient uptake systems. It has been previously shown

by Clark (2013) that deletion of the *mce* operon impedes colonisation of plant roots, potentially due to limited ability to transport sterols.

This thesis has demonstrated that growth of *S. coelicolor* in minimal media containing cholesterol is severely reduced by deletion of the *mce* operon, with the *mce* null mutant showing a specific growth rate of 0.09 h^{-1} compared to 0.57 h^{-1} in *S. coelicolor* M145. The impaired growth of the Δ*mce* strain in cholesterol containing minimal media strongly indicates that the *mce* operon of *S. coelicolor* encodes a sterol importer.

This work then sought to further elucidate the location, characteristics, and mechanisms of the Mce proteins in *S. coelicolor* to better understand how they facilitate sterol import. Bioinformatic investigation of the Mce proteins SCO2421 and SCO2420, believed to be the transmembrane domain components of the ABC transporter system, indicated that SCO2421 contains 5 transmembrane helices, with a cytoplasmic N-terminal and extracellular C-terminal, whilst SCO2420 contains 6 transmembrane helices, with both N and C-terminus located inside the cell.

The six Mce-domain containing proteins of *S. coelicolor* are hypothesised to act as the substrate binding proteins (SBPs) of the transporter. These proteins share significant homology with the Mce3 proteins of *Mtb*, and, though all are predicted by StrepDB to be secreted proteins, SignalP 5.0 analysis identifies potential signal sequences in only 4 of 6 (SCO2418, SCO2416, SCO2415 and SCO2414). Similarly, although most Actinobacterial Mce-domaining containing proteins are predicted to be lipoproteins, none of the Mce proteins of *S. coelicolor* possess a lipobox motif with conserved cystine residue that indicates they remained attached to the cell membrane (Casali and Riley, 2007). Lipobox motifs are typically found in the MceE of Actinobacteria, including in *Mycobacterium* and *Streptomyces avermitilis*, however they are absent in both Mce2E of *Mtb* and Mce2 of *S. coelicolor*, which share considerable homology.

Nevertheless, software used for the prediction of signal sequences, lipobox motifs and general protein structure remain fallible and limited, as can be seen in the differences between the AI predicted structure of *E. coli* MlaD and the experimentally determined structure of this protein (Ekiert *et al.*, 2017). Purification and crystallisation of the Mce-domain containing proteins will be necessary in order to conclusively determine their location and structure.

This work demonstrates that it is possible to express the Mce proteins of *S. coelicolor* in *E. coli* BL21 (DE3) for the purposes of detection and purification. Both MceA and SCO2421, his-tagged on the C-terminus, were detected in the whole cell lysate of BL21 (DE3) by Western Blot. That SCO2421 was only successfully detected when membrane protein specific methods of cell lysis and lysate preparation were used further indicates that it is a membrane protein.

Based on the evidence compiled in this thesis, it is highly likely that the Mce ABC transporter for sterols is located in the cell wall of *S. coelicolor*, with SCO2422 encoding the cytoplasmic nucleotide binding domains and SCO2421 and SCO2420 encoding membrane proteins as the permeases of the transporter. Based on homology with other Actinobacteria *mce* operons, the Mce-domain containing proteins likely compose the SBPs of the transporter (Casali and Riley, 2007; Clark *et al.*, 2013; Hemati *et al.*, 2019; Isom *et al.*, 2020). Some or all of these proteins are likely secreted, given the predicted presence of N-terminal signal sequences and their function requiring them to bind with sterols in the environment. Whilst no lipobox motifs are detected by predictive software in the Mce-domain containing proteins of *S. coelicolor*, it is not possible to rule out the proteins as lipoproteins due to the plasticity of the lipobox motif and limitations to bioinformatic techniques in predicting protein structure. Therefore, it remains possible that one or more of the Mce-domain containing proteins are lipoproteins which remain tethered to the cell membrane and may act as a point of contact between secreted Mce

proteins and the ABC transporter permease domains. Given the level of conservation of the six Mce-domain containing proteins within Actinobacterial *mce* operons, and understanding of the *E. coli* Mce protein MlaD, this study proposes that the Mce-domain containing proteins of *S. coelicolor* may function as a heteromeric complex to capture sterols in the environment and transport them to the TMD of the ABC transporter (Fig. 6.1).

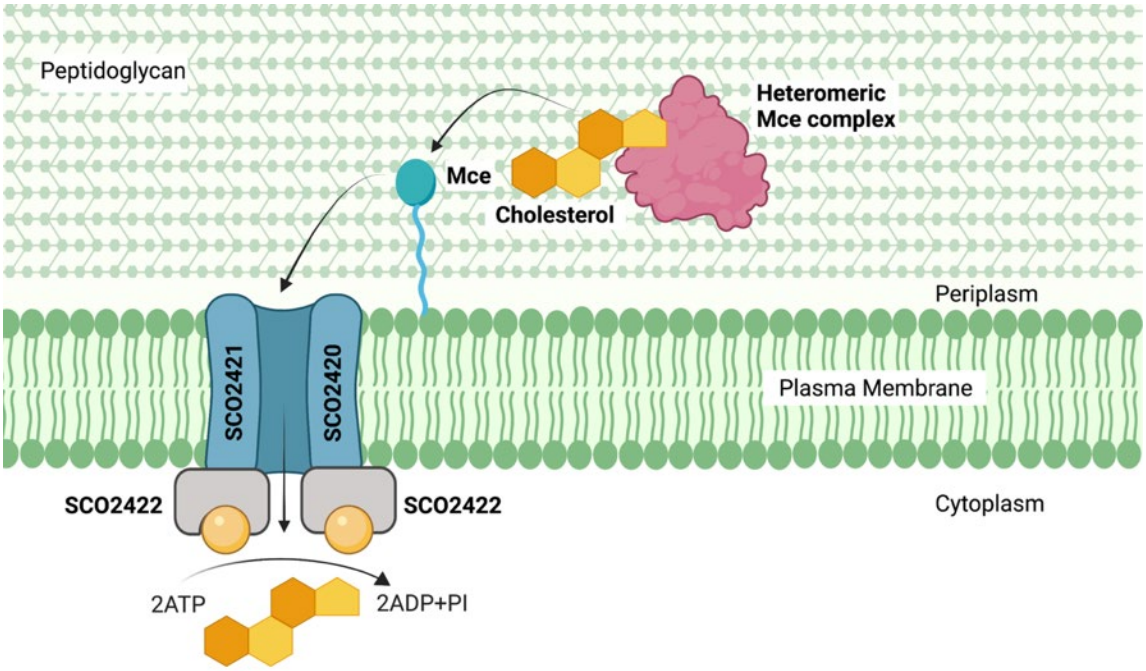

Figure 6.1: Predicted model of the *S. coelicolor* Mce ABC importer for sterols. SCO2422 form the nucleotide binding domains of the transporter within the cytoplasm. SCO2421 and SCO2420 form the TMD of the transporter, spanning the membrane. The Mce-domain containing proteins of *S. coelicolor* are likely secreted and form a heteromeric complex to capture environmental sterols. A single or multiple Mce-domain containing protein may remain anchored to the cell membrane as an intermediate point of contact between heteromeric complex and transporter.

Deletion of the mce operon causes profound phenotypic changes in *S. coelicolor*

Deletions of the Mce proteins of *S. coelicolor*, predicted to be localised within the cell wall of the bacterium, result in an abnormal spore envelope phenotype. The spore envelope of the Δ*mce* mutant possesses an atypical 'wrinkled' appearance, with smaller mean spore diameter, and spores are more prone to collapse then spores of *S. coelicolor* M145 (Clark *et al.*, 2013). Altered cell surface phenotypes in association with deletion of Mce proteins have been observed in other Actinobacteria and *E. coli* previously, and suggest that removal of these proteins may affect the integrity of the cell wall in some form (Möker *et al.*, 2004; Cangelosi *et al.*, 2006; Forrellad *et al.*, 2014; Ekiert *et al.*, 2017). Further, appendages seen upon Δ*mce* spores whilst still attached to the spore chain are suggestive of precocious germination, which this study has now confirmed to occur as a result of *mce* operon deletion. Work discussed in Chapter 3 of this thesis demonstrates that the Δ*mce* mutant displays both a precocious sporulation and a precocious germination phenotype. Interestingly, precocious germination has been previously linked with defective cell envelopes in *S. coelicolor* and theorised to be the result of weakened cell walls (Colson *et al.*, 2008). Potentially, deletion of the Mce proteins has similar effects, producing a weakened cell wall which leaves spores in a quasi-dormant state where they are less tolerant to stressors and quicker to germinate, a process that itself can be initiated by mechanical stress and in which the first step is breakdown of the spore envelope to allow peptidoglycan remodelling (Čihák *et al.*, 2017)

The effect of the altered spore envelope and precocious germination phenotype appears to lead to increased aggregation of *S. coelicolor* Δ*mce* spores when compared to those of M145. Various possibilities exist to explain this, including that the hydrophobic cell envelope, when damaged, becomes somewhat more adhesive. Of note, it has been observed recently that *S. coelicolor* spores are capable of "hitchhiking" on motile

bacteria, a phenomenon dependent upon the rodlin proteins which compose the outer spore coat (Muok, Claessen and Briegel, 2021). Furthermore, germinating spores produce extracellular glycans which have been shown to induce spore aggregation (Zacchetti *et al.*, 2016).

It was observed that the Δ*mce* strain produces the grey polyketide pigment associated with mature spores earlier than the M145 strain and appears to overproduce the characteristic blue actinorhodin (ACT) pigment. This study demonstrates that deletion of the *mce* operon may lead to earlier and excessive ACT production compared to the M145 strain, a phenotype likely linked with the strain's precocious germination and sporulation. Antibiotic production and development are closely linked in *Streptomyces*, with secondary metabolite production being switched on at specific stages of growth (Hasani, Kariminik and Isaazadeh, 2014). Stress has also been found to provoke production of antimicrobials in *Streptomyces* and it is possible that the deletion of the *mce* operon, now known to be a nutrient uptake system, results in additional stress upon the Δ*mce* mutant (Dyson, 2019).

Chapter 3 of this thesis hypothesised that the potential 'quasi-dormant' state of the spores, the altered spore envelope phenotype, and the linked precocious germination of these spores, may lead to their increased susceptibility to various stressors. The spore envelope is the protective layer of the spore and, as previously mentioned, is broken down upon initiation of germination. This work found that spores of the *mce* null mutant are indeed less tolerant to high temperatures and various chemicals. The *mce* null mutant, when exposed to temperatures between 60 – 100ºC showed reduced survival in comparison to the M145 strain and also did not display the heat activation characteristic of *Streptomyces* spores. This is likely due to the altered spore envelope and to the quasi-dormant state Δ*mce* spores appear to display as a result of Mce protein deletion.

The Δ*mce* mutant similarly demonstrated extreme susceptibility to the chemical triclosan, which inhibits fatty acid biosynthesis. A concentration of ≥ 0.625 ug/mL triclosan in YEME media is enough to completely inhibit growth of Δ*mce* spores, compared to M145 spores which are able to grow in the presence of 10 ug/mL triclosan. These results were mirrored with triclosan in minimal media and triclosan in minimal media with 0.193 ug/mL cholesterol. Therefore, it appears that loss of the *mce* sterol importer in the presence of a fatty acid biosynthesis inhibitor leads to complete abrogation of growth, whilst M145, which possess the native *mce* operon, and the complemented mutant, Δ*mce*+*mce,* are still able to grow. Interestingly, whilst M145 in the presence of triclosan does not reach the same optical density, and therefore biomass, the lag phase of growth for this strain is shortened in the presence of triclosan and specific growth rate increases. This may be due to upregulation of stress responses in the M145 strain, attempting to compensate for fatty acid biosynthesis inhibition.

Similar sensitivity of the Δ*mce* mutant was observed to sulfobetaines of various chain lengths, including lauryl sulfobetaine (LSB), myristyl sulfobetaine (MSB) and caprylyl sulfobetaine (CSB). Such increased susceptibility to chemical stressors is likely due to the altered spore envelope phenotype, and it was hypothesised that the Δ*mce* mutant may display increased permeability to or increased uptake of sulfobetaines via unknown secondary sterol transporters compared to *S. coelicolor* M145. Work in Chapter 3 of this thesis shows that there is a significant increase in permeability of Δ*mce* cells compared to those of M145. However, when cell walls of Δ*mce* and M145 spores were measured, the thickness of the cell wall of the *mce* null mutant did not differ in width from that of the M145 strain.

Dictyostelium is a highly efficient predator of *S. coelicolor*

A hypervirulence phenotype towards the soil amoeba *Acanthamoeba polyphaga* has been previously established for the *mce* null mutant, the virulence mechanism of which was proposed to be amoeba lysis due to precocious germination of Δ*mce* spores within the food vacuole following phagocytosis (Clark *et al.*, 2013). As this study has confirmed the precious germination phenotype of the Δ*mce* strain, Chapter 4 of this thesis examined the hypervirulence phenotype of this mutant in the soil protist *Dictyostelium discoideum.*

A. polyphaga and *Dictyostelium* are both free-living protozoa which likely encounter and predate *Streptomyces* in the environment. However, they are of evolutionary distant genera, with considerable differences in lifestyle, morphology, foraging strategies and interaction with prey organisms (Kuburich, Adhikari and Hadwiger, 2016; Leoni Swart *et al.*, 2018).

A. polyphaga may vary from 25 to 40 µm in size, and have a 120.6 Mb genome which is genetically intractable (Clarke *et al.*, 2013). They are motile organisms, but locomotion is slow and non-chemotactic. This is in contrast to *Dictyostelium*, which are typically 10 µm in size, and display rapid chemotactic motility. Further, their genome, at 34 Mb, is readily pliable to genetic manipulation. Recently, it has also been demonstrated that *Dictyostelium* alter their transcriptional profile and show differential gene expression depending on the food-source bacteria (Nasser et al., 2013; Lamrabet et al., 2020; Shi et al., 2020).

Examination of *Dictyostelium-Streptomyces* interactions in Chapter 4 of this work show that *Dictyostelium* is a rapid and incredibly efficient predator of *S. coelicolor*. *Dictyostelium* were seen to phagocytose spores within minutes of spore addition and association of spores with the V-ATPase was seen within five minutes of co-culture

initiation. Further, a single *Dictyostelium* was shown to be capable of phagocytosing many spores simultaneously. This study demonstrates that the hyper-virulence phenotype of the Δ*mce* strain in *Acanthamoeba* is not present in *Dictyostelium*. This is likely due to the rapid rate at which *Dictyostelium* associate with and phagocytose spores. *Acanthamoeba* were seen to take up to 12 hours to phagocytose *S. coelicolor* spores, with lysis of the amoeba occurring at 24 hours into co-culture, meaning spores remained viable for approximately 12 hours following phagocytosis (Clark, 2011). The hypervirulence mechanism appeared to be precocious germination of the strain inside the food vacuole, as M145 is also virulent towards *Acanthamoeba*, but germination and amoeba lysis do not occur with this strain until 35 hours into co-culture (Clark, 2011). Conversely, no amoeba lysis was visualised at any point during 40-hour co-culture with *Dictyostelium* with either Δ*mce* or M145 spores. This work hypothesises that lack of virulence of the Δ*mce* mutant towards *Dictyostelium* is due to the rapid rate of phagocytosis displayed towards the bacterium, which is prohibitory towards even precocious germination occurring within the food vacuole.

Based on prior work by Clark (2013), who demonstrated that the *mce* null mutant showed increased resistance to lysozyme, it was hypothesised that spores of the Δ*mce* strain may show increased intracellular survival within amoeba phagolysosomes. Comparisons of lysozyme tolerance in this work were done in suspension and carried out on both spores and germlings. Whilst germlings of the M145 and Δ*mce* strain showed similar resistance to lysozyme, lysozyme tolerance in spores was greater in the Δ*mce* mutant than M145. The *mce* null mutant further showed increased intracellular survival and increased survival post internalisation compared to M145 spores. However, interestingly, spores of the M145+*mce* mutant showed greatest resistance to lysozyme and greatest survival post internalisation into *Dictyostelium.* The M145+*mce* mutant, despite this, did not show hypervirulence towards *Dictyostelium* in co-culture.

It appears therefore that the mechanism of virulence of the *mce* null mutant towards *Acanthamoeba* is mechanical lysis caused by precocious germination, but that *Dictyostelium,* being highly efficient predators are able to circumvent this mechanism with the speed at which they phagocytose and break down *Streptomyces* spores. Though spores of the *mce* null mutant show increased resistance to lysozyme which appears to facilitate longer intracellular survival and greater viability post exocytosis, this does not enable ∆*mce* spores to persist long enough within *Dictyostelium* to germinate.

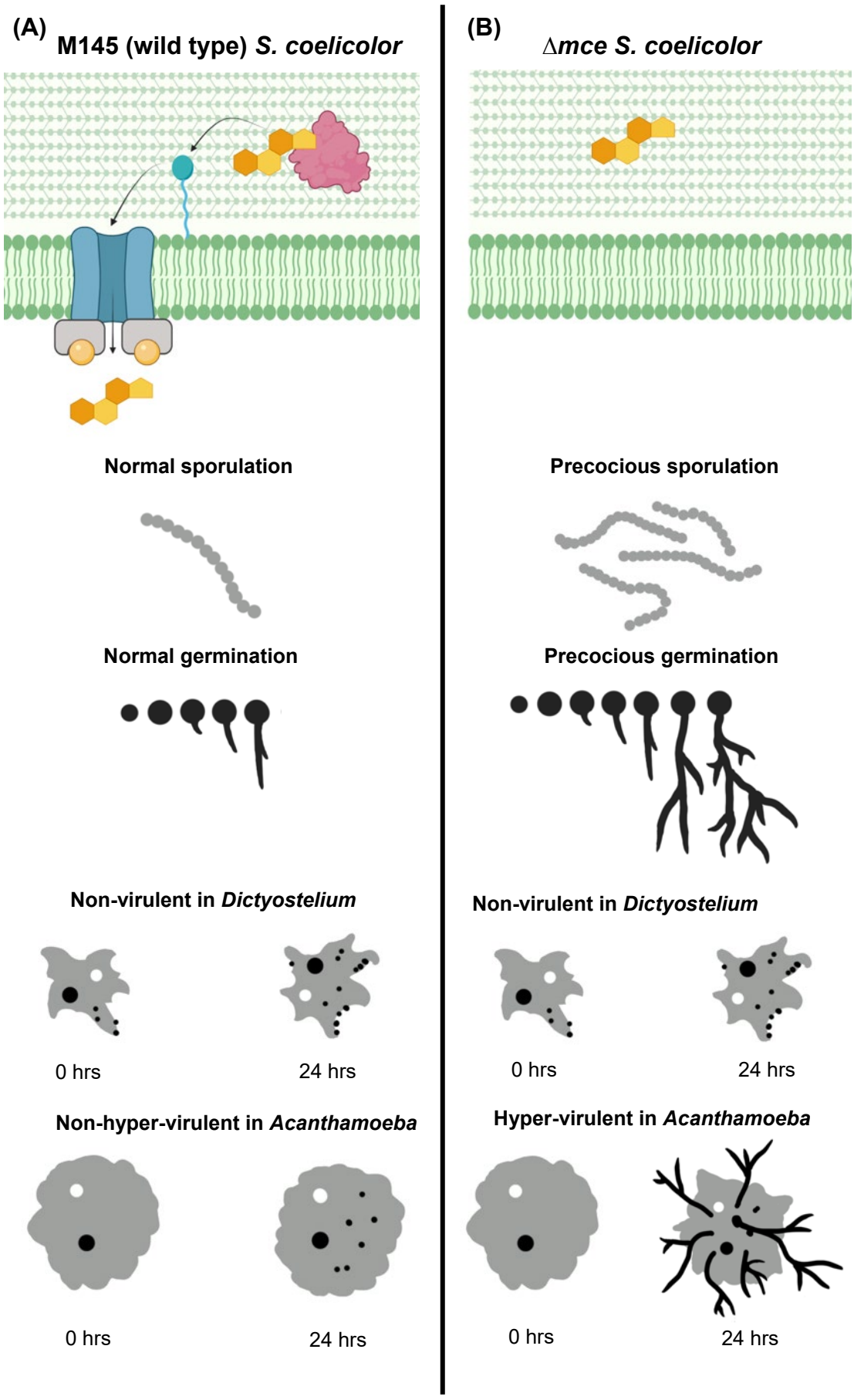
(A)
M145 (wild type) S. coelicolor
Normal sporulation
Normal germination
Non-virulent in Dictyostelium
0 hrs
24 hrs
Non-hyper-virulent in Acanthamoeba
0 hrs
24 hrs
(B)
Δmce S. coelicolor
Precocious sporulation
Precocious germination
Non-virulent in Dictyostelium
0 hrs
24 hrs
Hyper-virulent in Acanthamoeba
0 hrs
24 hrs

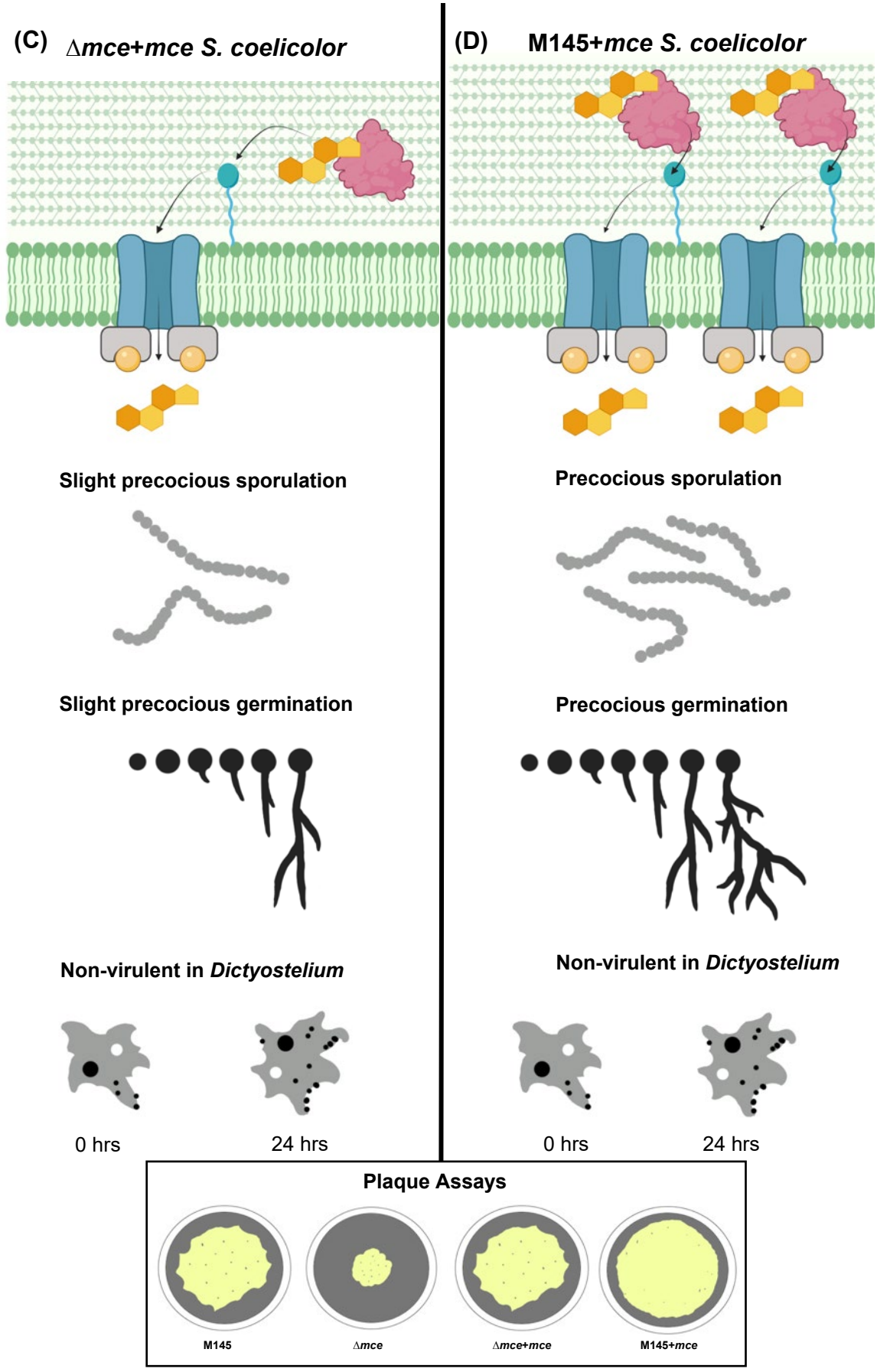
(C) Δmce+mce S. coelicolor
(D) M145+mce S. coelicolor
Slight precocious sporulation
Precocious sporulation
Slight precocious germination
Precocious germination
Non-virulent in Dictyostelium
Non-virulent in Dictyostelium
0 hrs
24 hrs
0 hrs
24 hrs
Plaque Assays
M145
Δmce
Δmce+mce
M145+mce

Figure 6.2: Summary of *mce S. coelicolor* mutants, predicted transport structure and confirmed phenotypes. The predicted structure of the ABC transporter for sterols encoded for by the *mce* operon in *S. coelicolor* and phenotypes associated with operon mutants. **(A)** *S. coelicolor* M145 contains the native *mce* operon encoding an ABC importer for sterols. This thesis predicts that the Mce-domain containing proteins of *S. coelicolor* are secreted and form a heteromeric complex to bind sterols. Potentially, one or more of the Mce-domaining containing proteins may remain tether to the membrane to facilitate substrate transport to the permeases of the transporter. *S. coelicolor* M145 displays typical sporulation and germination, is non-virulent in *Dictyostelium* and does not show enhanced virulence towards *Acanthamoeba*. **(B)** The *S. coelicolor* Δ*mce* mutant lacks the functional *mce* operon and encoded transporter and is thus unable to transport sterols via this system. This strain demonstrates precocious sporulation and germination and is non-virulent in *Dictyostelium* but displays hyper-virulence in *Acanthamoeba polyphaga.* **(C).** The *S. coelicolor* Δ*mce*+*mce* strain contains the *mce* operon integrated into a Δ*mce* background into an ectopic location and therefore one functional copy of the Mce ABC importer. This strain shows slightly precocious sporulation and slight precocious germination. It is non-virulent in *Dictyostelium.* **(D)** The *S. coelicolor* M145+*mce* strain contains both an ectopic *mce* operon and the native *mce* operon and therefore possess two copies of the Mce ABC importer. This strain shows precocious sporulation and precocious germination. It is non-virulent towards

Conclusions and Future work

This thesis presents strong evidence that the *mce* operon of *S. coelicolor* encodes an ABC transporter for sterols and demonstrates that deletion of this locus results in stark phenotypic changes in the bacterium. This work confirms that the Δ*mce* mutant displays precocious germination, precocious sporulation, possible increased actinorhodin production, and increased aggregation compared to *S. coelicolor* M145. This thesis also demonstrates that the Δ*mce* mutant does not display hypervirulence towards *Dictyostelium*, likely due to the rapid predation and phagocytosis of spores by the amoeba which outcompetes the precocious germination of the strain. Further, this body of work confirms that spores of the Δ*mce* mutant are highly sensitive to triclosan, LSB, MSB, CSB and heat, compared to spores of *S. coelicolor* M145, likely due to the altered spore envelope this mutant possess. Prior to this work, the Mce proteins of *S. coelicolor* had never been successfully expressed in or purified from *E. coli*, and this thesis demonstrates the successful expression of MceA and SCO2421 in BL21 (DE3) and enhances understanding of the location of Mce-domain containing proteins in *S. coelicolor*.

However, a considerable amount of work remains to be done to characterise the *mce* operon of *S. coelicolor*. Future experimental work would benefit greatly from knocking-out the individual genes of the *mce* operon, particularly Mce-domain containing proteins and subsequent phenotypic characterisation, e.g the growth of these mutants in the presence of cholesterol. For future investigation into the interaction of the Δ*mce* strain with *Dictyostelium,* quantification and characterisation of phagocytotic rate and processes could be performed via confocal microscopy and flow cytometry. Transparent soil has also emerged as a method of live-cell imagining of the rhizosphere and could be used to visualise amoeba-spore interactions in a biologically relevant manner.

Extensive avenues exist for further examination of the Mce-domain containing proteins of *S. coelicolor*. Future purification of MceA should utilise cobalt instead of nickel for IMAC, as higher specificity for the hexa-histidine tag appears to be required. Once purified, polishing steps should be performed by HPLC. Once MceA has been successfully purified, isothermal titration calorimetry measurements of the protein in the presence of cholesterol could be applied to show in vitro binding of cholesterol to MceA. Similarly, pull-down assays could be performed, potentially identifying how the Mce-domaining containing proteins of *S. coelicolor* interact. Overexpression of his-tagged Mce proteins in *S. coelicolor* was unsuccessful in this study due to time constraints but will likely prove a fruitful avenue for future investigations. This would allow for cell fractionation and subsequent Western Blotting of cell components, such as membrane, cell wall and cytoplasm, to be performed and may potentially reveal the location of these proteins within the cell.

In summary, this thesis advances the understanding of the *mce* operon in *S. coelicolor*, its function, the phenotypic consequences of its abrogation and how the operon affects interaction with protists.

The exploitation of the Mce protein in biotechnology holds considerable potential. For example, the high value conversion of sterols to steroids for use in medicine, and the efficient uptake of substrates for bioconversion of sterols to steroids offers several advantages over chemical conversion when considering selectivity, sustainability, and economics (Donova *et al.*, 2007; García, Uhía and Galán, 2012b; Galán *et al.*, 2017; Wang *et al.*, 2017). The use of heterologous, highly specific sterol uptake systems, such as the Mce systems, may prove highly useful in this area.

The Mce1 proteins of *Mycobacterium tuberculosis*, located at the cell surface, have shown some potential as vaccine candidates and may offer an alternative to the inefficient BCG vaccine (Obregón-Henao *et al.*, 2011; Mustafa, 2013).

Therefore, understanding the structure, function and role of the diverse Mce operons offers a range of potential applications in biotechnology and therapeutics.

References

Aguilar, L. D. *et al.* (2006) 'Immunogenicity and protection induced by *Mycobacterium tuberculosis mce-2* and *mce-3* mutants in a Balb/c mouse model of progressive pulmonary tuberculosis', *Vaccine*. doi: 10.1016/j.vaccine.2005.11.051.

Ahmad, S. *et al.* (2012) 'Probing protein stability and proteolytic resistance by loop scanning: A comprehensive mutational analysis', *Protein Science*, 21(3), pp. 433–446. doi: 10.1002/pro.2029.

Allué-Guardia, A., García, J. I. and Torrelles, J. B. (2021) 'Evolution of Drug-Resistant *Mycobacterium tuberculosis* Strains and Their Adaptation to the Human Lung Environment', *Frontiers in Microbiology*, 12(February), pp. 1–21. doi: 10.3389/fmicb.2021.612675.

Almagro Armenteros, J. J. *et al.* (2019) 'SignalP 5.0 improves signal peptide predictions using deep neural networks', *Nature Biotechnology*. Springer US, 37(4), pp. 420–423. doi: 10.1038/s41587-019-0036-z.

Angelini, S., Deitermann, S. and Koch, H. G. (2005) 'FtsY, the bacterial signal-recognition particle receptor, interacts functionally and physically with the SecYEG translocon', *EMBO Reports*. doi: 10.1038/sj.embor.7400385.

Annesley, S. J. and Fisher, P. R. (2009) '*Dictyostelium discoideum*-a model for many reasons', *Molecular and Cellular Biochemistry*. doi: 10.1007/s11010-009-0111-8.

Aoki, Y. *et al.* (2007) 'Isolation and characterization of a spore germination inhibitor

from *Streptomyces* sp. CB-1-1, a phytopathogen causing root tumor of melon', *Bioscience, Biotechnology and Biochemistry*, 71(4), pp. 986–992. doi: 10.1271/bbb.60649.

Arafah, S. *et al.* (2013) 'Setting Up and Monitoring an Infection of *Dictyostelium discoideum* with *Mycobacteria*', in. doi: 10.1007/978-1-62703-302-2_22.

Arruda, S. *et al.* (1993) 'Cloning of an *M. tuberculosis* DNA fragment associated with entry and survival inside cells', *Science*. doi: 10.1126/science.8367727.

Ashworth, J. M. and Watts, D. J. (1970) 'Metabolism of the cellular slime mould *Dictyostelium discoideum* grown in axenic culture.', *The Biochemical journal*. doi: 10.1042/bj1190175.

Aufderheide, K. J. and Janetopoulos, C. (2016) 'Migration of *Dictyostelium discoideum* to the chemoattractant folic acid', in *Methods in Molecular Biology*. doi: 10.1007/978-1-4939-3480-5_3.

Bagwell, C. E. *et al.* (2008) 'Survival in nuclear waste, extreme resistance, and potential applications gleaned from the genome sequence of *Kineococcus radiotolerans* SRS30216', *PLoS ONE*. doi: 10.1371/journal.pone.0003878.

Banchio, C. and Gramajo, H. C. (1997) 'Medium- and long-chain fatty acid uptake and utilization by *Streptomyces coelicolor* A3(2): First characterization of a Gram-positive bacterial system', *Microbiology*. doi: 10.1099/00221287-143-7-2439.

Barka, E. A. *et al.* (2016) 'Taxonomy, Physiology, and Natural Products of

Actinobacteria', *Microbiology and Molecular Biology Reviews*. doi: 10.1128/mmbr.00019-15.

Basu, S. *et al.* (2013) 'DictyBase 2013: Integrating multiple Dictyostelid species', *Nucleic Acids Research*. doi: 10.1093/nar/gks1064.

Ter Beek, J., Guskov, A. and Slotboom, D. J. (2014) 'Structural diversity of ABC transporters', *Journal of General Physiology*. doi: 10.1085/jgp.201411164.

Bentley, S. D. *et al.* (2002) 'Complete genome sequence of the model actinomycete *Streptomyces coelicolor* A3(2)', *Nature*. doi: 10.1038/417141a.

Bentley, S. D. *et al.* (2003) 'Sequencing and analysis of the genome of the Whipple's disease bacterium *Tropheryma whipplei*', *Lancet*. doi: 10.1016/S0140-6736(03)12597-4.

van Bergeijk, D. A. *et al.* (2020) 'Ecology and genomics of Actinobacteria: new concepts for natural product discovery', *Nature Reviews Microbiology*. Springer US, 18(10), pp. 546–558. doi: 10.1038/s41579-020-0379-y.

Berntsson, R. P. A. *et al.* (2010) 'A structural classification of substrate-binding proteins', *FEBS Letters*. Federation of European Biochemical Societies, 584(12), pp. 2606–2617. doi: 10.1016/j.febslet.2010.04.043.

Bibb, M. J. (2005) 'Regulation of secondary metabolism in *Streptomycetes*', *Current Opinion in Microbiology*, 8(2), pp. 208–215. doi: 10.1016/j.mib.2005.02.016.

Biemans-Oldehinkel, E., Doeven, M. K. and Poolman, B. (2006) 'ABC transporter architecture and regulatory roles of accessory domains', *FEBS Letters*. doi: 10.1016/j.febslet.2005.11.079.

Bignell, D. R. D. *et al.* (2010) 'What does it take to be a plant pathogen: Genomic insights from *Streptomyces* species', in *Antonie van Leeuwenhoek, International Journal of General and Molecular Microbiology*. doi: 10.1007/s10482-010-9429-1.

Bloomfield, G. *et al.* (2015) 'Neurofibromin controls macropinocytosis and phagocytosis in *Dictyostelium*', *eLife*. doi: 10.7554/eLife.04940.

Bobek, J., Šmídová, K. and Čihák, M. (2017) 'A waking review: Old and novel insights into the spore germination in *Streptomyces*', *Frontiers in Microbiology*. doi: 10.3389/fmicb.2017.02205.

Bodinier, R. *et al.* (2021) 'Role of LrrkA in the Control of Phagocytosis and Cell Motility in *Dictyostelium discoideum*', *Frontiers in Cell and Developmental Biology*, 9(March), pp. 1–11. doi: 10.3389/fcell.2021.629200.

de Boer, M. *et al.* (2019) 'Conformational and dynamical plasticity in substrate-binding proteins underlies selective transport in ABC importers', *Conformational and dynamic plasticity in substrate-binding proteins underlies selective transport in ABC importers*, p. 537308. doi: 10.1101/537308.

Bontemps, C. *et al.* (2013) 'Taxonomic and functional diversity of *Streptomyces* in a forest soil', *FEMS Microbiology Letters*. doi: 10.1111/1574-6968.12126.

Bozzaro, S., Bucci, C. and Steinert, M. (2008) ‘Chapter 6 Phagocytosis and Host-Pathogen Interactions in *Dictyostelium* with a Look at Macrophages’, *International Review of Cell and Molecular Biology*. doi: 10.1016/S1937-6448(08)01206-9.

Bozzaro, S. and Eichinger, L. (2011) ‘The Professional Phagocyte *Dictyostelium discoideum* as a Model Host for Bacterial Pathogens’, *Current Drug Targets*. doi: 10.2174/138945011795677782.

Bozzaro, S. and Roseman, S. (1983) ‘Adhesion of Dictyostelium discoideum cells to carbohydrates immobilized in polyacrylamide gels. Evidence for three sugar-specific cell surface receptors’, *Journal of Biological Chemistry*.

Bradshaw, C. S. *et al.* (2006) ‘ The Association of *Atopobium vaginae* and *Gardnerella vaginalis* with Bacterial Vaginosis and Recurrence after Oral Metronidazole Therapy ’, *The Journal of Infectious Diseases*. doi: 10.1086/506621.

Brennan, P. J. (2003) ‘Structure, function, and biogenesis of the cell wall of *Mycobacterium tuberculosis*’, in *Tuberculosis*. doi: 10.1016/S1472-9792(02)00089-6.

Brock, D. A. *et al.* (2011) ‘Primitive agriculture in a social amoeba’, *Nature*. Nature Publishing Group, 469(7330), pp. 393–396. doi: 10.1038/nature09668.

Brown, R. L. and Peterson, G. E. (1966) ‘Cholesterol Oxidation By Soil Actinomycetes’, *Journal of General Microbiology*. doi: 10.1099/00221287-45-3-441.

Bruheim, P. *et al.* (2002) ‘High-yield actinorhodin production in fed-batch culture by a *Streptomyces lividans* strain overexpressing the pathway-specific activator gene actII-

ORF4', *Journal of Industrial Microbiology and Biotechnology*, 28(2), pp. 103–111. doi: 10.1038/sj/jim/7000219.

Buckley, C. M. *et al.* (2016) 'WASH drives early recycling from macropinosomes and phagosomes to maintain surface phagocytic receptors', *Proceedings of the National Academy of Sciences of the United States of America*. doi: 10.1073/pnas.1524532113.

Bush, M. J. *et al.* (2015) 'C-di-GMP signalling and the regulation of developmental transitions in *Streptomycetes*', *Nature Reviews Microbiology*. doi: 10.1038/nrmicro3546.

Bush, M. J. (2018) 'The actinobacterial WhiB-like (Wbl) family of transcription factors', *Molecular Microbiology*. doi: 10.1111/mmi.14117.

Cangelosi, G. A. *et al.* (2006) 'The two-component regulatory system mtrAB is required for morphotypic multidrug resistance in *Mycobacterium avium*', *Antimicrobial Agents and Chemotherapy*. doi: 10.1128/AAC.50.2.461-468.2006.

Cantrell, S. A. *et al.* (2013) 'Free mycolic acid accumulation in the cell wall of the *mce1* operon mutant strain of *Mycobacterium tuberculosis*', *Journal of Microbiology*. doi: 10.1007/s12275-013-3092-y.

Cardenal-Muñoz, E. *et al.* (2018) 'When dicty met myco, a (not so) romantic story about one amoeba and its intracellular pathogen', *Frontiers in Cellular and Infection Microbiology*. doi: 10.3389/fcimb.2017.00529.

Casali, N. and Riley, L. W. (2007) 'A phylogenomic analysis of the Actinomycetales

mce operons', *BMC Genomics*. doi: 10.1186/1471-2164-8-60.

Chater, K. F. *et al.* (2010) 'The complex extracellular biology of *Streptomyces*: REVIEW ARTICLE', *FEMS Microbiology Reviews*. doi: 10.1111/j.1574-6976.2009.00206.x.

Chater, K. F. (2016) 'Recent advances in understanding *Streptomyces*', *F1000Research*. doi: 10.12688/f1000research.9534.1.

Chater, K. F. and Chandra, G. (2006) 'The evolution of development in *Streptomyces* analysed by genome comparisons', *FEMS Microbiology Reviews*. doi: 10.1111/j.1574-6976.2006.00033.x.

Chen, C. W. *et al.* (2002) 'Once the circle has been broken: Dynamics and evolution of *Streptomyces* chromosomes', *Trends in Genetics*. doi: 10.1016/S0168-9525(02)02752-X.

Chitale, S. *et al.* (2001) 'Recombinant *Mycobacterium tuberculosis* protein associated with mammalian cell entry', *Cellular Microbiology*. doi: 10.1046/j.1462-5822.2001.00110.x.

Čihák, M. *et al.* (2017) 'Secondary metabolites produced during the germination of *Streptomyces coelicolor*', *Frontiers in Microbiology*. doi: 10.3389/fmicb.2017.02495.

Clark, L. (2011) *Elucidating the function of a conserved gene cluster in a non-pathogenic actinomycete*. University of Strathclyde.

Clark, L. C. *et al.* (2013) 'Mammalian cell entry genes in *Streptomyces* may provide clues to the evolution of bacterial virulence', *Scientific Reports*. doi:

10.1038/srep01109.

Clarke, M. *et al.* (2002) ‘Dynamics of the vacuolar H+-ATPase in the contractile vacuole complex and the endosomal pathway of Dictyostellium cells’, *Journal of Cell Science*.

Clarke, M. *et al.* (2013) ‘Genome of *Acanthamoeba castellanii* highlights extensive lateral gene transfer and early evolution of tyrosine kinase signaling’, *Genome Biology*, 14(2). doi: 10.1186/gb-2013-14-2-r11.

Clarke, M. and Gomer, R. H. (1995) ‘PSF and CMF, autocrine factors that regulate gene expression during growth and early development of *Dictyostelium*’, *Experientia*. doi: 10.1007/BF01944730.

Coldham, N. G. *et al.* (2010) ‘A 96-well plate fluorescence assay for assessment of cellular permeability and active efflux in *Salmonella enterica* serovar *Typhimurium* and *Escherichia coli*’, *Journal of Antimicrobial Chemotherapy*, 65(8), pp. 1655–1663. doi: 10.1093/jac/dkq169.

Cole, S. T. *et al.* (1998) ‘Deciphering the biology of *Mycobacterium tuberculosis* from the complete genome sequence’, *Nature*. doi: 10.1038/31159.

Colosimo, M. E. and Katz, E. R. (2001) ‘Altered prestarvation response in a nystatin resistant *Dictyostelium discoideum* mutant’, *Differentiation*. doi: 10.1046/j.1432-0436.2001.067001001.x.

Colson, S. *et al.* (2008) ‘The chitobiose-binding protein, DasA, acts as a link between

chitin utilization and morphogenesis in *Streptomyces coelicolor*', *Microbiology*. doi: 10.1099/mic.0.2007/011940-0.

Constant, P., Poissant, L. and Villemur, R. (2008) 'Isolation of *Streptomyces* sp. PCB7, the first microorganism demonstrating high-affinity uptake of tropospheric H2', *ISME Journal*. doi: 10.1038/ismej.2008.59.

Cornillon, S. *et al.* (2006) 'An adhesion molecule in free-living Dictyostelium amoebae with integrin β features', *EMBO Reports*. doi: 10.1038/sj.embor.7400701.

Cosson, P. and Lima, W. C. (2014) 'Intracellular killing of bacteria: Is Dictyostelium a model macrophage or an alien?', *Cellular Microbiology*. doi: 10.1111/cmi.12291.

Craney, A. *et al.* (2012) 'Chemical perturbation of secondary metabolism demonstrates important links to primary metabolism', *Chemistry and Biology*, 19(8), pp. 1020–1027. doi: 10.1016/j.chembiol.2012.06.013.

Currie, C. R. *et al.* (1999) 'Fungus-growing ants use antibiotic-producing bacteria to control garden parasites', *Nature*. doi: 10.1038/19519.

Dassa, E. (2011) 'Natural history of ABC systems: Not only transporters', *Essays in Biochemistry*. doi: 10.1042/BSE0500019.

Davidson, A. L. *et al.* (2008) 'Structure, Function, and Evolution of Bacterial ATP-Binding Cassette Systems', *Microbiology and Molecular Biology Reviews*. doi: 10.1128/mmbr.00031-07.

Dellaire, G., Farrall, R. and Bickmore, W. A. (2003) 'The Nuclear Protein Database

(NPD): Sub-nuclear localisation and functional annotation of the nuclear proteome', *Nucleic Acids Research*, 31(1), pp. 328–330. doi: 10.1093/nar/gkg018.

Delogu, G., Sali, M. and Fadda, G. (2013) 'The biology of mycobacterium tuberculosis infection', *Mediterranean Journal of Hematology and Infectious Diseases*. doi: 10.4084/mjhid.2013.070.

Dennis, P. G., Miller, A. J. and Hirsch, P. R. (2010) 'Are root exudates more important than other sources of rhizodeposits in structuring rhizosphere bacterial communities?', *FEMS Microbiology Ecology*. doi: 10.1111/j.1574-6941.2010.00860.x.

Dias Mirandela, G. *et al.* (2018) 'Merging In-Solution X-ray and Neutron Scattering Data Allows Fine Structural Analysis of Membrane-Protein Detergent Complexes', *Journal of Physical Chemistry Letters*, 9(14), pp. 3910–3914. doi: 10.1021/acs.jpclett.8b01598.

van Dissel, D. *et al.* (2015) 'A novel locus for mycelial aggregation forms a gateway to improved Streptomyces cell factories', *Microbial Cell Factories*, 14(1), pp. 1–10. doi: 10.1186/s12934-015-0224-6.

Domínguez-Martín, E., Ongay-Larios, L., *et al.* (2018) 'IreA controls endoplasmic reticulum stress-induced autophagy and survival through homeostasis recovery', *Molecular and Cellular Biology*. doi: 10.1128/mcb.00054-18.

Domínguez-Martín, E., Hernández-Elvira, M., *et al.* (2018) 'Unfolding the Endoplasmic Reticulum of a Social Amoeba: Dictyostelium discoideum as a New Model for the Study of Endoplasmic Reticulum Stress', *Cells*. doi: 10.3390/cells7060056.

Donova, M. V. *et al.* (2007) 'Methyl-β-cyclodextrin alters growth, activity and cell envelop features of sterol-transforming mycobacteria', *Microbiology*, 153(6), pp. 1981–1992. doi: 10.1099/mic.0.2006/001636-0.

Douglas, T. E. *et al.* (2013) 'Collection and Cultivation of Dictyostelids from the Wild', in. doi: 10.1007/978-1-62703-302-2_6.

Dumon-Seignovert, L., Cariot, G. and Vuillard, L. (2004) 'The toxicity of recombinant proteins in Escherichia coli: A comparison of overexpression in BL21(DE3), C41(DE3), and C43(DE3)', *Protein Expression and Purification*. doi: 10.1016/j.pep.2004.04.025.

Dunn, J. D. *et al.* (2018) 'Eat prey, live: Dictyostelium discoideum as a model for cell-autonomous defenses', *Frontiers in Immunology*. doi: 10.3389/fimmu.2017.01906.

Dunn, J. and Grider, M. H. (2020) *Physiology, Adenosine Triphosphate (ATP)*, *StatPearls*.

Dunphy, K. Y. *et al.* (2010) ' Attenuation of Mycobacterium tuberculosis Functionally Disrupted in a Fatty Acyl–Coenzyme A Synthetase Gene fadD5 ', *The Journal of Infectious Diseases*. doi: 10.1086/651452.

Dyson, P. (2019) 'Streptomyces', in *Encyclopedia of Microbiology*. doi: 10.1016/B978-0-12-801238-3.02306-0.

Ekiert, D. C. *et al.* (2017) 'Architectures of Lipid Transport Systems for the Bacterial Outer Membrane', *Cell*. doi: 10.1016/j.cell.2017.03.019.

El-Awady, R. *et al.* (2017) 'The role of eukaryotic and prokaryotic ABC transporter

family in failure of chemotherapy', *Frontiers in Pharmacology*. doi: 10.3389/fphar.2016.00535.

El-Shazly, Sherief *et al.* (2007) 'Internalization by HeLa cells of latex beads coated with mammalian cell entry (Mce) proteins encoded by the mce3 operon of Mycobacterium tuberculosis', *Journal of Medical Microbiology*. doi: 10.1099/jmm.0.47095-0.

El-Shazly, S. *et al.* (2007) 'Utility of three mammalian cell entry proteins of Mycobacterium tuberculosis in the serodiagnosis of tuberculosis', *International Journal of Tuberculosis and Lung Disease*, 11(6), pp. 676–682.

Elibol, M. (2004) 'Optimization of medium composition for actinorhodin production by Streptomyces coelicolor A3(2) with response surface methodology', *Process Biochemistry*, 39(9), pp. 1057–1062. doi: 10.1016/S0032-9592(03)00232-2.

Ensign, J. C. (1978) 'Formation, Properties, and Germination of Actinomycete Spores', *Annual Review of Microbiology*. doi: 10.1146/annurev.mi.32.100178.001153.

Falke, D. *et al.* (2019) 'Activity of spore-specific respiratory nitrate reductase 1 of streptomyces coelicolor A3(2) requires a functional cytochrome bcc-aa3 oxidase supercomplex', *Journal of Bacteriology*. doi: 10.1128/JB.00104-19.

Falkenstein, K. and De Lozanne, A. (2014) 'Dictyostelium LvsB has a regulatory role in endosomal vesicle fusion', *Journal of Cell Science*. doi: 10.1242/jcs.138123.

Farajnia, S., Ansarin, K. and Sahebi, L. (2019) 'Effectiveness of bacillus Calmette–Guerin vaccination history on pulmonary tuberculosis symptoms', *Journal of Clinical*

Tuberculosis and Other Mycobacterial Diseases. Elsevier, 17, p. 100126. doi: 10.1016/j.jctube.2019.100126.

Fenn, K., Wong, C. T. and Darbari, V. C. (2020) 'Mycobacterium tuberculosis Uses Mce Proteins to Interfere With Host Cell Signaling', *Frontiers in Molecular Biosciences*. doi: 10.3389/fmolb.2019.00149.

Fey, P. *et al.* (2007) 'Protocols for growth and development of Dictyostelium discoideum', *Nature Protocols*. doi: 10.1038/nprot.2007.178.

Filipski, A. and Kumar, S. (2005) 'Comparative Genomics in Eukaryotes', in *The Evolution of the Genome*. doi: 10.1016/B978-012301463-4/50011-5.

Finlay, B. J. and Esteban, G. F. (2019) 'Protozoa', in *Encyclopedia of Microbiology*. doi: 10.1016/B978-0-12-809633-8.02281-0.

Fischer, M., Falke, D. and Sawers, R. (2014) 'Determination of Oxygen Respiration Rates in Wetted Developmentally Arrested Spores of Streptomyces Species', *BIO-PROTOCOL*. doi: 10.21769/bioprotoc.1153.

Fischer, M., Falke, D. and Sawers, R. G. (2013) 'A respiratory nitrate reductase active exclusively in resting spores of the obligate aerobe Streptomyces coelicolorA3(2)', *Molecular Microbiology*. doi: 10.1111/mmi.12344.

Flärdh, K. and Buttner, Mark J (2009) 'Streptomyces morphogenetics: dissecting differentiation in a filamentous bacterium', *Nature Reviews Microbiology*, 7(1), pp. 36–49. doi: 10.1038/nrmicro1968.

Flärdh, K. and Buttner, Mark J. (2009) ‘Streptomyces morphogenetics: Dissecting differentiation in a filamentous bacterium’, *Nature Reviews Microbiology*. doi: 10.1038/nrmicro1968.

Forrellad, M. A. *et al.* (2014) ‘Role of the Mce1 transporter in the lipid homeostasis of Mycobacterium tuberculosis’, *Tuberculosis*. doi: 10.1016/j.tube.2013.12.005.

Foulston, L. C. and Bibb, M. J. (2010) ‘Microbisporicin gene cluster reveals unusual features of lantibiotic biosynthesis in actinomycetes’, *Proceedings of the National Academy of Sciences of the United States of America*. doi: 10.1073/pnas.1008285107.

Fröjd, M. J. and Flärdh, K. (2019) ‘Apical assemblies of intermediate filament-like protein FilP are highly dynamic and affect polar growth determinant DivIVA in Streptomyces venezuelae’, *Molecular Microbiology*. doi: 10.1111/mmi.14253.

Froquet, R. *et al.* (2009) ‘Dictyostelium discoideum: A model host to measure bacterial virulence’, *Nature Protocols*. doi: 10.1038/nprot.2008.212.

Fyans, J. K. *et al.* (2013) ‘The ESX/type VII secretion system modulates development, but not virulence, of the plant pathogen Streptomyces scabies’, *Molecular Plant Pathology*. doi: 10.1111/j.1364-3703.2012.00835.x.

Galán, B. *et al.* (2017) ‘Mycobacterium smegmatis is a suitable cell factory for the production of steroidic synthons’, *Microbial Biotechnology*, 10(1), pp. 138–150. doi: 10.1111/1751-7915.12429.

Gao, B. and Gupta, R. S. (2012) ‘Phylogenetic Framework and Molecular Signatures

for the Main Clades of the Phylum Actinobacteria', *Microbiology and Molecular Biology Reviews*. doi: 10.1128/mmbr.05011-11.

García-Fernández, J. *et al.* (2017a) 'Molecular and functional analysis of the mce4 operon in Mycobacterium smegmatis', *Environmental Microbiology*. doi: 10.1111/1462-2920.13869.

García-Fernández, J. *et al.* (2017b) 'Unravelling the pleiotropic role of the MceG ATPase in Mycobacterium smegmatis', *Environmental Microbiology*. doi: 10.1111/1462-2920.13771.

García, J. L., Uhía, I. and Galán, B. (2012a) 'Catabolism and biotechnological applications of cholesterol degrading bacteria', *Microbial Biotechnology*. doi: 10.1111/j.1751-7915.2012.00331.x.

García, J. L., Uhía, I. and Galán, B. (2012b) 'Catabolism and biotechnological applications of cholesterol degrading bacteria', *Microbial Biotechnology*, 5(6), pp. 679–699. doi: 10.1111/j.1751-7915.2012.00331.x.

Gaudet, P. *et al.* (2008) 'An anatomy ontology to represent biological knowledge in Dictyostelium discoideum', *BMC Genomics*. doi: 10.1186/1471-2164-9-130.

Gerisch, G, Luderitz, O, Ruschmann, E (1967) 'Antibodies promoting phagocytosis of bacteria by amoebae'.

Gerisch, G. *et al.* (2004) 'GFP-golvesin constructs to study Golgi tubulation and post-Golgi vesicle dynamics in phagocytosis', *European Journal of Cell Biology*. doi:

10.1078/0171-9335-00393.

Gezelius, K. and Rånby, B. G. (1957) ‘Morphology and fine structure of the slime mold Dictyostelium discoideum’, *Experimental Cell Research*. doi: 10.1016/0014-4827(57)90141-6.

Gioffré, A. *et al.* (2005) ‘Mutation in mce operons attenuates Mycobacterium tuberculosis virulence’, *Microbes and Infection*. doi: 10.1016/j.micinf.2004.11.007.

Glaziou, P. (2020) ‘Predicted impact of the COVID-19 pandemic on global tuberculosis deaths in 2020’, *medRxiv*, 66. doi: 10.1101/2020.04.28.20079582.

Gotthardt, D. *et al.* (2002) ‘High-resolution dissection of phagosome maturation reveals distinct membrane trafficking phases’, *Molecular Biology of the Cell*. doi: 10.1091/mbc.E02-04-0206.

Grant, S. G. N. *et al.* (1990) ‘Differential plasmid rescue from transgenic mouse DNAs into Escherichia coli methylation-restriction mutants’, *Proceedings of the National Academy of Sciences of the United States of America*. doi: 10.1073/pnas.87.12.4645.

Grzegorzewicz, A. E. *et al.* (2016) ‘Assembling of the Mycobacterium tuberculosis cell wall core’, *Journal of Biological Chemistry*. doi: 10.1074/jbc.M116.739227.

Gueho, A., Bosmani, C. and Soldati, T. (2019) ‘Proteomic characterisation of the Mycobacterium marinum-containing compartment in Dictyostelium discoideum’, *bioRxiv*. doi: 10.1101/592717.

Gupta, R. S., Lo, B. and Son, J. (2018) ‘Phylogenomics and comparative genomic

studies robustly support division of the genus Mycobacterium into an emended genus Mycobacterium and four novel genera', *Frontiers in Microbiology*. doi: 10.3389/fmicb.2018.00067.

Hagedorn, M. and Soldati, T. (2007) 'Flotillin and RacH modulate the intracellular immunity of Dictyostelium to Mycobacterium marinum infection', *Cellular Microbiology*. doi: 10.1111/j.1462-5822.2007.00993.x.

Haile, Y. *et al.* (2002) 'Mycobacterium tuberculosis mammalian cell entry operon (mce) homologs in Mycobacterium other than tuberculosis (MOTT)', *FEMS Immunology and Medical Microbiology*. doi: 10.1016/S0928-8244(02)00302-4.

Haiser, H. J., Yousef, M. R. and Elliot, M. A. (2009) 'Cell wall hydrolases affect germination, vegetative growth, and sporulation in Streptomyces coelicolor', *Journal of Bacteriology*. doi: 10.1128/JB.00767-09.

Hameduh, T. *et al.* (2020) 'Homology modeling in the time of collective and artificial intelligence', *Computational and Structural Biotechnology Journal*. The Author(s), 18, pp. 3494–3506. doi: 10.1016/j.csbj.2020.11.007.

Hanson, P. I. and Whiteheart, S. W. (2005) 'AAA+ proteins: Have engine, will work', *Nature Reviews Molecular Cell Biology*. doi: 10.1038/nrm1684.

Hardisson, C. *et al.* (1978) 'Fine structure, physiology and biochemistry of arthrospore germination in Streptomyces antibioticus', *Journal of General Microbiology*. doi: 10.1099/00221287-105-2-203.

Harris, T. J. C., Ravandi, A. and Siu, C. H. (2001) 'Assembly of glycoprotein-80

adhesion complexes in Dictyostelium: Receptor compartmentalization and oligomerization in membrane rafts', *Journal of Biological Chemistry*. doi: 10.1074/jbc.M108030200.

Hasani, A., Kariminik, A. and Isaazadeh, K. (2014) 'Streptomycetes : Characteristics and Their Antimicrobial Activities', *International Journal of Advanced Biological and Biomedical Research*.

Haug, I. *et al.* (2003) 'Streptomyces coelicolor A3(2) plasmid SCP2*: Deductions from the complete sequence', *Microbiology*. doi: 10.1099/mic.0.25751-0.

Hemati, Z. *et al.* (2019) 'Mammalian cell entry operons; novel and major subset candidates for diagnostics with special reference to Mycobacterium avium subspecies paratuberculosis infection', *Veterinary Quarterly*. doi: 10.1080/01652176.2019.1641764.

Hett, E. C. and Rubin, E. J. (2008) 'Bacterial Growth and Cell Division: a Mycobacterial Perspective', *Microbiology and Molecular Biology Reviews*. doi: 10.1128/mmbr.00028-07.

Hirsch, C. F. and Ensign, J. C. (1976) 'Nutritionally defined conditions for germination of Streptomyces viridochromogenes spores', *Journal of Bacteriology*. doi: 10.1128/jb.126.1.13-23.1976.

Hopwood, D. A. (2015) *Streptomyces in Nature and Medicine*, *Oxford university press*. doi: 10.1017/CBO9781107415324.004.

Hoskisson, P. A. and Fernández-Martínez, L. T. (2018) ‘Regulation of specialised metabolites in Actinobacteria – expanding the paradigms’, *Environmental Microbiology Reports*, pp. 231–238. doi: 10.1111/1758-2229.12629.

Hoskisson, P. A., Hobbs, G. and Sharples, G. P. (2000) ‘Response of Micromonospora echinospora (NCIMB 12744) spores to heat treatment with evidence of a heat activation phenomenon’, *Letters in Applied Microbiology*. doi: 10.1046/j.1472-765x.2000.00680.x.

Hoskisson, P. A. and van Wezel, G. P. (2019) ‘Streptomyces coelicolor’, *Trends in Microbiology*. doi: 10.1016/j.tim.2018.12.008.

Huang, J. *et al.* (2005) ‘Cross-regulation among disparate antibiotic biosynthetic pathways of Streptomyces coelicolor’, *Molecular Microbiology*. doi: 10.1111/j.1365-2958.2005.04879.x.

Hürlimann, L. M. *et al.* (2016) ‘The heterodimeric ABC transporter EfrCD mediates multidrug efflux in Enterococcus faecalis’, *Antimicrobial Agents and Chemotherapy*. doi: 10.1128/AAC.00661-16.

Hutchings, M. I. *et al.* (2009) ‘Lipoprotein biogenesis in Gram-positive bacteria: knowing when to hold ’em, knowing when to fold ’em’, *Trends in Microbiology*. doi: 10.1016/j.tim.2008.10.001.

Ishikawa, J. *et al.* (2003) ‘Phagocytosis of Dictyostelium discoideum studied by the particle-tracking method’, *Experimental Cell Research*. doi: 10.1016/S0014-4827(03)00212-X.

Isom, G. L. *et al.* (2017) ‘MCE domain proteins: Conserved inner membrane lipid-binding proteins required for outer membrane homeostasis’, *Scientific Reports*. doi: 10.1038/s41598-017-09111-6.

Isom, G. L. *et al.* (2020) ‘LetB Structure Reveals a Tunnel for Lipid Transport across the Bacterial Envelope’, *Cell*. doi: 10.1016/j.cell.2020.03.030.

Jang, M. S. *et al.* (2016) ‘Genetic and transcriptional analyses of the flagellar gene cluster in Actinoplanes missouriensis’, *Journal of Bacteriology*. doi: 10.1128/JB.00306-16.

Janssen, K. P. *et al.* (2001) ‘Characterization of CD36/LIMPII Homologues in Dictyostelium discoideum’, *Journal of Biological Chemistry*. doi: 10.1074/jbc.M103384200.

Ji, X. *et al.* (2017) ‘Cloning, expression, invasion, and immunological reactivity of a mammalian cell entry protein encoded by the mce1 operon of Nocardia farcinica’, *Frontiers in Microbiology*. doi: 10.3389/fmicb.2017.00281.

John Jumper, Richard Evans, Alexander Pritzel, Tim Green, Michael Figurnov, Kathryn Tunyasuvunakool, Olaf Ronneberger, Russ Bates, Augustin Žídek, Alex Bridgland, Clemens Meyer, Simon A A Kohl, Anna Potapenko, Andrew J Ballard, Andrew Cowie, Bernardino Ro, D. H. (2020) ‘Critical Assessment of Techniques for Protein Structure Prediction’, *Abstract Book*, pp. 1–221.

Jones, P. M. and George, A. M. (2002) ‘Mechanism of ABC transporters: A molecular

dynamics simulation of a well characterized nucleotide-binding subunit', *Proceedings of the National Academy of Sciences of the United States of America*. doi: 10.1073/pnas.152439599.

De Jong, W. *et al.* (2009) 'NepA is a structural cell wall protein involved in maintenance of spore dormancy in Streptomyces coelicolor', *Molecular Microbiology*. doi: 10.1111/j.1365-2958.2009.06633.x.

Joshi, S. M. *et al.* (2006) 'Characterization of mycobacterial virulence genes through genetic interaction mapping', *Proceedings of the National Academy of Sciences of the United States of America*. doi: 10.1073/pnas.0603179103.

Juncker, A. S. *et al.* (2003) 'Prediction of lipoprotein signal peptides in Gram-negative bacteria', *Protein Science*, 12(8), pp. 1652–1662. doi: 10.1110/ps.0303703.

Kämpfer, P. *et al.* (2014) 'The family Streptomycetaceae', in *The Prokaryotes: Actinobacteria*. doi: 10.1007/978-3-642-30138-4_184.

Kapadia, M., Rolston, K. V. I. and Han, X. Y. (2007) 'Invasive Streptomyces infections: Six cases and literature review', *American Journal of Clinical Pathology*. doi: 10.1309/QJEBXP0BCGR54L15.

Kelley, L. A. *et al.* (2015) 'The Phyre2 web portal for protein modeling, prediction and analysis', *Nature Protocols*, pp. 845–858. doi: 10.1038/nprot.2015.053.

Khan, S. *et al.* (2016) 'Purification and structural characterization of Mce4A from Mycobacterium tuberculosis', *International Journal of Biological Macromolecules*.

Elsevier B.V., 93, pp. 235–241. doi: 10.1016/j.ijbiomac.2016.06.059.

Kieser, T. *et al.* (2000) 'Practical Streptomyces Genetics. 2nd ed.', *International microbiology: official journal of the Spanish Society for Microbiology*.

Kieser, T. (2000) *Practical Streptomyces Genetics*. 2000th edn. Norwich.

Kim, D. R. *et al.* (2019) 'A mutualistic interaction between Streptomyces bacteria, strawberry plants and pollinating bees', *Nature Communications*. doi: 10.1038/s41467-019-12785-3.

Kirby, R. (2011) 'Chromosome diversity and similarity within the Actinomycetales', *FEMS Microbiology Letters*. doi: 10.1111/j.1574-6968.2011.02242.x.

Kirby, R. *et al.* (2012) 'Draft genome sequence of the human pathogen Streptomyces somaliensis, a significant cause of actinomycetoma', *Journal of Bacteriology*. doi: 10.1128/JB.00534-12.

Kleinschnitz, E. M., Latus, A., *et al.* (2011) 'Genetic analysis of SCO2997, encoding a tagf homologue, indicates a role for wall teichoic acids in sporulation of streptomyces coelicolor A3(2)', *Journal of Bacteriology*. doi: 10.1128/JB.05782-11.

Kleinschnitz, E. M., Heichlinger, A., *et al.* (2011) 'Proteins encoded by the mre gene cluster in Streptomyces coelicolor A3(2) cooperate in spore wall synthesis', *Molecular Microbiology*. doi: 10.1111/j.1365-2958.2010.07529.x.

Klepp, L. I. *et al.* (2012) 'Impact of the deletion of the six mce operons in

Mycobacterium smegmatis', *Microbes and Infection*. doi: 10.1016/j.micinf.2012.01.007.

Koegelenberg, C. F. N., Schoch, O. D. and Lange, C. (2021) 'Tuberculosis: The Past, the Present and the Future', *Respiration*, 100(7), pp. 553–556. doi: 10.1159/000516509.

Kohwiwattanagun, J. *et al.* (2007) 'Mycobacterial mammalian cell entry protein 1A (Mce1A)-mediated adherence enhances the chemokine production by A549 alveolar epithelial cells', *Microbiology and Immunology*. doi: 10.1111/j.1348-0421.2007.tb03897.x.

Kronheim, S. *et al.* (2018) 'A chemical defence against phage infection', *Nature*. doi: 10.1038/s41586-018-0767-x.

Kuburich, N. A., Adhikari, N. and Hadwiger, J. A. (2016) 'Acanthamoeba and Dictyostelium Use Different Foraging Strategies', *Protist*. doi: 10.1016/j.protis.2016.08.006.

de La Paz, M. *et al.* (2009) 'Mce3R, a TetR-type transcriptional repressor, controls the expression of a regulon involved in lipid metabolism in mycobacterium tuberculosis', *Microbiology*. doi: 10.1099/mic.0.027086-0.

Lamb, D. C. *et al.* (2002) 'Sterol 14α-demethylase activity in Streptomyces coelicolor A3(2) is associated with an unusual member of the CYP51 gene family', *Biochemical Journal*. doi: 10.1042/BJ20011380.

Lamrabet, O. *et al.* (2020) 'Transcriptional Responses of Dictyostelium discoideum

Exposed to Different Classes of Bacteria', *Frontiers in Microbiology*, 11(March), pp. 1–12. doi: 10.3389/fmicb.2020.00410.

Leoni Swart, A. *et al.* (2018) 'Acanthamoeba and dictyostelium as cellular models for Legionella infection', *Frontiers in Cellular and Infection Microbiology*. doi: 10.3389/fcimb.2018.00061.

Lewis, N. E. and Brady, L. J. (2015) 'Breaking the bacterial protein targeting and translocation model: Oral organisms as a case in point', *Molecular Oral Microbiology*. doi: 10.1111/omi.12088.

Li, J. *et al.* (2015) ' Mycobacterium tuberculosis Mce3E Suppresses Host Innate Immune Responses by Targeting ERK1/2 Signaling ', *The Journal of Immunology*. doi: 10.4049/jimmunol.1402679.

Lim, J. P. and Gleeson, P. A. (2011) 'Macropinocytosis: An endocytic pathway for internalising large gulps', *Immunology and Cell Biology*. doi: 10.1038/icb.2011.20.

de Lima Procópio, R. E. *et al.* (2012) 'Antibiotics produced by Streptomyces', *Brazilian Journal of Infectious Diseases*. doi: 10.1016/j.bjid.2012.08.014.

Lima, W. C. *et al.* (2014) 'Two distinct sensing pathways allow recognition of Klebsiella pneumoniae by Dictyostelium amoebae', *Cellular Microbiology*. doi: 10.1111/cmi.12226.

Liot, Q. and Constant, P. (2016) 'Breathing air to save energy - new insights into the ecophysiological role of high-affinity [NiFe]-hydrogenase in Streptomyces avermitilis',

MicrobiologyOpen. doi: 10.1002/mbo3.310.

Locher, K. P. (2004) 'Structure and mechanism of ABC transporters', *Current Opinion in Structural Biology*. doi: 10.1016/j.sbi.2004.06.005.

Locher, K. P. (2016) 'Mechanistic diversity in ATP-binding cassette (ABC) transporters', *Nature Structural and Molecular Biology*. doi: 10.1038/nsmb.3216.

Logsdon, M. M. and Aldridge, B. B. (no date) 'Stable regulation of cell cycle events in mycobacteria: Insights from inherently heterogeneous bacterial populations', *Frontiers in Microbiology*. doi: 10.3389/fmicb.2018.00514.

Ludwig, E., Francisco, R.-C. and Francisco, R. (2006) *Dictyostelium discoideum Protocols*, *Dictyostelium discoideum Protocols*. doi: 10.1385/1597451444.

MacNeil, D. J. *et al.* (1992) 'Analysis of Streptomyces avermitilis genes required for avermectin biosynthesis utilizing a novel integration vector', *Gene*. doi: 10.1016/0378-1119(92)90603-M.

Maqbool, A. *et al.* (2015) 'The substrate-binding protein in bacterial ABC transporters: Dissecting roles in the evolution of substrate specificity', *Biochemical Society Transactions*. doi: 10.1042/BST20150135.

Marciano-Cabral, F. and Cabral, G. (2003) 'Acanthamoeba spp. as agents of disease in humans', *Clinical Microbiology Reviews*. doi: 10.1128/CMR.16.2.273-307.2003.

Marjanovic, O. *et al.* (2010) 'Mce2 operon mutant strain of Mycobacterium tuberculosis is attenuated in C57BL/6 mice', *Tuberculosis*. doi: 10.1016/j.tube.2009.10.004.

Marjanovic, O., Iavarone, A. T. and Riley, L. W. (2011) ‘Sulfolipid accumulation in Mycobacterium tuberculosis disrupted in the mce2 operon’, *Journal of Microbiology*. doi: 10.1007/s12275-011-0435-4.

Mazza, P. *et al.* (2006) ‘MreB of Streptomyces coelicolor is not essential for vegetative growth but is required for the integrity of aerial hyphae and spores’, *Molecular Microbiology*. doi: 10.1111/j.1365-2958.2006.05134.x.

McArthur, M. and Bibb, M. J. (2008) ‘Manipulating and understanding antibiotic production in Streptomyces coelicolor A3(2) with decoy oligonucleotides’, *Proceedings of the National Academy of Sciences of the United States of America*, 105(3), pp. 1020–1025. doi: 10.1073/pnas.0710724105.

McCormick, J. R. and Flärdh, K. (2012) ‘Signals and regulators that govern Streptomyces development’, *FEMS Microbiology Reviews*. doi: 10.1111/j.1574-6976.2011.00317.x.

McDonald, C. J. and Sampson, J. (1983) ‘The effects of inhibition of protein glycosylation on the aggregation of Dictyostelium discoideum’, *Journal of Embryology and Experimental Morphology*.

McLean, K. J. *et al.* (2006) ‘The preponderance of P450s in the Mycobacterium tuberculosis genome’, *Trends in Microbiology*. doi: 10.1016/j.tim.2006.03.002.

McLeod, M. P. *et al.* (2006) ‘The complete genome of Rhodococcus sp. RHA1 provides insights into a catabolic powerhouse’, *Proceedings of the National Academy of*

Sciences of the United States of America. doi: 10.1073/pnas.0607048103.

Mehling, A., Wehmeier, U. F. and Piepersberg, W. (1995) 'Nucleotide sequences of streptomycete 16S ribosomal DNA: Towards a specific identification system for streptomycetes using PCR', *Microbiology*. doi: 10.1099/13500872-141-9-2139.

Mendes, R., Garbeva, P. and Raaijmakers, J. M. (2013) 'The rhizosphere microbiome: Significance of plant beneficial, plant pathogenic, and human pathogenic microorganisms', *FEMS Microbiology Reviews*. doi: 10.1111/1574-6976.12028.

Mohn, W. W. *et al.* (2008) 'The actinobacterial mce4 locus encodes a steroid transporter', *Journal of Biological Chemistry*. doi: 10.1074/jbc.M805496200.

Möker, N. *et al.* (2004) 'Deletion of the genes encoding the MtrA-MtrB two-component system of Corynebacterium glutamicum has a strong influence on cell morphology, antibiotics susceptibility and expression of genes involved in osmoprotection', *Molecular Microbiology*. doi: 10.1111/j.1365-2958.2004.04249.x.

Moule, M. G. and Cirillo, J. D. (2020) 'Mycobacterium tuberculosis Dissemination Plays a Critical Role in Pathogenesis', *Frontiers in Cellular and Infection Microbiology*. doi: 10.3389/fcimb.2020.00065.

Muok, A. R., Claessen, D. and Briegel, A. (2021) 'Microbial hitchhiking: how Streptomyces spores are transported by motile soil bacteria', *ISME Journal*. doi: 10.1038/s41396-021-00952-8.

Mustafa, A. S. (2013) 'In silico analysis and experimental validation of mycobacterium

tuberculosis-specific proteins and peptides of mycobacterium tuberculosis for immunological diagnosis and vaccine development', *Medical Principles and Practice*, 22(SUPPL.1), pp. 43–51. doi: 10.1159/000354206.

Nass, N. M. *et al.* (2017) 'Revisiting unexploited antibiotics in search of new antibacterial drug candidates: The case of γ-actinorhodin', *Scientific Reports*, 7(1), pp. 1–11. doi: 10.1038/s41598-017-17232-1.

Nasser, W. *et al.* (2013a) 'Bacterial discrimination by dictyostelid amoebae reveals the complexity of ancient interspecies interactions', *Current Biology*. doi: 10.1016/j.cub.2013.04.034.

Nasser, W. *et al.* (2013b) 'Bacterial discrimination by dictyostelid amoebae reveals the complexity of ancient interspecies interactions', *Current Biology*. Elsevier Ltd, 23(10), pp. 862–872. doi: 10.1016/j.cub.2013.04.034.

Natale, P., Brüser, T. and Driessen, A. J. M. (2008) 'Sec- and Tat-mediated protein secretion across the bacterial cytoplasmic membrane-Distinct translocases and mechanisms', *Biochimica et Biophysica Acta - Biomembranes*. doi: 10.1016/j.bbamem.2007.07.015.

Nazarova, E. V. *et al.* (2017) 'Rv3723/LucA coordinates fatty acid and cholesterol uptake in Mycobacterium tuberculosis', *eLife*. doi: 10.7554/eLife.26969.

Nazarova, E. V. *et al.* (2019) 'The genetic requirements of fatty acid import by mycobacterium tuberculosis within macrophages', *eLife*. doi: 10.7554/eLife.43621.

Neujahr, R. *et al.* (1998) ‘Microtubule-mediated centrosome motility and the positioning of cleavage furrows in multinucleate myosin II-null cells’, *Journal of Cell Science*.

Nieselt, K. *et al.* (2010) ‘The dynamic architecture of the metabolic switch in Streptomyces coelicolor’, *BMC Genomics*, 11(1), pp. 1–9. doi: 10.1186/1471-2164-11-10.

Nouioui, I. *et al.* (2018) ‘Genome-based taxonomic classification of the phylum actinobacteria’, *Frontiers in Microbiology*. doi: 10.3389/fmicb.2018.02007.

O’Callaghan, A. and van Sinderen, D. (2016) ‘Bifidobacteria and their role as members of the human gut microbiota’, *Frontiers in Microbiology*. doi: 10.3389/fmicb.2016.00925.

Obregón-Henao, A. *et al.* (2011) ‘Vaccination of guinea pigs using mce operon mutants of Mycobacterium tuberculosis’, *Vaccine*, 29(26), pp. 4302–4307. doi: 10.1016/j.vaccine.2011.04.027.

Olanrewaju, O. S. and Babalola, O. O. (2019) ‘Streptomyces: implications and interactions in plant growth promotion’, *Applied Microbiology and Biotechnology*. doi: 10.1007/s00253-018-09577-y.

Oliver, W. T. and Wells, J. E. (2015) ‘Lysozyme as an alternative to growth promoting antibiotics in swine production’, *Journal of Animal Science and Biotechnology*. doi: 10.1186/s40104-015-0034-z.

Paget, M. S. B. *et al.* (1999) ‘Evidence that the extracytoplasmic function sigma factor σ(E) is required for normal cell wall structure in Streptomyces coelicolor A3(2)’, *Journal*

of Bacteriology. doi: 10.1128/jb.181.1.204-211.1999.

Pagmadulam, B. *et al.* (2020) 'Isolation and characterization of antiprotozoal compound-producing Streptomyces species from Mongolian soils', *Parasitology International*. doi: 10.1016/j.parint.2019.101961.

Pan, M. *et al.* (2016) 'Identification of a Chemoattractant G-Protein-Coupled Receptor for Folic Acid that Controls Both Chemotaxis and Phagocytosis', *Developmental Cell*. doi: 10.1016/j.devcel.2016.01.012.

Pandey, A. K. and Sassetti, C. M. (2008) 'Mycobacterial persistence requires the utilization of host cholesterol', *Proceedings of the National Academy of Sciences of the United States of America*. doi: 10.1073/pnas.0711159105.

Paquet, V. E. and Charette, S. J. (2016) 'Amoeba-resisting bacteria found in multilamellar bodies secreted by Dictyostelium discoideum: Social amoebae can also package bacteria', *FEMS Microbiology Ecology*. doi: 10.1093/femsec/fiw025.

Parte, A. C. (2014) 'LPSN - List of prokaryotic names with standing in nomenclature', *Nucleic Acids Research*. doi: 10.1093/nar/gkt1111.

Pears, C. J. and Gross, J. D. (2021) 'Microbe profile: Dictyostelium discoideum: Model system for development, chemotaxis and biomedical research', *Microbiology (United Kingdom)*, 167(3), pp. 1–3. doi: 10.1099/mic.0.001040.

Perkowski, E. F. *et al.* (2016) 'An orphaned Mce-associated membrane protein of Mycobacterium tuberculosis is a virulence factor that stabilizes Mce transporters', *Molecular Microbiology*. doi: 10.1111/mmi.13303.

Petersen, F. *et al.* (1993) ‘Germicidin, an autoregulative germination inhibitor of streptomyces viridochromogenes NRRLB-1551’, *Journal of Antibiotics*. doi: 10.7164/antibiotics.46.1126.

Pham, V. C. *et al.* (2014) *Complementary methods for the identification of substrates of proteolysis*. 1st edn, *Methods in Enzymology*. 1st edn. Elsevier Inc. doi: 10.1016/B978-0-12-417158-9.00014-5.

Pieters, J. (2008) ‘Mycobacterium tuberculosis and the Macrophage: Maintaining a Balance’, *Cell Host and Microbe*. doi: 10.1016/j.chom.2008.05.006.

Poolman, B. and van der Heide, T. (2002) ‘ABC transporters: one, two or four extracytoplasmic substrate-binding sites?’, *EMBO reports*, 3(10), pp. 938–43. Available at: http://www.nature.com/embor/journal/v3/n10/abs/embor057.html.

Prieß, M. *et al.* (2018) ‘Molecular Mechanism of ATP Hydrolysis in an ABC Transporter’, *ACS Central Science*. doi: 10.1021/acscentsci.8b00369.

Procko, E. *et al.* (2009) ‘The mechanism of ABC transporters: general lessons from structural and functional studies of an antigenic peptide transporter’, *The FASEB Journal*. doi: 10.1096/fj.08-121855.

Qiang, L. *et al.* (2019a) ‘Mycobacterium tuberculosis Mce2E suppresses the macrophage innate immune response and promotes epithelial cell proliferation’, *Cellular and Molecular Immunology*. doi: 10.1038/s41423-018-0016-0.

Qiang, L. *et al.* (2019b) ‘Mycobacterium tuberculosis Mce2E suppresses the macrophage innate immune response and promotes epithelial cell proliferation’, *Cellular and Molecular Immunology*. Springer US, 16(4), pp. 380–391. doi: 10.1038/s41423-018-0016-0.

Rahlwes, K. C., Sparks, I. L. and Morita, Y. S. (2019) ‘Cell Walls and Membranes of Actinobacteria’, in *Subcellular Biochemistry*. doi: 10.1007/978-3-030-18768-2_13.

Rahman, O. *et al.* (2008) ‘Methods for the bioinformatic identification of bacterial lipoproteins encoded in the genomes of Gram-positive bacteria’, *World Journal of Microbiology and Biotechnology*, 24(11), pp. 2377–2382. doi: 10.1007/s11274-008-9795-2.

Ranada, N. and Vining, L. C. (1993) ‘Accumulation of intracellular carbon reserves in relation to chloramphenicol biosynthesis by Streptomyces venezuelae’, *Canadian Journal of Microbiology*. doi: 10.1139/m93-055.

Rank, L., Herring, L. E. and Braunstein, M. (2021) ‘Evidence for the mycobacterial mce4 transporter being a multiprotein complex’, *Journal of Bacteriology*, 203(10). doi: 10.1128/JB.00685-20.

Rashidi, G. and Ostrowski, E. A. (2019) ‘Phagocyte chase behaviours: Discrimination between Gram-negative and Gram-positive bacteria by amoebae’, *Biology Letters*, 15(1). doi: 10.1098/rsbl.2018.0607.

Rath, A. *et al.* (2009) ‘Detergent binding explains anomalous SDS-PAGE migration of membrane proteins’, *Proceedings of the National Academy of Sciences of the United States of America*, 106(6), pp. 1760–1765. doi: 10.1073/pnas.0813167106.

Rathor, N. *et al.* (2016) ‘Expression profile of mce4 operon of Mycobacterium tuberculosis following environmental stress’, *International Journal of Mycobacteriology*. doi: 10.1016/j.ijmyco.2016.08.004.

Rees, D. C., Johnson, E. and Lewinson, O. (2009) ‘ABC transporters: The power to change’, *Nature Reviews Molecular Cell Biology*. doi: 10.1038/nrm2646.

Rice, A. J., Park, A. and Pinkett, H. W. (2014) ‘Diversity in ABC transporters: Type I, II and III importers’, *Critical Reviews in Biochemistry and Molecular Biology*. doi: 10.3109/10409238.2014.953626.

Romano-Armada, N. *et al.* (2020) ‘Potential of bioremediation and PGP traits in streptomyces as strategies for bio-reclamation of salt-affected soils for agriculture’, *Pathogens*. doi: 10.3390/pathogens9020117.

Rosel, D. *et al.* (2012) ‘TOR complex 2 (TORC2) in Dictyostelium suppresses phagocytic nutrient capture independently of TORC1-mediated nutrient sensing’, *Development*. doi: 10.1242/jcs.077040.

Rosenberg, K. *et al.* (2009) ‘Soil amoebae rapidly change bacterial community composition in the rhizosphere of Arabidopsis thaliana’, *ISME Journal*. doi: 10.1038/ismej.2009.11.

Rupper, A., Grove, B. and Cardelli, J. (2001) ‘Rab7 regulates phagosome maturation in Dictyostelium’, *Journal of Cell Science*.

Russell, D. G. (2001) ‘Mycobacterium tuberculosis: Here today, and here tomorrow’, *Nature Reviews Molecular Cell Biology*. doi: 10.1038/35085034.

Sandoval-Calderón, M., Guan, Z. and Sohlenkamp, C. (2017) ‘Knowns and unknowns of membrane lipid synthesis in streptomycetes’, *Biochimie*. doi: 10.1016/j.biochi.2017.05.008.

Schrempf, H. (2006) ‘The Family Streptomycetaceae, Part II: Molecular Biology’, in *The Prokaryotes*. doi: 10.1007/0-387-30743-5_23.

Segota, I. *et al.* (2013) ‘High fidelity information processing in folic acid chemotaxis of Dictyostelium amoebae’, *Journal of the Royal Society Interface*, 10(88). doi: 10.1098/rsif.2013.0606.

Seipke, R. F., Kaltenpoth, M. and Hutchings, M. I. (2012) ‘Streptomyces as symbionts: An emerging and widespread theme?’, *FEMS Microbiology Reviews*. doi: 10.1111/j.1574-6976.2011.00313.x.

Sekine, M. *et al.* (2006) ‘Sequence analysis of three plasmids harboured in Rhodococcus erythropolis strain PR4’, *Environmental Microbiology*. doi: 10.1111/j.1462-2920.2005.00899.x.

Sellers, R. S. *et al.* (2012) ‘Immunological variation between inbred laboratory mouse strains: Points to consider in phenotyping genetically immunomodified mice’, *Veterinary Pathology*. doi: 10.1177/0300985811429314.

Sexton, D. L. *et al.* (2015) ‘Resuscitation-promoting factors are cell wall-lytic enzymes

with important roles in the germination and growth of streptomyces coelicolor', *Journal of Bacteriology*. doi: 10.1128/JB.02464-14.

Shi, Y. *et al.* (2020) 'The Ecology and Evolution of Amoeba-Bacterium Interactions', *Applied and Environmental Microbiology*. doi: 10.1128/aem.01866-20.

Shi, Y. *et al.* (2021) 'crossm The Ecology and Evolution of Amoeba-Bacterium Interactions', 87(2).

Shimono, N. *et al.* (2003) 'Hypervirulent mutant of Mycobacterium tuberculosis resulting from disruption of the mce1 operon', *Proceedings of the National Academy of Sciences of the United States of America*. doi: 10.1073/pnas.2433882100.

Sigle, S. *et al.* (2015) 'Synthesis of the spore envelope in the developmental life cycle of Streptomyces coelicolor', *International Journal of Medical Microbiology*. doi: 10.1016/j.ijmm.2014.12.014.

Simpson, R. S. and Read, R. C. (2014) 'Nocardiosis and actinomycosis', *Medicine (United Kingdom)*. doi: 10.1016/j.mpmed.2013.10.012.

Sinai, L. *et al.* (2015) 'The molecular timeline of a reviving bacterial spore', *Molecular Cell*. doi: 10.1016/j.molcel.2014.12.019.

Singh, P. *et al.* (2016) 'Analysis of expression profile of mce operon genes (mce1, mce2, mce3 operon) in different Mycobacterium tuberculosis isolates at different growth phases', *Indian Journal of Medical Research*. doi: 10.4103/0971-5916.184305.

Smith, I. (2003) 'Mycobacterium tuberculosis pathogenesis and molecular determinants

of virulence', *Clinical Microbiology Reviews*. doi: 10.1128/CMR.16.3.463-496.2003.

Soldati, T. and Neyrolles, O. (2012) 'Mycobacteria and the Intraphagosomal Environment: Take It With a Pinch of Salt(s)!', *Traffic*. doi: 10.1111/j.1600-0854.2012.01358.x.

Som, N. F. *et al.* (2017) 'The MtrAB two-component system controls antibiotic production in streptomyces coelicolor A3(2)', *Microbiology (United Kingdom)*. doi: 10.1099/mic.0.000524.

Song, L. *et al.* (2006) 'Type III polyketide synthase β-ketoacyl-ACP starter unit and ethylmalonyl-CoA extender unit selectivity discovered by Streptomyces coelicolor genome mining', *Journal of the American Chemical Society*. doi: 10.1021/ja065247w.

Sousa, J. A. de J. and Olivares, F. L. (2016) 'Plant growth promotion by streptomycetes: Ecophysiology, mechanisms and applications', *Chemical and Biological Technologies in Agriculture*. doi: 10.1186/s40538-016-0073-5.

Stavrum, R. *et al.* (2012) 'Mycobacterium tuberculosis Mce1 protein complex initiates rapid induction of transcription of genes involved in substrate trafficking', *Genes and Immunity*. doi: 10.1038/gene.2012.24.

Steinert, M. (2011) 'Pathogen-host interactions in Dictyostelium, Legionella, Mycobacterium and other pathogens', *Seminars in Cell and Developmental Biology*. doi: 10.1016/j.semcdb.2010.11.003.

Strakova, E. *et al.* (2013) 'Global Features of Gene Expression on the Proteome and

Transcriptome Levels in S. coelicolor during Germination', *PLoS ONE*. doi: 10.1371/journal.pone.0072842.

Studier, F. W. (2005) 'Protein production by auto-induction in high density shaking cultures.', *Protein expression and purification*. doi: 10.1016/j.pep.2005.01.016.

Studier, F. W. and Moffatt, B. A. (1986) 'Use of bacteriophage T7 RNA polymerase to direct selective high-level expression of cloned genes', *Journal of Molecular Biology*. doi: 10.1016/0022-2836(86)90385-2.

Suarez, J. E., Barbes, C. and Hardisson, C. (1980) 'Germination of spores of Micromonospora chalcea: Physiological and biochemical changes', *Journal of General Microbiology*. doi: 10.1099/00221287-121-1-159.

Sunderland, M. E. (2009) 'Dictyostelium discoideum', *Embryo Project Encyclopedia*. ISSN: 1940. Available at: http://embryo.asu.edu/handle/10776/1792.

Sutcliffe, I. C. and Harrington, D. J. (2004) 'Lipoproteins of Mycobacterium tuberculosis: An abundant and functionally diverse class of cell envelope components', *FEMS Microbiology Reviews*. doi: 10.1016/j.femsre.2004.06.002.

Tabor, S. and Richardson, C. C. (1992) 'A bacteriophage T7 RNA polymerase/promoter system for controlled exclusive expression of specific genes. 1985.', *Biotechnology (Reading, Mass.)*.

Takatsuki, A., Arima, K. and Tamura, G. (1971) 'Tunicamycin, a new antibiotic. I. Isolation and characterization of tunicamycin', *The Journal of Antibiotics*. doi:

10.7164/antibiotics.24.215.

Talbot, E. A. and Raffa, B. J. (2014) ‘Mycobacterium tuberculosis’, in *Molecular Medical Microbiology: Second Edition*. doi: 10.1016/B978-0-12-397169-2.00092-5.

Tan, L. T. H. *et al.* (2015) ‘Investigation of antioxidative and anticancer potentials of Streptomyces sp. MUM256 isolated from Malaysia mangrove soil’, *Frontiers in Microbiology*. doi: 10.3389/fmicb.2015.01316.

Thilo, L. (1985) ‘Quantification of endocytosis-derived membrane traffic’, *BBA - Reviews on Biomembranes*. doi: 10.1016/0304-4157(85)90010-3.

Thomas, G. H. (2010) ‘Homes for the orphans: Utilization of multiple substrate-binding proteins by ABC transporters: MicroCommentary’, *Molecular Microbiology*. doi: 10.1111/j.1365-2958.2009.06961.x.

Thompson, B. J. *et al.* (2010) ‘Investigating lipoprotein biogenesis and function in the model Gram-positive bacterium Streptomyces coelicolor’, *Molecular Microbiology*. doi: 10.1111/j.1365-2958.2010.07261.x.

Thong, S. *et al.* (2016) ‘Defining key roles for auxiliary proteins in an ABC transporter that maintains bacterial outer membrane lipid asymmetry’, *eLife*. doi: 10.7554/eLife.19042.

Tran, A. *et al.* (2017) ‘C. elegans avoids toxin-producing Streptomyces using a seven transmembrane domain chemosensory receptor’, *eLife*. doi: 10.7554/eLife.23770.

Uchiya, K. ichi *et al.* (2013) ‘Comparative Genome Analysis of Mycobacterium avium Revealed Genetic Diversity in Strains that Cause Pulmonary and Disseminated Disease’, *PLoS ONE*. doi: 10.1371/journal.pone.0071831.

Ventura, M. *et al.* (2007) ‘Genomics of Actinobacteria: Tracing the Evolutionary History of an Ancient Phylum’, *Microbiology and Molecular Biology Reviews*. doi: 10.1128/mmbr.00005-07.

Vera, A. *et al.* (2007) ‘The conformational quality of insoluble recombinant proteins is enhanced at low growth temperatures’, *Biotechnology and Bioengineering*. doi: 10.1002/bit.21218.

Vissa, V. D. and Brennan, P. J. (2001) ‘The genome of Mycobacterium leprae: A minimal mycobacterial gene set’, *Genome Biology*. doi: 10.1186/gb-2001-2-8-reviews1023.

Vogel, G. *et al.* (1980) ‘Mechanism of phagocytosis in dictyostelium discoideum: Phagocytosis is mediated by different recognition sites as disclosed by mutants with altered phagocytotic properties’, *Journal of Cell Biology*. doi: 10.1083/jcb.86.2.456.

Vollmer, W., Blanot, D. and De Pedro, M. A. (2008) ‘Peptidoglycan structure and architecture’, *FEMS Microbiology Reviews*. doi: 10.1111/j.1574-6976.2007.00094.x.

Walls, D. and Loughran, S. (2017) *Methods in Molecular Biology: Protein Chromatography*, *Methods in Molecular Biology*.

Wang, J. *et al.* (2011) ‘Sequences in the nonconsensus nucleotide-binding domain of ABCG5/ABCG8 required for sterol transport’, *Journal of Biological Chemistry*. doi:

10.1074/jbc.M110.210880.

Wang, X. *et al.* (2017) ‘Characterization of new recombinant 3-ketosteroid-Δ1-dehydrogenases for the biotransformation of steroids’, *Applied Microbiology and Biotechnology*, pp. 6049–6060. doi: 10.1007/s00253-017-8378-2.

Watts, D. J. and Ashworth, J. M. (1970) ‘Growth of myxameobae of the cellular slime mould Dictyostelium discoideum in axenic culture.’, *The Biochemical journal*. doi: 10.1042/bj1190171.

Van Wely, K. H. M. *et al.* (2001) ‘Translocation of proteins across the cell envelope of Gram-positive bacteria’, *FEMS Microbiology Reviews*. doi: 10.1016/S0168-6445(01)00062-6.

Whittington, R. J. *et al.* (2012) ‘Comparative immunological and microbiological aspects of paratuberculosis as a model mycobacterial infection’, *Veterinary Immunology and Immunopathology*. doi: 10.1016/j.vetimm.2011.03.003.

WHO (2019) *Global TUBERCULOSIS Report 2019- Executive summary*, *Geneva: World Health Organization*.

Widdick, D. A. *et al.* (2006) ‘The twin-arginine translocation pathway is a major route of protein export in Streptomyces coelicolor’, *Proceedings of the National Academy of Sciences of the United States of America*. doi: 10.1073/pnas.0607025103.

Wilkens, S. (2015) ‘Structure and mechanism of ABC transporters’, *F1000Prime Reports*. doi: 10.12703/P7-14.

Willemse, J. *et al.* (2011) ‘Positive control of cell division: FtsZ is recruited by SsgB during sporulation of Streptomyces’, *Genes and Development*. doi: 10.1101/gad.600211.

Williams, T. D. and Kay, R. R. (2018) ‘The physiological regulation of macropinocytosis during Dictyostelium growth and development’, *Journal of Cell Science*. doi: 10.1242/jcs.213736.

Williams, T. and Kay, R. R. (2018) ‘High-throughput measurement of dictyostelium discoideum macropinocytosis by flow cytometry’, *Journal of Visualized Experiments*, 2018(139), pp. 1–8. doi: 10.3791/58434.

Williamson, G. *et al.* (2020) ‘A two-lane mechanism for selective biological ammonium transport’, *eLife*, 9, pp. 1–41. doi: 10.7554/eLife.57183.

Yagüe, P. *et al.* (2016) ‘Subcompartmentalization by cross-membranes during early growth of Streptomyces hyphae’, *Nature Communications*. doi: 10.1038/ncomms12467.

Yamasaki, M., Redenbach, M. and Kinashi, H. (2001) ‘Integrated structures of the linear plasmid SCP1 in two bidirectional donor strains of Streptomyces coelicolor A3(2)’, *Molecular and General Genetics*. doi: 10.1007/s004380000349.

Yanisch-Perron, C., Vieira, J. and Messing, J. (1985) ‘Improved M13 phage cloning vectors and host strains: nucleotide sequences of the M13mpl8 and pUC19 vectors’, *Gene*. doi: 10.1016/0378-1119(85)90120-9.

Yeagle, P. L. (2016) ‘The Lipids of Biological Membranes’, in *The Membranes of Cells*. doi: 10.1016/b978-0-12-800047-2.00002-4.

Yoon, V. and Nodwell, J. R. (2014) ‘Activating secondary metabolism with stress and chemicals’, *Journal of Industrial Microbiology and Biotechnology*, 41(2), pp. 415–424. doi: 10.1007/s10295-013-1387-y.

Zacchetti, B. *et al.* (2016) ‘Aggregation of germlings is a major contributing factor towards mycelial heterogeneity of Streptomyces’, *Scientific Reports*. Nature Publishing Group, 6(February), pp. 1–11. doi: 10.1038/srep27045.

Zaychikova, M. V. and Danilenko, V. N. (2020) ‘The Actinobacterial mce Operon: Structure and Functions’, *Biology Bulletin Reviews*. doi: 10.1134/s2079086420060079.

Zhang, F. and Xie, J. P. (2011) ‘Mammalian cell entry gene family of Mycobacterium tuberculosis’, *Molecular and Cellular Biochemistry*, 352(1–2), pp. 1–10. doi: 10.1007/s11010-011-0733-5.

Zhang, Y. *et al.* (2018) ‘Mycobacterium tuberculosis Mce3C promotes mycobacteria entry into macrophages through activation of β2 integrin-mediated signalling pathway’, *Cellular Microbiology*, 20(2), pp. 1–16. doi: 10.1111/cmi.12800.

Zhi, X. Y., Li, W. J. and Stackebrandt, E. (2009) ‘An update of the structure and 16S rRNA gene sequence-based definition of higher ranks of the class Actinobacteria, with the proposal of two new suborders and four new families and emended descriptions of the existing higher taxa’, *International Journal of Systematic and Evolutionary Microbiology*. doi: 10.1099/ijs.0.65780-0.

Zhou, Z. *et al.* (2016) ‘Genomic data mining reveals a rich repertoire of transport proteins in Streptomyces’, *BMC Genomics*. doi: 10.1186/s12864-016-2899-4.

Zuber, B. *et al.* (2008) ‘Direct visualization of the outer membrane of mycobacteria and corynebacteria in their native state’, *Journal of Bacteriology*. doi: 10.1128/JB.01919-07.

Zückert, W. R. (2014a) ‘Secretion of Bacterial Lipoproteins: Through the Cytoplasmic Membrane, the Periplasm and Beyond’, *Biochimica et Biophysica Acta - Molecular Cell Research*. doi: 10.1016/j.bbamcr.2014.04.022.

Zückert, W. R. (2014b) ‘Secretion of Bacterial Lipoproteins: Through the Cytoplasmic Membrane, the Periplasm and Beyond’, *Biochimica et Biophysica Acta - Molecular Cell Research*. Elsevier B.V., 1843(8), pp. 1509–1516. doi: 10.1016/j.bbamcr.2014.04.022.